SYNTHESIS AND CHARACTERIZATION OF
POROUS CARBONS
USING NATURAL ZEOLITES AND AlPO$_4$-5 AS TEMPLATES
AND
DIFFUSION OF VOLATILE ORGANIC CHEMICALS
IN THESE POROUS MEDIA

by
BİLLUR SAKİNTUNA

Submitted to the Graduate School of Engineering and Natural Sciences
in partial fulfilment of
the requirements for the degree of
Doctor of Philosophy

Sabanci University
Spring 2005

Dedicated to Duhter and Ender Sakintuna

SYNTHESIS AND CHARACTERIZATION OF

POROUS CARBONS

USING NATURAL ZEOLITES AND AlPO$_4$-5 AS TEMPLATES

AND

DIFFUSION OF VOLATILE ORGANIC CHEMICALS
IN THESE POROUS MEDIA

APPROVED BY:

Prof. Dr. Yuda Yürüm ……………………..
(Dissertation Supervisor)

Prof. Dr. Ferhat Yardım ……………………..

Prof. Dr. S. Ali Tuncel ……………………..

Assist. Prof. Dr. Alpay Taralp ……………………..

Assist. Prof. Dr. Gürsel Sönmez ……………………..

DATE OF APPROVAL: 17.06.2005

ACKNOWLEDGEMENT

First of all, I would like to express my deepest gratitude to Prof. Dr. Yuda Yürüm, my supervisor, dissertation chair and above all, my mentor. Right from the beginning of my studies at Sabanci University, I always felt his continual support and sincere interest in my success. He inspired me both with his academic success and gained my utmost respect as a reputable researcher with his kindness as a wonderful person. Thank you always being there for me…

I would also like to thank Enis Fakıoğlu, a very special person in my life. Enis always managed to support me and provided understanding during the long and arduous hours I devoted to the PhD experience. You made it all so much easier being there for me.

I can not forget admired supports of my dear friends Lerzan Aksoy and Şebnem Erseren. Within my last four years in Istanbul, they have always been with me even on my most difficult days. I also would like to thank Ahu Gümrah Dumanlı and all my friends at Sabanci University who made my whole PhD period a very pleasing four years.

Altough far away in Ankara, I always felt Duhter and Ender Sakintuna's presence right next to me. My beloved mother and father, my deepest thanks for everything you have done for me…

TABLE OF CONTENTS

LIST OF TABLES

LIST OF FIGURES

xii

ABSTRACT

The novel approach of template carbonization method has been successfully used in this study for the production of porous carbons templated from a Turkish natural zeolite and a microwave-assisted $AlPO_4$-5. The effect of different templating agents and different carbonization temperatures was studied. The carbon precursor used was furfuryl alcohol, FA. The structures of the carbons produced were compared using SEM, EDS, XRD, FT-IR, ^{13}C CPMAS, ^{29}Si CPMAS, ^{27}Al MAS NMR and ^{19}F MAS NMR and some surface analysis methods.

FA was polymerized and carbonized at 700°C, 800°C, 900°C and 1000°C in the channels of natural zeolite and $AlPO_4$-5. The d_{002} values, stacking heights of graphene sheets, L_c, lateral size, L_a, number of graphene sheets per stack of resultant carbons were calculated from the Debye-Scherer equation.

BET surface areas of natural zeolite templated carbons were 397, 350, 405 and 367 m^2/g at 700, 800, 900 and 1000°C, respectively. By using sol-gel method, 804 m^2/g BET surface area was obtained. EDS analyses showed that 91-99% C was obtained at 700-1000°C. In ^{13}C NMR, sp, sp^2 and sp^3 hybridized carbons were observed. Pore diameters were 11 nm, indicating the mesoporosity. L_c values and average number of graphene sheets per stack were increasing with carbonization temperature.

During removal of the zeolite template by washing with HF, some organoaluminium fluoride flower-like structures were observed in the SEM images which consisted of mainly fluorine, carbon and aluminium. According to ^{19}F MAS NMR spectra of these carbons, Al_2F_2, $AlFC_3$, AlF_2C_2, and AlF_3C groups were observed. In XRD pattern, peaks were belonging to aluminium hydroxide fluoride. The structural differences in the natural zeolite templated carbons obtained after HCl, NaOH, HCl-NaOH, and HF-NaOH washing solutions besides HF were investigated. HF washed porous carbon had the highest surface area with 397 m^2/g.

The systematic study of the parameters of the microwave synthesis of $AlPO_4$-5 was examined for the use of further templating purposes. Powdered $AlPO_4$-5 crystals of high quality could be synthesized using a microwave heating technique. Usage of microwave heating drastically reduced the crystallization times. The crystal growth depended on the

initial gel composition. Perfect hexagonal $AlPO_4$-5 products formed with ca. 5 μm length with characteristic morphologies of $AlPO_4$-5 crystals. BET surface area of selected $AlPO_4$-5 for the further steps was 107 m^2/g and average pore diameter was 1.7 nm.

BET surface areas of $AlPO_4$-5 templated carbons were measured as 149, 125, 122 and 108 m^2/g at 700, 800, 900 and 1000°C, respectively. The surface areas of natural zeolite templated porous carbons were higher than those of $AlPO_4$-5 templated porous carbons, due to higher accessibility to the pores in natural zeolite. Average pore diameters of $AlPO_4$-5 templated porous carbons were 1.7 nm, indicating microporosity. Carbon contents of the porous carbons detected in EDS were 96-82% at 700-1000°C. As observed in the natural zeolite templated carbons, L_c values and average number of graphene sheets per stack were increasing with carbonization temperature. The d_{002} values of the $AlPO_4$-5 templated porous carbons synthesized were 0.358-0.363 nm at 700-1000°C, respectively.

Diffusion of volatile organic chemicals in natural zeolites and natural templated porous carbons was investigated. Diffusion coefficients, mode of transport and activation energies of diffusion of methanol, ethanol, n-propanol, i-propanol and n-butanol into the porous structure of a Turkish natural zeolite and natural zeolite templated porous carbons were measured in the range of 24.0-28.0°C.

As the molecular weight of the alcohols increased diffusion coefficients into natural zeolite and natural zeolite templated carbons decreased, activation energy for diffusion increased, and time necessary to reach equilibrium increased. The diffusion constants increased linearly with an increase in the temperature. The diffusion of alcohols into zeolite and porous carbons obeyed the anomalous transport mechanism. Diffusion rate constants slightly increased as the temperature was increased.

The calculated coefficients of diffusion of volatile molecules in the porous carbons were lower than that of observed in the natural zeolite. It is interesting to compare the activation energies measured in natural zeolite and natural zeolite templated porous carbons. The activation energies for diffusion of methanol were 90.1 kJ/mol and 220.7 kJ/mol for natural zeolite and porous carbon, carbonized at 700°C, respectively. This is most likely due to the polarity of alcohols and stronger interaction with carbon surface.

ÖZET

DOĞAL ZEOLİT VE AlPO$_4$-5 KULLANILARAK KALIPLAMA YÖNTEMİYLE GÖZENEKLİ KARBON SENTEZİ VE KARAKTERİZASYONU
VE
UÇUCU ORGANİK KİMYASALLARIN BU GÖZENEKLİ YAPILARDAKİ DİFÜZYONU

Bu çalışmada, Manisa Gördes doğal zeolitinin ve mikrodalga enerjisi kullanılarak üretilen AlPO$_4$-5 'ın kalıp olarak kullanıldığı yöntemde gözenekli karbon sentezi başarıyla gerçekleştirilmiştir. Farklı kalıpların, doğal zeolit ve AlPO$_4$-5, ve farklı karbonizasyon sıcaklıkların, 700-1000°C, etkisi incelenmiştir. Furfuril alkol, karbon kaynağı olarak kullanılmıştır. Üretilen karbon malzemelerin özellikleri SEM, EDS, XRD, FT-IR, ^{13}C CPMAS, ^{29}Si CPMAS, ^{27}Al MAS NMR, ^{19}F MAS NMR ve yüzey analiz yöntemleri kullanılarak incelenmiştir.

Furfuril alkol, 700, 800, 900 and 1000°C sıcaklıklarda doğal zeolitin ve AlPO$_4$-5'in gözeneklerinde polimerize ve karbonize edilmiştir. Üretilen karbon malzemelerin d_{002} değerleri, grafit plakalar arasındaki uzunluk, L_c, plakaların uzunluğu, L_a, ve plaka sayısı Debye-Scherer denklemi kullanılarak hesaplanmıştır.

Doğal zeolitin kalıp olarak kullanıldığı deneylerden elde edilen gözenekli karbonların BET yüzey alanları 700, 800, 900 ve 1000°C'lerde sırasıyla 397, 350, 405 and 367 m^2/g'dır. EDS analizleri sonucunda 700-1000°C aralığında üretilen karbon malzemelerinin karbon içeriğinin %91-99 olduğu bulunmuştur. Elde edilen karbon malzemelerinde sp, sp^2 ve sp^3 hibritleşmiş karbon yapılarının olduğu ^{13}C NMR yöntemi kullanılarak gözlenmiştir. Bu malzemelerin gözenek çapları 11 nm olup, mezo gözenekli yapıdadır. L_c değerleri ve grafit plaka sayısı karbonizasyon sıcaklığı arttıkça artmaktadır.

Zeolit kalıbı uzaklaştırmak için HF kullanılan örneklerin SEM görüntülerinde çiçek şeklinde organoalüminyum florür yapılar gözlenmiştir. Bu yapılar başlıca flor, karbon ve alüminyum içermektedir. ^{19}F MAS NMR kullanılarak üretilen karbonda Al$_2$F$_2$, AlFC$_3$, AlF$_2$C$_2$, ve AlF$_3$C gruplar olduğu gözlenmiştir. X-ışını difraktogramlarında alüminyum hidroksit florür bileşiğine ait pikler bulunmaktadır. Kalıp olarak kullanılan doğal zeolit, HF yanında, HCl, NaOH, HCl-NaOH, ve HF-NaOH ile de uzaklaştırılmaya çalışılmış ve elde edilen gözenekli karbondaki değişiklikler gözlenmiştir.

İlerde kalıp olarak kullanılmak üzere çeşitli parametrelerin sistematik çalışılmasıyla mikrodalga yöntemiyle $AlPO_4$-5 sentezlenmiştir. Yüksek kalite $AlPO_4$-5 kristalleri mikrodalga yöntemi kullanılarak sentezlenebilmektedir. Mikrodalga yöntemi sentezleme zamanını oldukça düşürmektedir. Kristalin büyümesi başlangıç solüsyon kompozisyonuna bağlıdır. Mükemmel altıgen yapıda, yaklaşık 5 μm uzunluğunda $AlPO_4$-5 kristalleri elde edilmiştir. Kalıplama yönteminde kullanılmak üzere seçilen $AlPO_4$-5'ün BET yüzey alanı 107 m^2/g ve ortalama gözenek çapı ise 1.7 nm'dir.

$AlPO_4$-5 kullanılarak kalıplanan gözenekli karbonların BET yüzey alanları 700, 800, 900 ve 1000°C'lerde 149, 125, 122 and 108 m^2/g m^2/g'dır. $AlPO_4$-5 kullanılarak kalıplanan gözenekli karbonların yüzey alanları, gözeneklerin erişilebilirliği bakımından doğal zeolit kullanılarak üretilenlere kıyasla daha düşüktür. $AlPO_4$-5 kullanılarak kalıplanan gözenekli karbonların ortalama gözenek çapları 1.7 nm'dir. EDS analizleri at 700-1000°C aralığında 96-82% karbon elde edilmiştir. Doğal zeolit kullanılarak kalıplanan gözenekli karbonlarda olduğu gibi, L_c değerleri ve grafit plaka sayısı karbonizasyon sıcaklığı arttıkça artmaktadır. d_{002} değerleri 700-1000°C aralığında 0.358-0.363 nm arasındadır.

Uçucu organik kimyasalların doğal zeolitte ve doğal zeolit kullanılarak kalıplanan gözenekli karbonlarda difüzyonları incelenmiştir. Metanol, etanol, n-propanol, i-propanol ve n-butanol'ün doğal zeolitte ve doğal zeolit kullanılarak kalıplanan gözenekli karbonlarda difüzlenme katsayısı, difüzyon mekanizması ve aktivasyon enerjileri 24.0-28.0°C aralığında ölçülmüştür.

Hem doğal zeolitte, hem de doğal zeolit kullanılarak kalıplanan gözenekli karbonlarda, alkollerin molekül ağırlıkları arttıkça difüzyon katsayısının, aktivasyon enerjisinin ve dengeye ulaşmak için gerekli zamanın arttığı gözlenmiştir. Difüzyon katsayısı sıcaklık artıkça yükselmektedir. Difüzyon mekanizması, doğal zeolitte ve karbonlarda düzensiz difüzyondur. Difüzyon hız sabitleri sıcaklık arttıkça hafifçe yükselmektedir.

Doğal zeolit kullanılarak kalıplanan gözenekli karbonlarda difüzlenme katsayısı doğal zeolite göre düşüktür. Aktivasyon enerjileri ise daha yüksektir. Metanolün aktivasyon enerjisi doğal zeolitte ve karbonda sırasıyla 90.1 kJ/mol and 220.7 kJ/mol'dır. Bunun nedeni polar alkollerin karbon yüzeyi ile olan etkileşimidir.

LIST OF ABBREVIATIONS

d	Interlayer spacing
L_c	The stacking height of the graphene crystallites
L_a	The lateral size of the graphene crystallites
T	Tetrahedral atom
α_e	The electronic polarization
α_a	The atomic polarization
α_d	The dipolar polarization
α_I	The interfacial polarization
E	The magnitude of the internal electric field
ε_{eff}''	The relative effective dielectric factor
ε_0	The permittivity of free space
f	The microwave frequency
σ	The total effective conductivity
ε_r'	The relative dielectric constant
$tan\delta$	The energy loss required to store a given quantity of energy
T	Temperature
ρ	Density
C_p	Heat capacity
D	Depth of penetration
λ_0	Incident wavelength
J	Flux
x	Spatial coordinate
C_A	Solid phase concentration
r	Distance from the particle center
C	Initial solid phase concentration
r_o	Particle radius
PFG NMR	Pulsed field gradient nuclear magnetic resonance
QENS	Quasi-elastic neutron scattering
TEOM	Tapered element oscillating microbalance

ZLC	The zero-length column
TAP	Temporal-analysis-of-products
PEP	Positron Emission Profiling
EDS	Energy Dispersive Spectroscopy
PFA	Poly(furfuryl alcohol)
FA	Furfuryl alcohol
TEOS	Tetraethoxysilane
FWHM	Full width half maxima
$\mathbf{M_t}$	The amount of solvent diffused in the structure at time t
$\mathbf{M_\infty}$	The amount of solvent diffused at steady state
t	Release time
k	Rate constant
n	An exponent characteristic of the mode of transport
D	Coefficient of diffusion
$\mathbf{D_o}$	Temperature-independent pre-exponential
$\mathbf{E_A}$	Activation energy
TEA	Triethylamine
TPA	Tripropylamine
TPAOH	Tripropylamine hydroxide

SYNTHESIS AND CHARACTERIZATION OF

POROUS CARBONS

USING NATURAL ZEOLITES AND AlPO$_4$-5 AS TEMPLATES

AND

DIFFUSION OF VOLATILE ORGANIC CHEMICALS
IN THESE POROUS MEDIA

by

BİLLUR SAKİNTUNA

Submitted to the Graduate School of Engineering and Natural Sciences
in partial fulfilment of
the requirements for the degree of
Doctor of Philosophy

Sabanci University
Spring 2005

Dedicated to Duhter and Ender Sakintuna

SYNTHESIS AND CHARACTERIZATION OF
POROUS CARBONS
USING NATURAL ZEOLITES AND AlPO$_4$-5 AS TEMPLATES
AND
DIFFUSION OF VOLATILE ORGANIC CHEMICALS
IN THESE POROUS MEDIA

APPROVED BY:

Prof. Dr. Yuda Yürüm …………………..
(Dissertation Supervisor)

Prof. Dr. Ferhat Yardım …………………..

Prof. Dr. S. Ali Tuncel …………………..

Assist. Prof. Dr. Alpay Taralp …………………..

Assist. Prof. Dr. Gürsel Sönmez …………………..

DATE OF APPROVAL: 17.06.2005

ACKNOWLEDGEMENT

TABLE OF CONTENTS

LIST OF TABLES

LIST OF FIGURES

ABSTRACT

The novel approach of template carbonization method has been successfully used in this study for the production of porous carbons templated from a Turkish natural zeolite and a microwave-assisted $AlPO_4$-5. The effect of different templating agents and different carbonization temperatures was studied. The carbon precursor used was furfuryl alcohol, FA. The structures of the carbons produced were compared using SEM, EDS, XRD, FT-IR, ^{13}C CPMAS, ^{29}Si CPMAS, ^{27}Al MAS NMR and ^{19}F MAS NMR and some surface analysis methods.

FA was polymerized and carbonized at 700°C, 800°C, 900°C and 1000°C in the channels of natural zeolite and $AlPO_4$-5. The d_{002} values, stacking heights of graphene sheets, L_c, lateral size, L_a, number of graphene sheets per stack of resultant carbons were calculated from the Debye-Scherer equation.

BET surface areas of natural zeolite templated carbons were 397, 350, 405 and 367 m^2/g at 700, 800, 900 and 1000°C, respectively. By using sol-gel method, 804 m^2/g BET surface area was obtained. EDS analyses showed that 91-99% C was obtained at 700-1000°C. In ^{13}C NMR, sp, sp^2 and sp^3 hybridized carbons were observed. Pore diameters were 11 nm, indicating the mesoporosity. L_c values and average number of graphene sheets per stack were increasing with carbonization temperature.

During removal of the zeolite template by washing with HF, some organoaluminium fluoride flower-like structures were observed in the SEM images which consisted of mainly fluorine, carbon and aluminium. According to ^{19}F MAS NMR spectra of these carbons, Al_2F_2, $AlFC_3$, AlF_2C_2, and AlF_3C groups were observed. In XRD pattern, peaks were belonging to aluminium hydroxide fluoride. The structural differences in the natural zeolite templated carbons obtained after HCl, NaOH, HCl-NaOH, and HF-NaOH washing solutions besides HF were investigated. HF washed porous carbon had the highest surface area with 397 m^2/g.

The systematic study of the parameters of the microwave synthesis of $AlPO_4$-5 was examined for the use of further templating purposes. Powdered $AlPO_4$-5 crystals of high quality could be synthesized using a microwave heating technique. Usage of microwave heating drastically reduced the crystallization times. The crystal growth depended on the

initial gel composition. Perfect hexagonal AlPO$_4$-5 products formed with ca. 5 μm length with characteristic morphologies of AlPO$_4$-5 crystals. BET surface area of selected AlPO$_4$-5 for the further steps was 107 m^2/g and average pore diameter was 1.7 nm.

BET surface areas of AlPO$_4$-5 templated carbons were measured as 149, 125, 122 and 108 m^2/g at 700, 800, 900 and 1000°C, respectively. The surface areas of natural zeolite templated porous carbons were higher than those of AlPO$_4$-5 templated porous carbons, due to higher accessibility to the pores in natural zeolite. Average pore diameters of AlPO$_4$-5 templated porous carbons were 1.7 nm, indicating microporosity. Carbon contents of the porous carbons detected in EDS were 96-82% at 700-1000°C. As observed in the natural zeolite templated carbons, L_c values and average number of graphene sheets per stack were increasing with carbonization temperature. The d_{002} values of the AlPO$_4$-5 templated porous carbons synthesized were 0.358-0.363 nm at 700-1000°C, respectively.

Diffusion of volatile organic chemicals in natural zeolites and natural templated porous carbons was investigated. Diffusion coefficients, mode of transport and activation energies of diffusion of methanol, ethanol, n-propanol, i-propanol and n-butanol into the porous structure of a Turkish natural zeolite and natural zeolite templated porous carbons were measured in the range of 24.0-28.0°C.

As the molecular weight of the alcohols increased diffusion coefficients into natural zeolite and natural zeolite templated carbons decreased, activation energy for diffusion increased, and time necessary to reach equilibrium increased. The diffusion constants increased linearly with an increase in the temperature. The diffusion of alcohols into zeolite and porous carbons obeyed the anomalous transport mechanism. Diffusion rate constants slightly increased as the temperature was increased.

The calculated coefficients of diffusion of volatile molecules in the porous carbons were lower than that of observed in the natural zeolite. It is interesting to compare the activation energies measured in natural zeolite and natural zeolite templated porous carbons. The activation energies for diffusion of methanol were 90.1 kJ/mol and 220.7 kJ/mol for natural zeolite and porous carbon, carbonized at 700°C, respectively. This is most likely due to the polarity of alcohols and stronger interaction with carbon surface.

ÖZET

DOĞAL ZEOLİT VE AlPO$_4$-5 KULLANILARAK KALIPLAMA YÖNTEMİYLE GÖZENEKLİ KARBON SENTEZİ VE KARAKTERİZASYONU
VE
UÇUCU ORGANİK KİMYASALLARIN BU GÖZENEKLİ YAPILARDAKİ DİFÜZYONU

Bu çalışmada, Manisa Gördes doğal zeolitinin ve mikrodalga enerjisi kullanılarak üretilen AlPO$_4$-5 'ın kalıp olarak kullanıldığı yöntemde gözenekli karbon sentezi başarıyla gerçekleştirilmiştir. Farklı kalıpların, doğal zeolit ve AlPO$_4$-5, ve farklı karbonizasyon sıcaklıkların, 700-1000°C, etkisi incelenmiştir. Furfuril alkol, karbon kaynağı olarak kullanılmıştır. Üretilen karbon malzemelerin özellikleri SEM, EDS, XRD, FT-IR, ^{13}C CPMAS, ^{29}Si CPMAS, ^{27}Al MAS NMR, ^{19}F MAS NMR ve yüzey analiz yöntemleri kullanılarak incelenmiştir.

Furfuril alkol, 700, 800, 900 and 1000°C sıcaklıklarda doğal zeolitin ve AlPO$_4$-5'in gözeneklerinde polimerize ve karbonize edilmiştir. Üretilen karbon malzemelerin d_{002} değerleri, grafit plakalar arasındaki uzunluk, L_c, plakaların uzunluğu, L_a, ve plaka sayısı Debye-Scherer denklemi kullanılarak hesaplanmıştır.

Doğal zeolitin kalıp olarak kullanıldığı deneylerden elde edilen gözenekli karbonların BET yüzey alanları 700, 800, 900 ve 1000°C'lerde sırasıyla 397, 350, 405 and 367 m^2/g'dır. EDS analizleri sonucunda 700-1000°C aralığında üretilen karbon malzemelerinin karbon içeriğinin %91-99 olduğu bulunmuştur. Elde edilen karbon malzemelerinde sp, sp^2 ve sp^3 hibritleşmiş karbon yapılarının olduğu ^{13}C NMR yöntemi kullanılarak gözlenmiştir. Bu malzemelerin gözenek çapları 11 nm olup, mezo gözenekli yapıdadır. L_c değerleri ve grafit plaka sayısı karbonizasyon sıcaklığı arttıkça artmaktadır.

Zeolit kalıbı uzaklaştırmak için HF kullanılan örneklerin SEM görüntülerinde çiçek şeklinde organoalüminyum florür yapılar gözlenmiştir. Bu yapılar başlıca flor, karbon ve alüminyum içermektedir. ^{19}F MAS NMR kullanılarak üretilen karbonda Al$_2$F$_2$, AlFC$_3$, AlF$_2$C$_2$, ve AlF$_3$C gruplar olduğu gözlenmiştir. X-ışını difraktogramlarında alüminyum hidroksit florür bileşiğine ait pikler bulunmaktadır. Kalıp olarak kullanılan doğal zeolit, HF yanında, HCl, NaOH, HCl-NaOH, ve HF-NaOH ile de uzaklaştırılmaya çalışılmış ve elde edilen gözenekli karbondaki değişiklikler gözlenmiştir.

İlerde kalıp olarak kullanılmak üzere çeşitli parametrelerin sistematik çalışılmasıyla mikrodalga yöntemiyle $AlPO_4$-5 sentezlenmiştir. Yüksek kalite $AlPO_4$-5 kristalleri mikrodalga yöntemi kullanılarak sentezlenebilmektedir. Mikrodalga yöntemi sentezleme zamanını oldukça düşürmektedir. Kristalin büyümesi başlangıç solüsyon kompozisyonuna bağlıdır. Mükemmel altıgen yapıda, yaklaşık 5 μm uzunluğunda $AlPO_4$-5 kristalleri elde edilmiştir. Kalıplama yönteminde kullanılmak üzere seçilen $AlPO_4$-5'ün BET yüzey alanı 107 m^2/g ve ortalama gözenek çapı ise 1.7 nm'dir.

$AlPO_4$-5 kullanılarak kalıplanan gözenekli karbonların BET yüzey alanları 700, 800, 900 ve 1000°C'lerde 149, 125, 122 and 108 m^2/g m^2/g'dır. $AlPO_4$-5 kullanılarak kalıplanan gözenekli karbonların yüzey alanları, gözeneklerin erişilebilirliği bakımından doğal zeolit kullanılarak üretilenlere kıyasla daha düşüktür. $AlPO_4$-5 kullanılarak kalıplanan gözenekli karbonların ortalama gözenek çapları 1.7 nm'dir. EDS analizleri at 700-1000°C aralığında 96-82% karbon elde edilmiştir. Doğal zeolit kullanılarak kalıplanan gözenekli karbonlarda olduğu gibi, L_c değerleri ve grafit plaka sayısı karbonizasyon sıcaklığı arttıkça artmaktadır. d_{002} değerleri 700-1000°C aralığında 0.358-0.363 nm arasındadır.

Uçucu organik kimyasalların doğal zeolitte ve doğal zeolit kullanılarak kalıplanan gözenekli karbonlarda difüzyonları incelenmiştir. Metanol, etanol, n-propanol, i-propanol ve n-butanol'ün doğal zeolitte ve doğal zeolit kullanılarak kalıplanan gözenekli karbonlarda difüzlenme katsayısı, difüzyon mekanizması ve aktivasyon enerjileri 24.0-28.0°C aralığında ölçülmüştür.

Hem doğal zeolitte, hem de doğal zeolit kullanılarak kalıplanan gözenekli karbonlarda, alkollerin molekül ağırlıkları arttıkça difüzyon katsayısının, aktivasyon enerjisinin ve dengeye ulaşmak için gerekli zamanın arttığı gözlenmiştir. Difüzyon katsayısı sıcaklık artıkça yükselmektedir. Difüzyon mekanizması, doğal zeolitte ve karbonlarda düzensiz difüzyondur. Difüzyon hız sabitleri sıcaklık arttıkça hafifçe yükselmektedir.

Doğal zeolit kullanılarak kalıplanan gözenekli karbonlarda difüzlenme katsayısı doğal zeolite göre düşüktür. Aktivasyon enerjileri ise daha yüksektir. Metanolün aktivasyon enerjisi doğal zeolitte ve karbonda sırasıyla 90.1 kJ/mol and 220.7 kJ/mol'dır. Bunun nedeni polar alkollerin karbon yüzeyi ile olan etkileşimidir.

LIST OF ABBREVIATIONS

d	Interlayer spacing
L_c	The stacking height of the graphene crystallites
L_a	The lateral size of the graphene crystallites
T	Tetrahedral atom
α_e	The electronic polarization
α_a	The atomic polarization
α_d	The dipolar polarization
α_I	The interfacial polarization
E	The magnitude of the internal electric field
ε_{eff}''	The relative effective dielectric factor
ε_0	The permittivity of free space
f	The microwave frequency
σ	The total effective conductivity
ε_r'	The relative dielectric constant
$\tan\delta$	The energy loss required to store a given quantity of energy
T	Temperature
ρ	Density
C_p	Heat capacity
D	Depth of penetration
λ_0	Incident wavelength
J	Flux
x	Spatial coordinate
C_A	Solid phase concentration
r	Distance from the particle center
C	Initial solid phase concentration
r_o	Particle radius
PFG NMR	Pulsed field gradient nuclear magnetic resonance
QENS	Quasi-elastic neutron scattering
TEOM	Tapered element oscillating microbalance

ZLC	The zero-length column
TAP	Temporal-analysis-of-products
PEP	Positron Emission Profiling
EDS	Energy Dispersive Spectroscopy
PFA	Poly(furfuryl alcohol)
FA	Furfuryl alcohol
TEOS	Tetraethoxysilane
FWHM	Full width half maxima
$\mathbf{M_t}$	The amount of solvent diffused in the structure at time t
$\mathbf{M_\infty}$	The amount of solvent diffused at steady state
t	Release time
k	Rate constant
n	An exponent characteristic of the mode of transport
D	Coefficient of diffusion
$\mathbf{D_o}$	Temperature-independent pre-exponential
$\mathbf{E_A}$	Activation energy
TEA	Triethylamine
TPA	Tripropylamine
TPAOH	Tripropylamine hydroxide

CHAPTER 1. INTRODUCTION

In recent years, there has been growing interest in the new applications of porous carbons because of their ability to interact with molecules not only with their surfaces but also in the bulk of the material [25]. The size distribution and topology of pores in materials of similar compositions can be very different, depending on the method of synthesis.

Since they have hydrophobic surfaces, high surface area, large pore volumes, chemical inertness, good mechanical stability and good thermal stability, porous carbons are widely used as industrial adsorbents [25]. Application areas are wide including gas separation, water purification, catalyst support, chromatography columns, storage of natural gas, and use as electrodes of an electric double-layer capacitor.

In this study, a novel approach, templated carbonization method was proposed for the synthesis of porous carbons. Different inorganic templates have been used to synthesize a variety of porous carbon materials. Templating, the process of filling the external and / or internal pores of an inorganic material with a carbon precursor and chemically separating the resulting material from the template was used in this survey.

The template carbonization method allows one to control carbon structure in terms of various aspects such as pore structure and microscopic morphology, which makes this method very attractive. The synthesis conditions and type of the template introduce controllable features to the resulting carbon product. To control pore diameter of the porous carbons is very essential in industrial applications. The presence of micropores is essential for the adsorption of small gas molecules on activated carbons. However, when the adsorbates are polymers, dyes, or vitamins, only mesopores allow the adsorption of such giant molecules. Also nanostructured carbon materials are potentially great technological interest for the development of new catalysts, electronic components, fuel cell components and hydrogen storage equipment.

Turkish natural zeolite and microwave-assisted $AlPO_4$-5 was used as inorganic templates in the present study, because the dimensions of their cages and channels are quite similar to those of organic molecules that constitute the replica. Being cheap and abundant, Turkish natural zeolite is the best fit for our purposes.

As a templating agent, a zeolitic material, $AlPO_4$-5 was synthesized by microwave method which has a number of advantages, for instance, low processing costs, better production quality, reduced hazards to human health and the environment and enhanced quality of life. With proper understanding and control, many technically important materials can be heated rapidly, uniformly, selectively, less expensively and with greater control than the conventional methods.

It was expected that porous carbons with different pore diameters would be synthesized by using different templating agents. Mesoporous and highly microporous carbons expected to be synthesized by using natural zeolite and $AlPO_4$-5 respectively, since natural zeolite has a mesoporous and $AlPO_4$-5 has a microporous structure.

The size, shape and adsorptive selectivity of both natural and synthetic zeolitic materials have been used in advantage for a wide variety of heterogeneous catalytic processes. As an example of zeolite used as catalysts, the methanol to gasoline conversion process is of major commercial importance. This process has been the subject of numerous studies, but it is still not particularly well understood. The diffusion of small molecules in the intracrystalline void volume of zeolites has been a research topic for many years. To obtain information about the transport properties of zeolite crystals, it is important to understand fundamentals of the dynamics of small molecules inside the zeolite, which is relevant for all applications. In the present survey, diffusion into these porous materials has been investigated for the application purposes.

2

CHAPTER 2. STATE-OF-THE-ART

2.1 Carbon Materials and Zeolites

2.1.1 Carbon

The world carbon was coined in 1789 by Antoine L. de Lavoisier from the Latin *carbo,* charcoal [1]. At the close of the eighteenth century, graphite and diamond were known to be different forms of the same element. Then for a considerable time graphite and diamond were the only known forms of crystalline carbon. There exists a third major form, fullerenes that were discovered in 1985. Fullerene, the molecular allotrope of carbon, is a cage molecule. Fullerene is made from a single element and contains 60 carbon atoms.

With is central position in the first full row of the Mendeliev classification; the element carbon exhibits unique possibilities ($1s^2$, $2s^2$, $2p^2$). Carbon can bond to numerous other elements and can have different bondings with it. This gives to carbon extreme variations in physical properties. The principle feature is the multiple bonding available with catenation of carbon via π-orbitals and two principal regimes; either a single σ-bond as in diamond, or a double bond (σ- and π- bonds) as in graphite and graphitic compounds.

Graphitic carbons form as a carbonaceous residue during the pyrolysis of organic compounds (heating in absence of air). Graphitic means "all varieties of substance consisting of the element carbon (>90%) in the allotropic form of graphite irrespective of the presence of structural defects". Thus, graphitic carbons form a practically unbroken series of materials, based on defective graphite structures.

By heat treatment up to 2800°C at atmospheric pressure, some of them transform to graphite. Structure of all graphitic carbons can be simply described as the extent and perfection of a structural unit (i.e. the aromatic layer). Structure is defined by the layer extent (L_a) as well as layer stacking order (L_c and d_{002} spacing) which define paracrystalline structure of carbon, shown in Figure 2.1.
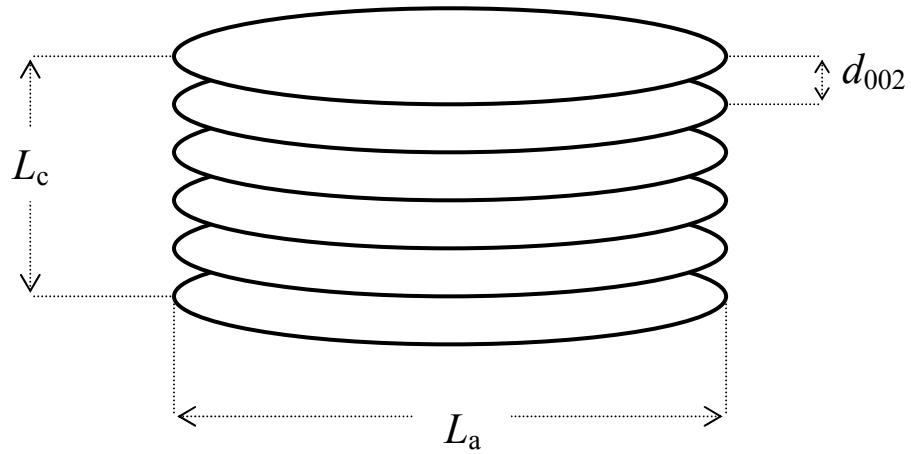
Figure 2.1. Model for a stack of layers of a carbon crystallite [2].

2.1.1.1 Graphitization and Structure by X-Ray Diffraction

Crystalline graphite consists of parallel sheets of carbon atoms, each sheet containing hexagonal arrays of carbon atoms (Figure 2.2). Each atom is connected to three nearest neighbours, within the sheets, by covalent bonds that separate them by a distance of 1.415 Å. This bonding arrangement results from the sp^2 hybridization of carbon's electronic orbitals. Another intriguing aspect of the bonding scheme within the graphite sheets is the distributed π- bonding between the carbon atoms. This distributed π- bonding gives rise to delocalized electrons that makes graphite electrically conducting. The sheets are held together by weak van der Waals forces and are separated from each other by a distance of 3.35 Å.

2.1.1.1.1 The Graphitization Process

Graphitization is a solid state transformation of thermodynamically unstable carbon into graphite by thermal activation [3]. During the process of the heat-treatment, the initially weak diffraction pattern becomes less diffuse, and the lines sharpen, with the appearance of new diffraction lines. The discovery and the explanation of this process started with the understanding of turbostratic (fully disordered) structures.
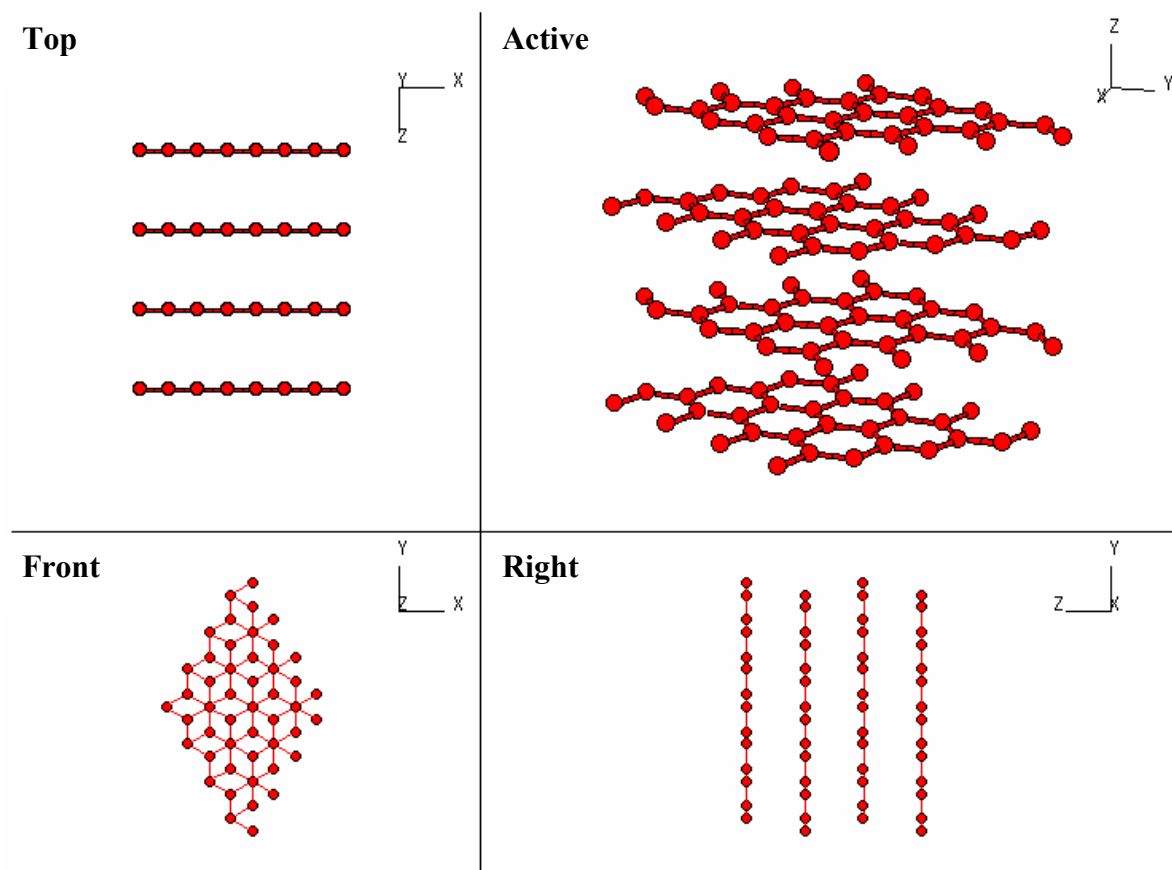
Figure 2.2. Schematic representation of graphite from different views.

2.1.1.1.1.1 Turbostratic structure

Carbonaceous materials like graphite, soot, chars, coke and coals have characteristic structural properties which differ from mostly amorphous to completely ordered graphitic crystalline structure. The degree of order in these structures clearly depends on the thermal treatment of the material as well as the type of precursor of the carbonaceous material. The structures can be characterized by various parameters such as interlayer spacing d, the stacking height L_c and the lateral size of the crystallites L_a, Figure 2.3.

Currently used X-ray diffraction techniques for the measurement of graphene sheet size and turbostratic crystallite thickness were developed by Warren [4,5] in 1941 and others [6-10]. In the most widely accepted model of the structure of "turbostratic" carbon, the atoms are arranged in layers but stacked randomly instead of the order ABABA... sequence of graphite and interlayer spacings also occur randomly. It is generally accepted [11] that the development of turbostratic structures of carbon takes place above 1200°C. Information about these parameters is significant to comprehend the processes like pyrolysis, gasification, graphitization etc.

The second decisive contribution in the field was made in 1951 by R. Franklin [12,13]. It was described that the thermal evolution of various precursors by means of the turbostratic model. It was recognized that the existence of graphitizable and non-graphitizable carbons as well as intermediate (partially graphitized carbons): Certain graphitic carbons, when heated to sufficiently high temperatures, show a gradual change from the random layer structure (turbostratic structure), to the ordered structure of crystalline graphite [13].

2.1.1.1.1.2 Measurement of L_a, L_c and d_{002}

Determination of the coherent lengths, L_c and L_a is one of the major concern as well as the interlayer spacing (d_{002}). Quantitative data can be obtained with a regular diffractometer. Several authors have published values of L_a and L_c based on the inverse peak widths with the aim to describe a "so-called" crystallite. In fact, line-broadening also arises from strain, defects of the lattice and from the finite domain size and their distribution. An apparent coherent length L, can be estimated from the amount of broadening, β using the Scherrer equation:

$$L = \frac{K\lambda}{\beta \cos\theta} \tag{2.1}$$

Where L is the coherence length, λ is the wavelength (154.18 pm for CuK$_\sigma$), β the width at the half peak-height, θ, the Bragg angle of the line, and K is the Scherrer parameter.

The measurement of the peak-width, β_{002}, from the *002* or *001* reflection, is used to measure the stack size, L_c. In this case, the Scherrer parameter is usually taken as $K = 0.9$. The 10 and 11 bands observed for turbostratic structures or the Debye-Scherrer rings observed for graphite powders have no preferred orientation and thus, the Scherrer equation applies directly with $K = 1.84$ [5]. The values usually quoted this way are only rough approximations of L_a and L_c.

The d_{002} spacing can be obtained with any modern X-ray diffractometer by measuring the 2θ angle at the maximum of the *002* peak (from $25° > 2\theta < 26.6°$ for Cu anti-cathode). The 2θ value at the maximum of the smoothed peak is used to calculate the mean d_{002}-spacing of the sample by means of the Bragg equation:

$$2d_{hkl}\sin(\theta_{hkl}) = n\lambda \qquad\qquad (2.2)$$

Where $2\theta_{hkl}$ is the scattering angle and d_{hkl} is the spacing *hkl* planes.

Oberlin [14] demonstrated that the 700-1500°C range is the most significant for the production of activated carbons of large surface areas. In this stage basic structural units are claimed to associate and the number of layers reaches to 8-10. Schematic representation of graphitic layers was shown in Figure 2.4. Sakintuna et al. [2] found that the lateral size of the crystallites, L_a, increases very faintly from 5.0 nm to 5.5 nm when the pyrolysis temperature of activated carbons was increased from 700°C to 1000°C. The lateral size of the crystallites of the chars is not change significantly within the pyrolysis temperature range studied but the stacking height and in relation with this the number of graphene sheets per stack increased about 60 percent within the same temperature range. The values of L_c for activated carbons stayed almost constant within 1.0-1.5 nm [2].

Kercher and Nagle [15] reported that with increased pyrolysis temperature, the crystallite boundary area decreased from turbostratic crystallite growth and number of graphene sheets increased. The reason for the increase in the stacking height could be related to heat treatment temperature only. Fujimoto and Shiraishi [16], observed that above 1000°C continuing growth of the carbon layer plane might be due to the increase of van der Waals forces between the layers which resulted in an increases of the stacking number, hence the coalescence of the units was probably accelerated also in temperatures between 700-1000°C, as it was also observed in the present work. Feng et al. [17] stated that L_a and L_c could be seen to increase slightly through the heat treatment at 1150°C for heating times up to 700 minutes, while the interlayer spacing d_{002} was essentially unchanged during heat treatment. It is also suggested that the impurities in the raw coal char enhanced the structural ordering during heat treatment [17].

The d_{002} results reported by Sakintuna et al. [2] seemed to change in the range of 0.35-0.39 nm. Similar values of d_{002} were also reported [18]. d_{002} values measured by Sharma et al. [18], for carbons produced at 1000°C and 1400°C were 0.38 nm and 0.37 nm, respectively. In particular, a carbon that is thermally treated at temperatures below 1800°C is generally very disordered; it contains turbostratic (fully disordered) structures. The reasons for this disorder are the presence of local stacking faults, random shifts between adjacent layers; variable interspacing values, unorganized carbons that are not a part of layer structure and strain in the layers [19]. The d_{002} values are typical of the turbostratic structure of carbon and it is also interesting to note that in a recent report [20] while the

development of turbostratic structures in untreated cellulose took place above 1200°C in the previous study [2] using a lignite as a carbon precursor, turbostratic structures started to appear at a much lower temperature range of 700-1000°C.
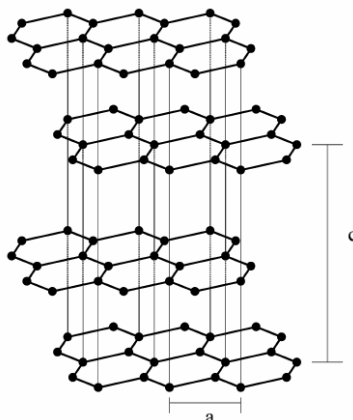
Figure 2.3. Schematic representation of graphite [21].

Figure 2.4. Schematic representation of graphite sheets [11].

2.1.1.2 Porosity in Carbons and Zeolites

Within the family of carbon materials, there exist the activated or porous carbons. Such carbons contain an extensive internal network of porosity. This network of porosity, in which the surfaces of the porosity are close to each other, confers on the carbons the properties of adsorption. That is, the carbons can take into themselves considerable quantities of small molecules, the adsorbate, and retain such small molecules, quite strongly within the porosity.

Porosity in solids should never be considered as a series of interconnected "drill-holes". In fact, porosity is simply where the solid adsorbent is not present. In this sense, the shapes and sizes of porosity are a direct function of the structure of the internal solid

surfaces. Porosity can be considered as a three-dimensional interconnected structure of spaces, different sizes and shapes.

The porosity of activated carbon and porous carbons is the all important controlling their applications. At the same time, it is one of the most elusive properties of carbons to visualize. Further, this visualization is all encompassing when it comes to understanding the phenomena or physical adsorption of gases and vapors by activated or porous carbons.

The zeolites, also microporous materials, are somewhat easier to understand in that they are crystalline solids, and as a result the porosity can be said to be also "crystalline", being regular and predictable in position. The crystalline nature of the porosity the shape and size of which is totally controlled by the mode of bonding of the silicon, aluminium and oxygen which constitute zeolites.

In one sense, porosity has no existence, it is space where the aluminosilicate material is absent within the material. But this space is different from space outside of the material. This difference is associated with the overlapping dispersive forces which emanate from the silicon, aluminium and oxygen atoms of the zeolite which trap or concentrate any atom or molecule which penetrates into such porosity. The strength of such trapping forces, i.e. adsorption potential is a function of the shape/size of porosity with the zeolites, in turn being a function of structure of the zeolite. The same argument applies to carbons. In order to best understand porosity in carbons, structure in carbons has to be understood as well as possible.

2.1.2 Zeolites

The zeolites are a group of compounds, some of which occur naturally which are named after their ability to evolve water when heated. The name "zeolites" comes from the Greek zeo to boil and lith stone. These materials form an extensive group. Both natural and synthetic zeolites are used for ion exchange, absorption and catalytic purposes.

Zeolites are compounds with low molar masses. Their structure consists of frame works that form cavities/channels, which may incorporate a range of small inorganic and organic species. The frameworks are constructed from linked tetrahedral. Many elements which form TO_4 groups, which T is a tetrahedral atom, can be the building block in zeolites. The most common groups are AlO_4, SiO_4, BO_4 and PO_4, but T can also be beryllium, gallium, germanium, etc. The majority of the materials are solely based on

silicon and aluminium. Materials containing elements other than aluminium and silicon are correctly termed zeotypes, reflecting the similar structure. The vast 3-dimensional networks are a result of all four corners for the tetrahedra being shared, producing low density microporous materials.

The general formula for zeolites may be obtained by starting from pure silica, in which all the tetrahedral are vertex linked. Replacement of some of the SiO_4 tetrahedra with AlO_4 tetrahedra upsets the charge balance, so counteractions have to be inserted inside the framework to maintain charge neutrality.

By dehydrating the zeolite, the cations are forced closer to the framework in order to achieve better coordination to the framework oxygen atoms. This means that dehydrate zeolites can often absorb small molecules other than water in their pores. Obviously, the larger the cavities in the zeolite, the larger the molecules it can absorb.

A defining feature of zeolites is that their frameworks are made up of 4-connected networks of atoms. One way of thinking about this is in terms of tetrahedra, with a silicon atom in the middle and oxygen atoms at the corners. These tetrahedra can then link together by their corners (Figure 2.5) to from a rich variety of beautiful structures. The framework structure may contain linked cages, cavities or channels, which are of the right size to allow small molecules to enter - i.e. the limiting pore sizes are roughly between 3 and 10 Å in diameter. In all, over 130 different framework structures are now known. In addition to having silicon or aluminium as the tetrahedral atom, other compositions have also been synthesised, including the growing category of microporous aluminophosphates, known as ALPOs. Zeolites are designated by three capital letters, following IUPAC rules. These codes are not dependant upon atomic composition, cell dimensions or geometry. They are derived from the names of the types of the materials.
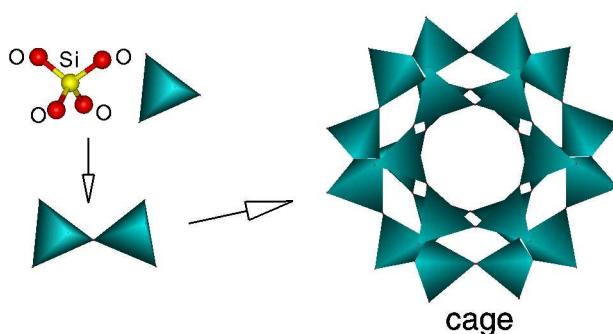
Figure 2.5. Schematic representation of tetrahedra found in zeolites.

2.1.2.1 Application of Zeolites

2.1.2.1.1 Catalysis

Zeolites have the ability to act as catalysts for chemical reactions which take place within the internal cavities. An important class of reactions is that catalysed by hydrogen-exchanged zeolites, whose framework-bound protons give rise to very high acidity. This is exploited in many organic reactions, including crude oil cracking, isomerisation and fuel synthesis. Zeolites can also serve as oxidation or reduction catalysts, often after metals have been introduced into the framework. Examples are the use of titanium ZSM-5 in the production of caprolactam, and copper zeolites in NO_x decomposition. Underpinning all these types of reaction is the unique microporous nature of zeolites, where the shape and size of a particular pore system exerts a steric influence on the reaction, controlling the access of reactants and products. Thus zeolites are often said to act as shape-selective catalysts. Increasingly, attention has focused on fine-tuning the properties of zeolite catalysts in order to carry out very specific syntheses of high-value chemicals, e.g. pharmaceuticals and cosmetics.

2.1.2.1.2 Adsorption and Separation

The shape-selective properties of zeolites are also the basis for their use in molecular adsorption. The ability preferentially to adsorb certain molecules, while excluding others, has opened up a wide range of molecular sieving applications. Sometimes it is simply a matter of the size and shape of pores controlling access into the zeolite. In other cases different types of molecule enter the zeolite, but some diffuse through the channels more quickly, leaving others stuck behind, as in the purification of *para*-xylene by silicalite (Figure 2.6).
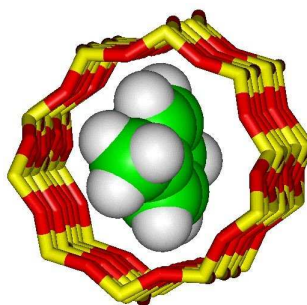
Figure 2.6. The shape of para-xylene means that it can diffuse freely in the channels of silicalite.

Cation containing zeolites are extensively used as desiccants due to their high affinity for water, and also find application in gas separation, where molecules are differentiated on the basis of their electrostatic interactions with the metal ions. Conversely, hydrophobic silica zeolites preferentially absorb organic solvents. Zeolites can thus separate molecules based on differences of size, shape and polarity.

2.1.2.1.3 Ion Exchange

The loosely-bound nature of extra-framework metal ions (such as in zeolite NaA, Figure 2.7) means that they are often readily exchanged for other types of metal when in aqueous solution. This is exploited in a major way in water softening, where alkali metals such as sodium or potassium prefer to exchange out of the zeolite, being replaced by the "hard" calcium and magnesium ions from the water. Many commercial washing powders thus contain substantial amounts of zeolite. Commercial waste water containing heavy metals, and nuclear effluents containing radioactive isotopes can also be cleaned up using such zeolites.
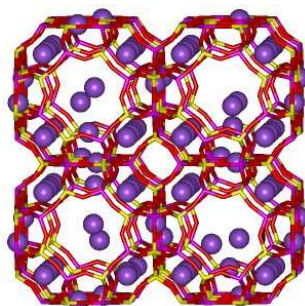
Figure 2.7. Sodium Zeolite A, used as a water softener in detergent powder.

Millions of years ago, zeolite deposits formed when volcanoes were erupted enormous amounts of ash–aluminosilicates of alkaline and alkaline earths. Some of the wind borne ash settled to form thick ash beds. In some cases the ash fell into lakes and in others, water percolated through the ash beds. In all cases, the chemical reaction of volcanic ash and salt water resulted in the formation of natural zeolites. Small natural differences such as temperature, geographic location and ash/water properties impart a different composition. Each natural zeolite property has distinctly unique properties. Over 40 natural zeolite structures (Clinoptilolite; Si/Al: 5/1, chabazite; Si/Al: 2/1, phillipsite, mordenite, etc.).

2.1.2.2 Clinoptilolite

Clinoptilolite, (Figure 2.8) with the simplified formula $(Na,K)_6Si_{30}Al_6O_{72}\cdot nH_2O$ is the most common natural zeolite found mainly in sedimentary rocks of volcanic origin. Such deposits aroused strong commercial interest because clinoptilolite tuffs are often rather pure and can be mined with simple techniques [22].

Characteristic clinoptilolite rocks consist of 60-90% clinoptilolite with the remaining being mainly feldspars, clays, glass, and quartz. In North America and Europe a large portion of the production goes into the area of animal hygiene including cat litter and other animal bedding products. The rest is divided among applications in animal feed, fertilizer, environmental absorption, and building materials.
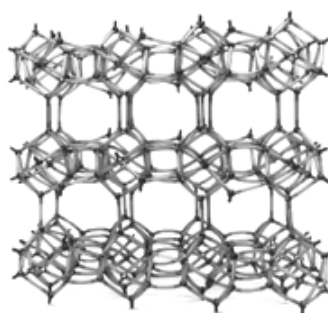
Figure 2.8. Clinoptilolite with its 8- and 10-member channels. (International Zeolite Association).

2.1.2.2.1 Mineralogical Nomenclature

Zeolite minerals species shall not be distinguished solely on the basis of the framework Si/Al ratio. Clinoptilolite is defined as the series with the heulandite framework topology and Si/Al $\geq$ 4.0.

Individual species in a zeolite mineral series with varying extraframework cations are named by attaching to the series name a suffix indicating the chemical symbol for the extraframework element that is most abundant in atomic properties, e.g. heulandite-Ca, heulandite-Na, clinoptilolite-K, clinoptilolite-Ca etc. [23].

2.1.2.2.2 Crystal Structure

The structural topology of the tetrahedral heulandite (HEU) framework [24] is well understood and possesses *C*2/*m* space group symmetry with oblate channels confined by ten-membered (7.5 × 3.1 Å) and eight-membered tetrahedral rings (4.6 × 3.6 Å) parallel to the *c*-axis. Additional eight-membered ring channels (4.7 × 2.8 Å) running parallel to [100] and [102] cross-link the former channels within (010), giving rise to a two-dimensional channel system parallel to (010) responsible for a layer-like structure (Figure 2.9).
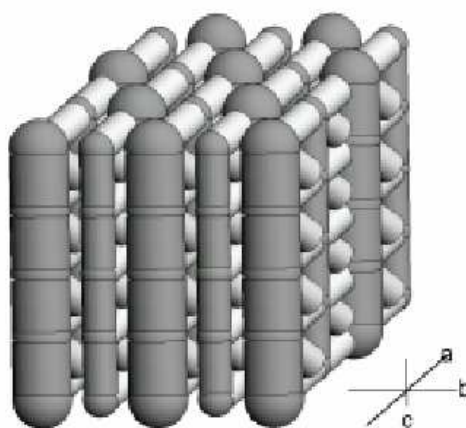
Figure 2.9. The model of the two-dimensional channel arrangement parallel to (010) in HEU frameworks. The dark gray columns parallel to [001] represent eight- and ten-membered ring channels. These channels are cross-linked by the light gray eight-membered ring channels running parallel to [100] and [102].

2.2   Templated Porous Carbons

2.2.1   Introduction

Sakintuna and Yürüm [25] reviewed templated porous carbons previously. In this review, they summarize recent reports on the synthesis of porous carbons using different kinds of templates. Syntheses of porous carbons were categorized by their different kinds of templates. After mentioning the earlier studies about the templating process, different types of inorganic templates such as ordered mesoporous molecular sieves, some silica sources, zeolites, clays and sol-gel processes that were used for the synthesis of porous carbons were discussed.

In recent years, there has been growing interest in new applications of porous carbons because of their ability to interact with molecules not only at their surfaces but also in the

bulk of the material. The synthesis of new porous materials is interesting for both practical and fundamental reasons. The size distribution and topology of pores in materials of similar compositions can be very different, depending on the method of synthesis. The types of pores are defined by IUPAC as micropore, pore with width not exceeding about 2.0 nm (20 Å), mesopore, pore with width between 2.0 nm (20 Å) and 50 nm (500 Å), and macropore, pore with width exceeding about 50 nm (500 Å) [26,27].

Porous carbons are widely used as industrial adsorbents because of the hydrophobic nature of their surfaces, high surface area, large pore volumes, chemical inertness, good mechanical stability and good thermal stability. Application areas are wide including gas separation, water purification, catalyst support, chromatography columns, storage of natural gas, and use as electrodes of an electric double-layer capacitor [28-30]. Recently, Davis [31] reviewed applications of porous materials. The presence of micropore is essential for the adsorption of small gas molecules on activated carbons. However, when the adsorbates are polymers, dyes, or vitamins, only mesopores allow the adsorption of such giant molecules. The importance of mesopores has been pointed out not only for giant molecule adsorption but also for new applications such as electric double-layer capacitors. The presence of wider pores would be advantageous in these cases [32-35] and also nanostructured carbon materials are potentially of great technological interest for the development of catalytic [36-38], electronic [29,39], fuel cells [40] and hydrogen-storage systems [41]. Recently Lee et al. [42] reviewed the synthesis of nanoporous carbon materials using nanostuctured silica materials as inorganic templates.

2.2.2   Preliminary Work

Porous carbons are usually obtained via carbonization of precursors of natural or synthetic origin, followed by activation. To meet the requirements, a novel approach, the template carbonization method, has been proposed. Many researchers have prepared novel porous carbons with this technique using a wide variety of inorganic porous templates. The templated synthesis of ordered mesoporous carbons is a remarkable achievement in the field of porous materials. The resulting high surface area materials with uniform pores poses to be suitable as adsorbents, catalyst supports, and materials for advanced electronics applications [43,44].

Replication, the process of filling the external and / or internal pores of a solid with a different material, physically or chemically separating the resulting material from the template, is a technique that is widely used in microporosity and printing. This method has been used to prepare nanotubules and fibrils of replica polymers [45,46], metals [47], semiconductors [48], carbons, and other materials [49] on the length scale of nanometers to microns. Some nanomaterials have been prepared using different nanoporous host matrixes. Q-state semiconductors are produced within the interlamellar region of a layered compound including layered materials [50] and semiconductors in the spherical cavities found in zeolite Y [51]. C cadmium telluride nanoclusters are synthesized by vapor-phase deposition of elemental tellurium in Na-zeolite A used a template [52]. The other example is the production of glass / conducting polymer nanocomposites prepared in the pores of porous Vycor glass[53].

Surfactants are also used to template the synthesis of porous silicates [54], sulfates [55] and layered organic-inorganic composites [56,57]. Liquid crystals are employed for the synthesis of mesoporous silicates or aluminoslicates [58,59], sulfide and selenide superlattices [60], as template. Layered double hydroxides and other layered structures [61,62] have been previously used as a pattern. Multiwalled carbon nanotubes are produced by catalytically pyrolyzing acetylene within the pores of an anodic aluminium oxide template [63].

Generally there are five steps in the production of a templated porous carbon, (i) synthesis of the inorganic template; (ii) impregnation of the template with an organic template (such as furfuryl alcohol, phenol-formaldehyde or acrylonitrile); (iii) polymerization of the precursor; (iv) carbonization of the organic material; (v) leaching of the inorganic template. Where commercially available templates are used, stage (i) is omitted. A variety of different methods are employed on each step, for example, leaching with HF, HCl or NaOH, impregnation from liquid and gas phase and carbonization at different temperatures.

Knox et al.[64] and Gilbert et al. [65] synthesize rigid mesoporous and some microporous carbon, with Brunauer-Emmett-Teller (BET) [66] surface area of 500 m^2/g, by carbonization of polymerized precursors in the silica gel. The resultant carbon is mesoporous, and it is now commercially available as a column packing material for liquid chromatography.

Different inorganic templates have been used to synthesize a wide variety of carbon materials. Alumina has been used as a template to produce carbon nanotubes [67] and nanofibers [68]. As well aluminium oxide was used as a model for carbon nanotubes [63,69]. Liu et al. [70] synthesized amorphous carbon nanotubes by using silver nanowires as templates. Carbon nanotubes and submicron-tubes that are comprised only of uniform hollow tubes with open ends are prepared in one dimensional channels using an anodic oxide film as a template. The infiltration of Poly (furfuryl alcohol) into the channels of the film and propylene followed by heat treatment led to the formation of bamboo like and uniform hollow tubes with open ends, carbon tubes. The outer diameter of carbons are 30-230 nm and 60-75 μm in length and reflect the channel diameter and the thickness of the template used, (Figure 2.10) [71]. Since the size of the channels in an anodic oxide film can easily be controlled, it is possible to control the diameter of the carbon tubes from ten to hundreds of nanometers and by changing the carbon deposition period, the wall thickness of the carbon tubes is controllable [72].

Poly(furfuryl alcohol), PFA, is a common thermosetting resin that forms carbon with a high yield on carbonization [73-75] that generally is used as an organic precursor for the production of templated carbons. PFA can be synthesized by a polycondensation reaction of furfuryl alcohol with various cationically active initiators, for example, silica, HCl, or Lewis acids [76]. The properties of pyrolized PFA have been previously investigated [77].
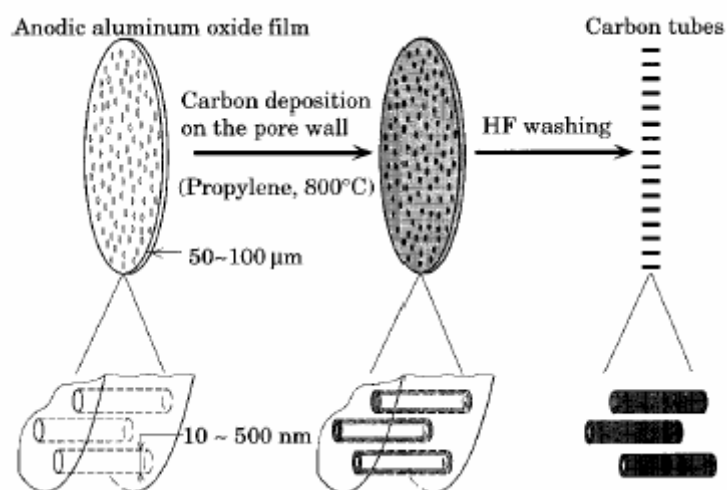
Figure 2.10. Schematic drawing of the formation process of carbon tubes [71].

2.2.3 Mesoporous Silica Materials as a Template

Ordered mesoporous carbon materials have been synthesized using mesostuctured silica templates, and the most important physicochemical properties of these materials have been described by various research groups [28,78-80].

Since the development of M41S [59] materials by Mobil Oil researchers in 1992, many different mesoporous inorganic materials have been prepared using various types of organic templates. Porous silica materials exhibiting structural periodicity are synthesized typically using organic amines, surfactants, block copolymers or polymer beads as a template.

The highly ordered mesoporous carbons have scientific and technological importance as a new shape-selective catalyst, adsorbent, sensor and electrode material. Ryoo et al. [81], have reported the synthesis of ordered carbon molecular sieves, CMK-1, by carbonization of sucrose inside the mesopores of the silica molecular sieve, MCM-48 [82] which has been characterized by Kruk et al. [83], using sulfuric acid as a catalyst. Sucrose is converted to carbon by carbonization under vacuum or in an inert atmosphere at 1073–1373 K. The silica template is removed using an aqueous solution of sodium hydroxide. Synthesized carbon molecular sieves have a uniform pore distribution (Figure 2.11).

The XRD pattern of carbon material showed no Bragg lines in the region 2θ greater than 10°, indicating that the carbon framework is atomically disordered. The changes in the peaks before and after the framework removal, and the appearance of the new peak (*110*), indicated that the structure of resultant carbon underwent a systematic transformation to a new ordered structure (Figure 2.12). The structure of synthesized carbon has micropores 0.5-0.8 nm diameter and 3.0 nm mesopores and has a 1380 m^2/g BET surface areas. The authors [84] suggest that the micropores are formed in the amorphous carbon framework prior to the removal of template, while the mesopores are formed upon the removal of the silica wall. Characterization of this carbon is reported by the same group [85]. They demonstrated that the unit-cell size of this carbon material can be tailored by choosing the MCM-48 type template of an appropriate unit-cell dimension, which is synthesized as described elsewhere [86-88]. CMK-1 carbon networks equally formed in two noninterconnecting channels of MCM-48 are displaced during the dissolution. The mesostructured carbon material CMK-1 is described as the ordered interwoven assembly

of two enantiomeric subframeworks reproducing the shape of the MCM-48 mesopores [89]. Joo et al. [90] investigate the effect of the sucrose-sulfuric acid ratio, pyrolysis temperature and the amount of sucrose. They showed that the synthesis method can be controlled to obtain highly ordered mesoporous carbon.
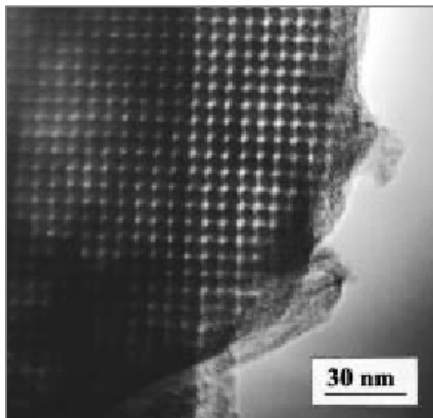
Figure 2.11. Transmission electron micrograph of the ordered carbon molecular sieve CMK-1, obtained by the template synthesis with the mesoporous silica molecular sieve MCM-48 [81].

Whereas their previous work using sucrose as a carbon source resulted in the formation of rod-type carbons under nitrogen [81,91], the polymerization of furfuryl alcohol by the designed catalytic function of the aluminosilicate frameworks leads to the formation of these pipe-like carbons under vacuum [92]. The synthesis of rodlike or rod-like mesoporous carbons does not depend on the carbon precursor but on the synthesis conditions used during carbonization. The carbon prepared using furfuryl alcohol instead of sucrose exhibited good structural ordering. The carbon prepared using MCM-41 [59] as a template collapses upon the template removal to yield a high-surface-area disordered microporous structure [43,84]. The detailed synthesis and characterization of MCM-41 is reported [93-97]. MCM-41 silica with a hexagonally ordered structure of approximately cylindrical one-dimensional pores, is found unsuitable as a template for ordered mesoporous carbon synthesis, and indeed its application yielded disordered high surface area microporous carbon [43,84]. The MCM-41 templated carbon had a featureless XRD spectrum (Figure 2.13a). The Al-MCM-41/carbon composite material still remains the hexagonal structure, but with much lower diffraction intensity because of the pore filling while the resultant carbon material after HF etching shows no Bragg angle in the small-angle region, confirming the absence of regular mesopores [43].
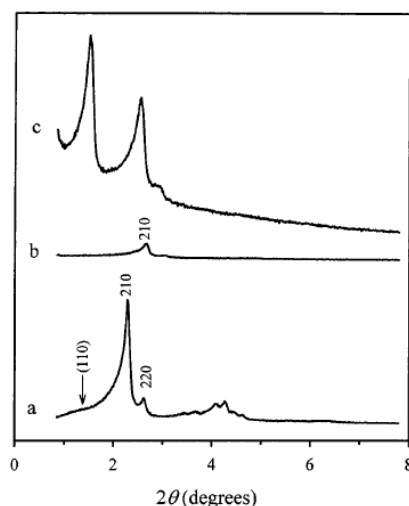
Figure 2.12. XRD patterns during synthesis of the carbon CMK-1 with its silica template MCM-48: (a) The mesoporous silica molecular sieve MCM-48, (b) MCM-48 after completing carbonization within pores, and (c) CMK-1 obtained by removing silica wall after carbonization [81].

After the first reported synthesis of a new type of mesoscopically ordered nanoporous carbon molecular sieve by using MCM-48 as a template, Lee et al. [98,99] synthesized an ordered nanoporous carbon material (CMK-3) using the ordered mesoporous silica molecular sieve SBA-15 [100] instead of MCM-48. SBA-15 has connected micropores and small mesopores in the walls of large-pore channels [91]. The SBA-15 silica is constructed with a hexagonal array of nanotubes with uniform diameter. This synthesis is the first example of an ordered mesoporous carbon molecular sieve retaining the structural symmetry for a silica template. Unlike the first example in which MCM-48 is used, this carbon is exactly an inverse replica. The carbon source is sucrose and the carbonization catalyst is the sulfuric acid. The carbon nanorods are 7 nm in diameter; the centers of the rods are 10 nm apart. The BET areas are 1520 m^2/g. and the total pore volume is 1.3 cm^3/g. The hexagonal structural order is retained in the carbon. The ordered arrangement of the carbon nanorods in CMK-3 gives rise to the XRD peaks (Figure 2.14). The main mesoporous channels in SBA-15 are interconnected through micropores inside the walls of the main channels, while the MCM-41 channels are not interconnected. In the case of MCM-41 silica, carbon infiltration leads to the formation of carbon rods that are not bonded to each other [91]. From the fact that the SBA-15 pore wall is thicker than that of MCM-48, the CMK-3 pore size is larger than that of CMK-1 [28].
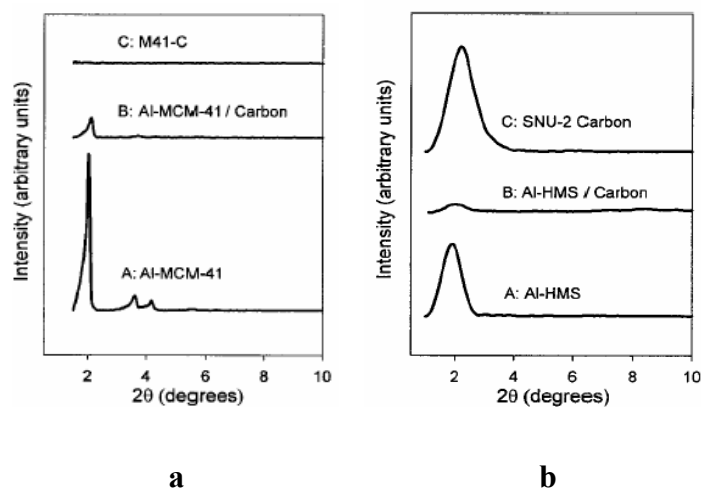
Figure 2.13. (a). A: XRD patterns of Al-MCM-41 template, B: Al-MCM-41/carbon composite, and C: replica carbon M41-C (b) XRD patterns of A: Al-HMS template, B: Al-HMS/carbon composite, and C: mesoporous SNU-2 carbon [43,44,101].

Shin et al. [102] synthesized two-dimensional hexagonally ordered CMK-3 carbons using SBA-15 templates calcined at a temperature of 1153 K to confirm not only that the typical SBA-15 silica has interconnected porous structure, but also the connecting pores are exceptionally persistent and are not eliminated even after calcination at 1153 K, although there is evidence that they are largely eliminated at somewhat higher temperatures. Whereas a disordered carbon is obtained using SBA-15 calcined at 1243 K, demonstrates that the pores connecting ordered mesopores in SBA-15 silica persist up to 1153 K, they are eliminated at temperatures close to 1243 K. The chemistry of the external surfaces of two carbons that synthesized from MCM-48 and SBA-15, is studied by X-ray photoelectron spectroscopy (XPS) and static secondary ion mass spectroscopy (SIMS) [103]. The outer surface of these ordered mesoporous carbons has polyaromatic character similar to that of carbon blacks or carbon fibers. Higher temperatures during pyrolysis or post-pyrolysis heat treatment increase the polyaromatic character. The structure of the silicate matrix has no influence on the polyaromatic character of the surface.
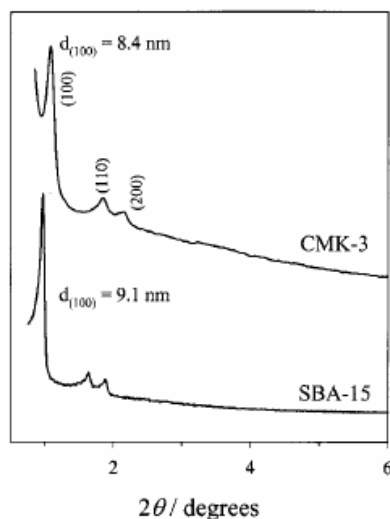
Figure 2.14. XRD patterns of CMK-3 carbon and SBA-15 silica used as template for the CMK-3 synthesis [91].

SBA-15 aluminosilicates with different Si/Al ratios ranging from 5 to 80 are used to synthesize ordered mesoporous carbon with a 2000 m^2/g BET surface area by using furfuryl alcohol [104]. During dissolution of the silicate matrix in HF, organic fluorine compounds are formed on the surface. A maximum surface fluorine concentration of 0.8 atom % is observed. Dissolution of the silica matrix in sodium hydroxide yields a less contaminated ordered mesoporous carbon as compared to that from dissolution in HF [104]. Sakintuna et al. [21] observed fluorine attachment on the carbon surfaces in zeolite templated carbons.

The physicochemical properties of the ordered mesoporous carbon depend significantly on Si/Al ratios. During carbonization, the acid sites of the matrix also catalyze reactions, which increase the order of the graphene layers. The increasing order of the graphene layers is accompanied by shrinkage of the nanopipes, which decreases the width of the pores inside the nanopipes and increases the width of the pores between the nanopipes.

Joo et al. [105] synthesized two-dimensional ordered mesoporous silicas with two different silica sources, TEOS and sodium silicate, and a poly(ethylene oxide)-poly(propylene oxide)-poly(ethylene oxide) triblock copolymer template. In all cases, the 2-D hexagonally ordered mesoporous carbons of CMK-3 type are obtained. This facilitates a prospective large-scale production of ordered mesoporous carbons, because both silica templates and carbon frameworks can be synthesized using cheap reagents.

22

Detailed investigation was done by Soloyov et al. [106] for the hexagonally packed mesostructured carbon material, CMK-3. Electron density distribution map agrees with carbon bridges, which seem to be attributed to the material interconnecting carbon nanorods in the CMK-3 mesostructure.

The combination of platinum and carbon in the SBA-15 structure readily results in the formation of two dimensional hexagonally ordered platinum [107] and carbon [91,92] nanostructures that retain the two-dimensional hexagonal order upon the SBA-15 template removal.

A mesoporous carbon (SNU-2) using the hexagonal mesoporous silica (HMS) aluminosilicate as a template by polymerization of formaldehyde and phenol inside the Al-HMS pores is synthesized [43]. A strong peak at 2θ =2.18 from the ordering of mesopores observed in the XRD pattern of the resultant carbon, demonstrating that the mesoporous structure is preserved even after the removal of the aluminosilicate framework by HF etching and also HMS has 3D interconnected pores, unlike the originally proposed tubular hexagonal pores, similar to those of MCM-41 (Figure 2.13b). The gas adsorption studies present the formation of regular mesopores from the 3D interconnected porous nature of HMS, and the surface area of resultant carbon is 1056 m^2/g [43]. The polymerization of phenol and formaldehyde to obtain the phenol resin inside the AlMCM-48, which has a three-dimensional channel structure, is carried out [44]. AlMCM-48 is formed by implanting Al onto MCM-48. A mesoporous carbon with regular three-dimensionally interconnected 2 nm pore arrays is synthesized and the resultant carbon exhibited excellent performance as an electrochemical double layer capacitor.

Mesocellular carbon foams with large cellular pores (20 nm) and disordered uniform pores (4 nm), and with a 716 m^2/g BET surface area, are fabricated using furfuryl alcohol as a carbon source and hydrothermally synthesized MSU-F [108] silica as a template [109].

2.2.4   Silica Sol, Silica Gel and Opals as a Template

Synthesis of templated carbon materials can be achieved with the organic polymer resins and hydrocarbon vapors by various kinds of silica materials other than ordered mesoporous molecular sieves.

Recently, the synthesis of mesoporous carbons was reported using mesophase pitch or polyacrylonitrile as a carbon precursor and silica sol [110] or silica gel [111] as a

template. Linden etal. [112] synthesized carbon containing wormhole-like mesoporous and macroporous materials using poly(ethylene glycol) and alkyltrimethylammonium bromide as a templates and furfuryl alcohol as a carbon precursor.

There are convenient methods for obtaining macroporous carbon nanotubules,vwith diameters greater than 30 nm [113] or arrays [114]. Li et al. [113] reported the production of highly ordered, isolated long carbon nanotubes, which are up to about 50 μm long, by using a method based on chemical vapor deposition catalyzed by iron nanoparticles embedded in mesoporous silica. The nanotubes are approximately perpendicular to the surface of the silica.

Surface templated inverse opals are interesting for such templating processes. Zakhidov et al. [114] produced three-dimensional periodic macroporous carbons by using porous silica opals as a template. Carbon inverse opals are synthesized by infiltrating silica opal plates with a phenolic resin, cutting the opal from the phenolic resin, removing residual surface phenolic, dissolving the SiO_2 from the infiltrated opal with aqueous HF, and pyrolyzing the resulting phenolic inverse opal. They also produce graphitic inverse opals by CVD on opal slabs and diamond inverse opals by plasma-enhanced CVD. The inverse opals are also of particular interest as photonic band-gap materials. A porous carbon that has low crystallinity when compared to that of graphite was produced by pyrolysis of PFA inside the pores of porous Vycor glass [115].

Kamegawa and Yoshida [116] used two replica methods, ester and CVD methods which consist of esterification of silica gel beads with alcohol or phenol, pyrolysis of the esterified silica gel, and dissolution of the silica gel with HF solution, yielding porous carbon beads with specific surface area ranging from 1100 to 2000 m^2/g. CVD method consists of the pyrolysis of benzene vapor on silica gel beads and the dissolution of the silica gel with HF solution, yielding porous carbon whose specific surface area is 640 m^2/g. Strano et al. [117] produced a series of carbons from mixtures of poly(ethylene glycol) and poly(furfuryl alcohol) with 25, 50 and 75% composition by weight. Templating process is dominated by both the molecular size of the template and the rate of expulsion of decomposed template material during the formation of the solid. In addition to PFA, different organic materials such as mesoporous organic aerogel [118] or a polymer blend, phenolic resin and poly(vinylbutyral) [119] are used.

Han et al. [120] synthesized different mesoporous carbon materials from the co-polymerization of cheap silica and carbon precursors, sodium silicate and sucrose, under various sucrose/silica ratios, followed by the carbonization and removal of the silica template. As the relative silica content increases in the sucrose - silica composite, the surface area and pore volume of the resulting mesoporous carbon are increased. Mesoporous carbon, with a surface area of 850 m^2/g, a pore volume of a 1.5 cm^3 /g, and well-interconnected pores of about 3 nm, is obtained. Silica nanoparticles were used as a template for the production of mesoporous carbons by the same research group [121]. Resorcinol and formaldehyde are polymerized in the presence of inorganic silica sol particles to generate composites. Pyrolysis followed by the HF etching of the composites produces porous carbons, which have pores ranging in size from 40 to 80 nm and a BET surface area of 1227 m^2/g [121]. These nanoporous carbons exhibited excellent adsorption capacities for bulky dyes [122]. To obtain a more uniform pore size distribution, isolated silica particles stabilized by surfactant are used as templates [123]. The BET surface area is found to be 1512 m^2/g. The pore size distribution of the carbon material is narrow with an average pore size of 12 nm along with a shoulder around 15 nm. The stabilized silica particles are acting as a true template for the formation of mesopores [123].

Fuertes and Nevskaia [124] used furfuryl alcohol and phenolic resin to produce mesoporous carbons with different pore size distribution. By changing the type of carbon precursor, it is possible to modulate the size of the mesopores derived from the silica framework. The difference between the carbons obtained by furfuryl alcohol and those by phenolic resin is 3 and 2.6 nm pores respectively. A route for tailoring the size of mesopores of templated carbons within a range of 2–10 nm with a spherical morphology by changing the synthesis temperature of the silica template has been developed by Alveraz and Fuertes [125]. The BET surface areas for the carbons obtained are between 1340 and 2000 m^2/g with unimodal or bimodal pore size distributions.

2.2.5 Zeolites and Clays as a Template

Zeolites, due their pore and channel properties, can also be used for the production of the porous carbon materials although the resultant carbons lost their structural order due to pore blockage and limited space within the micropores. Zeolites are highly crystalline aluminosilicates with a uniform pore structure; their channel apertures are in the range of

0.3-1.0 nm [126], depending on the type of zeolite and its preparation history (e.g., calcination, leaching, or various chemical treatments) [127]. Davis and Lobo [128] reviewed the synthesis of the zeolites.

One of the main reasons that the aluminosilicate zeolites have been so widely exploited for commercial applications is that their structures tend to be stable, even in the absence of pore-filling molecules such as solvent molecules and organic cations. Size and shape selectivity of zeolites makes them useful for several important technological processes, including ion exchange, separations, catalysis, and chemical sensing and host-guest chemistry.

Zeolites represent an interesting case for replication processes, because the dimensions of their cages and channels are quite similar to those of organic molecules that constitute the replica. If such a nanospace in a zeolite is packed with carbon and then the carbon is extracted from the zeolite framework, one can expect the formation of a porous carbon whose structure reflects the porosity of the original zeolite template. Owing to the disordered and inhomogeneous nature of the starting materials, the resulting carbon has a wide and poorly controlled distribution of pore sizes, and a carbon will contain a variety of impurities (sulfur, metals, etc.) characteristic of the precursor. Zeolites with three-dimensional pore structures are found to be suitable as templates [127,129], whereas zeolites with one-dimensional structures are not effective [130]. These carbons obtained using zeolite templates with three-dimensional pore structures retained the shapes of zeolite particles, but did not retain their internal periodic structure.

Pyrolizing the polyacrylonitrile, poly(furfuryl alcohol) and propylene gas as carbon sources, in the channels of zeolite Y and subjecting them to acid treatment to remove silica template, the resultant carbons, which have BET surface areas of more than 2000 m^2/g, reflect the similar morphology of the zeolite template [129]. The carbon in the channels did not have any regular stacking structure as carbon usually has, due to the spatial limitation in the zeolite channels. Sakintuna et al. [131] synthesized porous carbons using natural zeolite clinoptilolite. 400 m^2/g BET surface area was obtained. In the case of natural zeolite, such low surface areas were obtained.

The chemical vapor deposition, CVD carbons have higher surface area and larger pore volume than those of the polymer carbons [129]. Its porosity, however, consisted of not only micropores but also a large mount of mesopores. Long-range ordered microporous

carbons are prepared with the structural regularity of zeolite Y. Surface area and micropore volume reach 3600 m^2/g and 1.5 cm^3/g, respectively [132,133]. Cordero et al. [134] synthesized a carbon/zeolite complex by chemical vapor deposition of carbon from a propylene-nitrogen mixture, followed by HF and HCl treatment to leave the carbon. They discuss the oxidation behavior of the carbon extracted from zeolite in relation to its structure [127].

Microporous carbon with three-dimensional nanoarray structure, which has a 3600 m^2/g BET surface area, by using zeolite Y as a template, is synthesized [133]. The two-step method is employed for the filling of carbon into the nanochannels of zeolite Y, the carbon deposition from propylene CVD after the heat treatment of the zeolite-poly(furfuryl alcohol) composite. The carbons show a sharp peak around 6° in XRD, indicating that these carbons have a structural regularity with a periodicity of about 1.4 nm that corresponds to the (*111*) plane of zeolite Y. In addition, a broad peak around 25° is not detected and indicates that the carbon does not have any stacking structure of carbon layers. In ^{13}C NMR spectra one broad peak about at -130 ppm, due to *sp^2*-hybridized carbon in condensed aromatic rings, and two small peaks around 60 and 200 ppm, spinning sidebands from the aromatic band, is observed [133].

By using the simple CVD method, the carbons inherited the structural regularity of the zeolite. The extent of such transferability, however, strongly depends on zeolite type. Carbon filling into the zeolite channels in the two-step method (impregnation with furfuryl alcohol-propylene CVD) which produced the carbon with the highest long-range ordering in the case of zeolite Y does not work for zeolite β, ZSM-5 and mordenite. For obtaining porous carbon with higher regularity, the template zeolite should have a larger channel size (> 0.6–0.7 nm) and at the same time the channel system should be three-dimensional [135].

An ordered microporous carbon which has a BET surface area of 1910 m^2/g, preserves a long-range periodic ordering (*d* = 1.4 nm) and has been prepared by using zeolite Y in the case of CVD [132]. Low-temperature CVD and further heat treatment of the zeolite-carbon composite after CVD are key for the appearance of both good long-range periodicity and very high BET surface area with almost no mesoporosity in the carbons [136].

Poly(acrylonitrile) is carbonized inside the channels of zeolite NaY, Na-mordenite, and silicalite, and then the resultant carbon is liberated by using HF solution. Because of

the spatial limitations in the zeolite channels, the carbons obtained have much lower electronic conductivity than thet of the carbons from bulk polymerized poly(acrylonitrile) [137]. Johnson et al. [130] also used zeolites as a template to prepare microporous polymer and carbon replicas. Phenol-formaldehyde polymers are synthesized and cured within the channel networks of zeolites Y, β and L. The two monomers, phenol and formaldehyde, are transferred in the gas phase and so the filling of the pores by each is easily controlled. After the cross-linking of the polymer, the pyrolysis reaction of the resultant phenolic resin is performed to produce a porous carbon. In the case of zeolite Y and β the microporosity of the template is reflected in the replica polymer. Replication of zeolite β also results in a microporous material with a distribution of pore diameters very similar to that of the zeolite Y replicas. Complete collapse of the replica occurs upon removal of the zeolite L template.

The reaction of methylacetylene gas in acid forms of the molecular sieves mordenite, omega, L, Y, β, ZSM-5, and SAPO$_4$ is studied to produce oriented and isolated conjugated polymer chains. Methylacetylene reacts with the acid sites of zeolites to form reactive, conjugated oligomers. Differences in spatial restraints imposed by the zeolites, such as the open, branched pore structure of Y versus mordenite, omega, and L, did not produce obvious differences in any properties of the included organic compounds [138]. High-surface-area, microporous carbons, with wide microporosity, well-developed mesoporosity and high adsorption capacity pyrolytic carbon materials were prepared by the propylene chemical vapor infiltration of a microporous zeolite Y followed by removal of the zeolitic substrate (Figure 2.15). Their O$_2$-reactivity profiles exhibited a two-stage behavior, with the inflection point between the two stages occurring at different conversion levels depending on the deposition temperature [127].
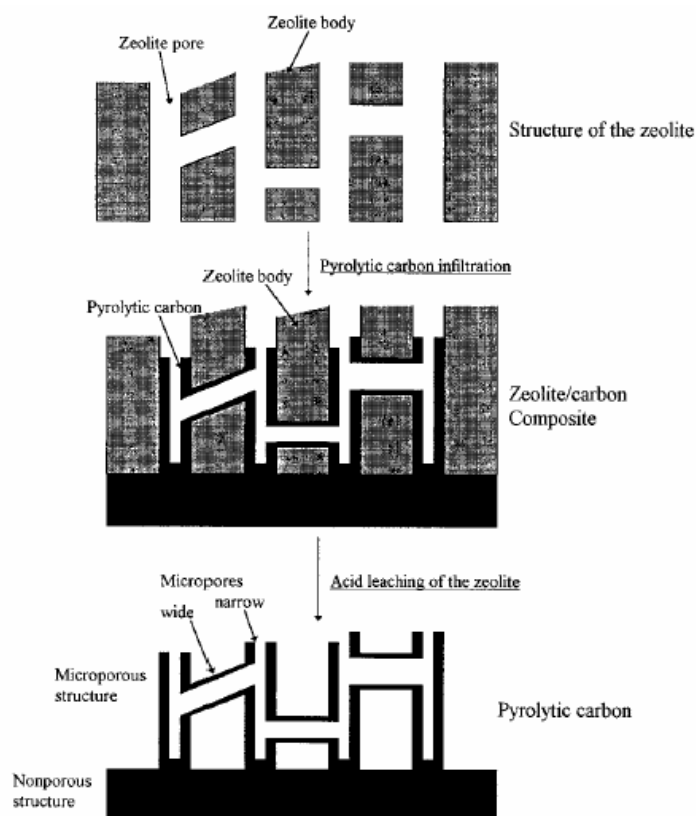
Figure 2.15. Scheme of pyrolytic carbon infiltration of zeolite, followed by removal of the zeolitic substrate [127].

Clays are used as a template to synthesize porous carbons. Some investigators prepare thin graphite films by the carbonization of organic polymers in the two dimensional opening between the lamellae of a layered clay. Sonobe et al. [139] carbonized poly(acrylonitrile) (PAN), poly(furfuryl alcohol) (PFA) and poly(vinyl acetate) (PVAC) [140] using the interlamellar opening of montmorillonite. PFA is carbonized using a two-dimensional opening between the lamellae of taeniolite [141], a sodium form of Wyoming smectite [142,143] and the lithium form of taeniolite, intercalated with hydroxyaluminium and hydroxyaluminium-zirconium cations, with high content of micropores [62]. Bandosz et al. [62] obtained carbons which possess pores no larger in diameter than the interlayer space of the clay. PFA and PVAC carbons prepared between the lamellae of montmorillonite are easily graphitized by further heat treatment; the resultant products are two-dimension like graphite, consisting of highly oriented layer planes which are stacked thin and wide [144].

Sandi et al. [145] used pillared clays, layered silicates whose sheets have been permanently propped open by sets of thermally stable molecular props as a template for five organic precursors, namely pyrene, styrene, pyrene/trioxane copolymer, ethylene, and propylene. The pore radii of resultant carbons range from 4 to 11 Å which are accessible to lithium ions when the intercalation process takes place in a lithium secondary battery.

A flexibility graphite film is prepared from poly(acrylonitrile) by using a Na-taeniolite clay film, which produced crystallized and oriented graphite film [146]. In an other study [147], commercial cationic clay, bentonite, a commercial zeolite, H-β, and a synthetic mesoporous aluminosilicate (Al-MCM-48) as inorganic templates are used, where furfuryl alcohol and complemented in some materials by an additional treatment using propylene carbon vapor deposition was used as a carbon source as described earlier [132,133]. The templated carbon proved to be more ordered than nontemplated carbon. The clay-templated carbon showed little or no ordering at low 2θ angles and had a relatively small surface area (446 m^2/g). However the zeolite and mesoporous aluminosilicate templated carbons had surface areas around 1000 m^2/g, which could be doubled in the zeolite series with the additional propylene carbon vapor deposition step. The carbon produced with additional propylene shows more densely packed crystals than the carbon produced from the furfuryl alcohol impregnation only, which could be an indication of a stronger carbon network left after leaching the template.

Meyers et al. [148] synthesized carbon materials from acrylonitrile with BET surface areas in the ranges between 458-504 m^2/g and 245-636 m^2/g and 333-947 m^2/g from furfuryl alcohol, pyrene and vinyl acetate respectively, by using zeolite (Y, β, and ZSM-5) and montmorillonite clay templates. The generally high surface areas of these carbons might result from the kinetics of dehydroxylation, which are faster than the kinetics of carbonization and which may cause the carbons to separate from the template and develop into small microporous particles.

2.2.6   Sol-Gel Process Used as a Template

It is well-known that a sol-gel process is a useful technique to prepare a nanocomposite of organic and inorganic materials. The sol-gel process, which is mainly based on inorganic polymerization reactions, is a chemical synthesis method to make pure

30

and well-controlled composition organic/inorganic hybrid materials at low temperatures [149,150].

The carbon/silica nanocomposite is obtained by using tetraethoxysilane (TEOS) in the presence of furfuryl alcohol as a carbon precursor and then silica template is removed from the composite by HF treatment [151]. The mesoporous and mesopore structure (pore size and distribution) strongly depend on the sol-gel reaction conditions. The mole ratio of FA/TEOS should be in the range of 1-2. Maximum BET area obtained is 1170 m^2/g. Under optimum sol-gel conditions and at a high gelation temperature (120°C) mesoporous carbon with a very narrow pore size distribution centered at 4 nm is prepared [151]. FA is compatible with TEOS and water. PFA/silica hybrid materials were also synthesized by a cationic polycondensation of FA and a sol-gel process with TEOS for producing nanostructural carbon/silica materials by their thermally induced transformation by Müller et al. [76].

The template carbonization method allows one to control carbon structure in terms of various aspects such as pore structure and microscopic morphology, which makes this method very attractive. Taking into account all studies, the conclusion is that some features of the template are carried out in the replicated carbon at the morphological level. The synthesis conditions and the type of template introduce controllable features into the resulting carbon. The interaction between template and synthesis conditions is subtle and it is hard to generalize about optimum conditions. Where a three-dimensional pore structure is present in the template it is usually possible to achieve a good carbon replica, with long range order reflecting the template and structural replication down to the nanometer level. The synthesis of porous carbon with structural periodicity becomes difficult as the pore diameter of the template decreases. The carbonization in macropores leads to a thick carbon coat that can remain stable and undergo no structural transformations upon removal of the silica template. While efforts have been made to understand and improve the templated synthesis of these latter materials, systematic studies need to be conducted on their controlled synthesis.

2.3   Preparation and Characterization of AlPO$_4$-5 by Microwave Heating

2.3.1   Introduction

Among the porous materials, those which present well defined channels and regular pore systems, as the crystalline zeolites, are adsorbents of great interest. The main characteristics of the zeolites are the molecular dimensions of their pores and the existence of strong acid sites located on their inner surface. As a consequence, they are of great industrial importance in the gas separation and purification processes and in the petroleum catalytic cracking. The zeolites present a rich variety of micropore frameworks. Generally speaking, both their micropore networks, which are composed of cages and/or channels, and their inner surfaces, are complex. The most widely known molecular sieves are the aluminosilicate zeolites [152] and the microporous silica polymorphs [153].

During the last few years considerable attention has been focused on the zeotypic or microporous aluminophosphates (AlPO$_4$). The family of aluminophosphate materials (AlPO$_4$-n), include about 20, three-dimensional framework structures, of which at least 14 are microporous and 6 are two-dimensional layer-type materials [154]. Most of the three-dimensional structures appear to be structurally related to the zeolite family, with framework topologies of the erionite/offretite type (AlPO$_4$-17), the sodalite type (AlPO$_4$-20), and the analcime type (AlPO$_4$-24).

Aluminium phosphate (AlPO-n) molecular sieves have physical/chemical properties similar to the zeolites, and have potentials as adsorbents for separations and purifications of molecular species and as catalysts or catalyst supports [154-156]. In aluminophosphate molecular sieves, it is said to that the silicon atoms in aluminosilicate molecular sieves are replaced by the phosphorus atoms and no extra-framework cations [157]. The molecular sieve aluminium phosphate number 5 (AlPO$_4$-5) (IUPAC code AFI [158]) was the first discovered [154] and the most frequently investigated member of the nanoporous aluminophosphate family. The regular well-defined pores offer a route to preferentially adsorb molecules based upon size or shape and to organize adsorbed molecules into one-dimensional columns.

Numerous studies including synthesis, catalysis, application and modification, etc. on the aluminophosphate type molecular sieves such as AlPO$_4$-n, silicoaluminophosphate (SAPO-n) and metal aluminophosphate (MeAPO-n) [159] have been undertaken. Besides their potential application as catalysts, dye-modified AFI materials have been increasingly

tested as novel materials for optical data storage [160,161] or optical frequency doubling (second harmonic generation, SHG) [162-166].

The aluminosilicate zeolites are characterized by the presence of cations of compensation, which neutralize the negative charge of the framework. Such cations occur in the zeolite micropore framework and act as impurities; they induce an inner surface energetic heterogeneity. As a consequence of its electrically neutral framework, the $AlPO_4$-5 micropore network is free of any cations. The thermal stability of $AlPO_4$-5 molecular sieves is higher than that of aluminosilicate structures [154]. It can be heated at temperatures as high as 1000°C without any amorphization [167].

Interest in the AFI-type materials arises from their microporous architecture, which is composed exclusively of one-dimensional linear 12-ring channels characterized by polar micropore walls. That microporous material can be considered as a host material is particularly interesting for the confinement of a large number of quasi one-dimensional solids, ranging from the van der Waals elements to the metallic ones, which presents only one type of sorption sites used as containers for nano-materials. The guest materials can be isolated and stabilized one dimensionally in their channels. These properties indicate that aluminophosphates can be used for the preparation of porous carbons.

Therefore, the synthetic condition of large AFI crystals with high quality has been widely investigated. Large $AlPO_4$-5 crystals with good optical quality were synthesized from HF-containing mixtures [168] or diluted solutions with high water conten t[156,169]. The loading of some organic materials, such as para-xylene and para-nitroaniline [170], into pores has been attempted after the synthesis.

Hydrothermal synthesis of $AlPO_4$-5 molecular sieves in conventional ovens is typically performed from aluminophosphate gels containing organic templates at 150-200 °C and times ranging from several hours to several days. The influence of the concentration of organic template and the crystallization temperature on the $AlPO_4$-5 molecular sieve formation was reported [164,171-173]. In this study, $AlPO_4$-5 crystals were synthesized by using a microwave oven.

2.3.2 Structure of AlPO$_4$-5

AlPO$_4$-5 has a hexagonal symmetry, and contains one-dimensional channels bounded by 12-membered rings with alternate composition of AlO$_4$ and PO$_4$ tetrahedrons [154]. The AlPO$_4$-5 framework can be constructed by connecting T12 rings, with T = Al or P in strict alternation. 12-Rings are connected through O-bridges into sheets parallel to c, shown in Figure 2.16a. Sheets are connected through O-bridges along c-axis, shown in Figure 2.16b. In this way, cylinders are formed consisting of fused 6-rings, as shown in Figure 2.17. The three-dimensional hexagonal AFI structure can also be described as a hexagonal close packing of these cylinders.

AlPO$_4$-5 can be built using the crankshaft chain shown in Figure 2.18a, running along c-axis. The repeat unit of the chain consists of 4 T atoms. Six of these chains are connected around a 6-fold axis to form the Periodic Building Unit (PBU), shown in Figure 2.18b. The PBU is a cylinder with a T12-ring pore. The cylinder wall consists of fused T6-rings. The repeat unit of the PBU is a cylindric T6-ring band of 24T atoms. Neighbouring PBU's are connected around a 3-fold axis through T4-rings as shown in Figure 2.16. Crankshaft chains are formed.
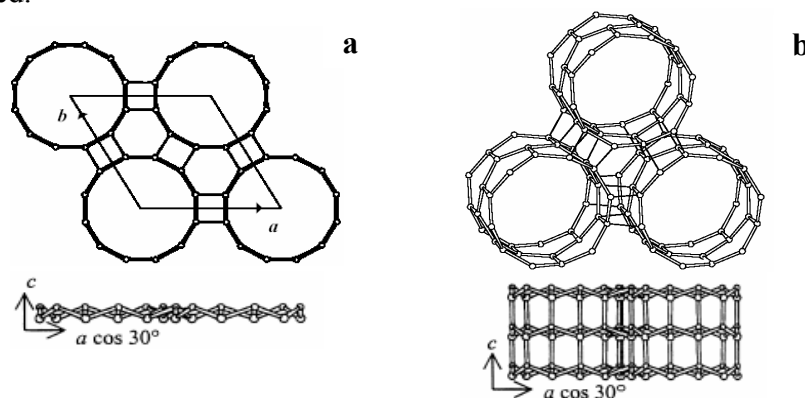
Figure 2.16. a. Connection mode and unit cell content in AFI seen along c in perspective view and **b.** in parallel projection. For clarity, only 1½ repeat units of the PBU's are drawn.
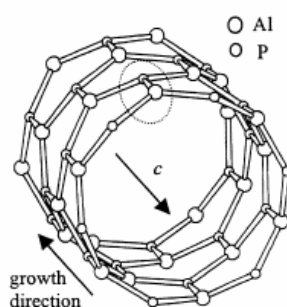
Figure 2.17. Cylinders of fused 6-rings along c.

AlPOs are found to be with a P/Al ratio near one, possessing both Lewis and Brønsted acidities [174]. AlPO$_4$-5 has electrically neutral cylindrical channels. Unlike zeolites, the AlPO$_4$-5 surface is reported to possess mild hydrophilicity and has no extra-framework cations.

Both for the orthorhombic and hexagonal symmetries, the crystallographic a and b axes lie in the plane of the figure, and the c axis runs along the channels, perpendicular to the plane of the Figure 2.19 [175].
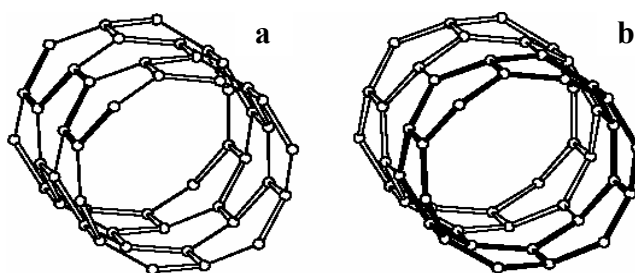
Figure 2.18. **a.** PBU constructed from six crankshaft chains; **b.** PBU constructed from T24 units.

The nominal diameter of the 12-membered ring is 7.3 Å [176,177]. The existence of Al-O-P angles near to 180° found in hexagonal structures of the first refinements [168] gave reason for subsequent studies focused on whether they are average angles as a consequence of disorder of the oxygen around Al-P axis or they are actually the angles present in this material.
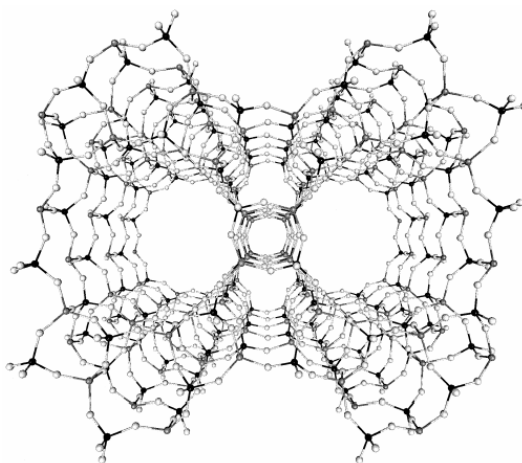
Figure 2.19. A pictorial view of the AlPO$_4$-5 structure.

2.3.3   Microwave Processing

2.3.3.1   Introduction

Microwave energy has been developed primarily for communications and some areas of processing such as cooking food, tempering and thawing, and curing of wood and rubber products [178]. Although there is extensive consumer and industrial use of microwave energy, interaction of microwaves with materials is poorly understood. Furthermore, there are numerous reports in the literature of non-thermal 'microwave effects' that accelerate reaction rates, alter reaction pathways and result in unique properties in polymers, ceramics, composites and zeolites. The origins of these microwave effects are unknown. Thus, a fundamental understanding of how microwave energy interacts with materials is the key to unlocking the technology for future and widespread use.

The advantages observed with microwave processing warrant serious, focused attention on this technology. Tangible benefits to be produced by microwave–material research include: reduced processing costs, better production quality, new materials and products, improved human health, reduced hazards to humans and the environment and enhanced quality of life. With proper understanding and control, many technically important materials can be heated rapidly, uniformly, selectively, less expensively and with greater control than is possible with conventional methods. Moreover, the unique internal heating phenomenon associated with microwave energy can lead to products and processes that cannot be achieved using conventional methods.

2.3.3.2   Working Principles of Microwave Ovens

At its most basic, the microwave oven consists of a microwave source, control and power circuits and a cavity for the sample. The cavity has reflective metal walls, which not only act to prevent leakage of radiation from the oven, but also improve its efficiency. The walls act to reflect the microwaves repeatedly through the sample where they are partially absorbed on each pass [179]. This process is particularly important for samples which are either dimensionally very small.

In the microwave ovens, AC power enters the oven and after the transformer, the magnetron begins to work. The magnetron which is a device for generating fixed frequency microwaves. It is a thermionic diode and consists of a directly heated cathode

and an anode separated under high vacuum by a high voltage in strong axial magnetic field. The anode consists of even cavities, generally eight cavities, behaves as a tuned circuit with the open end acting as a capacitance. Each cavity therefore acts as an electrical oscillator which resonates at a specific frequency [179]. The microwave power at the microwave oven frequency of 2.45 GHz is transmitted through a waveguide [180]. Whether or not a sample is present, the microwaves which enter the cavity are reflected from the walls and give rise to complex standing wave patterns. Oven manufacturers average out the energy which a sample receivers by moving the sample through the field on a turntable.

Power control in a domestic microwave oven is achieved by switching the magnetron on and off according to a duty cycle. The duty cycle is typically of the order of 20 seconds, and 50% power, for example, is achieved by repeatedly switching the magnetron on and off every 10 seconds.

2.3.3.3 Fundamentals of Microwave Heating

Microwaves are electromagnetic radiation, whose frequencies lie in the range of 0.3–300 MHz between infrared radiation and radio frequencies. Only narrow frequency windows centered at 900 MHz and 2.54 GHz are allowed for microwave heating purposes. These frequencies are indicated in the electromagnetic wave spectrum in Figure 2.20.
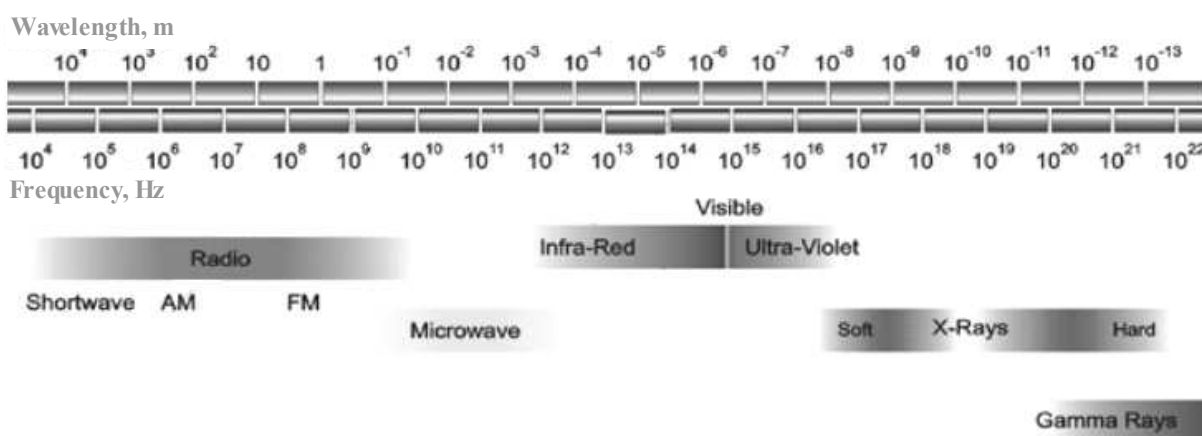
Figure 2.20. Electromagnetic spectrum including microwave frequencies between infrared and radio frequencies.

Microwave energy is a nonionizing radiation that causes molecular motion by migration of ions and rotation of dipoles, but does not cause changes in molecular structure

because it corresponds to excitation of rotational motion of molecules. An understanding of the microwave interaction with materials has been mainly based on concepts of dielectric heating and of the resonance absorption due to rotational excitation [181]. Thus energy transfer from microwaves to the material is believed to occur either through resonance or relaxation, which results in rapid heating. However, the exact nature of microwave interaction with reactants in the synthesis of inorganic solids is somewhat unclear yet Rao et al. [182] have also reviewed recent reports of microwave synthesis of inorganic solids.

Microwave frequencies correspond to rotational excitation energies in materials. Thus the incident microwaves excite rotational modes in a material and the energy absorption occurs by resonance. The absorbed energy may be completely dissipated as heat during de-excitation via internal mode coupling. The role of microwave irradiation in chemical reactions can be readily appreciated because the regime of rotational–vibrational excitations is essential for chemical reactions. Microwave energy is typically lost to the sample by two mechanisms [181]: Ionic conduction and dipole rotation. In many practical applications of microwave heating, ionic conduction and dipole rotation take place simultaneously. Ionic conduction is the conductive migration of dissolved ions in the applied electromagnetic field. Dipole rotation refers to the alignment, due to the electric field, of molecules in the sample that have permanent or induced dipole moments.

It is known that the interaction of dielectric materials with microwaves leads to what is generally described as dielectric heating due to dipole rotation [183]. Dielectric heating in microwaves can occur either via resonance modes of absorption, or via relaxational mechanisms as a result of phase lag between alternating microwave field and the motion of the polar species in the material [181,184]. Gabriel et al. [181] has described the factors which play a role in microwave heating: (1) superheating in the presence of a large number of ions; (2) more rapid achievement of the reaction temperature and (3) efficient mixing and boundary effects.

A microwave has an electric and a magnetic component which are in phase and perpendicular to each other in amplitude. Both wave components are perpendicular to the direction of travel. The heating effect in all types of materials that can interact with microwaves is mainly caused by the electric component. The total polarization (α_t) of the material based on the displacement of electrons, nuclei, permanent dipoles and quadrupoles and charges at interfaces is the sum of the following parameters:

$$\alpha_t = \alpha_e + \alpha_a + \alpha_d + \alpha_I, \qquad\qquad (2.3)$$

In which, α_e is the electronic polarization, displacement of electrons, α_a is the atomic polarization, polarization of nuclei, α_d is the dipolar polarization, polarization of permanent dipoles and quadrupoles, α_i is the interfacial polarization, polarization of charges in the interface in equation (2.3).

As both the electronic and atomic polarization operate at time scales that are smaller than required for microwave frequency field oscillations, these polarizations do not result in conversion of microwave into heat energy. The time-scale of the orientation of permanent dipoles is, however, comparable to the time scale of microwave oscillations. Thus when the amplitude of the electric field increases, the dipoles align themselves accordingly. Next, as the field amplitude decreases to zero intensity, the dipoles return to their random orientation. The change in orientation in both operations results in an energy conversion from electric into thermal energy. The interfacial polarization contributes to dielectric heating when conducting particles are suspended in a non-conducting phase. This effect is not substantial at microwave frequencies and thus results in a modest contribution to the heating. Conduction effects can also contribute to the dielectric heating. Since ions are charged, they accelerate in an electric field. Herein, the electromagnetic energy is converted in kinetic energy which is transferred to neighboring molecules resulting in unordered kinetic energy, actually heat.

A convenient measure of the heating effect which occurs in an applied field is $\tan \delta = \varepsilon'' / \varepsilon'$ is the phase difference between the electric field and the polarization of the material. In materials where the dipoles rotate freely, such as in liquids, the rotational frequency of the dipole determines the dissipation of energy from the applied field. In general, the dipolar species in any medium possesses a characteristic relaxation time, s, and the dielectric constant is, therefore, frequency-dependent.

The dielectric constant is a measure of a sample's ability to obstruct the microwave energy as it passes through, and the loss factor measures the sample's ability to dissipate that energy [185]. The word ''loss'' in the loss factor is used to indicate the amount of input microwave energy that is lost to the sample by being dissipated as heat. When microwave energy penetrates a sample, the energy is absorbed by the sample at a rate dependent upon its dissipation factor. Magnetic polarization may also contribute to the heating effect observed in materials with magnetic properties.

The complex dielectric constant ε can be expressed as:

$$\varepsilon = \varepsilon' - i\varepsilon'' \tag{2.4}$$

In which, ε' is the real component, ε'' is the imaginary component and i is $\sqrt{-1}$, indicating a 90° phase shift between ε' and ε'' in equation (2.4).

The dielectric relaxation time is defined as the time that it takes for the molecules in the sample to achieve 63% of their return to disorder. The loss tangents of the molecules, which may be related to the ability of the solvent to absorb energy in a microwave cavity, depend on the relaxation times of the molecules. These relaxation times depend critically on the nature of the functional groups and the volume of the molecule. It is interesting that functional groups capable of hydrogen bonding have a particularly strong influence on the relaxation times [181].

Generally, there are three qualitative ways in which a material may be categorized with respect to its interaction with the microwave field: transparent (low dielectric loss materials), microwaves pass through with little, if any, attenuation; opaque (conductors), microwave are reflected and do not penetrate; and, absorbing (high dielectric loss materials), absorb microwave energy to a certain degree based on the value of the dielectric loss factor [186].

The efficient coupling of microwaves and polar organic solvents can be utilized to heat rapidly reaction solutions and thereby accelerate chemical reactions. If the reactants are enclosed in a closed vessel which is transparent to microwaves the vessel has to be able to sustain the pressures which are generated by rapidly heating the volatile organic solvents. There are a number of plastic materials which are microwave transparent and also sufficiently chemically inert to be used as materials for high pressure reactors. The use of steel vessel which could effectively sustain the high pressures generated is not possible because metals such as steel are not transparent to microwaves. The pressures and temperatures generated in an autoclave which is transparent to microwaves depend on the microwave power, the dielectric loss of the solution, the volatility of the solvent, the volume of the container occupied by the solvent and the extent of gas formation during the reaction.

A fourth type of interaction is that of a mixed absorber. This type of interaction is observed in composite or multi-phase materials where one of the phases is a high-loss material while the other is a low-loss material. Mixed absorbers take advantage of one of

the significant characteristics of microwave processing, that of selective heating. The microwaves are absorbed by the component that has high dielectric loss while passing through the low loss material with little drop in energy. In some processes and products heating of a specific component while leaving the surrounding material relatively unaffected would be of great advantage. This selective heating process is not possible in conventional heating environments.

Two important parameters for microwave processing are power absorbed, P and depth of microwave penetration, D. Unlike conventional heating, these parameters are highly dependent on the dielectric properties of the material and, in practice, can provide another degree of process flexibility.

Microwave heating is the result of absorption of microwave energy by a material exposed to the electromagnetic field distributed within a reflective cavity. It is based on the power absorbed per unit volume given in equation (2.5) [186]:

$$P = \sigma |E|^2 = 2\pi f \varepsilon_0 \varepsilon_{eff}^{"} |E|^2 = 2\pi f \varepsilon_0 \varepsilon_r^{'} \tan\delta |E|^2 \tag{2.5}$$

where E is the magnitude of the internal electric field, $\varepsilon_{eff}^{"}$ is the relative effective dielectric factor, ε_0 is the permittivity of free space, f is the microwave frequency, σ is the total effective conductivity, $\varepsilon_r^{'}$ is the relative dielectric constant, and $tan\delta$ is the energy loss required to store a given quantity of energy. As can be seen from this equation, the dielectric properties ($\varepsilon_r^{'}, \varepsilon_{eff}^{"}$ and $tan\delta$) assume a significant role in the extent of power absorbed by a material. The majority of the absorbed microwave power is converted to heat within the material, as shown in equation (2.6):

$$\frac{\Delta T}{\Delta t} = \frac{2\pi f \varepsilon_0 \varepsilon_{eff}^{"} |E|^2}{\rho C_p} \tag{2.6}$$

where T is the temperature, t is the time, ρ is the density, and C_p is the heat capacity. Notice that there are no structural parameters (atomic, microstructural or otherwise) in the equation. Structural features are assumed to be accounted for by changes in the dielectric properties ($\varepsilon_r^{'}, \varepsilon_{eff}^{"}$ and $tan\delta$).

The dielectric properties also are important parameters in determining the depth to which the microwaves will penetrate into the material. As can be seen by equation (2.7),

the higher the values of *tanδ* and $\varepsilon_r^{'}$ the smaller the depth of penetration for a specific wavelength:

$$D = \frac{3\lambda_0}{8.686\pi \tan\delta \left(\dfrac{\varepsilon_r^{'}}{\varepsilon_0}\right)^{\frac{1}{2}}} \qquad (2.7)$$

where *D* is the depth of penetration at which the incident power is reduced by one half, λ_0 is the incident wavelength. The depth of penetration is important since it will determine the uniformity of heating, curing, etc., throughout the material. High frequencies and large values of the dielectric properties will result in surface heating, while low frequencies and small values of dielectric properties will result in more volumetric heating.

It has been reported that microwave dielectric heating has the following advantages compared to conventional heating for chemical conversions [181,187]; (a) the introduction of microwave energy into a chemical reaction which has at least one component which is capable of coupling strongly with microwaves can lead to much higher heating rates than those which are achieved conventionally; (b) there is no direct contact between the energy source and the reacting chemicals because the microwave energy is introduced into the chemical reactor remotely; (c) it is volumetric and instantaneous (or rapid) heating with no wall or heat diffusion effects; (d) it is specific and selective heating because chemicals and the containment materials for chemical reactions do not interact equally with the commonly used microwave frequencies for dielectric heating; (e) these selective interactions mean that microwave dielectric heating is an ideal method for accelerating chemical reactions under increased pressure conditions.

2.3.3.4 Synthesis of Microwave-Assisted AlPO$_4$-5

Microwave techniques have been now extended to serve very versatile areas in chemical research and practice including drying of chemicals [188], dehydration and synthesis of solid materials [182,189,190], catalyst preparation [191-195], acid hydrolysis of proteins [196], cleaning of metal surfaces [197], chemical desulfurization of lignite [198] sintering of ceramics [186], and promotion of many inorganic and organic reactions [186,199,200]. In particular, the microwave assisted technique is regarded as a novel method in synthesis of inorganic solids and is rapidly developing area of research [201,202].

Although it was not in the field of microwave synthesis, microwave and zeolites received first combined attention to microwave dehydration of zeolite 13X [189]. However, Mobil researchers have first claimed in 1988 that microwave energy is effective for synthesizing microporous zeolites [203]. According to this patent, microwave heating could be successfully used in the unseeded preparation of zeolite A and the seeded preparation of ZSM-5. Since the appearance of the Mobil patent, many groups reported microwave-assisted syntheses of microporous such as zeolites-A [203,204], X [204], Y [205], ZSM-5 [203,205], $AlPO_4$-type materials [206], VPI-5 [207], and mesoporous materials such as MCM-41 [208-212], MCM-48 [213], SBA-15 [214,215], Ti-SBA-15 [216], Zr- SBA-15 [216], and SBA-16 [217]. Microwave heating has been applied to the preparation of zeolites such as Y [205] and ZSM-5 [205], $AlPO_4$-11 [218] as well as FeAlPO-5 [219] crystals. Cundy [199] has reviewed microwave techniques in the synthesis and modification of zeolite catalysts in 1998 and this review covered several aspects of microwave synthesis which differ from traditional thermal methods.

The effect of microwave in the synthesis of zeolites can be divided into two parts; the ''thermal effect'' and the ''microwave effect''. The ''thermal effect'' refers to the fast and homogeneous heating of microwave. The ''microwave effect'' means the changes of the characteristic of the substance in the microwave field. In the synthesis of zeolites, the ''microwave effect'' mainly refers to the change of the characteristic of water in the microwave field. Xu et al. [220] considered that the hydrogen bridges of the water molecules are destroyed in the microwave field and the ''active'' water forms. The ''active'' water has a high activation energy, and the synthesis gel can be easily dissolved by ''active'' water. Therefore, the synthesis of zeolite was promoted.

Three predominant variables influence the heating period of the reaction gel under microwave conditions [221]. These variables are the starting gel volume, the water content, and the microwave energy penetrates the gel mixture, the energy is absorbed by the sample at a rate depending on the dissipation factor of defined magnitude for absorptive samples [221]. Because the frequency of the applied microwave radiation (2450 MHz) corresponds to the reciprocal of the dielectric relaxation time for water dipole rotation, an aqueous solution exhibits a high dissipation factor and, consequently, quick heating (170°C/0.3 min) [221]. This explains the faster processes for zeolite crystallization for the microwave-assisted synthesis compared to the one using a conventional heating system.

The larger fraction of water, required for the former synthesis method, is responsible for the demand of a larger fraction of template for a more diluted synthesis batch.

The synthesis of many kinds of zeolites, materials related to zeolites and mesoporous materials using microwave heating method have already been reported [206,207,212,218,222-230]. In this method, it is believed that a large number of crystal nuclei are simultaneously generated during the rapid increase in the gel temperature [224]. Therefore, it is believed to be promising technique for preparing zeolite crystals with a narrow pore size distribution. This is because the chemical composition of the synthesis mixture depends largely on the position in the autoclave, namely, the chemical composition in the gel under the conventional synthesis condition is not homogeneous. The heating by the conduction is also the cause of the non-uniform condition in the autoclave [224]. Structural studies about microwave-assisted zeolites were also recently carried out [231,232].

Recently, microwave heating has been used for the synthesis of $AlPO_4$-5 [15,154,156,168,205,218,225,233-236], its potential applications as advanced materials [160,162,164,166] and the protecting encapsulation of dyes $AlPO_4$-5 [221,237]. A microwave-heated, continuous-flow, high-pressure tube reactor is described, for the synthesis of $AlPO_4$-5 based a commercially available equipment [237]

Compared to the conventional hydrothermal crystallization, microwave heating of zeolite synthesis mixtures can drastically reduce the crystallization time [205]. The heat is supposedly induced by the friction of molecular rotation enhanced by microwave irradiation, and thus, it is possible to heat the reactants selectively and homogeneously from the inside. Some reports [226,238] showed that the reaction rate was 1 or 2 orders faster than that of a conventional heating.

$AlPO_4$-5 with an AFI structure, is possible candidate as containers in which one-dimensional guest materials may be isolated and stabilized in their channels [163]. $AlPO_4$-5 crystals are known to be easily synthesized in sizes larger than 100 mm in the *c*-axis direction. The anisotropy of the structure can be observed in the optical spectra using one single crystal. It is, however, well known that large crystals of $AlPO_4$-5 obtained by the conventional heating methods are often accompanied by a wide size distribution, aggregations, and byproducts. A few years ago, Girnus et al. [225] systematically investigated the synthetic conditions of $AlPO_4$-5 using the microwave heating method.

They succeeded in synthesizing large crystals within a short synthetic time using hydrofluoric acid. For obtaining high quality products, they also used a secondary synthetic procedure, which is the re-irradiation with the microwave of the supernatant liquid after the removal of the large $AlPO_4$ crystals with the byproducts.

The structures and morphology of $AlPO_4$-5 molecular sieves depend on the composition of the gel mixture and other factors such as hydrothermal temperature, hydrothermal reaction time, and pH value of the gel mixture [174]. The formation rate of hexagonal pillar crystals to form a dense $AlPO_4$ phase is favorable under acidic conditions, and an amorphous $AlPO_4$-5 structure forms under basic conditions [174]. The AFI molecular sieves were synthesized under microwave irradiation in various conditions by Jhung et al. [239]. In acidic conditions, the silica accelerates the crystallization, whereas in alkaline condition the silica hinders the crystallization to form plate-like crystals.

Kodaira et al. [224] also synthesized pure $AlPO_4$-5 crystals with a narrow size distribution by the microwave heating technique. They reported that the crystal morphology is initially hexagonal disk-like and changes into rod-like, i.e., the increase in the aspect ratio (the *c*-axis:*a*-axis ratio) during the synthesis. This behavior seems to be attributable to the change in the chemical composition of the synthesis mixture.

From previous studies of the microwave synthesis of $AlPO_4$-5, it is known that $AlPO_4$ hydrates of different crystal structures may form in the earliest stages of the reaction [240]. In some cases, it is shown that crystals formed in the early stages of synthesis may act as nucleation points for epitaxial growth of a second crystalline phase [240]. It is speculated that an $AlPO_4$ hydrate that forms octahedral bipyramidal crystal, such as variscite, may be at the center of the tetrapod [241]. Hexagonal $AlPO_4$-5 crystals then grow outward from four faces of the octahedral core. Powder XRD of the tetrapod crystals only shows the pattern corresponding to the AFI structure of $AlPO_4$-5. The bipyramidal crystals at the tetrapod core may be present in such small amounts that they are undetected by powder XRD [241].

The growth kinetics of AFI crystals was systematically studied using the XRD method so far. The influence of the synthesis variables, such as heating temperature, chemical composition of the mixture, pH and the types of Al/Si sources on the crystallization behavior, have been examined [172,242]. However, the growth behaviour of AFI crystals has not yet been clarified because a broad size distribution exists among

crystals synthesized by conventional heating methods [169,224]. Since the growth process of individual crystals cannot be easily followed, the nucleation time of crystals with different size is still under question.

Previously, Iwasaki et al. [243] have developed an optical microscope system to observe the growth process of MFI type zeolite crystals three-dimensionally and have already reported that the aspect ratio of crystals is significantly influenced by the growth environment. The obtained results suggest that the crystallization process is affected by the chemical composition of the starting synthesis gel and the surface structure and pore direction of zeolite crystal. The aspect ratio of the crystals changed with the increase in the synthesis time [244]. The silica species controlled the growth of AFI crystals, especially in the c-axis direction. The common characteristics with MFI crystals are that the aspect ratio of the crystal is largely influenced by the dilution, as well as the minor components in the framework. The prolonged synthesis time caused secondary nucleation and the formation of a growth ring pattern. Therefore, to utilize AFI crystals as host materials, the synthesis time must be controlled properly [244].

It has been reported that anions such as sulfate, chloride and fluoride are detrimental to the synthesis of AFI structure to form dense phases [172,245]. However, Kodaira et al. [224] and Finger et al. [156] synthesized well-defined $AlPO_4$-5 crystals under the pH control using sulfuric acid. Ahn and Chon [245] utilized the acetic acid to synthesize AFI molecular sieve in the presence of high concentration of magnesium or cobalt. Kornatowski et al. [246] could decrease the aspect ratio of CrAPO-5 by using acetic acid and chromium species.

Fluoride has been widely utilized in the synthesis of microporous zeolites and aluminophosphate molecular sieves [247]. The mineralizing effect in the synthesis of $AlPO_4$-n molecular sieves may not be so evident as in the case of zeolites because the $AlPO_4$-based materials have generally been synthesized in acidic conditions. Nevertheless, various beneficial effects have been observed in the presence of fluoride [247]. Girnus et al. [225] reported that large $AlPO_4$-5 crystals were formed using much diluted gel in the presence of fluoride. The crystal size decreased with increasing HF concentration. Another beneficial effect of the fluoride is a role of the structure-directing agent. In spite of much work on influence of anions in the synthesis of AFI molecular sieve, their exact role is still remained unclear.

The AFI molecular sieves such as AlPO$_4$-5 and SAPO-5 were synthesized in the presence of anions such as chloride, nitrate, sulfate, acetate and fluoride by Jhung et al. [248]. The crystallization yield and crystal size increase with a decrease in pH except for the fluoride anion. On the contrary, the fluoride showed an opposite trend, i.e., the crystallization yield decreased as the pH of the reaction gel decreased. Moreover, the rod-like AFI molecular sieve was produced with the addition of fluoride anion. The decrease of crystallization yield and formation of very long crystals may be attributable to the dissolution of the reaction gel by forming metal–fluoride bonds [248].

The AlPO$_4$-5 was crystallized through microwave heating of reagents initially confined in water-in-toluene microemulsion droplets [241]. The surfactant cetyltrimethylammonium bromide and cosurfactant butanol were used to form the microemulsion. By adjusting the microemulsion composition, the crystal morphology could be altered. The diversity of the observed crystal morphology suggests that there is a complex interplay of reagent confinement, crystal growth rate, and adsorption of some of the microemulsion components onto the growing crystal surface in affecting crystal nucleation and growth [241].

2.3.4   AlPO$_4$-5 as a Templating Agent

Carbon nanotubes, originally discovered as a byproduct of fullerene research [249], are attracting increasing interest as they offer new prospects to fundamental as well as nanotechnological applications. An important recent advance in carbon nanotube science is the synthesis of single-wall carbon nanotubes (SWCNs) in high yield using the laser ablation method [250] and the electric arc technique [251]. In each case, a small amount of transition metal was added to the carbon target as a catalyst. However, it is still a big challenge to produce mono-sized SWCNs with well-defined symmetry, and to make a good electrical contact to a single nanotube for carrying out experimental investigations.

The zigzag nanotubes inside AlPO$_4$-5 zeolite (AFI) channels and the double-walled nanotubes were recently investigated [252]. Carbon nanotubes can be found in two types of structures, where they are surrounded by a channel-like framework: (i) they can be found inside of another nanotube in form of multi-walled (MWNT) or doublewalled (DWNT) carbon nanotubes (ii) singlewalled carbon nanotubes (SWNTs) can be grown in channels of zeolite crystals [252].

While the nanotubes grown in zeolite crystalls have probably the smallest possible diameter, are aligned and due to diameter restrictions, only few chiralities can form, they are considered to contain a large amount of defects. The inner tubes of the DWNTs bridge the gap between these extremely narrow tubes and wider singlewalled nanotubes (SWNTs) that are usually present in the available samples.

The synthesis of mono-sized and parallel-aligned SWCNs in channels of microporous single crystal of $AlPO_4$-5 by pyrolysis of tripropylamine (TPA) was reported [253]. Microporous aluminophosphate $AlPO_4$-5 crystals (AFI) with elongated hexagonal prisms of dimensions 110 mm in cross-section diameter and 300 mm in length were used as the hosts to encapsulate the SWCNs. TPA molecules were encapsulated in the channels during the crystal growth. The synthesis procedure of the SWCNs involves the pyrolysis of TPA molecules in the AFI channels in a vacuum and exposed in free space after removing the AFI framework using HCl acid. SEM image of the AFI single crystal used to synthesize SWNTs shown in Figure 2.21.

The diameter of SWNTs was as small as 0.4 in the 1 nm sized channels of $AlPO_4$-5 single crystals, shown in Figure 2.22. These nanotubes have been observed directly by transmission electron microscopy [254], as well as indirectly by diffuse X-ray scattering [255], micro-raman measurements of the nanotube-breathing mode [256] and also electronic and superconductivity properties were tested [257]. It was reported that the formation of the SWCNs is very sensitive to the quality of the AFI crystal, the encapsulation of hydrocarbon molecules in the AFI channels, and the pyrolysis conditions [253].

Frequency doubling in zeolite-based guest/host systems was first discovered by Cox and Stucky [162] in 1988. They investigated the optical properties of several such materials, using different hosts as well as different guest molecules. High doubling efficiencies were observed with *p*-nitroaniline (PNA) as guest molecule, and molecular sieves with unidimensional channel systems as host, such as the aluminophosphate $AlPO_4$-5, a molecular sieve with a channel diameter of approximately 0.73 nm.

These experiments were later repeated in more detail on single crystals by Caro et al. [164], Caro and Marlow [258] and Miyake et al. [259]. The first system investigated by this group was again PNA in $AlPO_4$-5 with its channels running along the long crystal axis

(*c*-axis). Experiments on single crystals with polarized incident light revealed that the PNA is well ordered in the channel system of the molecular sieve.

Which factor controls the relatively perfect alignment of the PNA molecules is still an open question. In order to give rise to observable results, it is not only necessary that the orientation of all molecules in one channel is identical, the same orientation needs to be present in all channels, or at least in the majority of the channels [260]. Two explanations seem to be possible: the macroscopic polarity of the crystals could be responsible for the alignment, or the surface properties of the crystals could allow entry of the molecules into the channel system in only one orientation.

A set of measurements of the pyroelectric effect on a single crystal by Marlow and co-worker [261] suggests that the PNA molecules enter the pore system from both sides with the nitrogroup entering first. However, if the crystals were twinned with the two twins growing from the center rotated by 180° against each other, the orientation by the macroscopic dipole of the crystals might still be the major influence. This question has not been unambiguously answered yet

The morphology of some molecular sieve crystals suggests their use as optical resonators in lasers. Here again the $AlPO_4$-5 system seems to be promising. The hexagonal prism with its planparallel ends could be directly used as a laser cavity if the ends would be coated, for instance with a dielectric multilayer, to create a mirror [260]. The resonator with planparallel mirrors is certainly not optimal with respect to the laser quality, but the synthesis of such crystals in large amounts would be very easy, and thus the development of laser materials based on this class of substance is an interesting challenge. Such laser materials could offer several advantages. They would provide a highly flexible matrix, since many different guest species could be incorporated. Due to the open channel system the guest species could be further modified, for instance through complexation, and the integration of additional functions in one crystal could be possible, for instance by introducing additional frequency-conversion systems [260].

Synthesis of the host material in sufficiently high optical quality is relatively difficult. The structure of $AlPO_4$-5 is easy to synthesize, but usually the material forms as a fine, polycrystalline powder, which is not suitable for optical applications. A synthesis of high-quality $AlPO_4$-5 was developed by Finger and Kornatowski [262], but in this synthesis procedure a special aluminium source (AlOOH-sol; CTA Saureschutz) was used which is

no longer available. Although many parameters need to be optimized in order to synthesize high-quality $AlPO_4$-5, the aluminium source is the crucial component. In order to substitute the original aluminium source, many different aluminium sources, either commercially available or self-prepared, were tested by Demuth [169]. The reason for these strong differences between different precursors is not clear, yet. It might be related to the release rates of suitable building blocks for the $AlPO_4$-5 synthesis.
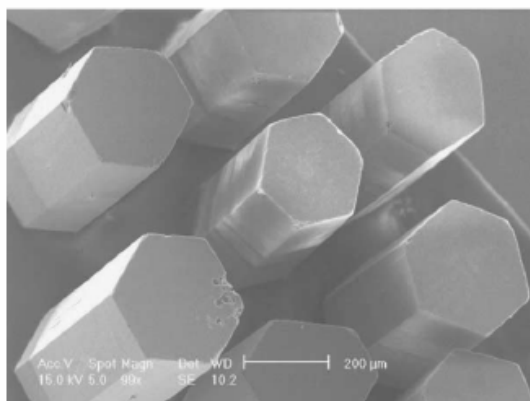
Figure 2.21. SEM image of the AFI single crystals [257].

Ion exchange to introduce the laser-active species is not directly possible for $AlPO_4$-5, since due to the electroneutral framework, no exchangeable cations are present, in contrast to the aluminosilicate zeolites. However, it is possible to incorporate silicon into the AlPO-framework, where the silicon substitutes primarily for phosphorus. Thus, for each silicon incorporated, one negative framework charge is created which leads to ion-exchange properties. The resulting silicoaluminophosphates are then called SAPOs.

Organic laser-active species was introduced into the channel system of the $AlPO_4$-5 [260]. Incorporation works best if the dye is added to the synthesis gel for the molecular sieve. Analysis of the resulting crystals with polarized light reveals that the dye is encapsulated in the crystal with a high degree of orientation.

Molecular sieves of the $AlPO_4$-5 type represent an especially suitable host material for the incorporation of dye molecules by conventional [263-267] or microwave- assisted crystallization inclusion [221,238], preserving the ability of a chromophore for fluorescence [160] or laser emission. Rhodamine dyes like rhodamine B, rhodamine 3B and the newly synthesized rhodamine Dyes were monomolecularly encapsulated in $AlPO_4$-5 by either conventional or microwave-assisted crystallization inclusion [268].
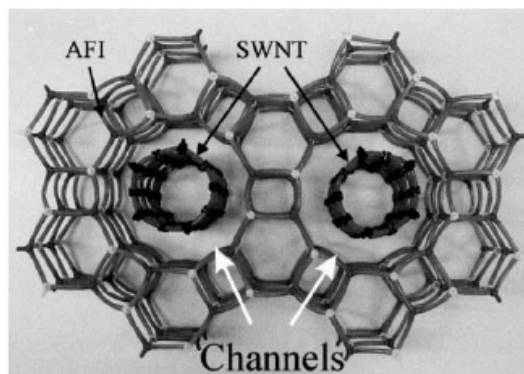
Figure 2.22. Schematic of the porous zeolite $AlPO_4$-5 (AFI) crystal structure and the SWNTs formed in the channels of the AFI [269].

2.4   Diffusion in Zeolites

The diffusion of small molecules in the intracrystalline void volume of zeolites has been a research topic for many years. To obtain information about the transport properties of zeolite crystals is important to understand the dynamics fundamentals of small molecules inside a zeolite which is relevant for all applications.

The size, shape and adsorptive selectivity of both natural and synthetic zeolitic materials have been used to advantage in a wide variety of heterogeneous catalytic processes. As an example of zeolite used as catalysts, the methanol to gasoline (MTG) conversion process, using a zeolite catalyst, is of major commercial importance. This process has been the subject of numerous experimental [270,271] and theoretical studies [272,273], but it is still not particularly well understood.

In zeolites the catalytically active sites are not directly accessible to the reacting molecules. As is usually the case for heterogeneous catalysts, a number of different steps are needed in order to convert the reactants into the desired products. As the feed stream is usually in the gas or liquid phase, adsorption on the zeolite surface and into the zeolite pores first has to take place. In order to react, the molecules then have to be transported to the reactive sites inside these pores. This transport process is called diffusion. Once the reactants have reached the catalytically active sites, the necessary chemical reactions can finally take place, and the conversion into products takes place.

Diffusion is caused by the thermal motion and subsequent collisions of the molecules. Two types of diffusion can be distinguished; transport diffusion resulting from

51

a concentration gradient, and self-diffusion which takes place in a system which is at equilibrium. The flux due to transport diffusion can be described using Fick's First Law of Diffusion:

$$\vec{J} = -D.\nabla c \tag{2.8}$$

in which D is the diffusion constant and c the concentration. Self-diffusion is usually expressed in terms of a self-diffusion constant D_c.

Diffusion plays an essential role in most phenomena occurring to molecules in zeolites, e.g. it favors adsorption, makes separation of similar molecules effective, and drives chemical reactions both on the reagent side to lead the reactants into the active sites and on the product side to select and extract the species resulting from the reaction.

In zeolites, the molecules have to move through channels of molecular dimensions and there is an interaction between the diffusing molecules and the zeolite framework. Besides concentration and temperature of the system, the size and the shape of the channels are important parameters in diffusion in zeolites. So the exact values of diffusivity constants are much harder to predict for zeolites. There is a large difference in the diffusivities of different alkane isomers, as the more bulky branched isomers have a much larger interaction with the zeolite framework.

For industrial applications, a better understanding of diffusion will promote the optimization and development of industrial applications of these materials in separation and catalytic processes. The study of diffusion in zeolites is an interesting subject as the different diffusion behaviours of different organic volatile molecules in zeolite channels at different temperatures. This will aid in understanding the interaction between the organic volatile material and the pore walls and the reactivity in these materials. The results found in this thesis can act as a diffusion models.

Various techniques for the measurement of intracrystalline diffusion have been developed [274-276] which widely vary in scope, degree of experimental and theoretical sophistication, and range of applicability. For a large number of the indirect methods, the diffusing species, or its concentration profile in the microporous material, is not directly observed; the diffusivity is rather calculated from the external measurement of pressure, concentration, or sample weight. Such computations require suitable models which describe all transport phenomena and possible sorption processes that can occur in the experimental setup. There is however no reliable theory that can easily predict the

diffusivity for different components in different zeolites [277]. There are large divergences between different techniques when comparing microscopic and macroscopic ones.

2.4.1 Fickian Diffusion

Configurational diffusion is takes place in the micropores of a zeolite [278]. The diffusivity in configurational regime depend strongly on the pore diameter, the structure of the pore wall, the interactions between the surface atoms and the diffusing molecules, the shape of the diffusing molecules and the way the channels are connected. As a result, it is very difficult to derive generalized equations.The values of diffusion coefficients is in the range from 10^{-8} to 10^{-20} m^2/s in the literature [279].

Whenever a species concentration gradient, $\partial C / \partial x$, exists in a finite volume of a matrix substance, the species will have the natural tendency to move in order to distribute itself more evenly within the matrix and decrease the gradient. Given enough time, this flow of species will eventually result in homogeneity within the matrix. The mathematics of this transport mechanism was formalized in 1855 by Fick, who postulated that the flux of material across a given plane is proportional to the concentration gradient across the plane [280]. Thus, Fick's First Law states:

$$J = -D \left(\frac{\partial C(x,t)}{\partial x} \right) \tag{2.9}$$

where J is the flux, D is the diffusion constant for the material that is diffusing in the specific solvent, x is the spatial coordinate and $\partial C(x,t) / \partial x$ is the concentration gradient. The diffusion constant of a material is also referred to as "diffusion coefficient". It is expressed in units of length^2/time. The negative sign of the right side of the equation indicates that the species are flowing in the direction of lower concentration

Fick's First Law does not consider the fact that the gradient and local concentration of the impurities in a material decreases with an increase in time, an aspect that's important to diffusion processes. Fick's Second Law states that the change in impurity concentration over time is equal to the change in local diffusion flux, or

$$\partial C(x,t) / \partial t = -\partial J / \partial x \tag{2.10}$$

or, from Fick's First Law,

$$\partial C(x,t)/\partial t = -\partial(D\partial C(x,t)/\partial x)/\partial x \qquad (2.11)$$

If the diffusion coefficient is independent of position, such as when the species concentration is low, then Fick's Second Law may be further simplified into the following equation:

$$\frac{\partial C(x,t)}{\partial t} = -D\left(\frac{\partial^2 C(x,t)}{\partial x^2}\right) \qquad (2.12)$$

This equation gives the change of concentration in a finite volume element with time. According to Barrer and Jost [281], the diffusivity is assumed to be isotropic throughout the crystal, as D is independent of the direction in which the particles diffuse. Assuming spherical particles, Fick's second law can be readily solved in radial coordinates. As a result, all information about the exact shape and connectivity of the pore structure is lost, and only reflected by the value of the diffusion constant.

When a porous adsorbent system is placed in contact with a solvent (penetrant) gas, diffusion of the penetrant in the porous material may be followed by measuring the uptake of the solvent. Diffusion in the silicalite crystals can be described by Fickian diffusion with concentration independent diffusivity, D. In Fick formulation the driving force for diffusive transport is the gradient of chemical potential of concentration, rather than the gradient of concentration [282]. The kinetics of the diffusion into the sphere in Fick formulation is expressed by equation (2.14) [283].

The diffusion coefficient is supposed to be constant. The basic equation, in spherical coordinates, to be solved is

$$\frac{\partial C_A}{\partial t} = D(\frac{\partial^2 C_A}{\partial r^2} + \frac{2}{r}\frac{\partial C_A}{\partial r}) \qquad (2.13)$$

with the initial conditions

$$C_A = C_\infty \qquad \text{for} \quad r = r_0 \qquad \text{at } t > 0$$

$$C_A(r) = C = const \qquad \text{for} \quad 0 < r < r_0 \quad \text{at } t = 0$$

where C_A is the solid phase concentration (mol/m^3), D is the diffusion coefficient, constant throughout the process (m^2/s), t is the time (s), r is the distance from the particle center (m), C is the initial solid phase concentration (mol/cm^3), and r_0 is the particle radius

(m). The exact solution of equation (2.13) is equation (2.14) for gas phase diffusion to the solid solute [284].

Assuming the zeolite particles are of spherical shape, the solution of Fick's second law of diffusion in spherical systems gives [285,286].

$$\frac{M_t}{M_\infty} = 1 - \frac{6}{\pi^2} \sum_{n=1}^{\infty} \frac{1}{n^2} \exp(-Dn^2\pi^2 \frac{t}{a^2}) \tag{2.14}$$

where M_t and M_∞ represent the amount of solvent diffused entering the spheres with radius a, at times t and steady state, respectively and n is an integer coming from the solvation of Fick's second law. D is the coefficient of diffusion of the solvent. This equation is based on the assumption that the particle radius does not change, which is true for zeolite particles. The solution to equation (2.14) for is given by the equation (2.15) [287].

$$\frac{M_t}{M_\infty} = 6(\frac{Dt}{a^2})^{1/2} \left[\pi^{-1/2} + 2\sum_{n=1}^{\infty} ierfc \frac{na}{\sqrt{(Dt)}} \right] - 3\frac{Dt}{a^2} \tag{2.15}$$

For small times equation (2.15) approximates to

$$\frac{M_t}{M_\infty} = 6\left[\frac{Dt}{\pi a^2} \right]^{1/2} - \frac{3Dt}{a^2} \tag{2.16}$$

Neglecting the contribution of the term $3Dt/a^2$, the value of D is found from the slope of a plot of M_t/M_∞ versus $t^{1/2}$.

2.4.2 Activation Energy of Diffusion

Diffusion is an activated process, *i.e.*, to occur it requires overcoming an energy barrier. Other activated processes are found in zeolites, the commonest examples being the adsorption of a molecule, which from a gas or a liquid enters into the micropores and, especially, chemical reactions occurring in the channel and cavities. Activation energies of diffusion are calculated using the equation below [288]:

$$D = D_o e^{\frac{-E_A}{RT}} \tag{2.17}$$

$$\ln D = \ln D_0 - \frac{E_A}{RT} \tag{2.18}$$

where, D_o is temperature-independent pre-exponential (m^2/s), and E_A is the activation energy for diffusion (kJ/mol) [289].

According to Riekert [290], diffusion takes place by means of series of jumps. The pre-exponential term D_o is related to the elementary rate at which particles attempt to jump to a neighbouring adsorption site. The exponential expresses the chance that the particles are able to overcome the free energy barrier E_A between these sites. Although this will certainly be an oversimplified picture of the true diffusion process, many experimental and theoretical studies have shown that it is capable of accurately describing the temperature dependence in diffusion systems.

The activation energy, E_A can thus be determined by measuring the diffusion coefficient at different temperatures. The measured activation energies can be much higher than the real activation energy, and it is also depend on the gas phase pressure at which the measurements are performed.

The concentration of molecules inside the zeolite also depends on the temperature and measurements are often performed at finite loadings. While measuring the activation energy is measuring, the combined effect of temperature and loading dependence is measured. With increasing temperature, the loading of the zeolite crystals usually decreases. In addition to the increased mobility of the molecules due to the higher temperatures, this can also lead to an increase of the diffusion rate. Thus it is complicated to compare the activation energies of diffusion for different experimental conditions.

2.4.3 Mode of Transport

The determination of diffusion coefficients is based on uptake measurement of the volatile component by sorbents. Analysis of the sorption data can be accomplished by various means. A convenient method of analysis involves fitting the sorption data to empirical equation (2.19). It is possible to express the initial rate of diffusional solvent penetration in terms of the equation:

$$\frac{M_t}{M_\infty} = kt^n \tag{2.19}$$

where, M_t is the amount of solvent diffused in the macromolecular structure at time t, M_∞ is the amount of solvent diffused at steady state, t is the release time, k is the rate constant

which depends on structural characteristics of the system and n is an exponent characteristic of the mode of transport of the solvent in the porous structure, varies with diffusion mechanism and particle geometry.

Sorption mechanisms in macromolecular systems may be defined in terms of two limiting cases of Fickian diffusion and Case II transport [291]. When $n = 0.5$, the solute diffuses through and is released from the adsorbent with a quasi-Fickian diffusion mechanism. For values of n > 0.5, non-Fickian solute diffusion is observed. When $n = 0.85$, Case II transport occurs and values of n between 0.5 and 1.0 indicates anomalous transport. There is a completely different behaviour of diffusing molecules in zeolites compared to the gas phase is the occurrence of anomalous diffusion in some zeolites.

Values above $n = 0.85$ are possible and are termed "super-Case II". It is important that the expected values of n are sensitive to the assumed particle shape. For an infinite plan sheet, the values would be 0.5 and 1.0 for Fickian and pure Case II respectively, and in the case of an infinite cylinder, 0.45 and 0.89, respectively [291]. There may be differences in the diffusion behavior of different sections of the zeolite. Thus the values of n can be used only as a rough guide as to the nature of the process. Different n and k values can be found in the literature [292]. Equation (2.19) is useful for preliminary analysis of sorption data, although it may be used up to 60% of the final weight of penetrant imbibed and it has no provisions for analysis of details, such as inflections or penetrant loss with time [285,293]. In the graph of ln (M_t/M_∞) versus ln t, ln k is the intercept and n is the slope [284,294].

2.4.4 Different Experimental Techniques

Conventionally, molecular diffusion in zeolites has been performed by subjecting the sample under study to a step in the pressure of the surrounding atmosphere and by recording the sample response [295-298], i.e., in general, by monitoring the time dependence of the thus induced change of the amount adsorbed, e.g., gravimetrically.

Besides intracrystalline diffusion, this process may be affected by a number of different processes such as the sorbate access to the sample, sorbate permeation through the bed of crystallites, overcoming transport resistances at the external surface of the crystallites and dissipation of the heat of adsorption.

An alternative access to diffusion phenomena is provided by the Pulsed Field Gradient (PFG) NMR [299-301] and quasi-elastic neutron scattering (QENS) [302]. In these techniques, either by studying their interaction with thermal neutrons (QENS) or by recording the time dependence of the Larmor frequency of (NMR-active) nuclei (PFG NMR), one is able to determine the propagator of the diffusants or, more accurately, of the nuclei under study. In both techniques, the smallest diffusivities still accessible are on the order of 10^{-14} m^2/s, while there is essentially no upper limit. Owing to the range of observable displacements, PFG NMR is able to observe both intracrystalline and long-range diffusion, while the diffusivities attained by QENS refer to a submicroscopic scale, involving even the elementary processes of diffusion.

Experimental techniques can be divided in two essential features [303]: Uptake measurements are carried out under non-equilibrium conditions and are based on the observation of macroscopic phenomena, like the change in the overall mass or pressure, while PFG NMR, QENS are equilibrium techniques, sensitive to a microscopic scale of observation.

2.4.4.1 Macroscopic Techniques

Uptake methods are based on the measurement of the response of the zeolitic host-guest system to a change in the pressure or concentration of the surrounding gas phase [295,304]. Usually, this analysis relies on analytical solutions of the diffusion equations stated above.

For the measurement of the response of the system, different techniques can be used. Examples are the gravimetric method, which uses a vacuum microbalance to measure the change in weight of the zeolite sample after exposure to a change in the gas phase, and volumetric methods, which measure the change in the amount of gas phase molecules in the sorption vessel.

Using gravimetric method, Seferinoğlu and Yürüm [294], recently measured the diffusion coefficients of pyridine in raw and acid-washed low rank coals. The method they used was simple and precise for the measurement of diffusion coefficients of solvents in coals. The same method was used previously for the measurement of diffusion coefficient of different organic volatile materials into the natural zeolite by Sakintuna et al. [305,306]. Ritger and Peppas [307], and Howell and Peppas [308] studied diffusion processes in

describing the transport kinetics for pyridine in coal using the same empirical equation (2.19).This method can also be used for the measurement of diffusion constants of several solvents in natural and synthetic zeolites. Bludau et al. [309] studied the uptake of pyridine into mordenite and H-ZSM-5. Their data evaluation was based on the solution of Fick's second law using diffusion coefficients for the whole process. Dyer and White [310] studied cation diffusion in a natural zeolite clinoptilolite and compared three different approaches to determine diffusion coefficients including Fick's second law of diffusion (equation (2.14)), which was found to produce similar results with other approaches. The applicability of various models for the determination of ion exchange diffusion coefficients in clinoptilolite was examined in an other study [284], in which equation (2.14) was found to be acceptable for the calculations. Marecka and Mianowski [311] used Fick's second law to determine sorption of carbon dioxide and methane on a highly metamorphosed coal and the results of the model are compared with the experimental kinetics of nitrogen sorption on type A zeolite.

More recently, the tapered element oscillating microbalance (TEOM) technique has been introduced, which measures the uptake in a zeolite sample via a change in eigen frequency of the oscillating tube holding the sample [312].

For the calculation of diffusion coefficient the following assumptions are made; the diffusion mechanism obeys the Fick's law of diffusion, the crystallites possess spherical shape, the concentration profile of the sorbed gas in these spheres shows radial symmetry. The diffusion is assumed to be isotropic; it can be described by a single diffusion coefficient rather than a diffusion tensor and the diffusion coefficient does not depend on sorbate concentration.

It is proposed that there are at least five limiting types of diffusion for the molecules flowing through the zeolitic material [313]:

Case a: Unrestricted intracrystalline diffusion: the molecule moves in the channels and cavities of a crystallite without crossing the surface of the solid or extended crystal defects.

Case b: Modified intracrystalline diffusion: the particle crosses extended (*e.g.,* dislocations, mosaic boundaries) or localized (*e.g.,* vacancies, cations in noncrystallographic positions) crystal defects hindering or, sometimes, enhancing its motion.

Case c: Restricted intracrystalline diffusion: the molecule is reflected at the crystal boundary due to a very low probability of desorption.

Case d: Intercrystalline diffusion: the molecule migrates between different crystals, so it is sorbed most of the time but not confined to the same crystal. Sometimes this type of diffusion involves surface film formation and diffusion on the zeolite surface.

Case e: Diffusion in the fluid phase: the particle remains in the gas or liquid phase, confined only by the walls of the vessel containing the sample.

Permeation measurements are one of the earliest ways to determine the diffusivity through porous solids [296]. With this technique, the flux of the adsorbate through a parallel sides slab or membrane is measured under conditions in which the concentrations at both faces are known. As the flux is related to the diffusivity of the adsorbate via Fick's law, this quantity can thus be directly calculated.

The another uptake method used is the chromatographic methods [314,315]. The technique is based on the measurement of the response of a chromatographic column filled with pellets composed of zeolite crystals to a perturbation in the sorbate concentration at the inlet A number of variations on the traditional chromatographic techniques have been introduced in the passed decades. The zero-length column (ZLC) method [316] uses a very small gas volume which is equilibrated with the sorbate of interest and subsequently purged with an inert gas at a high flowrate in order to further decrease external mass transfer resistances. More recently, TAP (temporal-analysis-of-products) [317,318] experiments have been introduced that measure the pulse response of a bed under ultra-high vacuum conditions using a mass spectrometer. The TAP reactor system permits to apply a transient technique in vacuum, suppressing high surface concentrations, to the measurement of molecules diffusing through a packed layer of zeolite particles and leaving this layer.

The other technique is Positron Emission Profiling (PEP) [319] method. In principle, PEP is a chromatographic technique using labelled molecules, but instead of measuring the response at the exit of the reactor, this technique is capable of measuring the concentration at different positions inside the reactor. As the technique furthermore uses a standard laboratory-scalepacked-bed reactor, experiments can be performed under typical reaction conditions.

2.4.4.2 Microscopic Techniques

The Pulsed Field Gradient (PFG) NMR [300,320] techniques makes use of the spatial dependence of the nuclear magnetic resonance frequency in an inhomogeneous magnetic field. This inhomogeneous magnetic field increases linearly with the spatial coordinate z, and is superimposed over the constant magnetic field. In the PFG-NMR technique, this field is only applied during two equal, short time intervals, separated by time t. The resulting NMR signal, generated by an appropriate sequence of radiofrequent pulses, will be proportional to the propagator of the diffusing molecules. This propagator denotes the propability density that during a time interval t a molecule is shifted over a certain distance, which is determined by the field gradient that is applied during the experiments. As a result, from these experiments the self-diffusion constant and mean-square displacement can be calculated inside the zeolite crystals.

There are some other NMR techniques apart from PFG-NMR. Nuclear spin interactions probed by solid-state NMR are generally anisotropic, and as a result encode for the molecular orientation with respect to the external magnetic field. By studying the motional averaging or time-correlation functions of these interactions, information can be obtained about the rotational motion of the molecules [321-323]. By assuming a certain relation between rotational and translational mobility the elementary diffusion rates can be extracted. Although the above-mentioned techniques can only be applied to a small number of zeolite-sorbate systems, their main advantage is that they are capable of measuring systems with extremely low mobility (D in the order of 10^{-20} m^2/s^1).

Quasi-elastic neutron scattering (QENS) [324] has been introduced as an alternative to PFG-NMR measurements to measure the intracrystalline diffusion in zeolites. This technique is based on the analysis of the quasi-elastic broadening in the energy of the scattered neutron beam. The broadening is caused by an energy transfer between the incident wave and the diffusing molecules, which in its turn depends on the elementary diffusion process of the particles. From these experiments, the self-diffusivity can be determined, and the mean jump length may be estimated. The application of this technique is limited to species with higher mobilities, and the diffusion paths covered during a measurement are typically of the order of a few nanometers.

A technique that has recently been introduced in the study of diffusion in zeolite crystals is interference microscopy [325]. It is based on the measurement of the change in

optical density of the zeolite crystallites during transient adsorption or desorption. The optical density in the zeolite is determined by the integral of the sorbate concentration in the observation direction. By using a microscope localized concentration measurements on zeolite crystals can be performed. As the method measures concentration changes, this technique is capable of measuring the transport-diffusion on a microscopic scale.

There is a vast amount of techniques available for studying the diffusion in zeolites. These techniques all vary in their basic principles and the assumptions made to analyze the experiments. The range of diffusivities accessible to the different methods is different and given in Figure 2.23 [317,318].
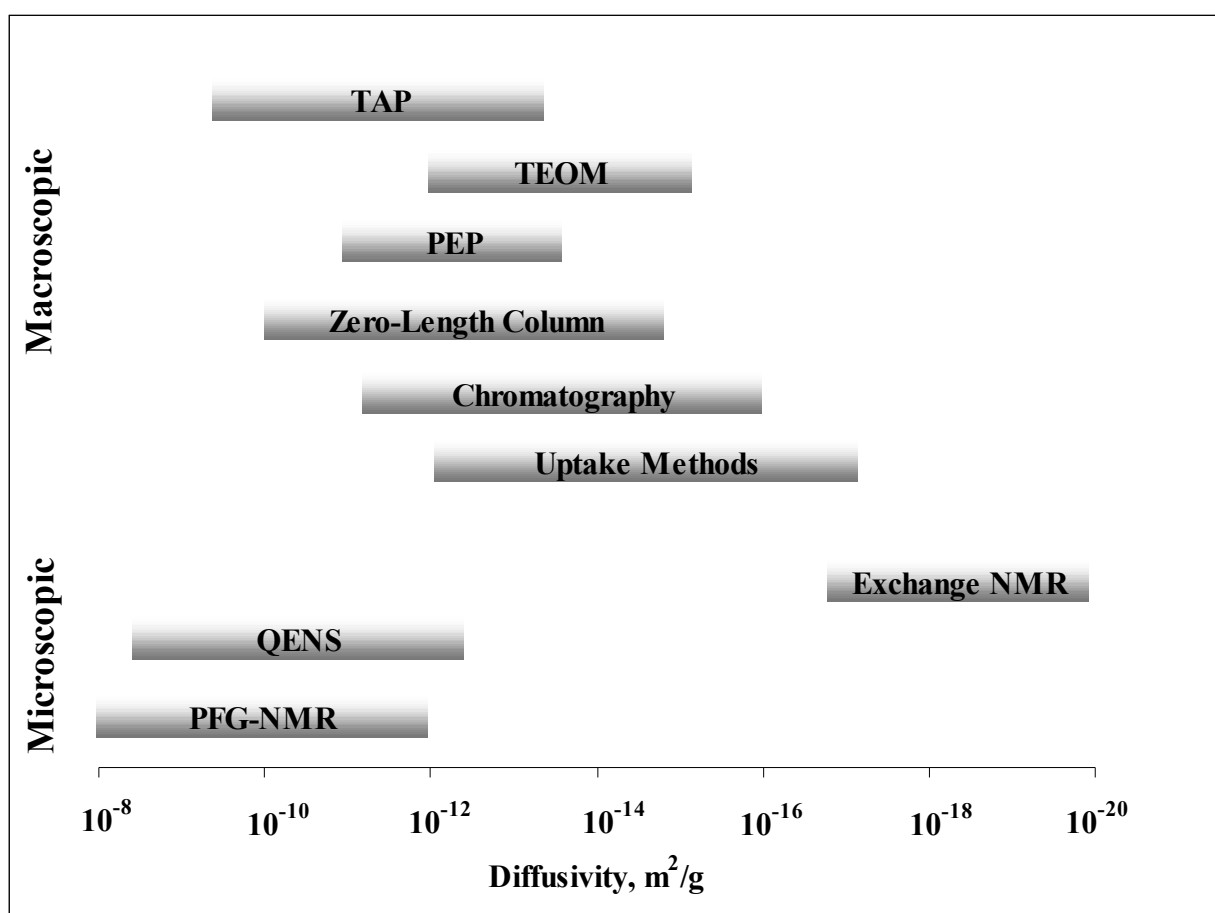
Figure 2.23. The range of diffusivities determined in different techniques.

Motivated by vast differences in the intracrystalline diffusivities obtained by different techniques, zeolite science and technology is reinforced by a continuously increasing number of novel theoretical concepts and experimental techniques of diffusion studies. The measurement of diffusion in zeolites can be expected to remain a challenging task also over the next decades.

2.5 The Techniques used to Sharpen and Maximize Nuclear Inducion in NMR

The total Hamiltonian defining any single-level energy transition between non-degenerate (non-equivalent) nuclear spin-states is a composite of several parts [326]. In theory, Zeeman term by itself would afford a very sharp peak, but in reality, the observed peak is typically dispersed by the chemical shielding anisotropy term and/or split by the indirect spin-spin coupling term.

In solid-state NMR, the dipole-dipole couplings and chemical shielding anisotropy effects are strong and would afford very broad spectra if not for the use of specific measurement techniques. Three spin systems are generally investigated. One is abundant spin ½ system, which is dominated by the homonuclear dipole-dipole interaction.

A second spin system defines that of rare spin ½ nuclei. Typical organic molecules containing ^{13}C, ^{29}Si or ^{31}P nuclei surrounded by numerous protons describe classic spin systems of this category. In this system, the total Hamiltonian and resonance condition is dominated by the heteronuclear dipole-dipole interaction between nucleus and proton nucleus, and by the chemical shielding anisotropy term. Clearly the spectrum obtained would contain very broad line if energy terms are not removed. Again, high-resolution spectra can be obtained in principle by rapidly rotating the sample at the magic angle, thereby cancelling the heteronuclear dipole-dipole coupling term. This rotation must be rapid enough on the NMR time scale to time-average all internuclear vectors.

Indeed, in ideal case, high rates of spinning can average the chemical shielding anisotropy of a sample and mimic the isotropic chemical shielding constant, which gives rise to the chemical shift in classical isotropic solution-phase samples. With lower rotation speeds, however, spinning sidebands are observed that may or may not pose a problem in spectral interpretation. A third spin system is defined by the quadrapolar nucleus. Here, the quadrapolar interaction is dominant.

The solid-state NMR experiments carried out in this work are all based on rare spin ½ nuclear systems and the method stated above is implemented to reduce or eliminate the effects of chemical shift anisotropy as well as heteronuclear dipole-dipole coupling.

CHAPTER 3. EXPERIMENTAL

3.1 Materials

Turkish Manisa Gördes zeolite, obtained from Enli Mining Corp., Izmir, Turkey, was used as the porous medium in the present study. Clinoptilolite was the predominant zeolite mineral (95% clinoptilolite) produced in Turkey, especially in the Gördes area, about 130 km northeast of Manisa. Average radius of the particles of the clinoptilolite, was 30 μm, with 59.44 m^2/g BET surface area. SEM image of the clinoptilolite sample is presented in Figure 3.1. Chemical analyses of the natural zeolite, are given in Table 3.1.
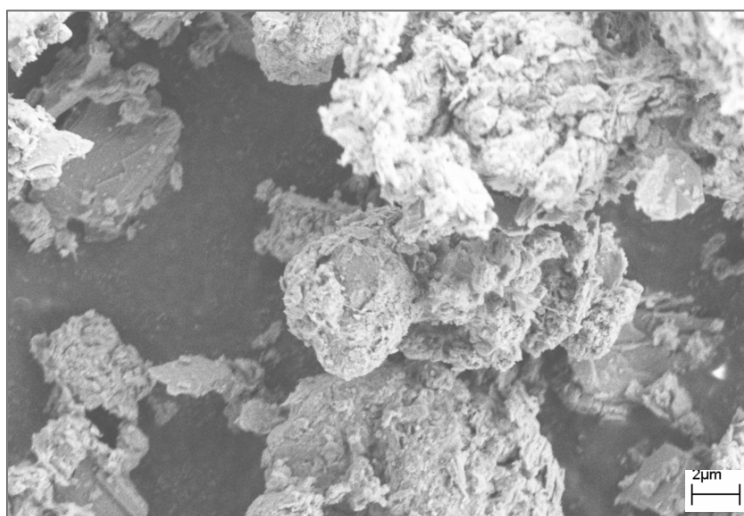
Figure 3.1. SEM images of Turkish Manisa Gördes natural zeolite.

Table 3.1. Analyses of Turkish Manisa Gördes natural zeolite.

% Clinoptilolite	95
Particle size	30 μm
Surface Analysis	**%, by volume**
Micropores	40.2
Mesopores	57.9
Macropores	1.9
Chemical Analysis	**%**
SiO_2	70.9
Al_2O_3	12.4
K_2O	4.46
CaO	2.54
Fe_2O_3	1.21
MgO	0.83
Na_2O	0.28
TiO_2	0.09
P_2O_5	0.02
MnO	<0.01

3.2 Synthesis Procedure of Templated Porous Carbons

3.2.1 Natural Zeolite Templated Porous Carbon Obtained from Sol–Gel Process using Tetraethoxy Silane (TEOS) in the Presence of Furfuryl Alcohol (FA)

A silica sol was prepared by stirring a mixture of tetraethoxy silane (TEOS),, ethyl alcohol, water and zeolite at 80°C for 3 hours. The mole ratio of TEOS, ethyl alcohol, and water was 1:4:2. Zeolite was used as an acid source. 6 g zeolite was mixed with 60 ml TEOS. After the mixture was cooled in ice bath, furfuryl alcohol (FA), as a carbon precursor, was added to the silica sol in the ratio of 2.00. This mixture was dried at 120°C for 2 hours. Gelation and polymerization took place in this step. Then the polymerized FA / silica gel was heated at a rate of 5°C/min to 700°C under 110 ml/min argon flow and held there for 3 hours to carbonize the polymerized FA. The carbonized composite was washed with excess amount of aqueous HF solution at room temperature to dissolve silica framework for 24 hours. The resulting carbon (TEOS-FA) was filtered and washed three times with water (200 ml each), and dried in an oven at 100°C.

3.2.2 Natural Zeolite Templated Porous Carbons Obtained from Furfuryl Alcohol (FA)

An excess of FA was mixed with zeolite in ratio of 10 ml FA / g zeolite, at room temperature for 5 days. The zeolite and FA mixture was then centrifuged at 2500 rpm for 30 minutes. The FA impregnated zeolite was polymerized at 80°C for 24 h under argon flow at 110 ml/min, after which the temperature was raised to 150°C for 8 hours. In order to carbonize, the polymerized FA / zeolite composite was heated to 700-1000°C at a 5°C/min rate and dwelled there for 3 h. the carbonized FA / zeolite composite was mixed with HF for 24 h. In addition to HF, concentrated HCl, HCl-NaOH (1:1, w/w), NaOH and HF-NaOH (1:1, w/w) solutions were used for carbon / zeolite composite carbonized at 700°C, for 24 h. The resulting carbon was filtered and washed three times with water (200 ml each), and dried in an oven at 100°C.

3.2.3 Natural Zeolite Templated Porous Carbon Obtained From 90% Furfuryl Alcohol (FA) – 10% Tetraethoxy Silane (TEOS) Mixture

An excess of 90 %FA and 10 %TEOS mixture was mixed with zeolite in ratio of 10 ml mixture/g zeolite, at room temperature for 5 days. The zeolite and FA mixture was then centrifuged at 2500 rpm for 30 minutes. The FA impregnated zeolite was polymerized at 80°C for 24 h under argon flow at 110 ml/min, after which the temperature was raised to 150°C for 8 hours. In order to carbonize, the polymerized FA / zeolite composite was heated to 700°C at a 5°C/min rate and dwelled there for 3 h. the carbonized FA / zeolite composite was mixed with HF for 24 h. The resulting carbon was filtered and washed three times with water (200 ml each), and dried in an oven at 100°C.

3.2.4 Polymerized Furfuryl Alcohol (FA) with Oxalic Acid

A blank experiment was done on 5 mg furfuryl alcohol mixed with 1 ml oxalic acid, as a catalyst. This mixture was carbonized under the same conditions to that of the furfuryl alcohol impregnated templates.

3.2.5 Microwave Assisted AlPO$_4$-5 Templated Porous Carbons Obtained from Furfuryl Alcohol (FA)

The same procedure for the synthesis of natural zeolite templeted porous carbons was applied to the microwave assisted AlPO$_4$-5 templated porous carbons. Oxalic acid was used as an acid source. The difference is the templating agent was AlPO$_4$-5.

3.3 Synthesis Procedure of Microwave Assisted AlPO$_4$-5

The preparation details of AlPO$_4$-5 crystallization using different initial solutions and conditions of hydrothermal crystallization using domestic microwave is given in Table 3.2.

The AlPO$_4$-5 samples were obtained by hydrothermal synthesis at 150-200°C in Teflon-lines autoclave. The reactants were 85% H$_3$PO$_4$, aluminium isopropoxide, tripropylamine hydroxide (TPAOH), tripropylamine (TPA), triethylamine (TEA) and 40% hydrofluoric acid (HF). The samples that contained the AlPO$_4$-5 crystals prepared from the starting mixture with the molar compositions given inTable 3.2.

3.3.1 The Synthesis Procedure of AlPO$_4$-5 Labeled A, H, J, K, L and M

The aluminium isopropoxide was first hydrolyzed in water, and H$_3$PO$_4$ were added. TPAOH, TPA or TEA added to the mixture according to the synthesis procedure. After the addition of HF, the gel was aged at room temperature for 2 hours and heated in the microwave oven.

3.3.2 The Synthesis Procedure of AlPO$_4$-5 Labeled B

The materials presented in Table 3.2 were mixed in three steps. Solution A was prepared by dropwise adding alumina sol into two-thirds of total water content. Solution B was prepared by dropwise addition of TEA to ice-cold diluted H$_3$PO$_4$ containing one-third the total water content. Solution B was added dropwise to solution A under vigorous stirring using a mechanical mixer at room temperature.

3.3.3 The Synthesis Procedure of AlPO$_4$-5 Labeled C and D

The H$_3$PO$_4$ dissolved in 15% of the water, is given to the Al$_2$O$_3$ suspended in 85% of the water, under strong stirring. After 5 min the uniform gel is obtained. The template was added dropwise under stirring, the agitate gel is aged for 12 h at room temperature.

3.3.4 The Synthesis Procedure of AlPO$_4$-5 Labeled E, F and G

The H$_3$PO$_4$ was diluted by adding water to 40%, and TEA was then added dropwise. At 0°C, aluminium isopropoxide was added to this mixture with strong stirring. Then the slurry was stirred for 2 h at room temperature, HF was added, and the mixture was stirred for another 2 h. the resulting gel was diluted with water.

Table 3.2. Parameters of the microwave synthesis of AlPO$_4$-5's.

| Sample Name | Molar Gel Composition | | | | | | | Mode of Heating | | | |
| | | | | | | | | First Step | | Second Step | |
	Al$_2$O$_3$	P$_2$O$_5$	TPAOH	TPA	TEA	HF	H$_2$O	Power, W	Heating Time, s	Power, W	Heating Time, s
A1	1	1	1.1	-	-	1.7	318	120	480	-	-
A2	1	1	1.1	-	-	1.7	318	120	600	-	-
A3	1	1	1.1	-	-	1.7	318	120	720	-	-
A4	1	1	1.1	-	-	1.7	318	200	300	-	-
A5	1	1	1.1	-	-	1.7	318	200	600	-	-
B1	1	1.03	-	-	3.56	-	250	120	300	-	-
B2	1	1.03	-	-	3.56	-	250	120	600	-	-
B3	1	1.03	-	-	3.56	-	250	120	1200	-	-
B4	1	1.03	-	-	3.56	-	250	120	1500	-	-
B5	1	1.03	-	-	3.56	-	250	120	1800	-	-
B6	1	1.03	-	-	3.56	-	250	200	600	-	-
B7	1	1.03	-	-	3.56	-	250	200	900	-	-
B8	1	1.03	-	-	3.56	-	250	200	1200	-	-
C1	1	1	-	-	1.5	-	150	800	60	120	600
C2	1	1	-	-	1.5	-	150	120	1200	-	-
C3	1	1	-	-	1.5	-	150	200	600	-	-
D1	1	1.1	-	-	0.7	-	50	120	300	-	-
D2	1	1.1	-	-	0.7	-	50	120	600	-	-

Table 3.2. *Continued*

Sample Name	Molar Gel Composition							Mode of Heating			
								First Step		Second Step	
	Al_2O_3	P_2O_5	TPAOH	TPA	TEA	HF	H_2O	Power, W	Heating Time, s	Power, W	Heating Time, s
E1	1	1.3	-	-	1.6	1.7	445	800	60	-	-
E2	1	1.3	-	-	1.6	1.7	445	800	60	120	120
E3	1	1.3	-	-	1.6	1.7	445	800	60	120	300
E4	1	1.3	-	-	1.6	1.7	445	800	60	120	480
E5	1	1.3	-	-	1.6	1.7	445	800	60	120	600
E6	1	1.3	-	-	1.6	1.7	445	800	60	120	900
E7	1	1.3	-	-	1.6	1.7	445	800	60	120	1200
E8	1	1.3	-	-	1.6	1.7	445	120	1200	-	-
E9	1	1.3	-	-	1.6	1.7	445	120	1500	-	-
E10	1	1.3	-	-	1.6	1.7	445	120	1800	-	-
E11	1	1.3	-	-	1.6	1.7	445	200	300	-	-
E12	1	1.3	-	-	1.6	1.7	445	200	600	-	-
E13	1	1.3	-	-	1.6	1.7	445	560	120	-	-
E14	1	1.3	-	-	1.6	1.7	445	560	180	-	-
E15	1	1.3	-	-	1.6	1.7	445	400	120	-	-
F1	1	1.3	-	-	1.6	1.7	200	800	60	120	300
F2	1	1.3	-	-	1.6	1.7	200	800	60	120	600
F3	1	1.3	-	-	1.6	1.7	200	800	60	120	900

Table 3.2. *Continued*

Sample Name	Molar Gel Composition							Mode of Heating			
								First Step		Second Step	
	Al_2O_3	P_2O_5	TPAOH	TPA	TEA	HF	H_2O	Power, W	Heating Time, s	Power, W	Heating Time, s
G1	1	1.3	-	-	1.6	1.3	440	800	60	-	-
G2	1	1.3	-	-	1.6	1.3	440	800	60	120	120
G3	1	1.3	-	-	1.6	1.3	440	800	60	120	300
G4	1	1.3	-	-	1.6	1.3	440	800	60	200	120
G5	1	1.3	-	-	1.6	1.3	440	800	60	200	300
G6	1	1.3	-	-	1.6	1.3	440	800	60	200	600
H1	1	1	-	-	1.3	1	70	120	300	-	-
H2	1	1	-	-	1.3	1	70	120	600	-	-
H3	1	1	-	-	1.3	1	70	120	900	-	-
H4	1	1	-	-	1.3	1	70	200	180	-	-
H5	1	1	-	-	1.3	1	70	200	240	-	-
H6	1	1	-	-	1.3	1	70	200	270	-	-
H7	1	1	-	-	1.3	1	70	200	285	-	-
H8	1	1	-	-	1.3	1	70	200	300	-	-
H9	1	1	-	-	1.3	1	70	200	315	-	-
H10	1	1	-	-	1.3	1	70	200	330	-	-
H11	1	1	-	-	1.3	1	70	200	360	-	-
H12	1	1	-	-	1.3	1	70	200	420	-	-

Table 3.2. *Continued*

Sample Name	Molar Gel Composition							Mode of Heating			
								First Step		Second Step	
	Al_2O_3	P_2O_5	TPAOH	TPA	TEA	HF	H_2O	Power, W	Heating Time, s	Power, W	Heating Time, s
H13	1	1	-	-	1.3	1	70	200	600	-	-
H14	1	1	-	-	1.3	1	70	200	900	-	-
H15	1	1	-	-	1.3	1	70	800	60	-	-
H16	1	1	-	-	1.3	1	70	800	60	120	300
H17	1	1	-	-	1.3	1	70	800	60	120	600
H18	1	1	-	-	1.3	1	70	800	60	200	300
J1	1	1	-	-	2.6	1	70	200	240	-	-
J2	1	1	-	-	2.6	1	70	200	300	-	-
K1	1	1	-	-	1.3	1	35	120	300	-	-
K2	1	1	-	-	1.3	1	35	120	420	-	-
K3	1	1	-	-	1.3	1	35	200	300	-	-
L1	1	1	-	1.3	-	1	70	120	60	-	-
L2	1	1	-	1.3	-	1	70	120	180	-	-
L3	1	1	-	1.3	-	1	70	120	300	-	-
L4	1	1	-	1.3	-	1	70	200	180	-	-
L5	1	1	-	1.3	-	1	70	200	240	-	-
L6	1	1	-	1.3	-	1	70	200	300	-	-
L7	1	1	-	1.3	-	1	70	200	360	-	-

Table 3.2. *Continued*

Sample Name	Molar Gel Composition							Mode of Heating			
								First Step		Second Step	
	Al_2O_3	P_2O_5	TPAOH	TPA	TEA	HF	H_2O	Power, W	Heating Time, s	Power, W	Heating Time, s
L8	1	1	-	1.3	-	1	70	200	420	-	-
L9	1	1	-	1.3	-	1	70	800	60	-	-
L10	1	1	-	1.3	-	1	70	800	60	200	60
L11	1	1	-	1.3	-	1	70	800	60	200	180
L12	1	1	-	1.3	-	1	70	800	60	200	300
L13	1	1	-	1.3	-	1	70	800	60	200	600
M1	1	1	-	2.6	-	1	70	200	180	-	-
M2	1	1	-	2.6	-	1	70	200	240	-	-
M3	1	1	-	2.6	-	1	70	200	300	-	-

3.4 Diffusion Experiments

An adiabatic isothermal setup [294], designed and built in our laboratories was used in the diffusion experiments. Sartorius CP 124S analytical balance with a 0.0001 g accuracy was placed in a Memmert Modell 300 laboratory oven. Porous carbons were grinned and sieved to 30 μm. At the start of experiment approximately 1.0000 g of 100% degassed with heating, zeolite and porous carbons were evenly distributed in a Petri dish and its initial weight was recorded. Four wide beakers filled with total 200 ml alcohol were used in each experiment and they were placed in the closest vicinity of the balance pan. The temperature of the experiment was set and the system was closed. After the temperature reached a constant set value between 24.0– 28.0°C, the weight increase of the samples due to alcohol vapor uptake was recorded at every 5 seconds with the aid of Sarto Connect software installed in the PC. Experiment was continued until the software collected 2000 data and a constant weight was attained. All experiments were at least repeated five times.

For the calculation of diffusion coefficient the following assumptions are made; the diffusion mechanism obeys Fick's law, the crystallites possess spherical shape, the concentration profile of the sorbed gas in these spheres shows radial symmetry, the diffusion is assumed to be isotropic, it can be described by a single diffusion coefficient rather than a diffusion tensor and the diffusion coefficient does not depend on sorbate concentration.

3.5 Characterization Methods

3.5.1 Surface Analysis

Surface areas of samples were measured by ASAP 2000 Accelerated Surface Area and Porosimetry system manufactured by Micromeritics Co., USA at 77K. Before the experiments the samples were heated for 12 h at 120°C and outgassed for 2 h at 350 °C. Surface area of the samples was determined by using Brunauer, Emmett and Teller (BET) method [66] in the relative pressure range of between 0.05 and 0.25, over five adsorption points. Pore size distributions were calculated using Barrett, Joyner and Halenda (BJH) method [327].

3.5.2 XRD Measurements

XRD measurements of the samples of were done with a Bruker axs advance powder diffractometer fitted with a Siemens X-ray gun and equipped with Bruker axs Diffrac PLUS software. The sample was rotated (15 rpm) and swept from $2\theta = 5^\circ$ through to 80° using default parameters of the program. The X-ray generator was set to 40kV at 40 mA. All the XRD measurements were repeated at least three times and the results reported were the average of these measurements.

The XRD patterns were analyzed for the structural parameters using the classical Debye-Scherer equations:

$$L_c = 0.90 \ \lambda / \ \beta_{002} \cos \theta_{002},$$

$$L_a = 1.94 \ \lambda / \ \beta_{100/101} \cos \theta_{100/101}$$

$$n = L_c / d_{002}$$

where

β: Full Width Half Maxima, FWHM (in radians of theta)

n: number of graphene sheets.

The peak positions of the (002) peak was measured and Bragg's Law was used to calculate the interlayer spacing d_{002}. L_c, L_a and d_{002} are indicated in our previous study[2]. The full widths were calculated at the half maxima (FWHM) with the Bruker axs Diffrac PLUS software provided with the Bruker axs advance powder diffractometer of the peak positions of (002) and (100)/(101) peaks.

3.5.3 NMR Measurements

Samples were probed further by ^{13}C CPMAS, ^{29}Si CPMAS, ^{19}F MAS and ^{27}Al MAS NMR using an Inova 500MHz NMR Varian system. ^{13}C CPMAS, ^{29}Si CPMAS, ^{27}Al MAS NMR and ^{19}F MAS spectra were acquired at 125 MHz, 100 MHz, 130 MHz and 8-15 kHz fields respectively, using Si_3N_4 rotors set to 6 Hz. In the ^{19}F MAS spectra, spinning at different speeds is necessary to ensure no spectral overlap of spinning sidebands with the signals. Pulses were separated by a 1s delay in the case of carbon, 2s delay in the case of silicon and 0.25s delay in the case of aluminium.

3.5.4 FT-IR Analyses

FT-IR spectra of samples were measured with a Bruker EQUINOX 55 FT-IR spectrometer. Samples were dried under a nitrogen atmosphere at 110^oC for 24 hours. KBr pellets were prepared by grinding 2.5 mg of dry sample with 200 mg of dried KBr. Spectra were obtained with 200 scans at a resolution 2 cm^{-1}.

3.5.5 Scanning Electron Microscopy (SEM)

Leo Supra 35VP Field emission scanning electron microscope, Leo 32 and energy dispersive spectrometer (EDS) software was used for images and analysis. Before analysis samples were coated with carbon by Emitech, T950x Turbo Evaporatore. Imaging was generally done at 2-5 keV accelerating voltage, using the secondary electron imaging technique.

CHAPTER 4. RESULTS AND DISCUSSION

4.1 Synthesis of Porous Carbons Using Natural Zeolite as a Template

Natural zeolite was used as a template for the synthesis porous carbons. BET surface area of natural zeolite was 59 m^2/g. N$_2$ adsorption/desorption isotherms and pore size distribution were given in Figure 4.1. Average pore diameter of natural zeolite was 39 Å, indicating mesoporosity.
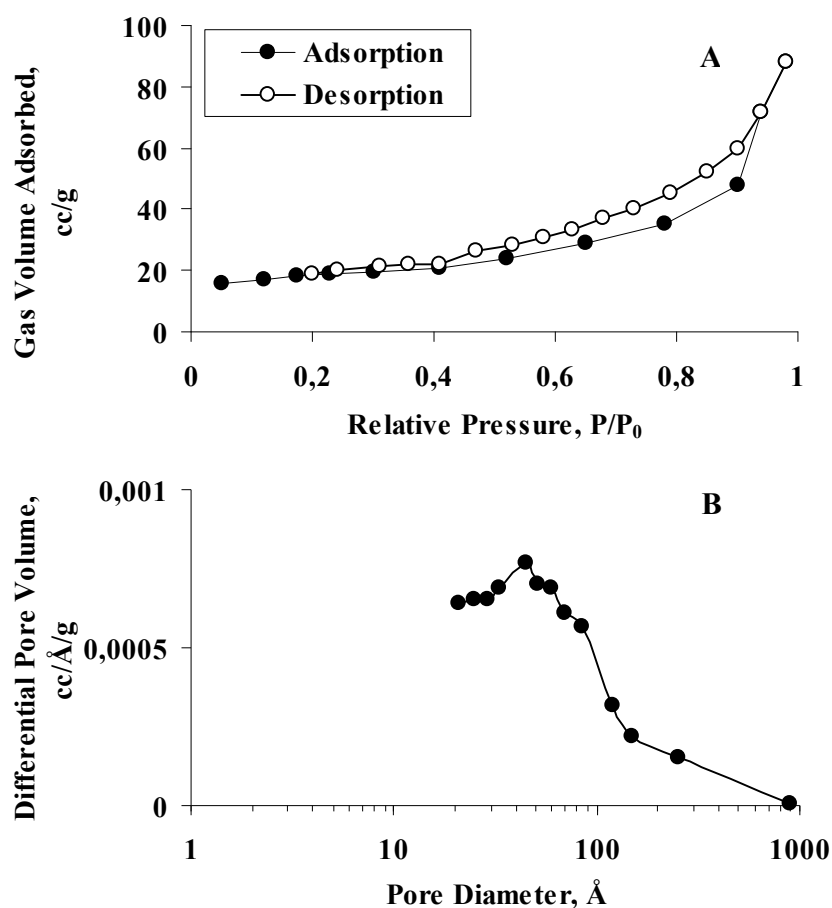
Figure 4.1. A. N$_2$ adsorption/desorption isotherms and **B.** Pore size distribution of the natural zeolite.

Poly(furfuryl alcohol), PFA, is a common typical thermosetting resin that forms carbon with a high yield on carbonization that generally used as an organic precursor for the production templated carbons [73-75]. In order to have an indication about carbonization of the PFA, a blank experiment was done. SEM image of non-templated carbon was shown in Figure 4.2. According to the Energy Dispersive Spectroscopy, EDS, analysis, the composition of non-templated carbon consisted of 100% C, which had a BET area 18 m^2/g.
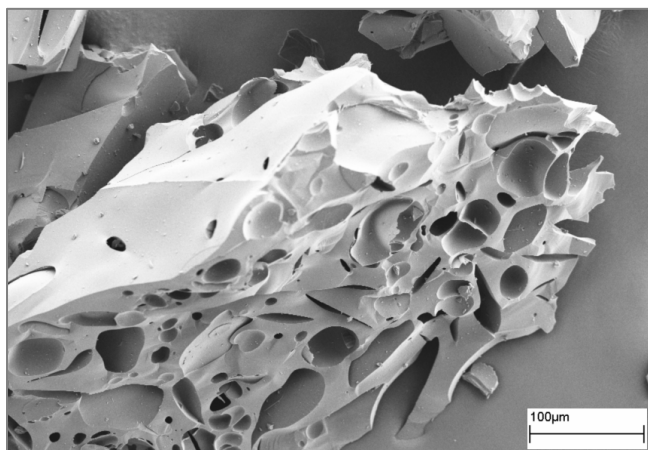
Figure 4.2. SEM image of non-templated polymerized and carbonized furfuryl alcohol.

Natural zeolite was used as an acid source for catalysis in the sol-gel process at which TEOS was utilized in the presence of FA. Hydroxyl groups adjacent to aluminium in the aluminosilicate framework catalyze the polymerization reaction of the FA as Brønsted acid sites [104]. After dissolution of silica network with HF, TEOS-FA carbon was produced that consisted of 100% C and BET area was 804 m^2/g. SEM image of TEOS-FA carbon was shown in Figure 4.3.

Figure 4.3. SEM image of TEOS-FA carbon.

PFA was carbonized inside the natural zeolite channels at different temperatures. Porous carbons were obtained after HF washing of the template. BET surface area of zeolite-carbon composite was 63 m^2/g, before the acid treatment. BET surface areas of natural zeolite templated carbons were measured as 397, 350, 405 and 367 m^2/g at 700, 800, 900 and 1000°C, respectively, and they are presented in Figure 4.4. BET surface areas seemed not to change with increasing temperature. SEM images of the natural zeolite templated carbons shown in Figure 4.5, indicated that zeolite framework is mimiced in the templated porous carbons. N_2 adsorption/desorption isotherms and pore size distribution of natural zeolite templated carbons were presented in Figure 4.6 and Figure 4.7, respectively. All of the isotherms of porous carbon are similar. Closure at P/P_0 indicates that the presence of small mesopores and the hysteresis indicates the capillary condensation in mesopores. Average pore diameter of porous carbons, carbonized at 700, 800, 900 and 1000°C, were measured as 11 nm, this indicated the presence of pores of mainly mesoporous.
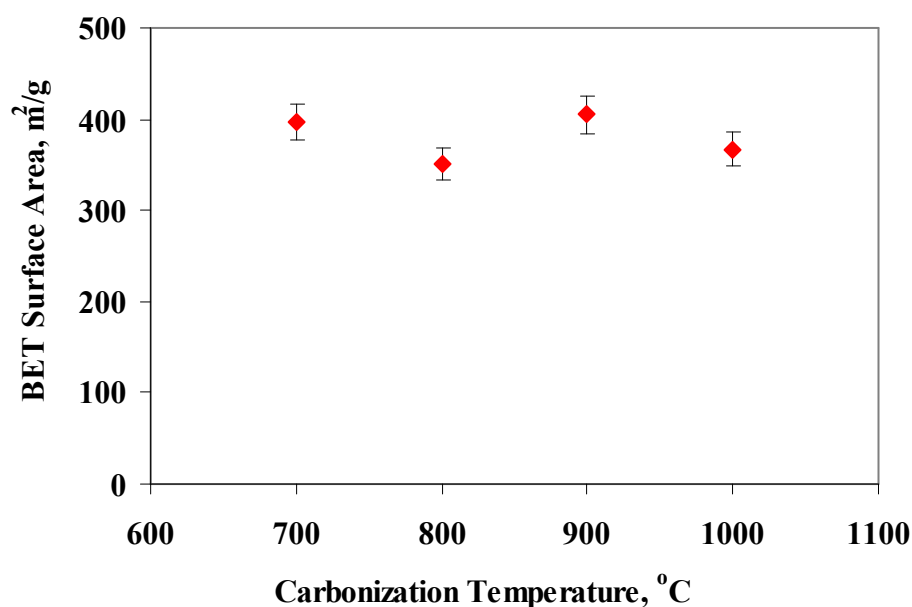
Figure 4.4. Change of BET surface area of natural zeolite templated carbons carbonized at different temperatures.
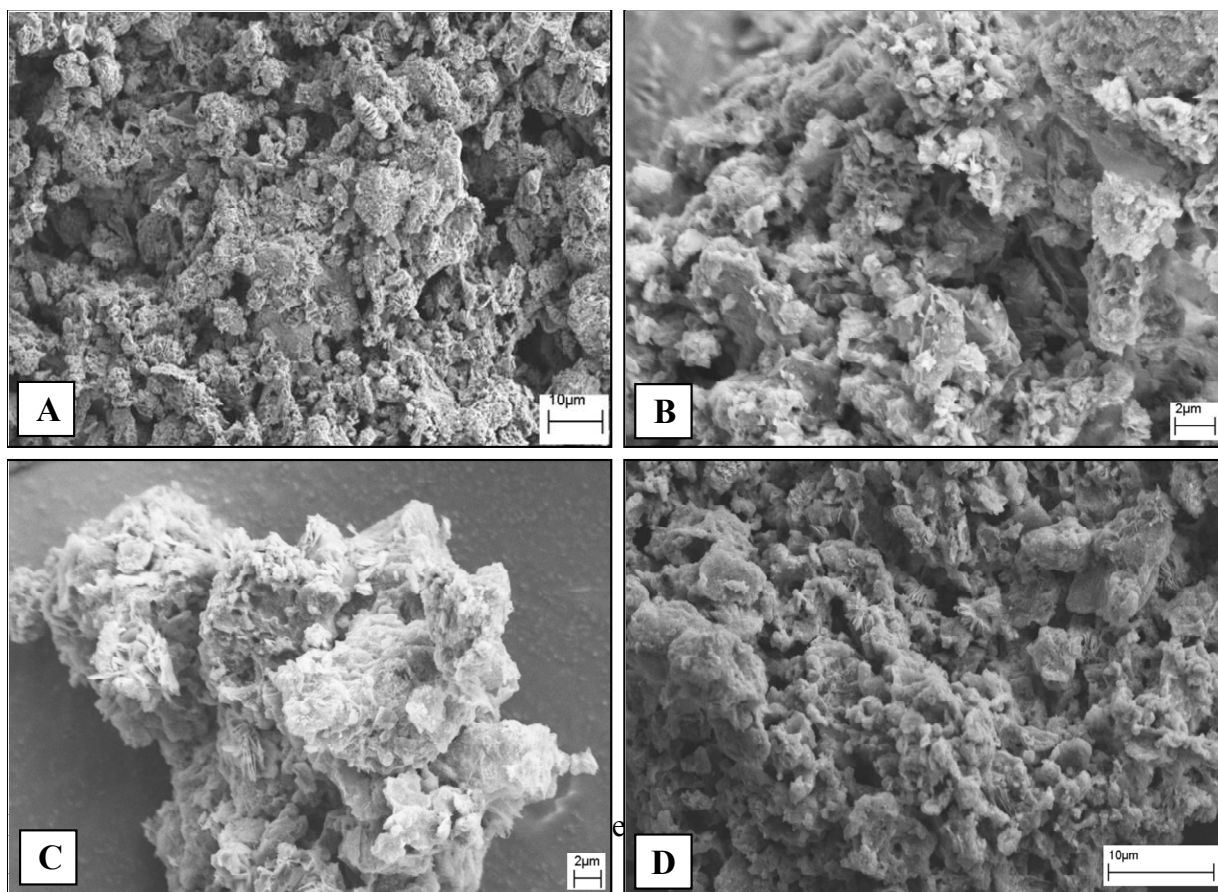
EDS analyses of natural zeolite templated carbons at different temperatures are presented in Table 4.1. Carbon contents of the porous carbons were 91%, 96%, 99% and 92% C at 700, 800, 900 and 1000°C respectively. The success of the demineralization step was indicated by both the high carbon content and the small quantities of silicon and aluminium. Porous carbons contained some amount of fluorine resultant of the HF treatment, which reduced from 5.4% to 1.5% as the temperature was increased from 700 to 1000°C.

Table 4.1. EDS analyses of natural zeolite templeted carbons.

Element	Atom. C, At. %			
	700°C	800°C	900°C	1000°C
Carbon	91.14	95.79	98.79	92.03
Fluorine	5.39	2.22	0.78	1.51
Magnesium	0.09	0.12	-	035
Aluminium	0.14	0.33	0.13	0.41
Oxygen	3.24	1.47	0.30	5.46
Silicon	-	0.07	-	0.24

Carbonization of pure FA in the zeolite channels at 700°C produced a carbon material with BET area of 397 m^2/g, whereas addition of 10% TEOS (90%FA-10%TEOS carbon) into the system increased BET surface area of the material produced to 430 m^2/g. The porous carbons obtained from intercalated matrix templates has 400 m^2/g BET surface reported previously [62]. Meyers et al. [148] synthesized porous carbon materials from acrylonitrile as a carbon source, has BET surface area between 458 and 504 m^2/g by using FA, between 245 and 636 m^2/g by using pyrene as a carbon source inside the zeolite (Y, Beta, and ZSM-5) channels. The generally high surface areas of these carbons might result from the kinetics of dehydroxylation, which are faster than the kinetics of carbonization and which may cause the carbons to separate from the template and develop into small microporous particles [148].

After filtration of the used-FA filtrate, the filtrated FA was used to synthesize porous carbon to understand the efficiency of the process. The second used-FA was utilized for the carbonization process. BET surface areas of the used-FA and new-FA which was carbonized at 700°C, were measured as 398 m^2/g and 397 m^2/g. In conclusion, this indicated that recycled-FA could be used for this process.
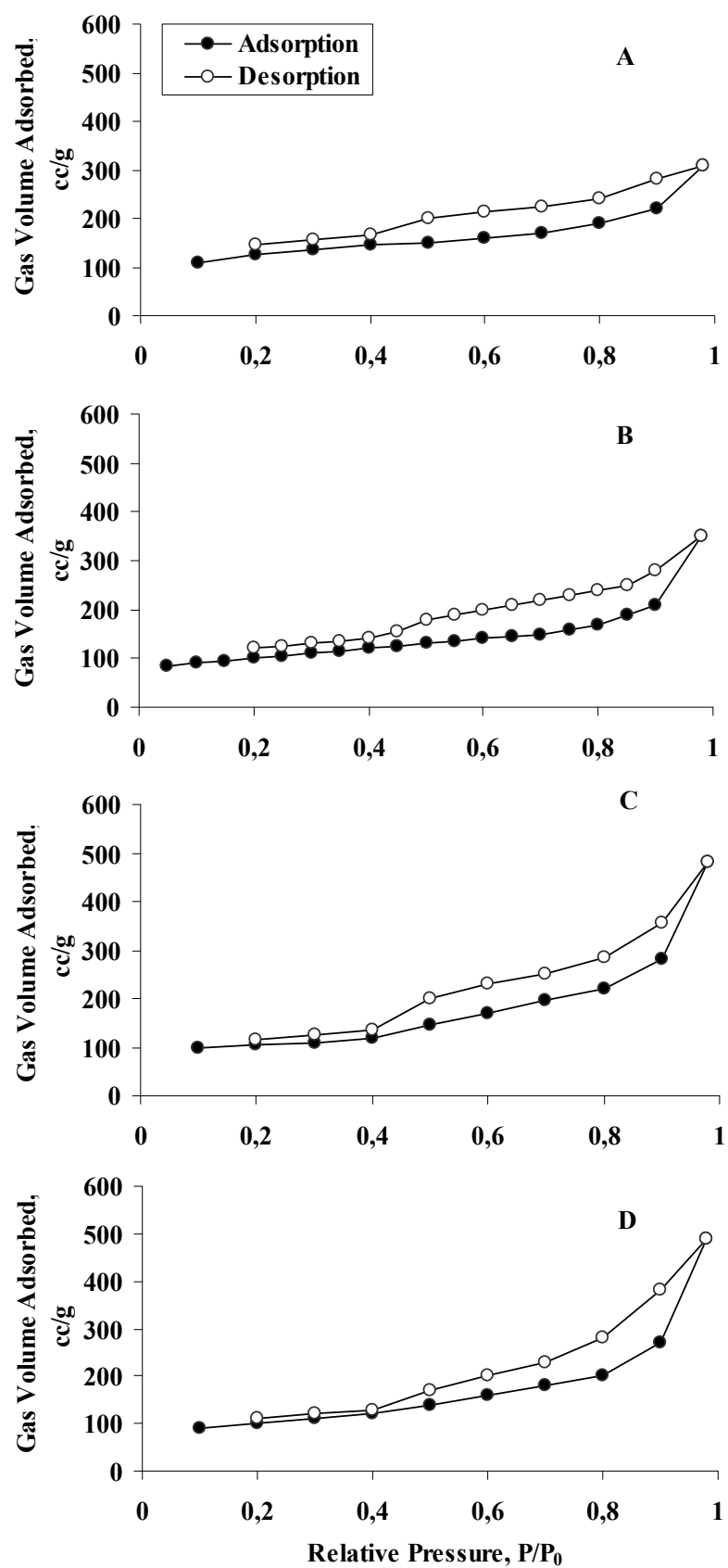
Figure 4.6. N_2 adsorption/desorption isotherms of natural zeolite templated carbons, carbonized at **A.** 700°C, **B.** 800°C, **C.** 900°C and **D.**1000°C.
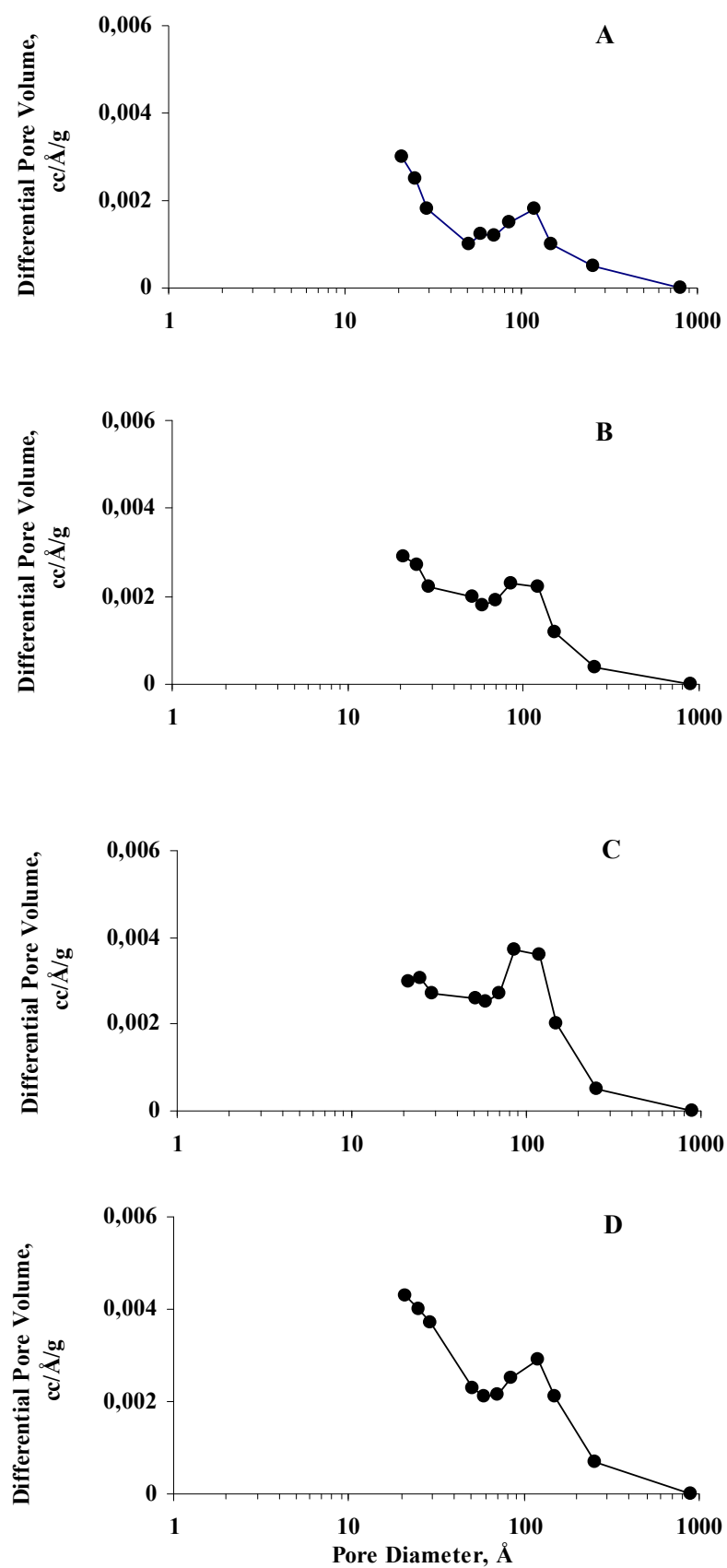
Figure 4.7. Pore size distribution of natural zeolite templated carbons, carbonized at
A. 700°C, **B.** 800°C, **C.** 900°C and **D.**1000°C.
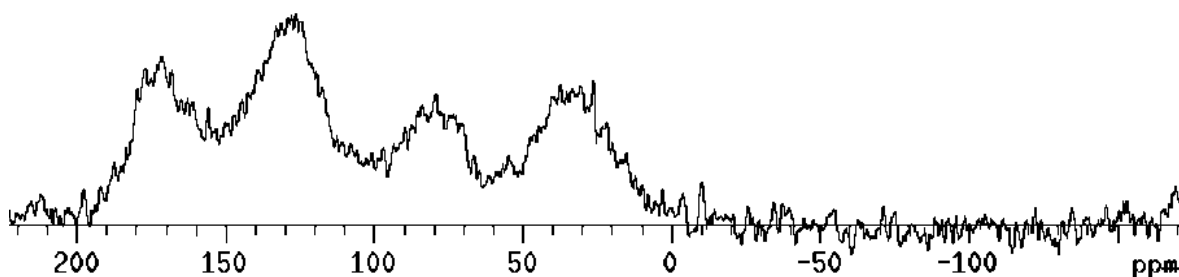
Figure 4.8. ^{13}C NMR of natural zeolite templated carbon, carbonized at 700°C.

A representative ^{13}C NMR spectrum of the natural zeolite templated carbon, produced at the temperature of carbonization of 700°C is shown in Figure 4.8. The peaks in the ^{13}C NMR spectrum were found to be real peaks and there were no side bands whatsoever. The *sp³*-hybridized carbon at 30 ppm [328], *sp*–hybridized carbon at 80 ppm, *sp²*-hybridized carbon due to graphite or graphite-like domains at 127 ppm [133,328-330] and alkoxy and OH substituted carbon at 175 ppm were observed in the spectrum. 700°C was considered as medium range temperature in the carbonization of coals and the presence of all types of carbon bands at this range of temperatures seemed to be quite evident. A small line observed at 42 ppm can be attributed to –CH and –CH₂ groups. Broad signal at 39 ppm shows crosslinking between oligo FA and PFA sequences [76] and due to the cross-linking through these methylene groups [115]. The ^{13}C signals for the olefinic carbon atoms are not resolved, but they are clearly detectable in the solid-state ^{13}C NMR spectrum as a broad signal between 120 and 140 ppm [76].

The FT-IR spectra of porous carbons, obtained at at 700, 800, 900 and 1000°C were presented in Figure 4.9. In all of the recorded spectra, in the 3500-3400 cm^{-1} ranges, a band of O-H stretching vibrations, due to the existence of surface hydroxylic groups was observed. The asymmetry of this band at lower wave numbers indicates the presence of the strong hydrogen bonds [331-333]. Peaks observed at 3135 cm^{-1}, between 1450-1200 cm^{-1} and 1259 cm^{-1} due to =C-H stretching band, -C=C-H in-plane C-H bend and -C≡C-H bend overtone respectively [332,333].

The presence of adsorption bands characteristics of -CH₃ and/or -CH₂- structures (2946-2958, 2915-2916 and 2847-2854 cm^{-1}) in all spectra suggests the existence of some asymmetric and symmetric C-H stretching vibrations, *sp³* hybridized carbons, in aliphatic

species on the porous carbons [333]. The presence of these bonds seemed to decrease with increasing the carbonization temperature.

The band observed in the region of 1631-1664 cm^{-1} is olefinic C=C stretching band, the absorption maximum of this band shifted toward lower wavenumbers with increasing the carbonization temperature until 900°C, when the C=C bond is conjugated with another C=C bond, an aromatic nucleus, or a C-O bond [334]. The 1250-1100 cm^{-1} band is associated with the C-F stretching vibrations [332]. The band around 1735 cm^{-1} is attributed to AlH_4^+ due to undissolved zeolite residues [332]. Broad bands at 1300–1000 cm^{-1} have been assigned to C–O stretching [335].
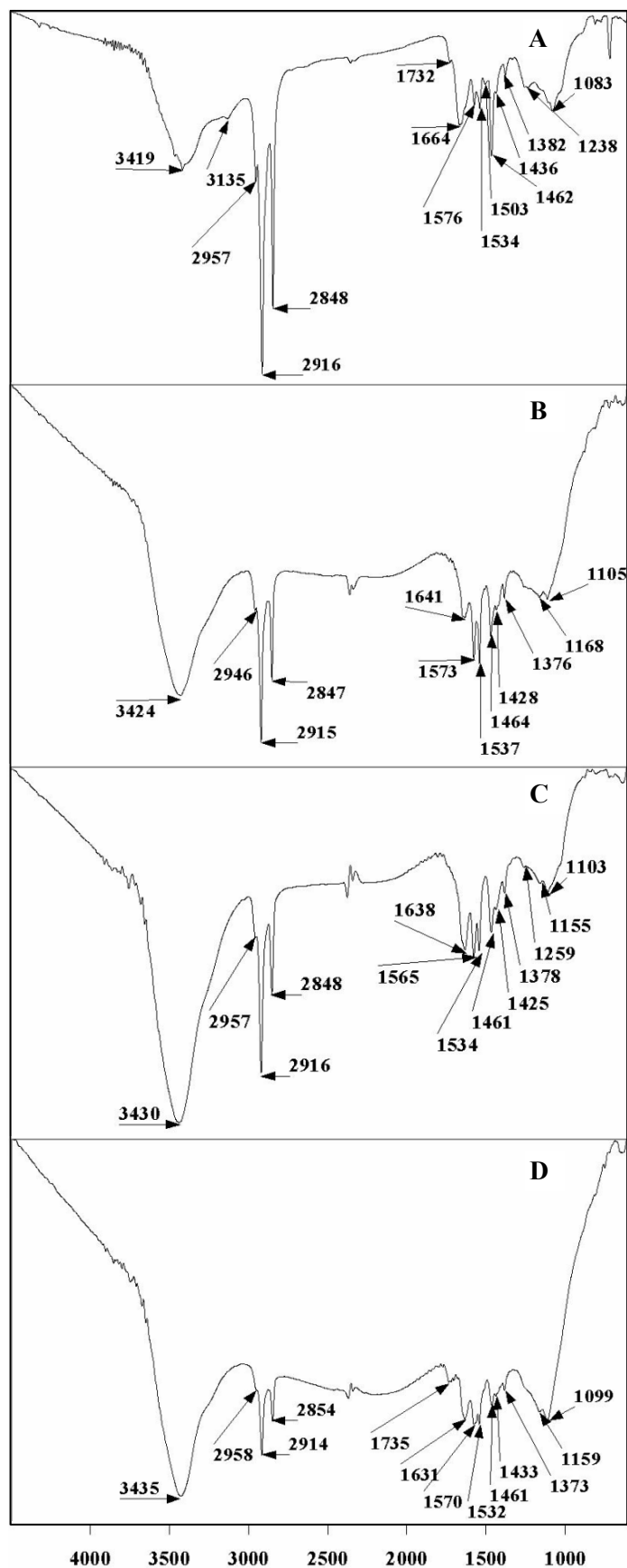
Figure 4.9. FT-IR spectra of natural zeolite templated carbons, carbonized at **A**. 700°C, **B.** 800°C, **C.** 900°C and **D.** 1000°C.

The XRD patterns of the porous carbons produced at different temperatures are presented in Figure 4.10. The d_{002} values of the carbons were calculated from the XRD patterns. The resultant porous carbons display two large diffraction peaks near $2\theta = 26°$ and $44°$, which are characteristic of a disordered carbonaceous structure. By analogy with disordered carbon, two peaks can be indexed as the (*002*) and (*100*) reflections of the hexagonal structure of graphite. A broad peak at $2\theta = 26°$ represents *(002)* reflection of carbon due to the stacking structure of aromatic layers [2]. The interlayer spacing (d_{002}) of the carbon is traditionally used to estimate a graphitizaton degree of the carbon and, in general, growing disorder in the materials is reflected in increased values of d_{002}.
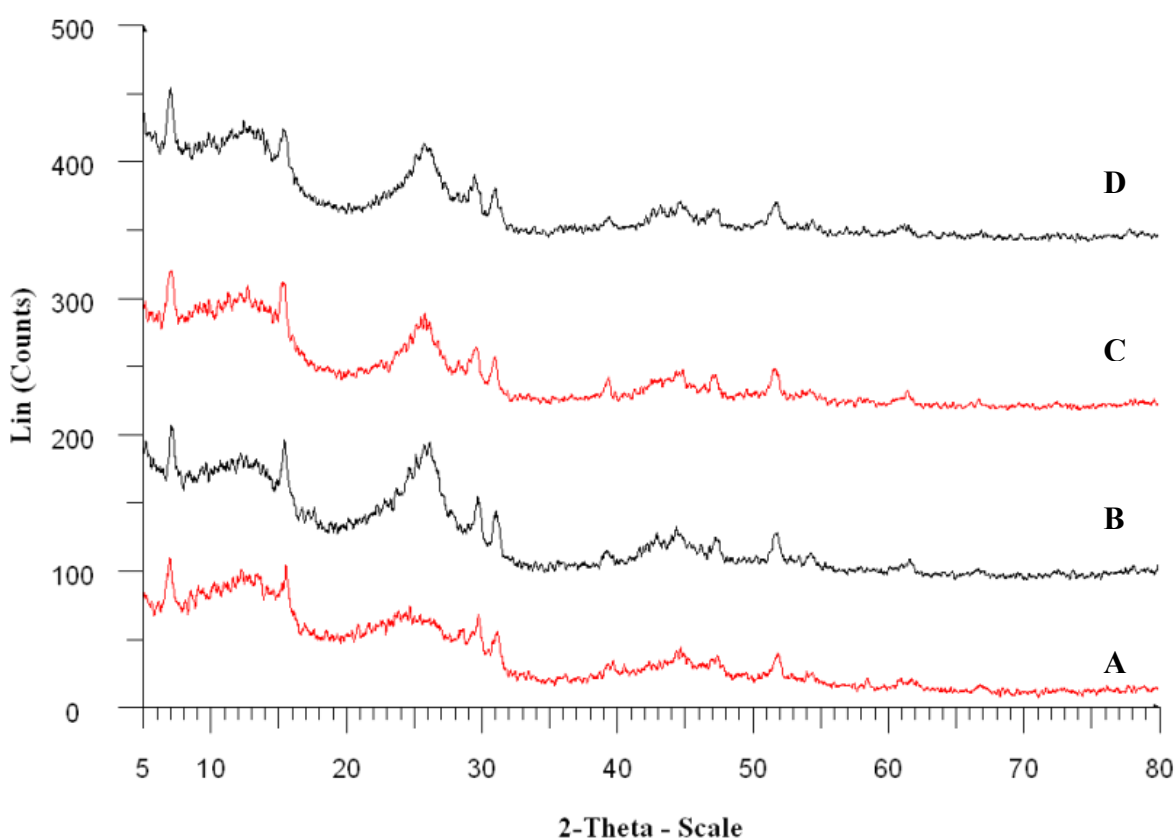
Figure 4.10. XRD patterns of natural zeolite templated carbons, carbonized at **A.** 700°C, **B.** 800°C, **C.** 900°C and **D.**1000°C.

The d_{002} values of the carbon synthesized by carbonization of 100% FA in the channels of zeolite were presented in Table 4.2. The results presented in the present work might be considered as indications for the present of turbostratic (fully disordered) structures in the temperature range of 700-1000°C.

Table 4.2. Change of interlayer spacing of carbons natural zeolite templated carbons carbonized at different temperatures.

Carbonization Temperature, °C	d_{002}, nm	Relative intensity of (002) peak
700°C	0.358	1.00
800°C	0.347	0.85
900°C	0.349	0.61
1000°C	0.346	0.70

The relative intensities of (002) peaks were 1.00, 0.85, 0.61 and 0.70 for 700, 800, 900 and 1000°C, respectively. The d_{002} intensities decreased with increasing temperature after 700°C. The decrease of the intensity of the (002) peaks in the present report could be explained by the loss of amounts of carbon from large turbostratic crystallites which is quite evident that as the temperature is increased carbon losses are expected to increase in pyrolysis reactions [2]. Addition of 10% TEOS (90%FA-10%TEOS carbon) into the system caused a decrease in the d_{002} value from 0.358 nm to 0.353 nm, at 700°C.

Barata-Rodriques et al. [147] observed d_{002} = 0.342 nm for the zeolite templeted carbon which is larger then the ideal graphite indicating that the carbon was formed disorder.

XRD patterns of the non-templated carbon and TEOS-FA carbon was shown in Figure 4.11. The d_{002} value of ideal graphite is 0.3354 nm, same as the d_{002} value of non-templated carbon. The d_{002} value of TEOS-FA carbon was 0.364 nm. Sakintuna et al. [2] recently reported d_{002} values of activated carbons as 0.35–0.39 nm.

The literature on templated carbons that were reported previously [133] showed a sharp peak around 2θ = 6° in addition to a broad peak around 25° in the XRD patterns, indicating that these carbons had a structural regularity that was not detected in the present study.

Graphene layers are the basic building block of carbon particles and these layers exhibit numerous distortions and discontinuities. Some regions, however, have a more regular, graphite-like arrangement. The dimensions of these graphitic domains are characterized by the average stacking height of the parallel layers in the ''c'' direction (L_c) and by the average diameter of the c parallel layers in the ''a'' direction (L_a). These two dimensions can be determined by Debye–Sherrer equation [2].

According to Debye-Scherer equations, calculated values of L_c and L_a values of non-templated carbon were 1.44 nm and 5.96 nm respectively and L_c and L_a values of TEOS–FA carbon were 2.29 nm and 5.35 nm respectively.
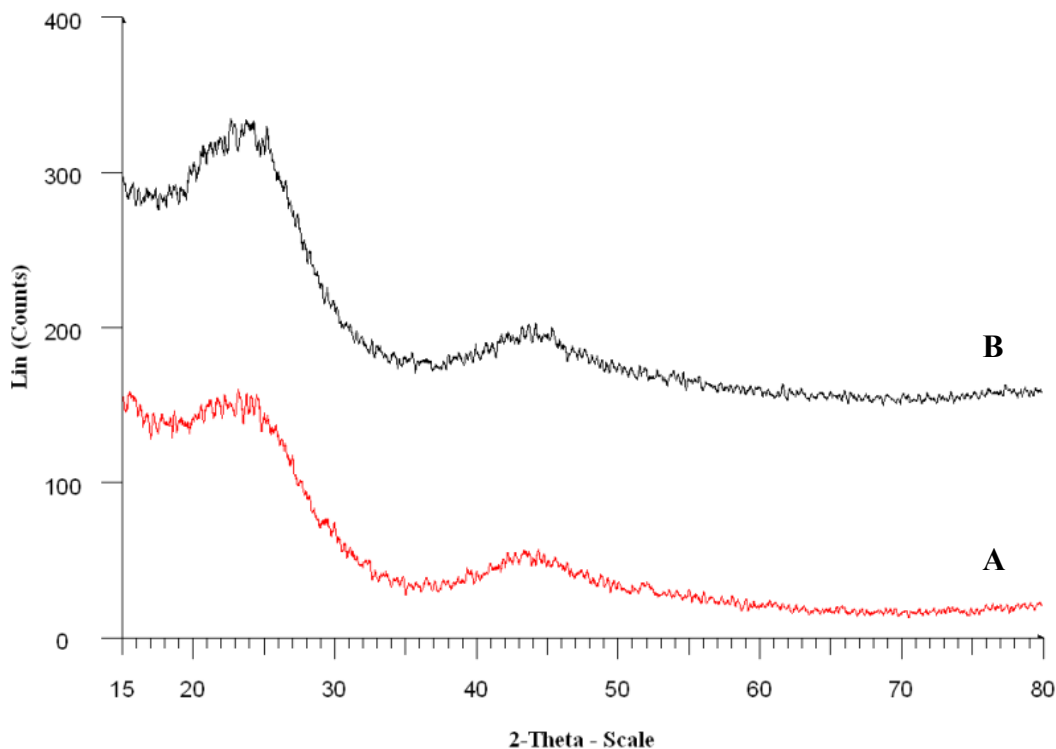
Figure 4.11. XRD patterns of **A.** non-templated carbon, **B.** TEOS-FA carbon.

Stacking height, L_c values and the average number of graphene sheets per stack increased with increasing temperature which was calculated from XRD patterns shown in Figure 4.12 and Figure 4.13 respectively. L_c values increased from 2.79 nm to 6.64 nm, and average number of graphene sheets increased from 8 to 19 when temperature was increased from 700°C to 1000°C. Calculated values of L_c from the XRD pattern of natural zeolite templated process using 90%FA-10%TEOS mixture was 3.00 nm. In general terms, the results indicated that L_c increased monotonically with temperature of pyrolysis as we discussed in our previous study [2]. Kercher and Nagle [15] reported that with increased pyrolysis temperature, the crystallite boundary area decreased from turbostratic crystallite growth and number of graphene sheets increased. The reason for the increase in the stacking height could be related to heat treatment temperature only. The growth of the carbon layer plane might be due to the increase of van der Waals forces between the layers which resulted in increases of the stacking number; hence the coalescence of the units was

probably accelerated also in temperatures between 700-1000°C, as it was also observed in the present work.
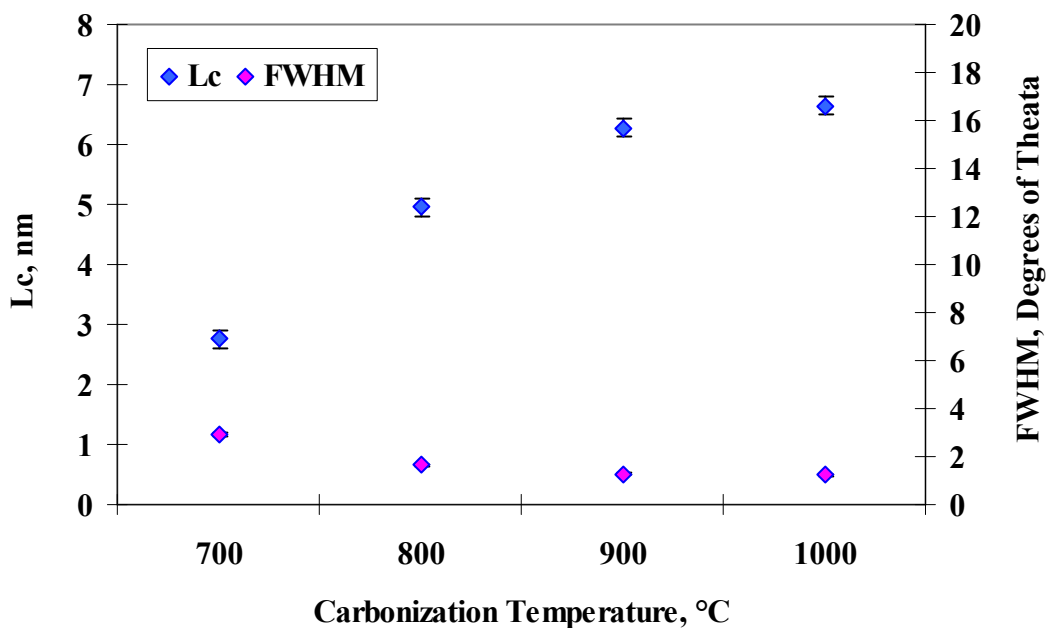
Figure 4.12. Change of FWHM and L_c values of natural zeolite templated carbons carbonized at different temperatures.

Previously three critical temperatures were found on pyrolyzing PFA [77]. The molecular structure of PFA is degraded at about 400°C and carbonization begins. Then, when the temperature reaches 550°C a large number of small graphitic crystalline nuclei are formed. As the temperature is further increased to about 700°C the nuclei grow and large crystalline grains are observed. The size of the microcrystallites increases quickly with increasing pyrolytic temperature as well as with increasing heat-treatment time at this period. The three critical temperatures are called carbonization temperature, nucleation temperature and crystallite growth temperature, respectively. 600°C is a temperature at which microcrystallites of graphite are expected to form but their size is smaller than that obtained above the crystallite growth temperature [77].
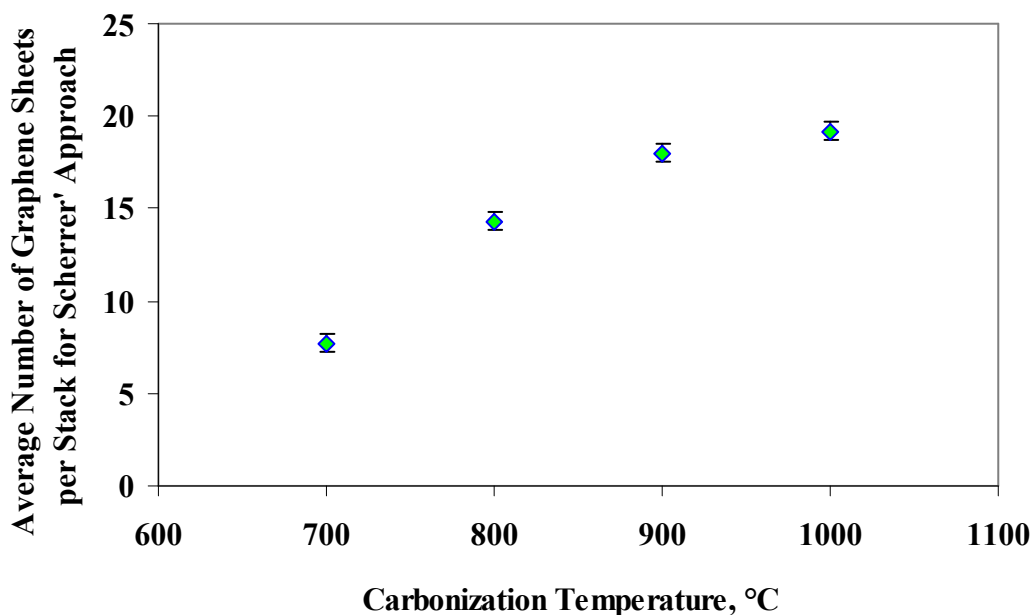
Figure 4.13. Change of the average number of graphene sheets of carbons natural zeolite templated carbons carbonized at different temperatures.

4.1.1 Organoaluminium Fluoride Structures

During removal of the zeolite template by HF washing in addition to the carbon structures some flower-like shaped organoaluminium fluoride compounds which consisted of mainly fluorine, carbon, oxygen and aluminium were observed in the SEM images. Organoaluminium fluorides constitute a very distinct family of chemical compounds. They contain both strong and highly polar Al–F bonds (580–670 kJ/mol) and also more covalent and much weaker Al–C bonds (255–280 kJ/mol) [336]. This ambivalence plays a major role throughout their chemistry. They were originally synthesized by Ziegler with the aim of employing them as intermediates in the synthesis of trialkylalanes that were applied, at that time new, catalytic system for the polymerization of olefins [337]. In spite of their growing number, organoaluminium fluorides remain rare in comparison with other halide derivatives.

The reactions with HF or other protic reagents with AlR_3 were not frequently considered as suitable routes to organoaluminium fluorides because of the possible uncontrolled alkane elimination from labile Al–C bonds. A patent claiming only a partial alkyl displacement in the synthesis of organoaluminium difluorides by the reactions of AlR_3 with HF for a variety of alkyl and aryl substituents was filed [336].

^{27}Al and ^{29}Si MAS NMR spectra of natural zeolite are shown in Figure 4.14A and Figure 4.14B, respectively. ^{29}Si MAS NMR and ^{27}Al MAS NMR spectra of the zeolite used gave information about the Si atoms coordinated (via oxygen) with neighbouring Al atoms and about tetrahedrally coordinated Al atoms, respectively. The peak near ~60 ppm in the ^{27}Al MAS NMR spectrum was due to aluminium atoms that are tetrahedrally connected to the framework (Al(OSi)$_4$) [338,339]. Since the tetrahedrally coordinated Al atoms in the lattice of zeolites, are positively charged, these are the sites to which the acid OH groups are coordinated. The ^{29}Si MAS NMR spectral resolution deteriorates due to chemical shift dispersion introduced by lattice distortions upon Al incorporation in the zeolite lattice, further complicated by spectral overlap among the various inequivalent tetrahedral Si sites [340]. According to Figure 4.14A and Figure 4.14B, Si^{+4} and Al^{+3} are present in tetrahedral environment of shared oxides ion in natural zeolite.
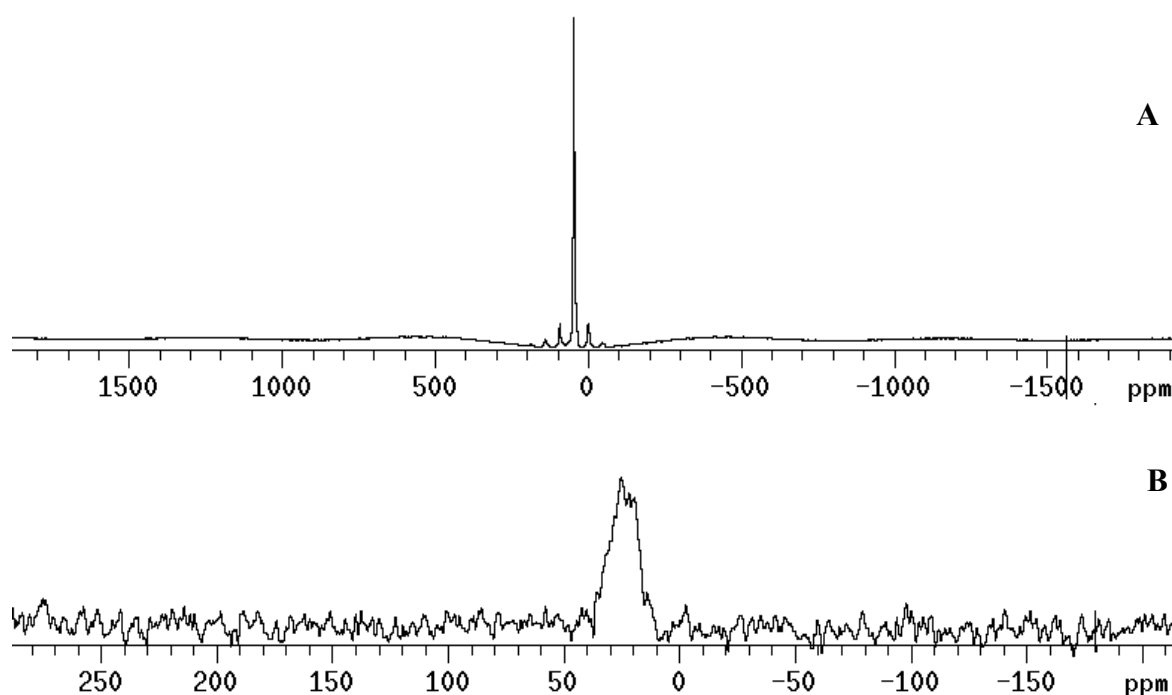
Figure 4.14. A. ^{27}Al NMR, **B.** ^{29}Si MAS NMR spectra of the natural zeolite.

The band observed at 1083 cm^{-1} in FT-IR spectrum shown in Figure 4.9, is due to O-H and C-O stretchings. The 1250-1100 cm^{-1} band is associated with C-F stretching vibrations [332]. The band around 1735 cm^{-1} and 1436 and 1462 cm^{-1} is attributed to AlH$_4^+$ and Al species due to organoaluminium fluorides [332,341]. A broad band at 1382 cm^{-1} have been assigned to C-H$_2$ bending and CF$_2$H stretchings [332].

The L_c value of the HF washed carbon was 2.76 nm. Giraudet et al. [342] calculated the d_{002} values of the treated CF are between 0.34 and 0.37 nm and L_c values are between 1.2 and 6.9 nm. Fluorine can easily accept electron from graphite in the presence of a fluoride such as HF to form mobile HF_2^- anions and is easily intercalated between graphene layers [343]. If fluorine atoms make a single intercalated layer between each pair of graphene layers, L_c values of carbonfluorides are in the range of 0.50–0.60 nm [343]. These values indicated that fluorine was attached to the carbon surface, not bonded inside the graphite layers.

SEM images of the zeolite templated carbons that were washed with HF contained flower-like structures were shown in Figure 4.15. Flower-like structures were of about 10 μm in diameter in porous carbon, carbonized at 700°C, while about 4 μm in diameter and in different shape at carbon, carbonized at 1000°C. EDS analyses of these structures were presented in Table 4.3. Compositions of the flower–like structures changed with the carbonization temperature. They were mainly formed from fluorine, carbon, oxygen and aluminium. With the increase in carbonization temperature, while the fluorine and carbon contents indicated a decreasing trend, the contents of oxygen and aluminium seemed to increase. Almost all silicon was washed away with HF washing; this was confirmed also with ^{29}Si NMR spectra. Upon removal of the matrix by the hydrofluoric acid, very reactive sites on the carbon surface became accessible. These sites were so active that they reacted with hydrofluoric acid. Fluorine, which is the most electronegative element, had a marked effect on the core-level binding energies of the heteroatom to which it is linked [344]. Fluorine up to 60% were found to be present in these flower-like structures while the carbon structures obtained in the same experiments contained only 0.78 % fluorine on the mesoporous carbons, liberated from matrix by HF. Darmstadt et al. [103] also found 0.8% fluorine on the surface of mesoporous carbons.

The raw natural zeolite was washed with excess hydrofluoric acid to check whether HF washing also formed similar flower-like structures. Flower–like structures were also formed, as shown in Figure 4.16, but these are comparably much small in size and their analysis with EDS indicated 57.5% fluorine, 37.5% oxygen and 3.0% aluminium but no carbon. The adsorption of H^+ on surface functional species, leads to dissolution of silicon and to the formation of Al-O, and facilitates the detachment of Al-OH. Because of their high electronegativity, terminal fluorine atoms show a remarkable propensity for forming bridging bonds to electropositive centers [336]. Acid leaching causes (i) Al and

extraframework cation depletion on the surface leading to an amorphous silica layer and (ii) depletion of extra framework cations in the core of the crystals where the zeolite framework is still intact [345]. The other leaching solutions, HCl, NaOH, HCl-NaOH, and HF-NaOH used did not produce any of the flower-like structures.
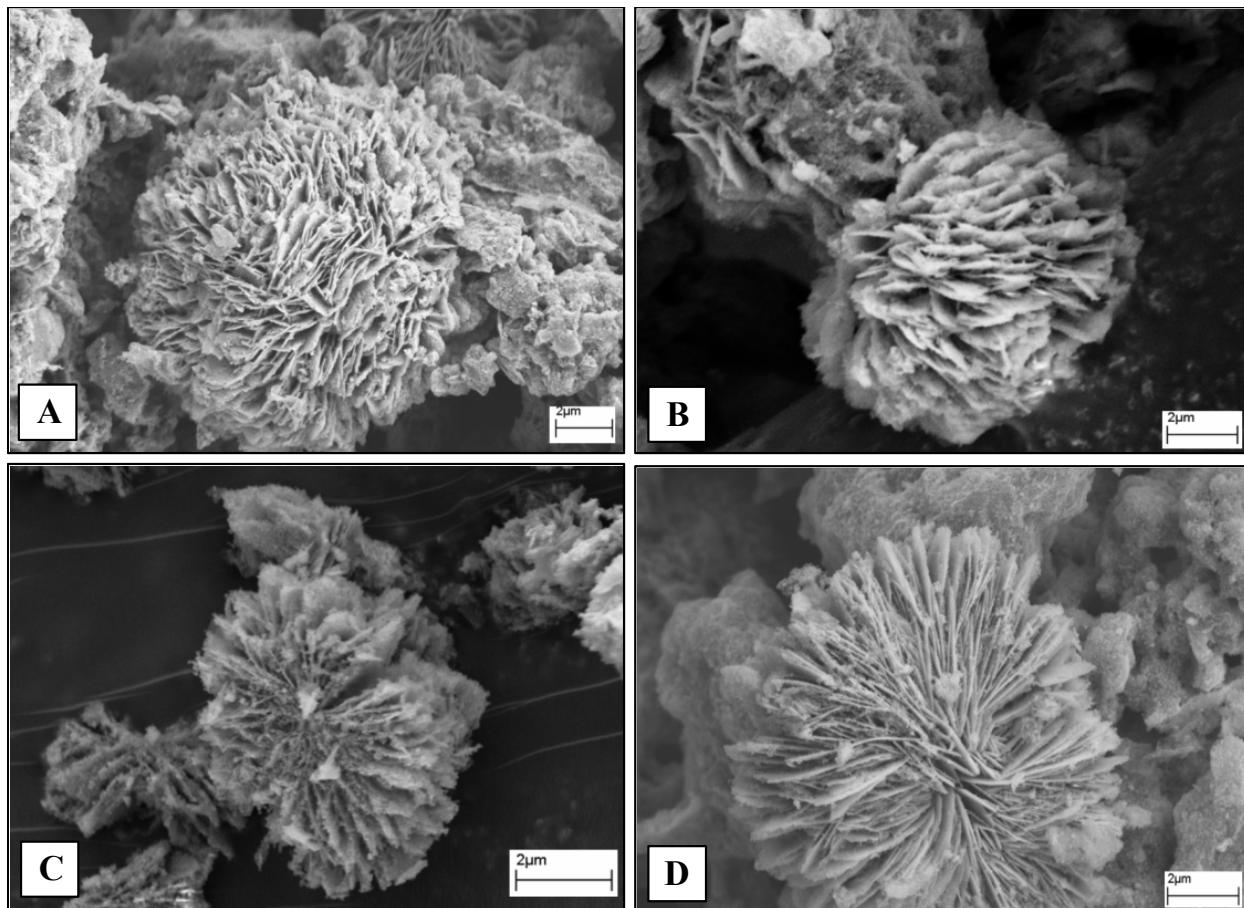
Figure 4.15. SEM image of HF washed natural zeolite templated carbons, carbonized at **A**. 700°C, **B.** 800°C, **C.** 900°C and **D.** 1000°C.

Table 4.3. EDS analyses of flower-like structures of the HF washed natural zeolite templated carbons, carbonized at different temperatures.

Element	Atom. C, At. %			
	700°C	**800°C**	**900°C**	**1000°C**
Carbon	12.98	31.11	18.01	13.25
Fluorine	69.69	54.00	52.03	62.07
Magnesium	-	0.01	0.88	0.75
Aluminium	1.50	3.14	4.92	4.93
Oxygen	9.86	11.75	24.17	18.73
Silicon	-	-	-	0.28

Figure 4.16. SEM image of HF washed raw natural zeolite.

According to XRD pattern of zeolite templated carbons that were washed with HF, peaks were matched to aluminium hydroxide fluoride, $Al(OH,F)_3$ [346], evaluated with XRD software, shown in the Figure 4.10. Aluminium hydroxide fluoride is a face-cantered cubic that has a peak with highest intensity, was *(111)* plane with 0.57 nm *d* spacing. Since AlF_2^+ ions compete successfully for F^- over Ca^{2+} and Mg^{2+}, insoluble CaF_2 and MgF_2 do not form [339]
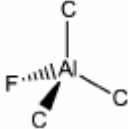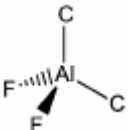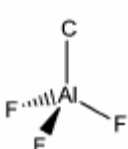
The solid-state ^{19}F MAS NMR spectra of the natural zeolite templated carbon, carbonized at 700°C, were presented in Figure 4.17, with varying spinning rates between 6 kHz and 14 kHz to eliminate the effect of spinning side bands, as described in a previous study [347]. High-resolution spectra with separated signals were obtained at spinning speeds higher than 12 kHz. Spinning at 14 kHz gave a spectrum almost free from the spinning side bands-overlap problems. After the elimination of spinning-side bands, the sharp peaks observed at -103, -118, -140, -149, -165 and -183 ppm. A qualitative observation can be made based on the presented ^{19}F MAS NMR spectroscopic data. According to ^{19}F MAS NMR spectra, Al_2F_2, $AlFC_3$, AlF_2C_2, and AlF_3C groups were observed, shown in Table 4.4. The resultant porous carbons contained organoaluminium fluoride constitutes.
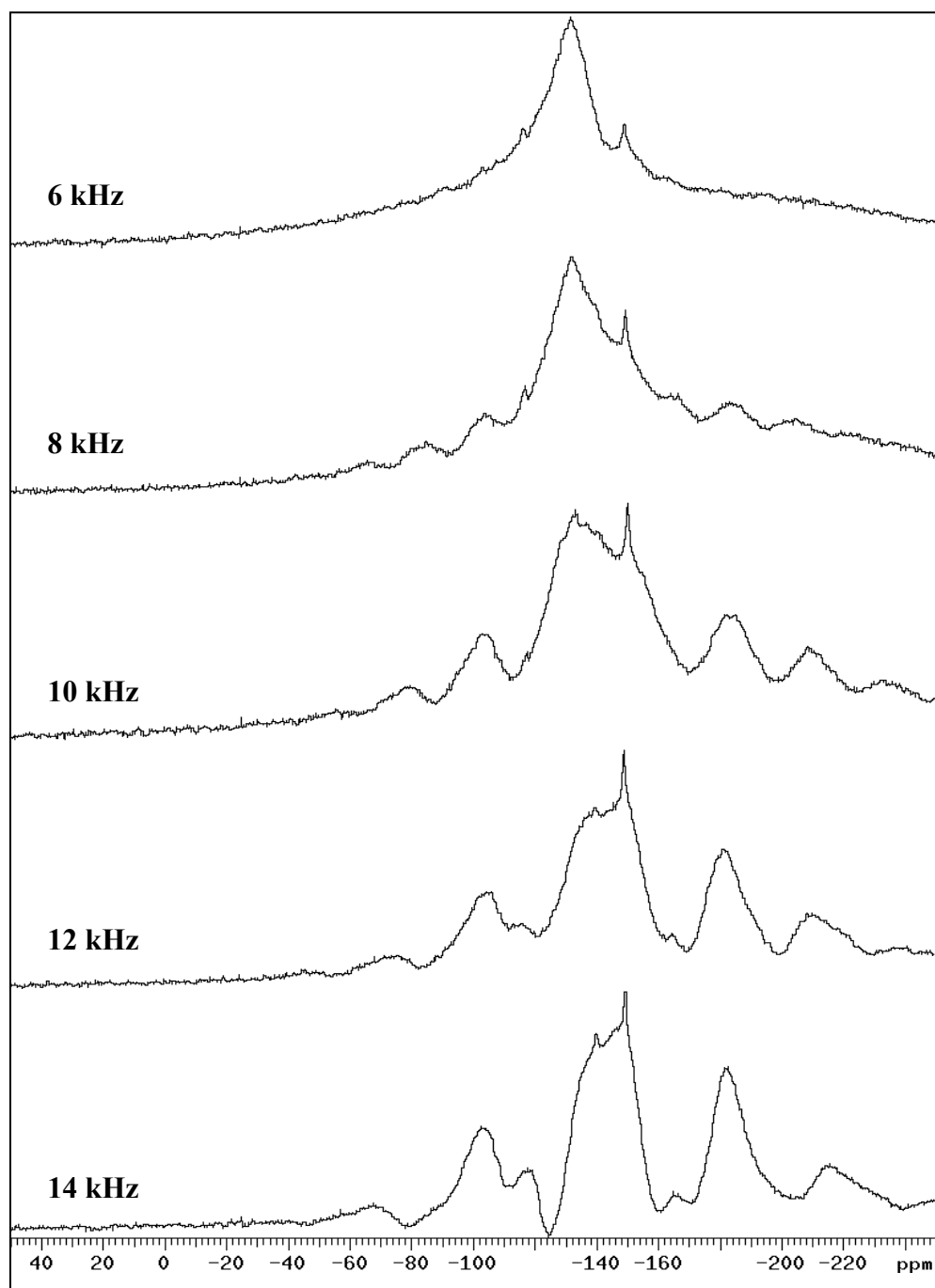
Figure 4.17. ^{19}F NMR of HF washed natural zeolite templated carbon, carbonized at 700°C.

Table 4.4. ^{19}F NMR chemical shifts, observed in natural zeolite templated carbon, carbonized at 700°C.

Aluminium Fluorides	Chemical shift, ppm
	-118
	-140
	-149
	-165

The nature of C–F bond in C_xF is ionic to semi-covalent with increasing concentration of fluorine on the external surface, border of mesopores, quaternary sp^3 C and sp^3 C of (-CH,-), (>CH-) groups or (-CH$_2$-)$_n$ sequences bridging polyaromatic structural units, sp^3 C of cycles or saturated C chains linked to defects, gaps or discontinuities of the graphitic structure and which belong to the carbon skeleton of the starting material, functionalized (oxygenated or nitrogenated) sp^3 C and sp^2 C, sp^2 C of cycles of the border of the graphene layers, of non-conjugated aromatic cycles and non-aromatic unsaturated carbon [344]. For this sample the ^{27}Al NMR was also measured, presented in Figure 4.18. Raw natural zeolite showed only tetra-coordinated aluminium at ca. 60 ppm. By contacting with HF, a peak ascribed to the hexacoordinated species at ca. 0 ppm became large [348]. Although there remains a possibility that an NMR-invisible extra-framework aluminium species had been formed on the sample carbonized at 700°C and HF treated and that the hydration of the surface made it visible [349,350].
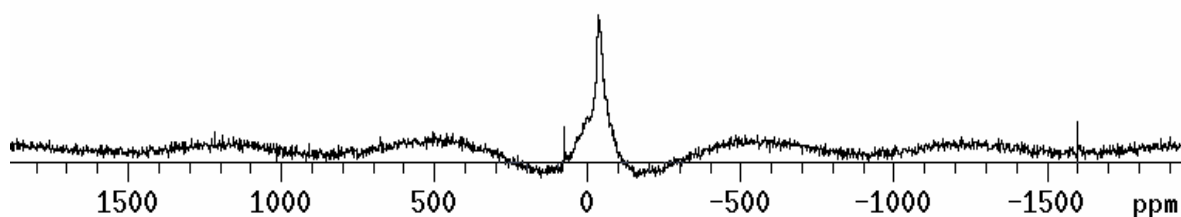
Figure 4.18. ^{27}Al MAS NMR spectra of HF washed natural zeolite templated carbon, carbonized at 700°C.

4.1.2 Different Washing Solutions

Different washing solutions were used for the removal of the zeolite templates. Some structural features of templated porous carbons obtained from HF washing, was explained in the previous sections. In this section the structural differences in the resultant carbons obtained after HCl, NaOH, HCl-NaOH, HF and HF-NaOH washings will be discussed.

The d_{002} values of the carbons were calculated as 0.341, 0.329, 0.330, 0.358 and 0.313 nm for those washed with HCl, NaOH, HCl-NaOH, HF and HF-NaOH solutions, respectively. The results presented might be considered as indications for the presence of turbostratic (fully disordered) structures. The percentage of the superficial fluorinated carbon atoms (i.e. the amount of fluorine fixed by covalent binding at low temperature) is more important when the starting material presents a lower degree of order (low degree of graphitization) [344].

L_c values of resultant carbons obtained from different washing solutions were shown in Figure 4.19. The L_c values of the HCl and HF washed carbons were 5.22 and 2.76 nm, respectively Stacking height of carbons obtained after HCl-NaOH treatment decreased from 5.22 nm to 3.16 nm. L_c value of NaOH washed carbon, was 4.47 nm whereas the L_c value decreased to 2.14 nm in the case of HF-NaOH washing. Average numbers of graphene sheets per stack were calculated as 15, 13, 9, 8 and 7 when resultant carbons were washed with HCl, NaOH, HCl-NaOH, HF and HF-NaOH respectively, as shown in Figure 4.20.
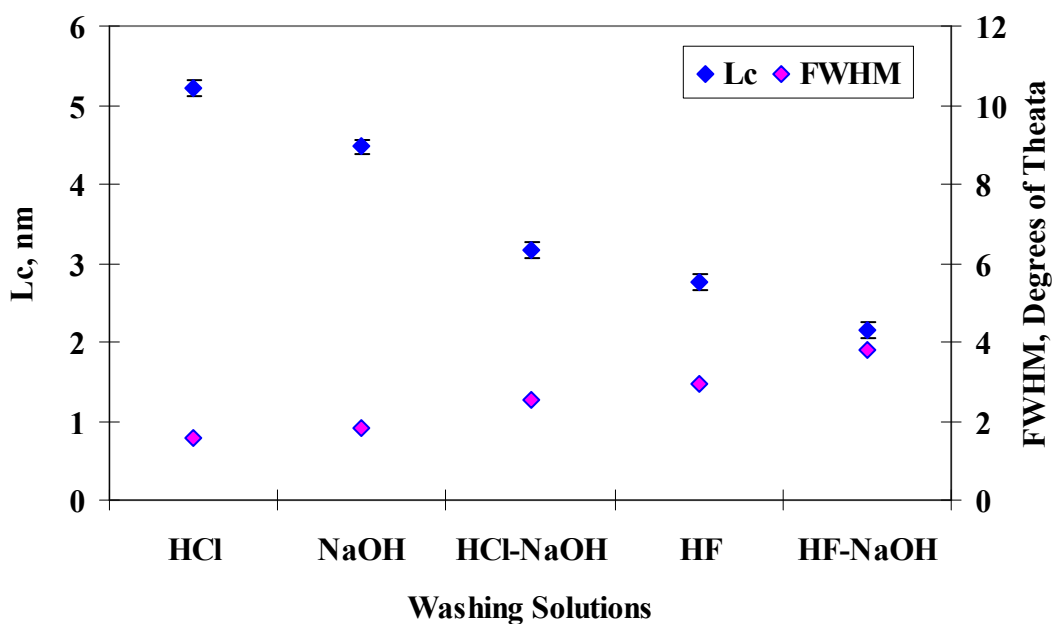
Figure 4.19. Change of FWHM and L_c values of natural zeolite templated carbons, carbonized at 700°C washed with different solutions.

BET surface areas of the porous carbons washed with different solutions shown in Figure 4.21. Average pore diameter was 11 nm for HCl washed carbon, which has a 58 m^2/g BET surface area due to undissolved silicon, confirmed with ^{29}Si NMR spectra. In the case of HCl-NaOH solution, BET surface area was increased to 140 m^2/g. The NaOH washed carbon, had 163 m^2/g BET surface area. HF washed carbon has the highest surface area with 397 m^2/g. Average pore diameters were 9 nm for NaOH and HCl-NaOH washed carbons.

SEM images of templated porous carbons obtained after washings with HCl, HCl-NaOH, NaOH, and HF-NaOH solutions are shown in Figure 4.22. EDS analyses of the samples in general view given in Table 4.5. According to EDS analyses, the cubic structures in the SEM image of the sample washed with HCl, contains 3.4 % silicon and 0.7 % aluminium. Some silicon residues are still remains in the case of HCl, HCl-NaOH and NaOH washed samples. Small amounts of sodium were detected in the HCl-NaOH and NaOH washed porous carbons. .
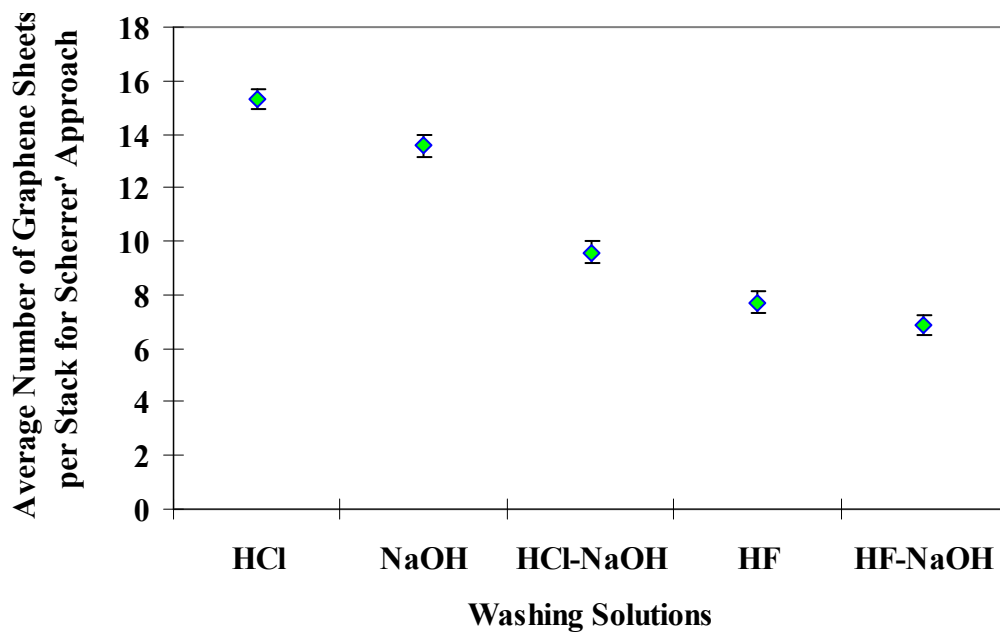
Figure 4.20. Change of the average number of graphene sheets of carbons natural zeolite templated carbons, carbonized at 700°C washed with different solutions.
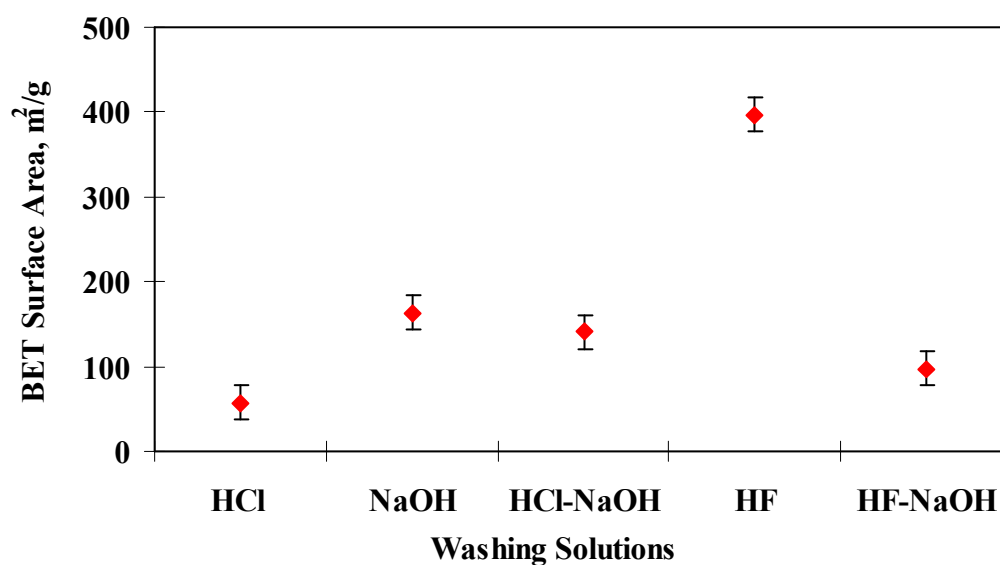
Figure 4.21. Change of the BET surfaces of natural zeolite templated carbons carbonized at 700°C washed with different solutions.
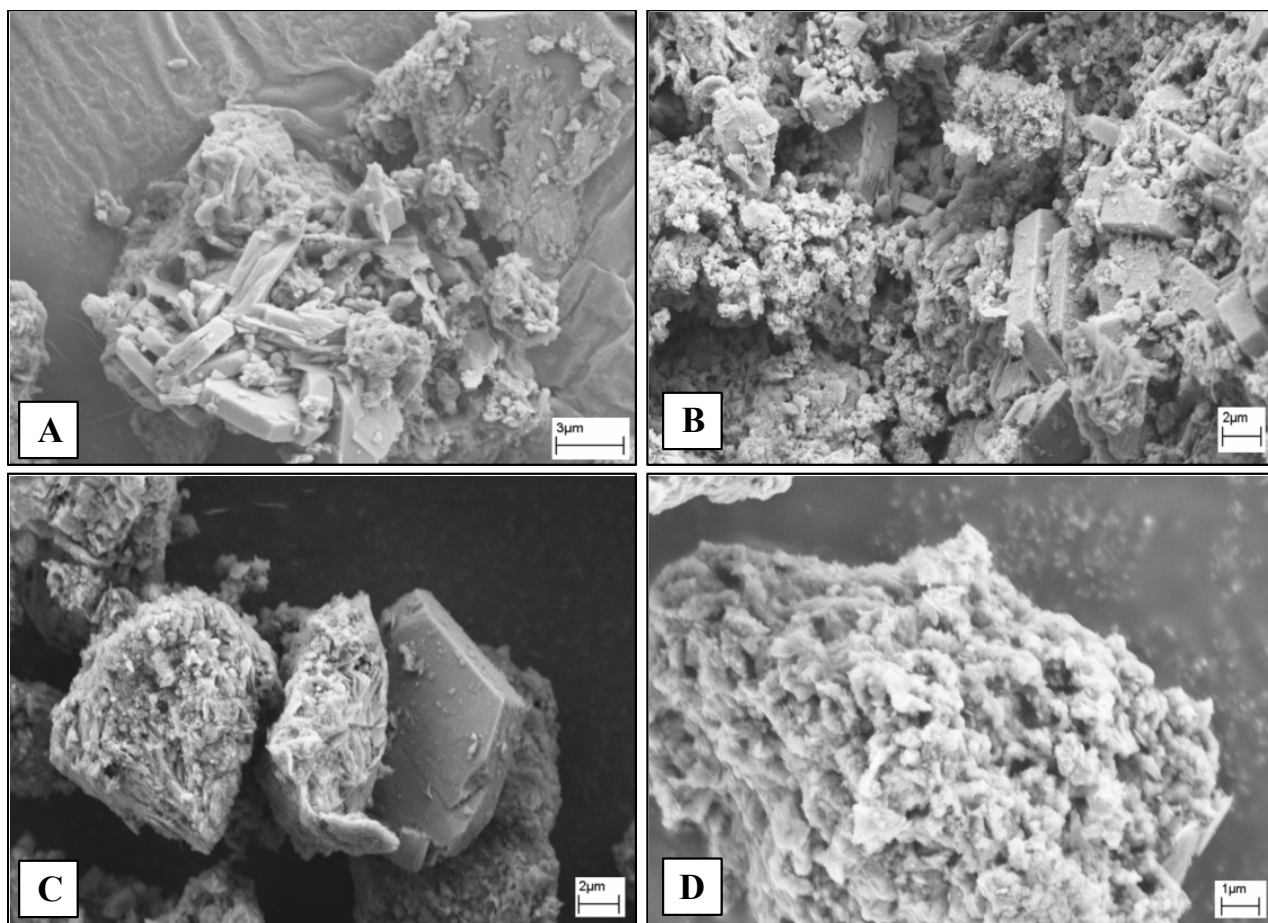
Figure 4.22. SEM image of natural zeolite templated carbon, carbonized at 700°C washed with **A.** HCl, **B.** HCl-NaOH, **C.** NaOH and **D.** HF-NaOH.

Table 4.5. EDS analyses of zeolite templated carbons, carbonized at 700°C washed with different solutions.

	Atom. C, At. %			
Element	**HCl**	**HCl-NaOH**	**NaOH**	**HF-NaOH**
Carbon	64.71	64.46	74.71	42.96
Aluminium	0.68	0.48	0.21	0.03
Oxygen	31.21	32.24	23.87	14.34
Silicon	3.40	1.95	1.06	0.05
Sodium	-	0.87	0.15	8.02
Flourine	-	-	-	34.64

4.2 Synthesis of Microwave-Assisted AlPO$_4$-5

The possible fields of applications for molecular sieves have been extended greatly over the last years with the possibility of generating new supramolecular structures by in situ inclusion of guest molecules into the pores of molecular sieves. AlPO$_4$-5 is very attractive for preparation of one-dimensional systems by introduction of some guest materials into their channels with diameters less than 1 nm [351].

In the present survey, the systematic study of the parameters of the microwave synthesis of AlPO$_4$-5 was examined to use for the further templating purposes. Usage of microwave heating for the synthesis of AFI type structures drastically reduced the crystallization times.

It is well known that the synthesis of AlPO$_4$-5 is strongly influenced by organic gel, the crystallization conditions and the presence or mineralizers such as F$^-$ [168]. The preparation details of AlPO$_4$-5 crystallization using different initial solutions and conditions of hydrothermal crystallization using domestic microwave oven are presented in Table 3.2. Because aluminium isopropylate was used as Al source as described in the experimental section, a fixed amount of three isopropyl alcohol moles per mole of Al was always present in the gel. This remarkable amount of alcohol could have influenced the experiments in two ways: (i) as a dipolar molecule which effectively couples with the microwave field, thus contributing to the heating, and (ii) as an amphiphilic molecule which could cause the formation of hydrophilic-hydrophobic gel structures [225].

The products of the whole set of experiments was investigated by scanning electron micrography (SEM) and X-ray diffraction (XRD). The XRD patterns of the samples point out their high level of crystallinity. The structure and morphology of the AlPO$_4$-5 molecular sieves depend on the gel composition and heating periods. The phase purity is also dependent on the composition of the gels. All synthesis batches produced nearly identical fractions of AlPO$_4$-5, i.e., 0.1 g per 1 g of the gel. Braun et al.[237] synthesized AlPO$_4$-5 crystals, yielding 0.1 g of AlPO$_4$-5 crystals from 2 g of gel.

The H labeled AlPO$_4$-5's, had good crystallinity, and perfectly matched between experimental and expected XRD patterns corresponding to the AFI type structure. In this section H labeled samples which were selected for the subsequent sections were discussed. They were used as synthetic zeolitic templates for the production of porous carbons. The

details of synthesis of AlPO$_4$-5's with different crystalline structures are presented in the Appendix II.

Perfect hexagonal AlPO$_4$-5 products with rod-like shape, well-defined edges and faces formed in H1 are shown in Figure 4.23. This shape is one of the characteristic morphologies of AlPO$_4$-5 crystals [156,168,225]. The direction of the *c*-axis is parallel to the six-fold axis of this rod-like shape. The *a-b* plane is perpendicular to the *c*-axis. The average crystal sizes in length along the *c*-axis were obtained ca. 5 μm length from the SEM images.
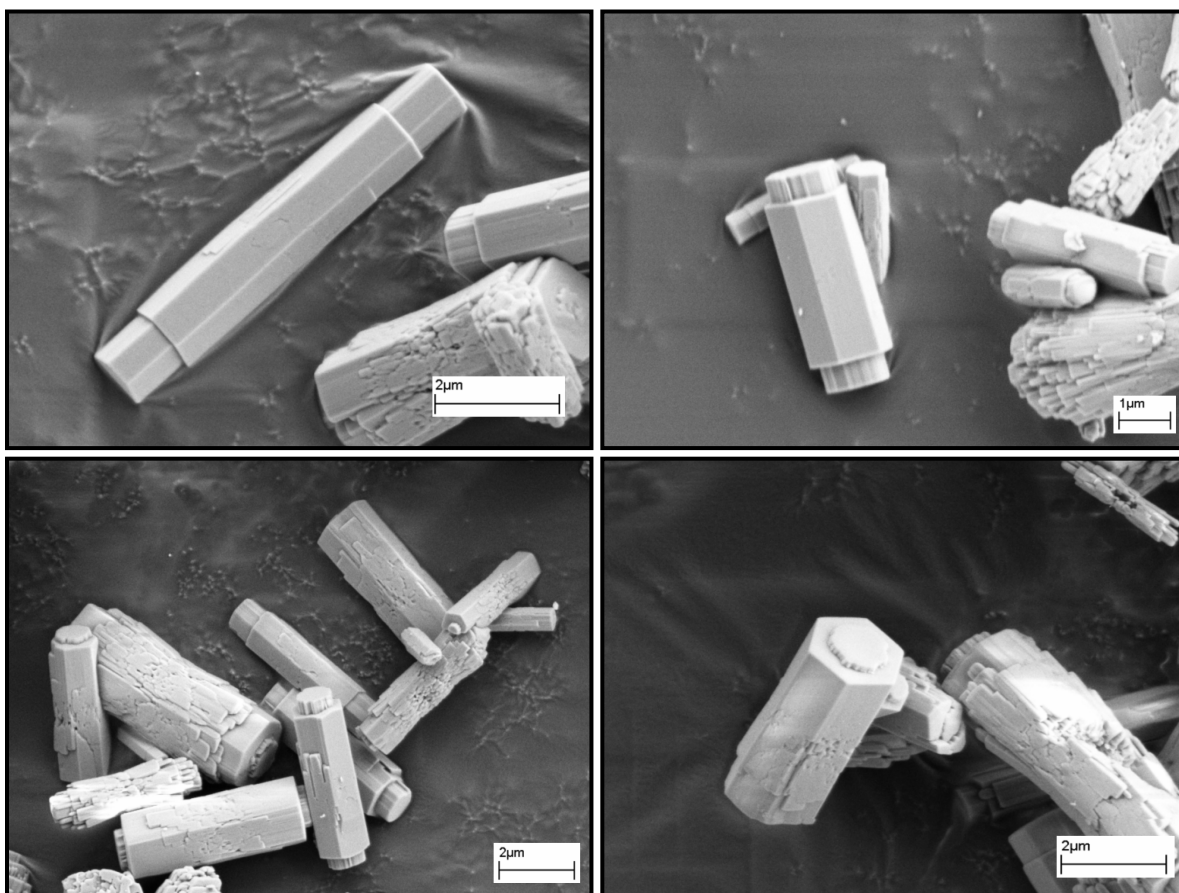
Figure 4.23. SEM micrographs of H1.

Different heating rates and heating times were studied in H composition. Increasing crystallization time, in H2 and H3, shown in Figure 4.24, the same crystals were obtained with some unreacted gels in the surroundings. Increasing the microwave power for heating, from 120 W to 200W, at 180 s, resulted in perfect AlPO$_4$-5's with ca. 5 μm length. XRD patterns of H1, H2 and H3 were shown in Figure 4.25 corresponding to the AFI structure [168,352].

SEM micrograph of H4 was shown in Figure 4.26. Both H1 and H4 were matched with perfect AlPO$_4$-5 crystals XRD patterns recently published [231,352]. The frameworks of H1 and H4 were consistent with the AFI-structure type found in Qui et al. [168]. Four-, 6-, and 12-rings of the corner sharing PO$_4$ and AlO$_4$ tetrahedra was present. In H1 and H4, the crystals nuclei were mostly formed with homogeneously distributed.
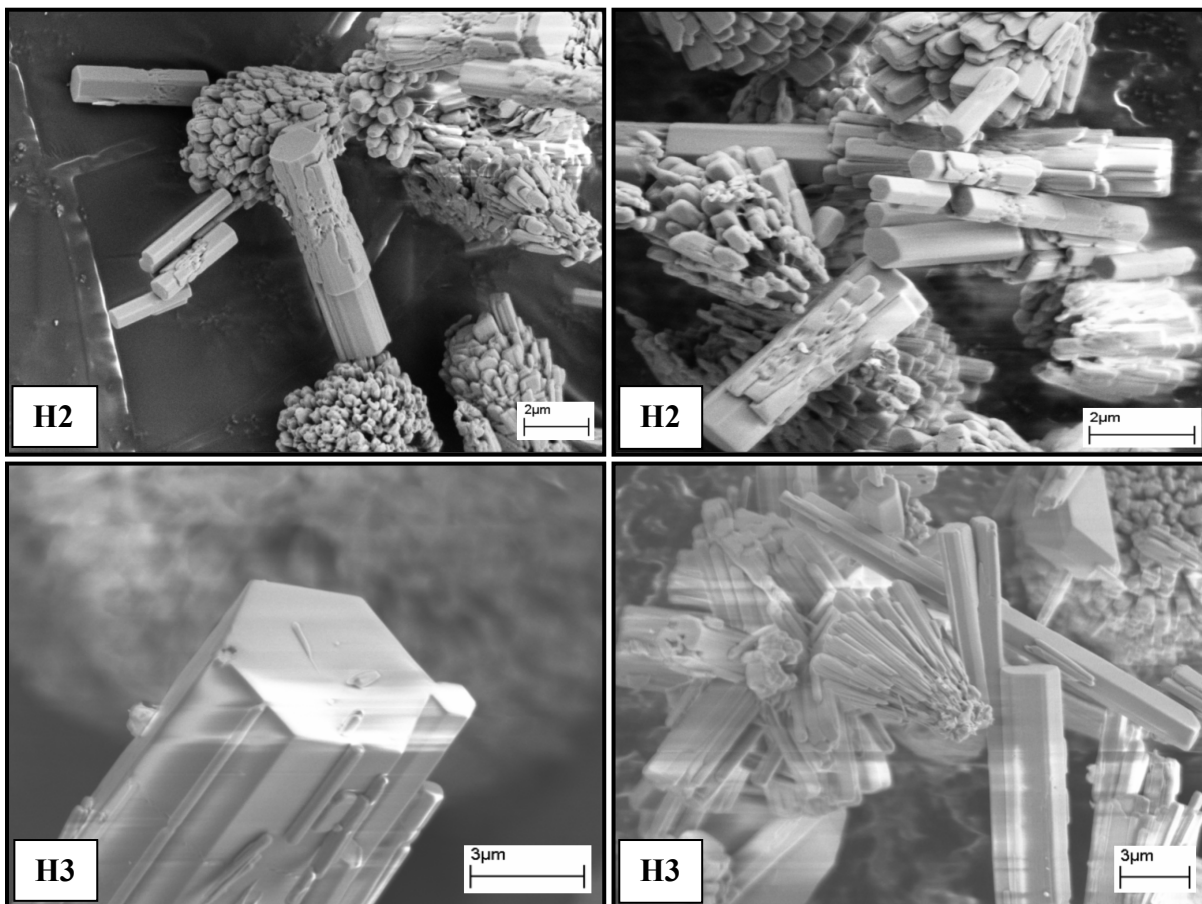
Figure 4.24. SEM micrographs of H2, and H3.

The morphology of a molecular sieve is very important for special applications. Both H1 and H4 contain some structures that not completely formed into hexagonal crystals. The perfect hexagonal crystals grow from hourglass shaped crystals. Diffraction patterns of both samples point out their high level of crystallinity, shown in Figure 4.27. In the XRD patterns recorded for the AlPO$_4$-5 crystals, the *(100), (210), (002)* and *(211)* peaks were detected at *d* values 11.92 Å, 4.51 Å, 4.19 Å and 3.97 Å respectively, in addition to small features around 15° 2θ.

BET surface area of H1 and H4 was 61 m^2/g and 107 m^2/g, respectively. N$_2$ adsorption/desorption isotherms and pore size distributions of H1 and H4 were given in

Figure 4.28 and Figure 4.29, respectively. Average pore diameters of H1 and H4 were measured as 1.9 nm and 1.7 nm, respectively. H4 was chosen for the rest part of the study, template synthesis of porous carbons due to higher BET surface area and lower pore diameter.

SEM micrographs of H1 and H4 from different view of point were shown in Figure 4.30. The crystallization times were 300 s and 180 s at 120 W and 200W respectively, however Demuth et al. [169] reported that the nucleation occurred even during the heating to the set temperature. It could be concluded that the growing of the crystals began to form the hourglass orientation. It was shown that the AlPO$_4$-5 crystals, freely grown in solution, always consisted of two half-crystals with opposite growth direction along the c axis of the crystal.
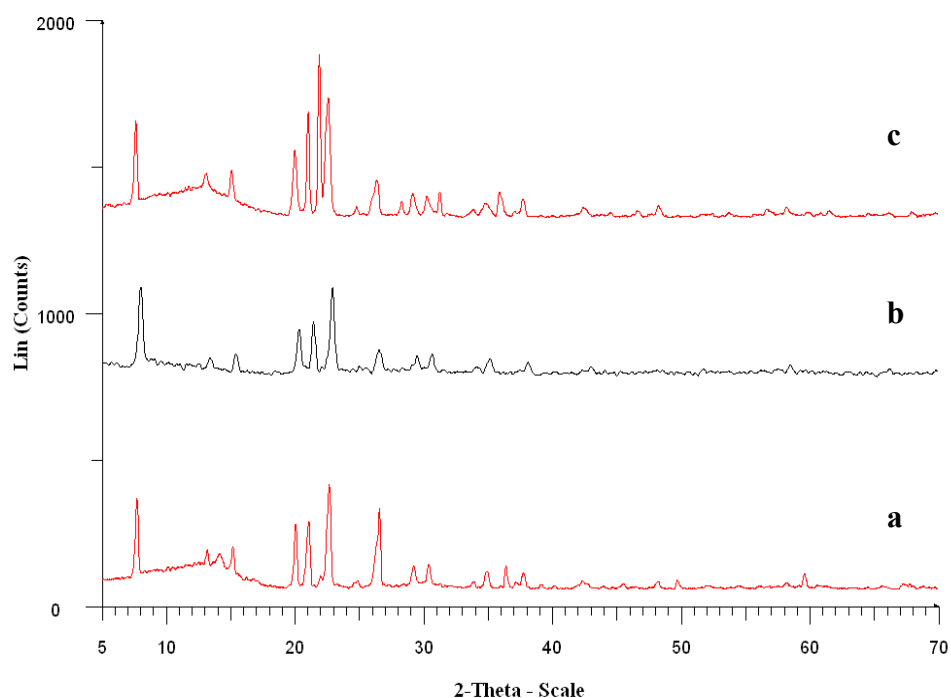
Figure 4.25. XRD patterns of **a.** H1, **b.** H2 and **c.** H3.

There are two alternatives to correlate the two half-crystals [232]. The first option is that the two halves of the AFI crystal are related by a 180° rotation about a diagonal in the hexagonal plane as shown in Figure 4.31a. Both half-crystals have the same absolute configuration. Another possibility is that the structures in the two half-crystals are related by a mirror plane (Figure 4.31b) or, equivalently, by inversion. Consequently, the two half-crystals have a different absolute structure. In both cases, the two end faces of a crystal are

identical [232]. The end face of crystals, perpendicular to the main growth direction, terminated with Al atoms. Although $AlPO_4$-5 crystals are found to have twinned structure, the growth process has not yet been clarified [244].

Lin et al. [241] synthesized "dumbbell" or "half-dumbbell" shaped $AlPO_4$-5's.The central part of the crystal is a hexagonal prism. At the ends of the crystals, smaller twinned crystals radiate out from the central hexagonal part. Other researchers have observed dumbbell-shaped $AlPO_4$-5 crystals in traditional hydrothermal synthesis under certain conditions [353]. In the present study, obtained crystals belonged to hexagonal space group P6/mcc according to XRD patterns [168]. The hexagonal unit cell parameters and volume are $a = 13.770$ Å, $c = 8.379$ Å, and $V = 1376.04$ Å^3.
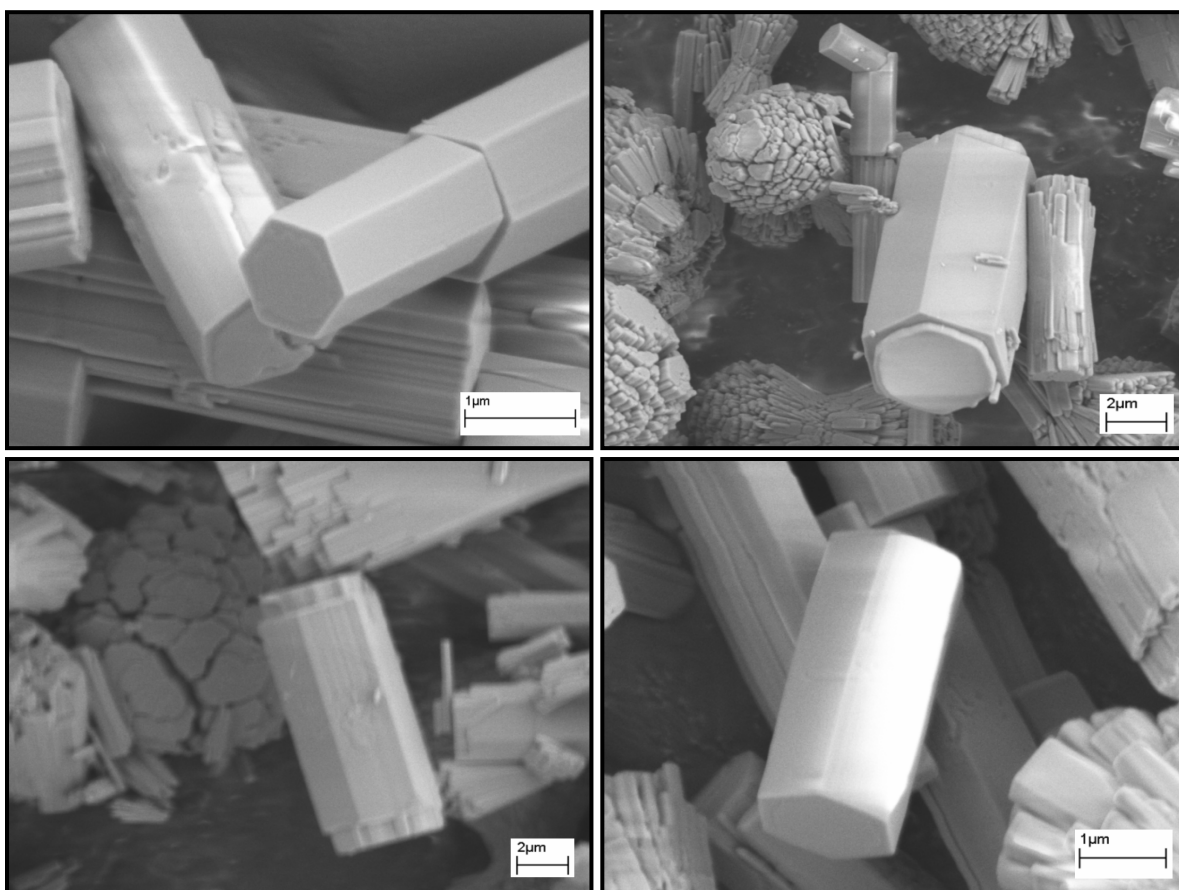
Figure 4.26. SEM micrographs of H4.

Increasing the microwave power to 200 W and crystallization time to 240 s - 300 s caused formation of hexagonal as well as hourglass shaped and conical crystals, in the samples labeled as in H5, H6, H7 (Figure 4.32) and H8 (Figure 4.33). With the increase in the microwave heating time to 240 s in H5, the crystals growed only in the *c*-axis direction

and close to hexagonal rod-like shape with no size change in the *a-b* plane. Nucleation of the needle-like crystals were observed near the large crystals in H6, also observed in a previous study [244]. The AlPO$_4$-5 product of sample H9 and H10 (Figure 4.33) transformed hexagonal crystals into convex ended and angled surface. Increasing the crystallization time 330 s, caused the formation of the conical crystals before transformed into larger amounts of hexagonal and convex ended crystals. Increasing the microwave heating times up to 315 s and 330 s, in H9 and H10, respectively, brought about the crystals in H9 and H10 to grow in the *a-b* direction.

XRD patterns of H4, H5, H6, H7, H8, H9 and H10 were shown in Figure 4.34. Diffraction patterns of H4, H5, H6, H7, H8 and H9 correspond to the AFI type structure, similar to those published in the literature [168,352]. Diffraction pattern of H10 was more likely synthetic berlinite [354] matched with patterns found XRD software. The intensities of *(100)*, *(210)*, *(002)* and *(211)* decreased from H4 to H7, due to the elongation of the crystals [239].
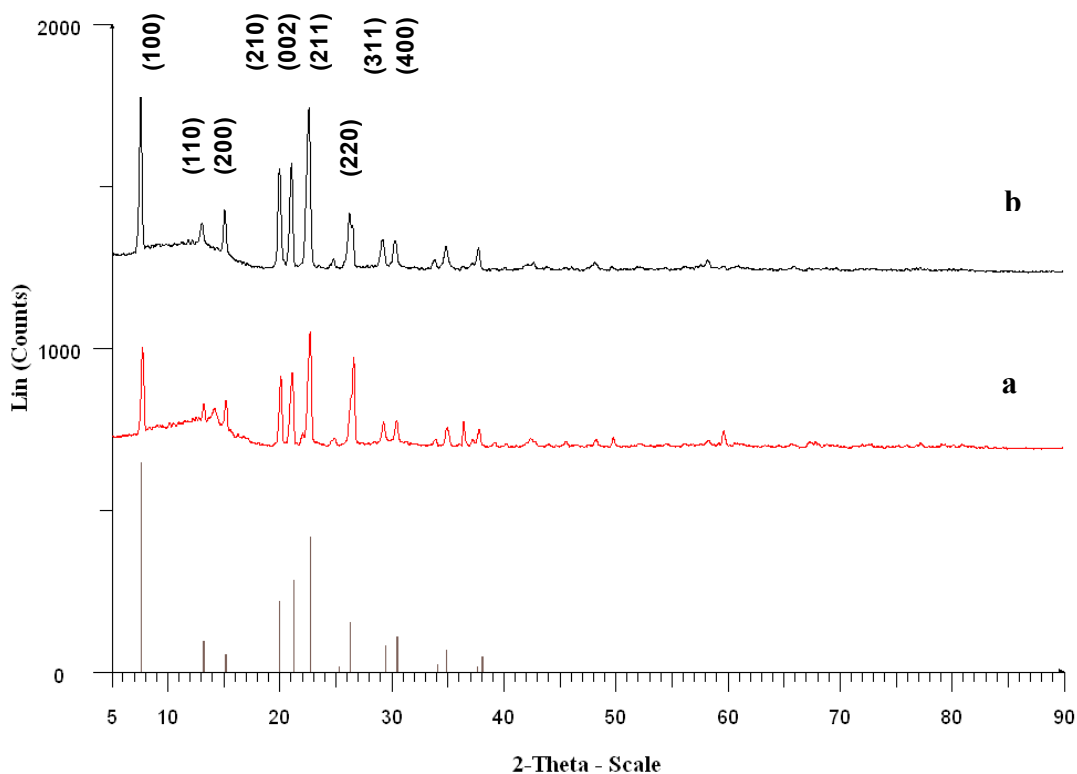
Figure 4.27. XRD patterns of **a.** H1, **b.** H4.

A survey of the literature indicates that a number of additional phases such as AlPO$_4$, boehmite, augelita or AlPO$_4$.2H$_2$O [168,355-357] may form during the synthesis of the

AlPO$_4$-5 material, depending on the starting gel composition and the synthesis conditions. However, reasons such as small quantities, poor crystallinity, or short-range crystals may explain a weak efficiency of XRD patterns to detect these additional phases. The crystalline form of the natural mineral augelite Al$_2$PO$_4$(OH)$_3$, which has a single type of PO$_4$ tetrahedra and two types of Al polyhedra, i.e., five-coordinated AlO$_2$(OH)$_3$ and six-coordinated AlO$_4$(OH)$_2$ were reported was a by-products previously [358,359].
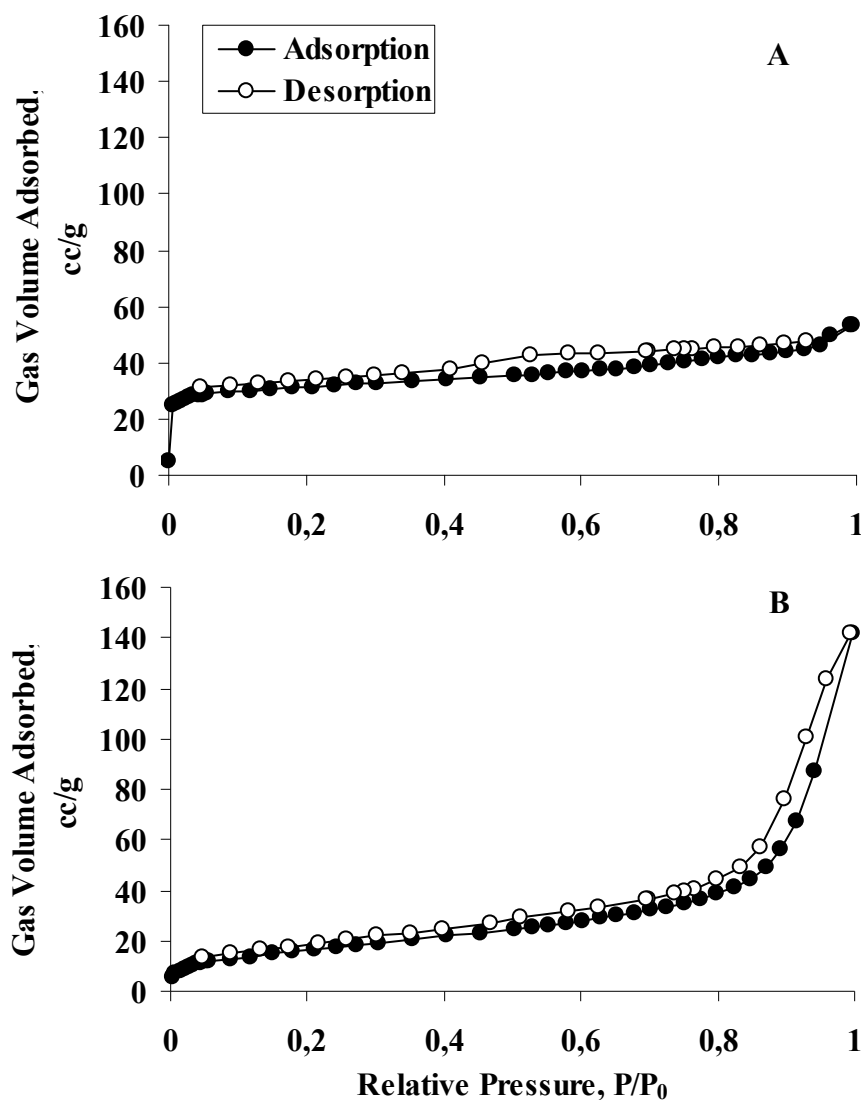
Figure 4.28. N$_2$ adsorption/desorption isotherms of **A.**H1 and **B.**H4.
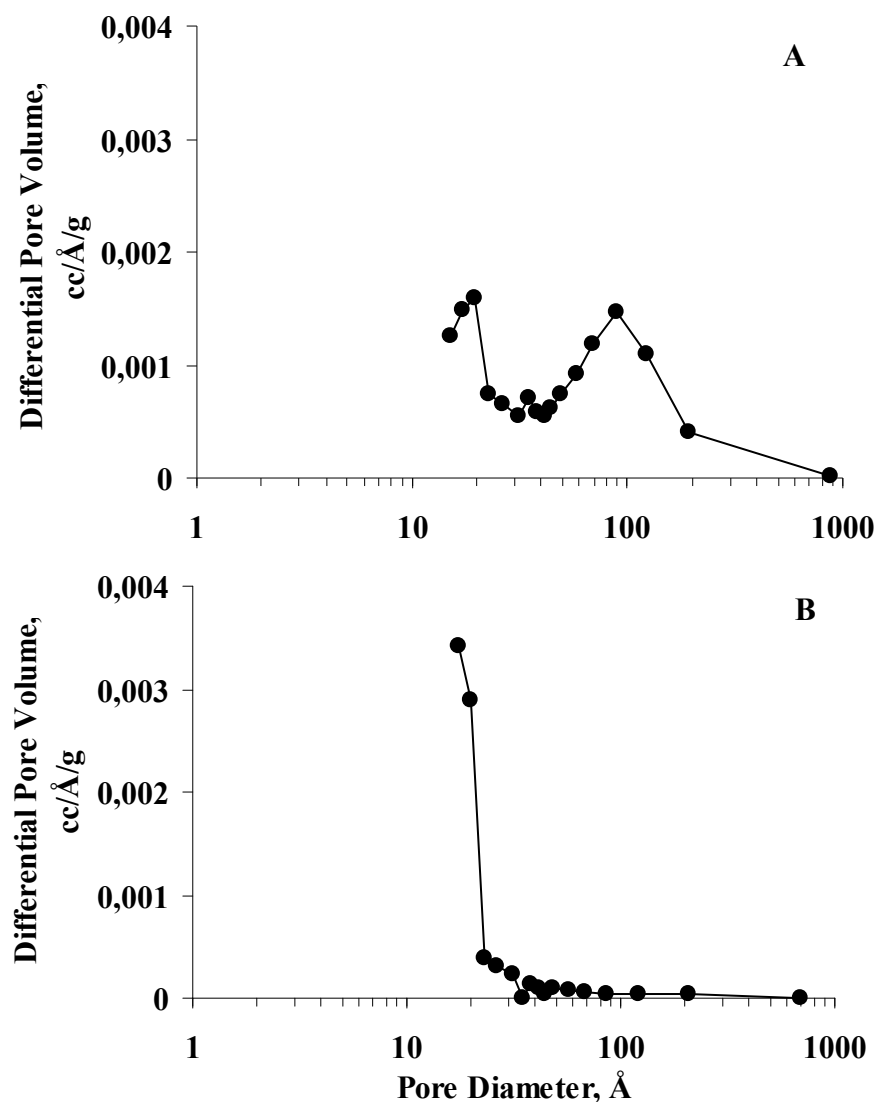
Figure 4.29. Pore size distributions of **A.**H1 and **B.**H4.

In the H11 and H12 samples (Figure 4.35), ca. 4 μm width and 6 μm length lime type and unreacted crystals formed when the crystallization time was increased to 360 and 420 s respectively at 200W power exposure. In sample H13 (Figure 4.35) angled and longer crystals with narrower ends were examined at 600s at the same power, whereas in sample H14, at 900 s more incoherent crystals were detected. As the crystallization time was increased from 180 s to 900 s, AlPO4-5 crystals began to grow longer and aligned in certain angles. XRD patterns of H11, H12 and H13 were shown in Figure 4.37, corresponding to the berlinite structure [354]. As this model, we propose that the hexagonal shape is formed readily due to a small barrier of activation and gradually transform into the rounded shapes over time.

The aspect (length-per-width) ratio of the AlPO4-5 crystals varied during synthesizing. The crystals grow mainly in the both *c*-axis and *a-b* plane during the first

180 s at 200W. After 180 s, the crystals did not grow in the *c*-axis any more but in the *a-b* plane direction. The ratio of TEA molecules to other chemical species increased at the late stage of the synthesis because phosphate species are consumed faster than TEA in the synthesis mixture [224].

Perfect hexagonal $AlPO_4$-5's formed at 800W and 60 s crystallization time. It is necessary to heat the starting solution very quickly to the crystallization temperature in order to synthesize pure $AlPO_4$-5 (Sample H15). When the starting solution is heated slowly, the presence of an amorphous phase indicates incomplete conversion or changing the crystallization behavior, presumably due to slower nucleation and crystallization rates. The perfect crystallites formed in the samples H1, H4 and H15, which has lower crystallization times and enough power in order to form pure $AlPO_4$-5 crystallites.

When second step was added to the$AlPO_4$-5 crystallite formation after 800W and 60 s, in H16, H17 and H18 (Figure 4.38), amorphous phase was observed. XRD patterns of H15, H16 and H17 corresponding to the AFI structure [168,352], aluminium phosphate structure [360] and berlinite structure [360], respectively. The XRD patterns intensity of H17 was higher than that of H18.

The use of microwave heating leads to improved control of the synthesis of molecular sieve crystals. The results showed that the morphology, orientation, and the size of the $AlPO_4$-5 crystals could be controlled by varying the gel composition, water content, and amount of organic template, heating power and crystallization time.

Generally, in the microwave heating method, the solution is directly warmed by the dielectric loss of the microwave. The dielectric loss occurs all over the solution. In contrast, in the case of the conventional heating method, the solution is warmed in the autoclave by the conduction of heat. Therefore, using microwave irradiation, the gel is quickly and uniformly heated compared with the conventional heating method. For the microwave heating, the temperature over all the gel quickly reaches the condition that starts the reaction.

Many crystal nuclei are simultaneously formed all over the gel. Once the nuclei are generated with a high density, the residual Al and P sources are used only for the growth of these nuclei that form crystals. This explains why the crystals have a tendency to have a homogeneous size.
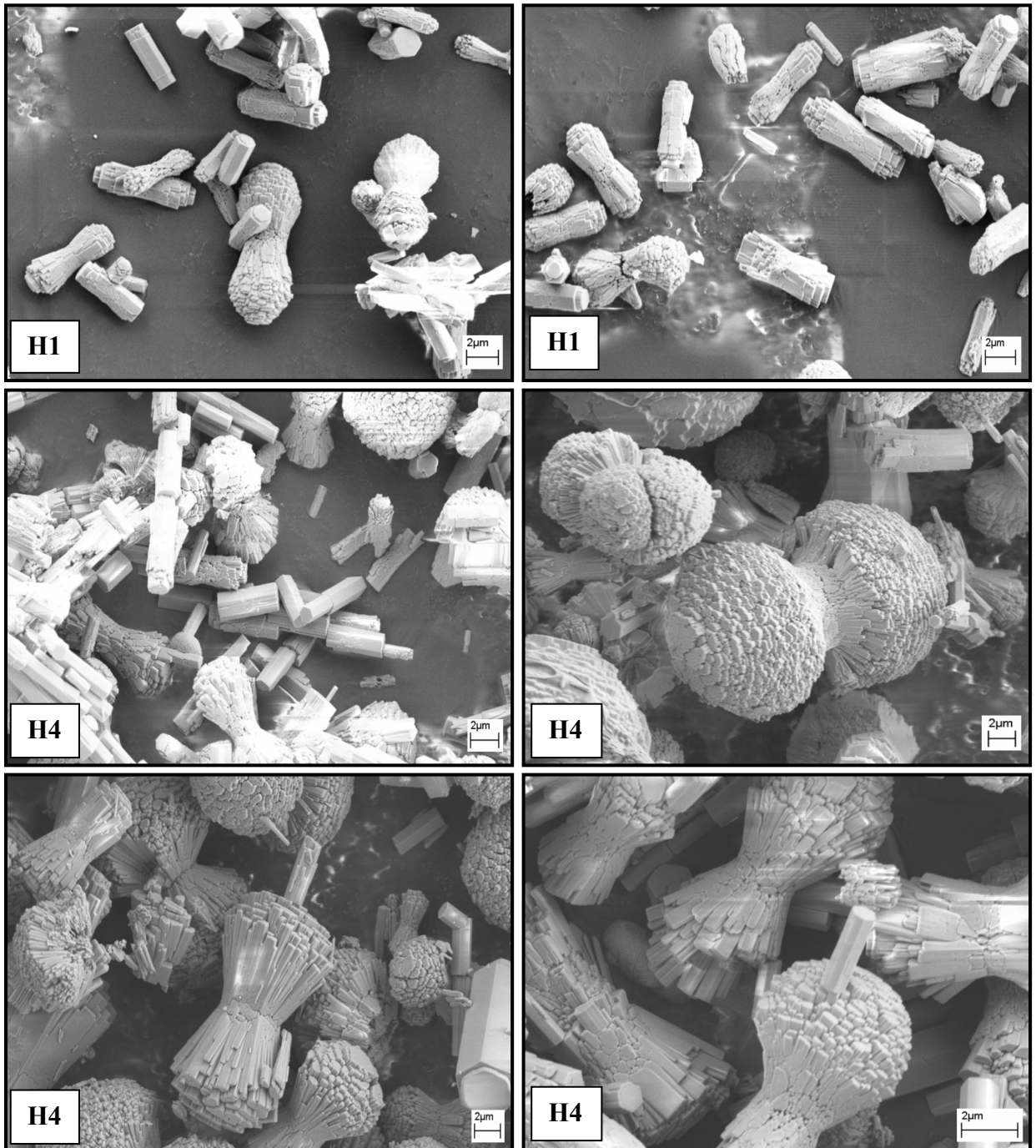
Figure 4.30. SEM micrographs of H1 and H4.
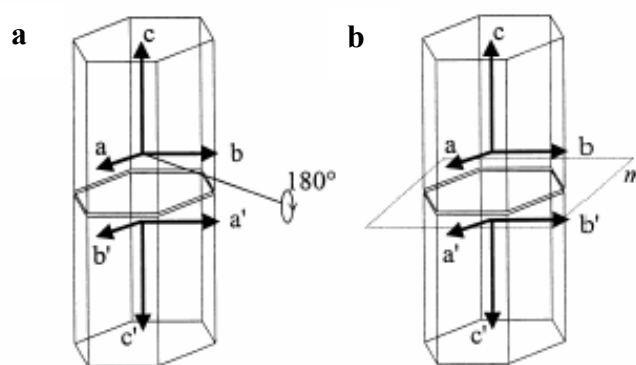
Figure 4.31. Explanation of the two possible symmetry operations between the two half-crystals. In both cases the polarization of the end faces is the same. **a.** rotation, **b.** reflection.

The duration of synthesis of the $AlPO_4$-5 crystals needed to terminate the crystal growth was ca. 300 s at 200W in the present work. The synthesis duration is shorter than that using the conventional methods heating methods [224]. In a previous study using the microwave heating method, $AlPO_4$-5 crystals were obtained also in only a few minutes [225]. Thus, HF is believed to accelerate the speed of the crystal growth, and the use of aluminium isopropylate may lead to a more uniformly dispersed Al source. Girnus et al. [225] proposed a model to explain the significantly short synthesis time in microwave heating from a microscopic view point. Hydrogen bonds between the water molecules are destroyed by the microwave irradiation forming active water molecules which accelerate the speed of the crystal growth.
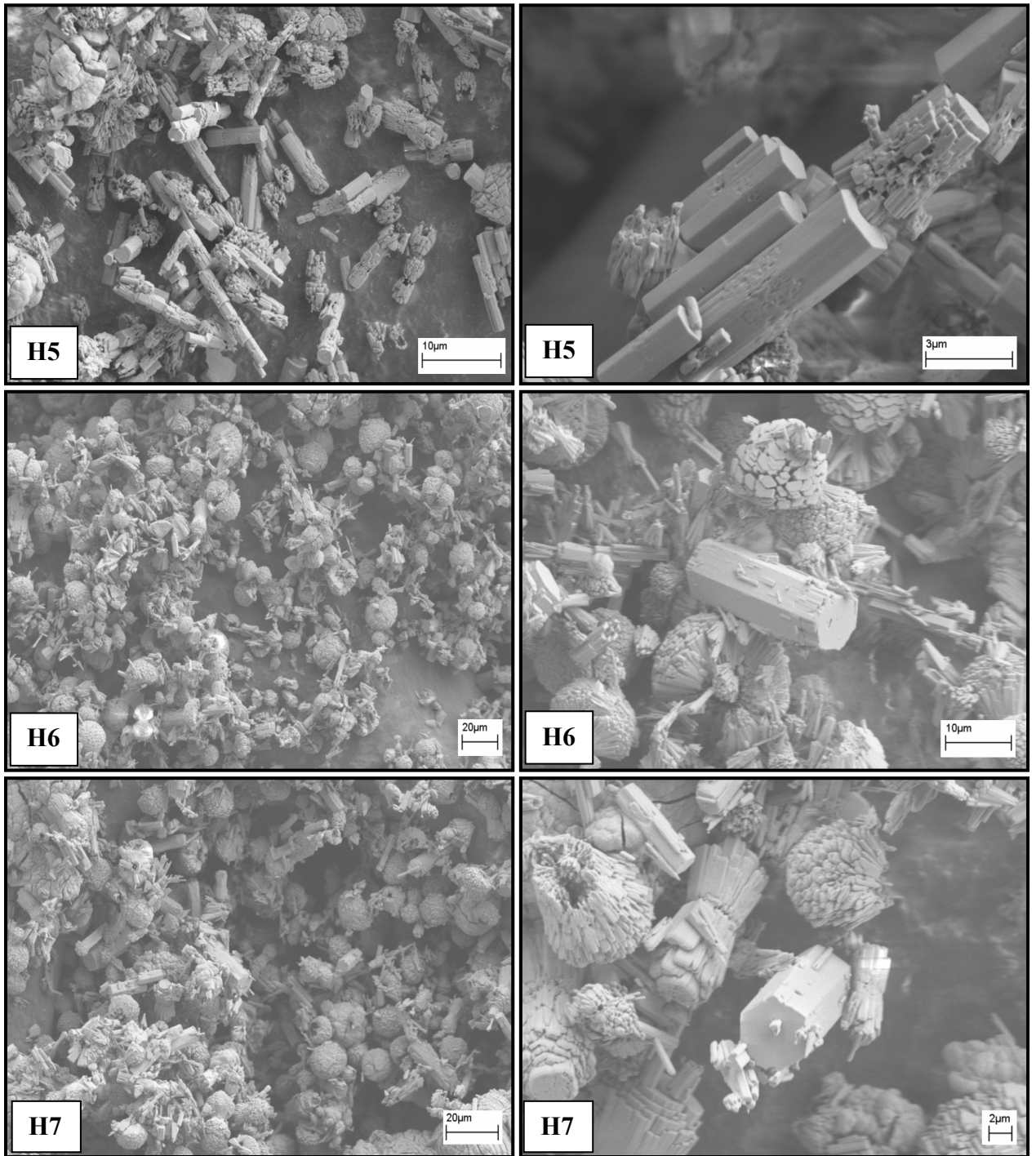
Figure 4.32. SEM micrographs of H5, H6 and H7.
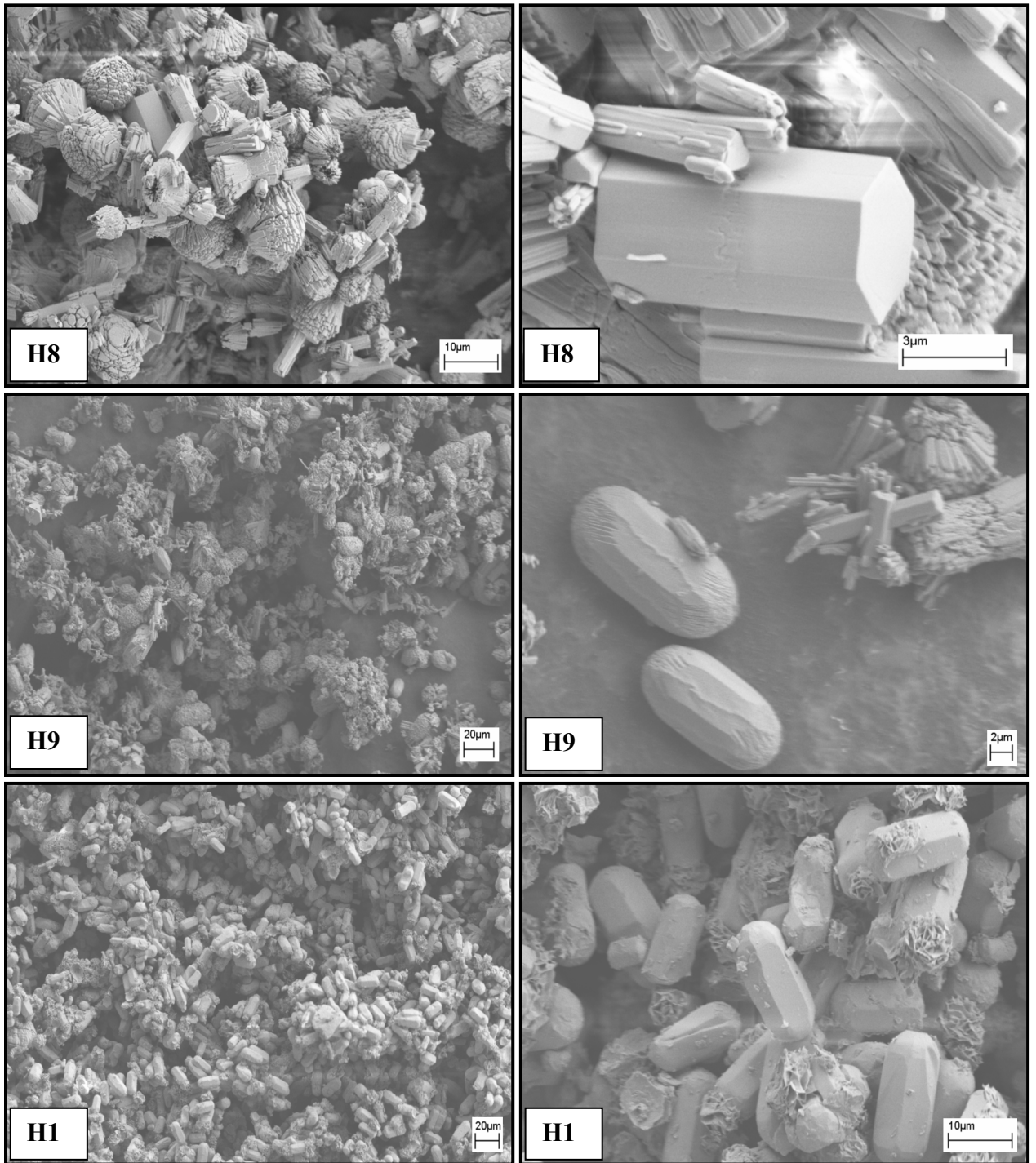
Figure 4.33. SEM micrographs of H8, H9 and H10.
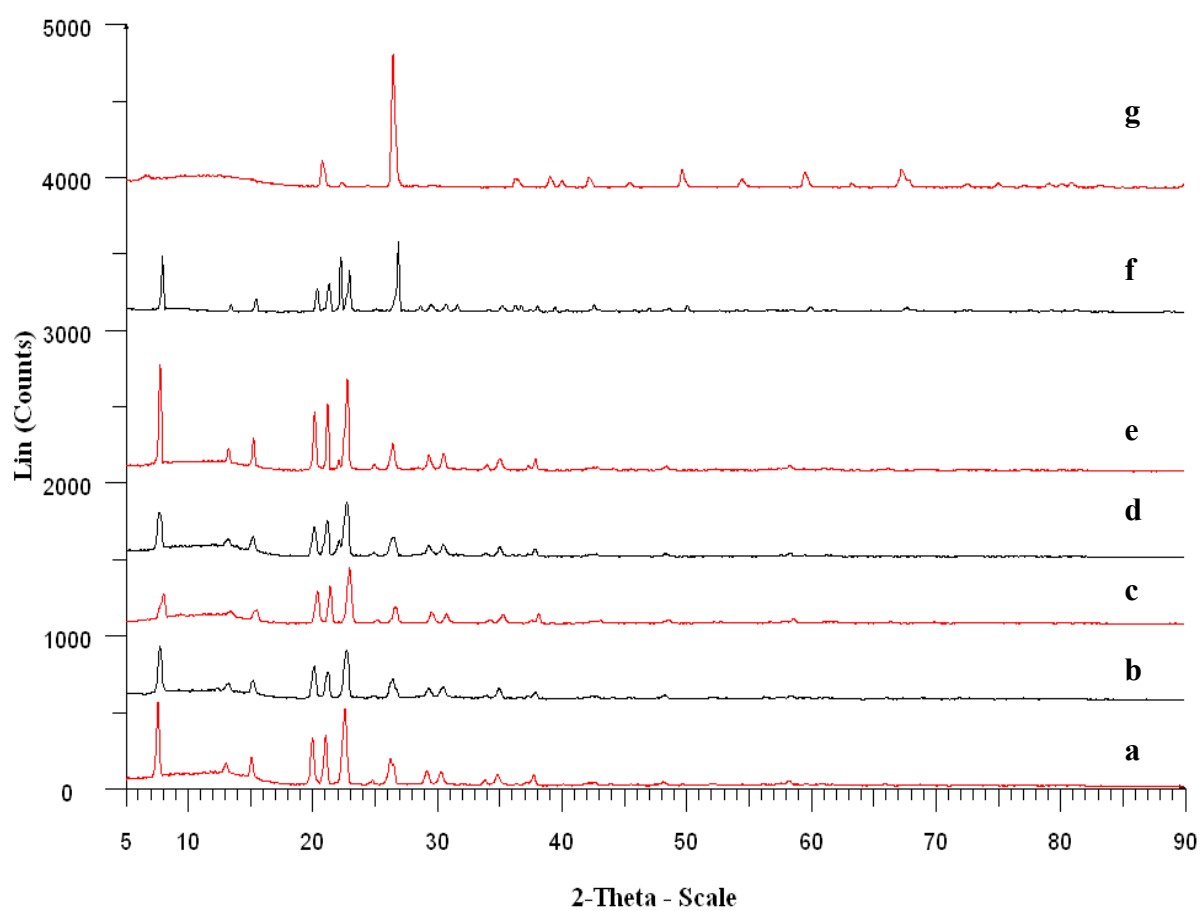
Figure 4.34. XRD patterns of **a.** H4, **b.** H5, **c.** H6, **d.** H7, **e.** H8, **f.** H9 and **g.** H10.
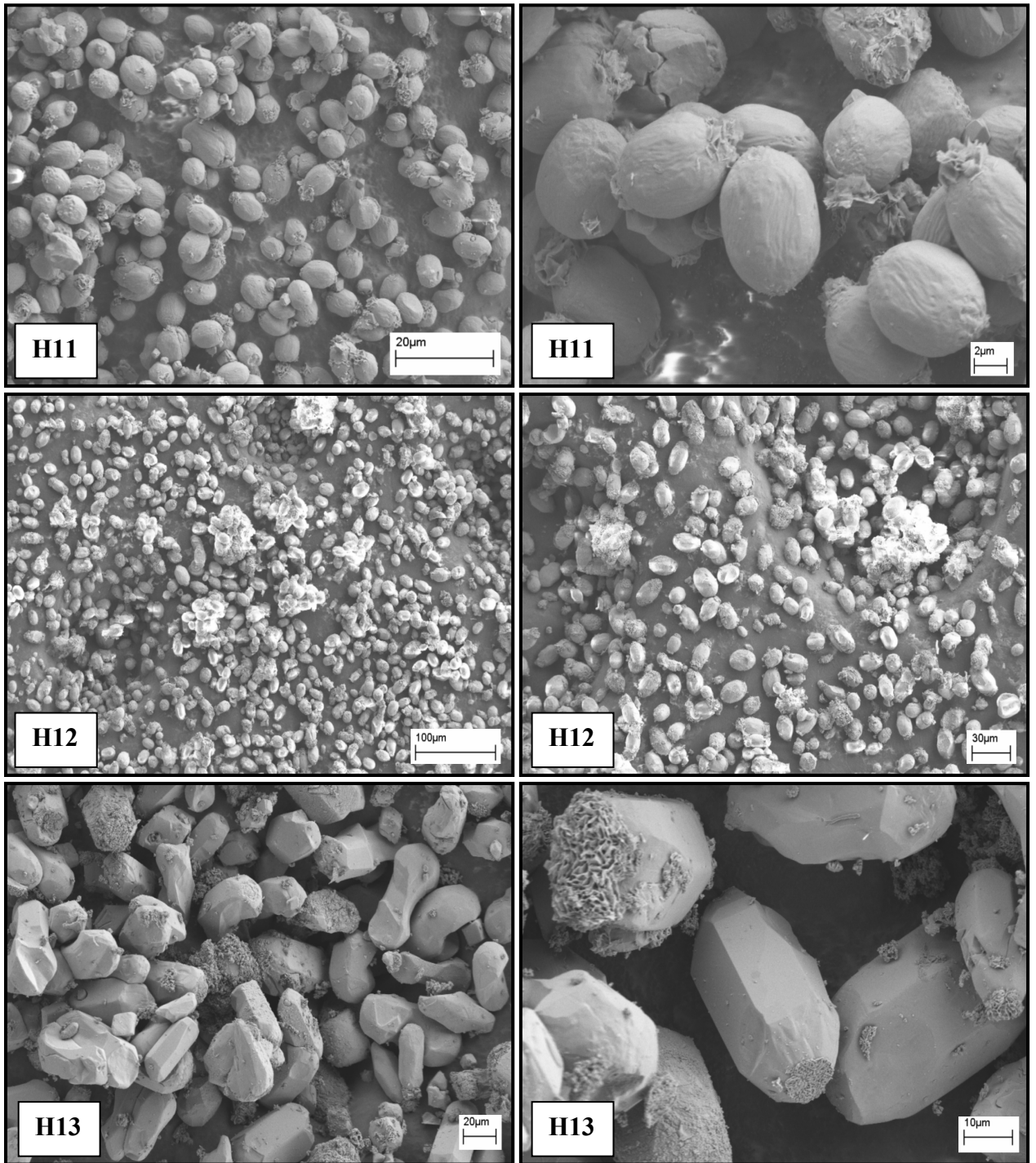
Figure 4.35. SEM micrographs of H11, H12 and H13.
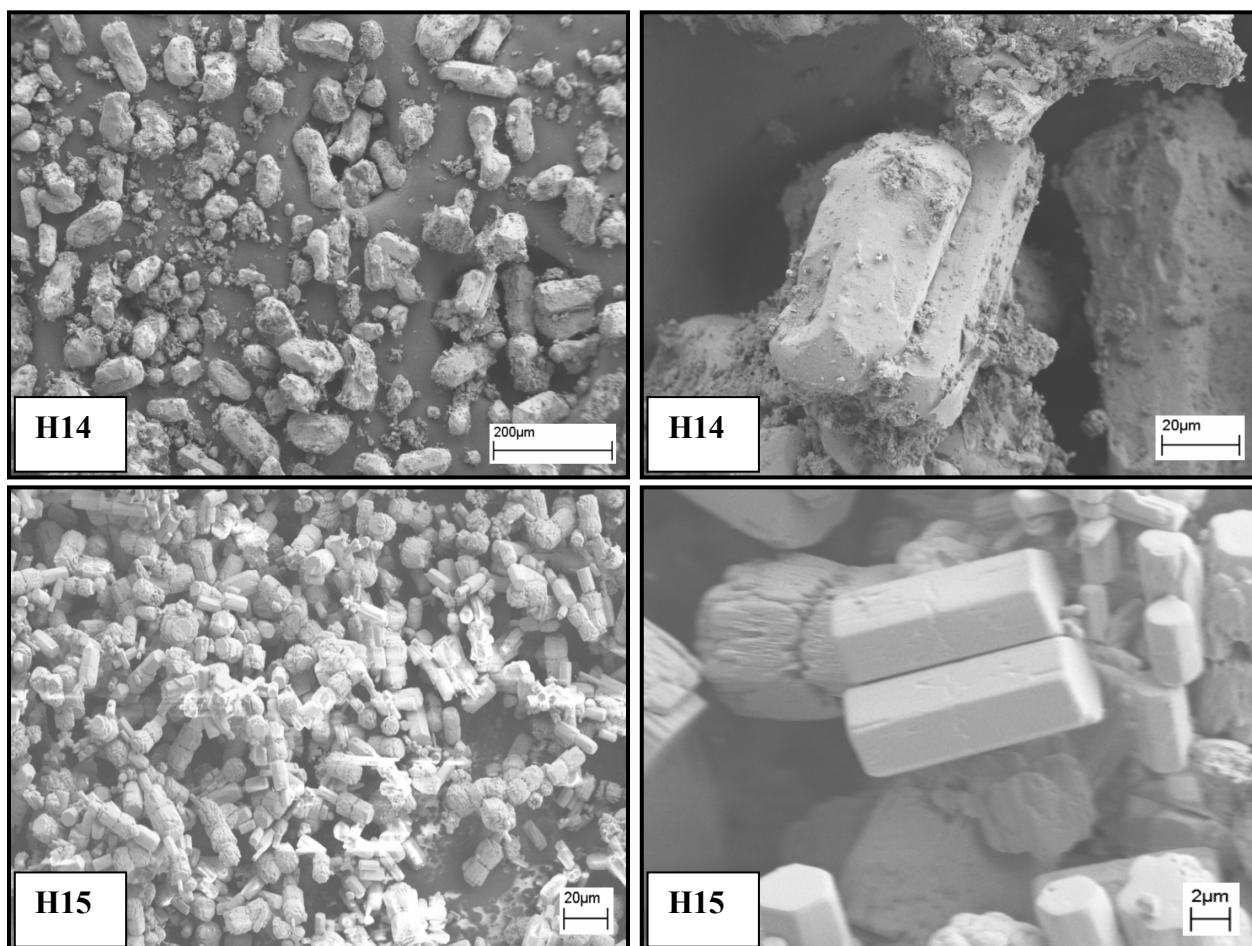
Figure 4.36. SEM micrographs of H14 and H15.
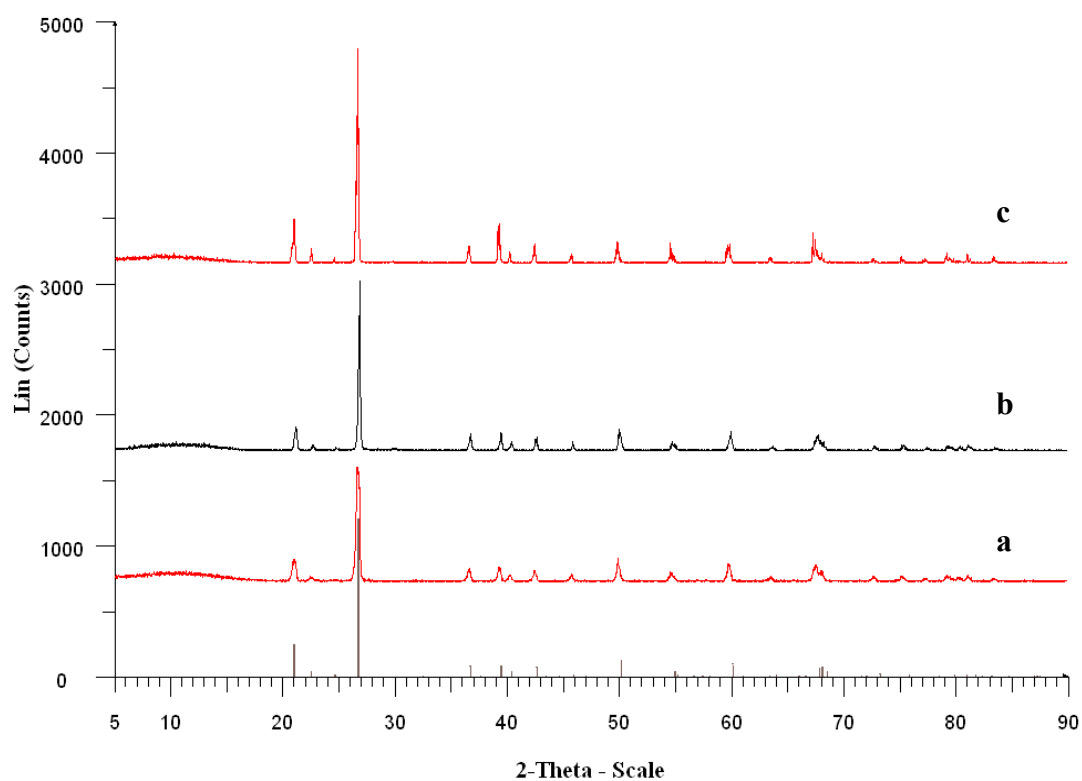
Figure 4.37. XRD patterns of **a.** H11, **b.** H12 and **c.** H13.
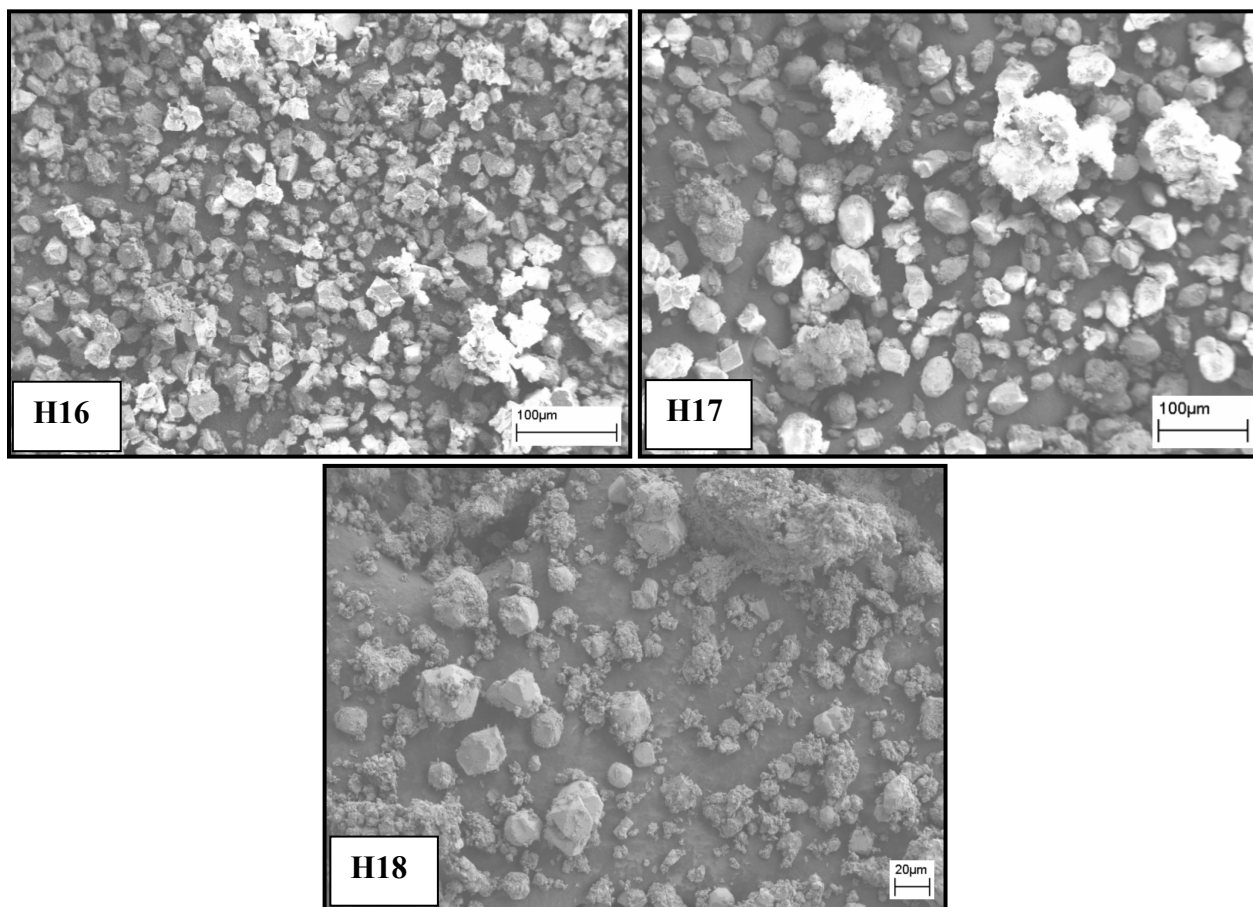
Figure 4.38. SEM micrographs of, **A.**H16, **B.**H17, **C.**H18.
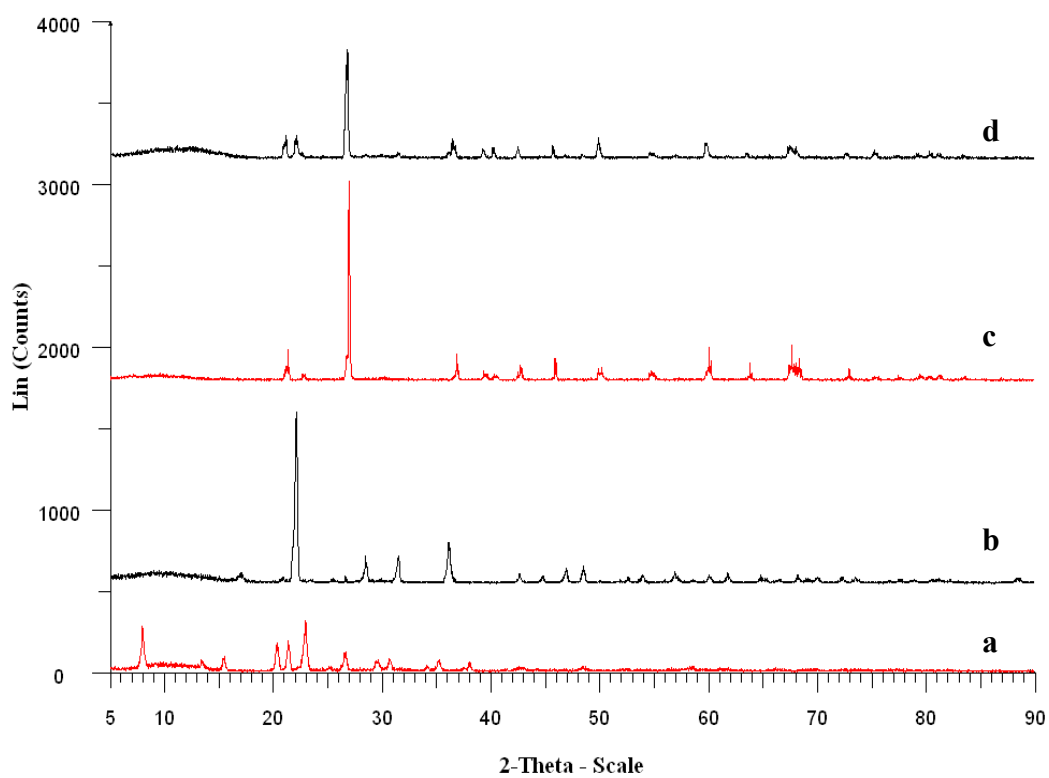
Figure 4.39. XRD patterns of **a.** H15, **b.** H16, **c.** H17 and **d.** H18.

It was observed that the crystallinity of AlPO$_4$-5 crystals was obtained in low crystallization times in the microwave method. The exact crystallization mechanism that occurs by applying microwave heating is still not understood completely The low crystallization times in the crystallization period was considered to result from the high potential of the active water to dissolve the gel constituents under microwave irradiation [205]. In microwave system the microwave irradiation destroys the hydrogen bridges of the water molecules by ion oscillation and water dipole rotation, to result in so called active water [361,362]. The lone pair of OH group of active water molecules has higher potential to dissolve the gel constituents than normal water. Another factor could be influenced of a microwave field on the condensation rate of Al-O-P bondings and simultaneous separation of water. Such effects could become important if the crystallization took place as a direct transformation of gel particles. Such models have recently been proposed by Brunner [363], who discussed the gel as a sponge-like organic-inorganic assembly, and Handerson and White [364], who believe that in the ZSM-5 synthesis the TPA template molecules induce a local structure of the same approximate density as the final crystalline material.

The mechanism of zeolite formation is very complicated [365]. There are two alternative mechanisms are proposed for crystal growth. These include the "solution mediated transport" mechanism, in which amorphous gel is supposed to be dissolved to provide reactants for nucleation that ultimately changes into crystal [366]. The other mechanism is "solid phase transformation" mechanism, in which amorphous gel is assumed to be converted in to crystal [367]. In our case the solution mediated transport mechanism may be occurring as the exposure to microwave dissolve the gel contents.

Powdered AlPO$_4$-5 crystals of high quality can be synthesized using a microwave heating technique. In the microwave heating method, the procedure for the preparation of the gel affects the quality of the final AlPO$_4$-5 product. It is concluded that the crystal growth depends on the initial gel composition. During the microwave heating, the AlPO$_4$-5 crystals grow mainly in the *c*-axis first, and then in the *a–b* plane direction. It is confirmed that the AlPO$_4$-5 powder of H4, produced by the method described in the present study is of sufficient quality to be used as the container for guest material and for studying its properties in detail [327].

4.3   Synthesis of Porous Carbons Using Microwave-Assisted AlPO₄-5 as a Template

Poly(furfuryl alcohol), PFA, used as carbon precursor and microwave assisted AlPO₄-5, labeled H4 was chosen as a templating agent. PFA was carbonized with AlPO₄-5 molecular sieves at different temperatures. Porous carbons were obtained after HF washing of the template.

BET surface areas of AlPO₄-5 templated carbons were measured as 149, 125, 122 and 108 m^2/g at 700, 800, 900 and 1000°C, respectively, are shown in Figure 4.40. BET surface areas seemed to decrease slightly with increasing temperature. The surface areas of natural zeolite templated porous carbons as shown in Figure 4.4 were higher than those of AlPO₄-5 templated porous carbons, due to higher accessibility to the pores in natural zeolite. N_2 adsorption/desorption isotherms and average pore diameter of porous carbons, carbonized at 700, 800, 900 and 1000°C, shown in Figure 4.41 and Figure 4.42, respectively. Rouded knee onserved in all isotherms indicates approximate location of monolayer formation. Low slope region in the middle of the isotherms pointed out the first few multilayers. The presence of hystersis showed that the existence of mesopores. Average pore diameters of all the porous carbons were 1.7 nm, carbonized at 700, 800, 900 and 1000°C, indicating that highly microporosity. This showed that, carbons were mostly formed inside the pores of the AlPO₄-5. Distribution of pore diameters of AlPO₄-5 templated porous carbons, shown in Figure 4.42, was evidence of presence of bigger pores between 6 nm and 9 nm pore diameter, besides smaller ones that have 1.7 nm pore diameters. These results indicated that synthesized porous carbon structures mimiced the structures of the AlPO₄-5 crystals.
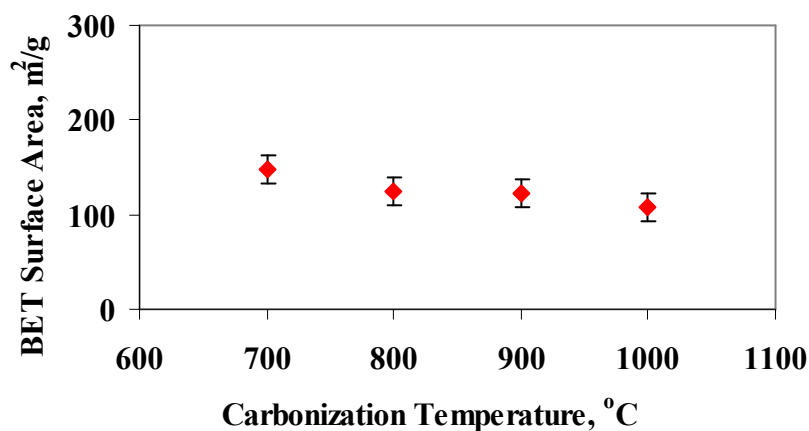
Figure 4.40. Change of BET surface area of AlPO₄-5 templated carbons carbonized at different temperatures.
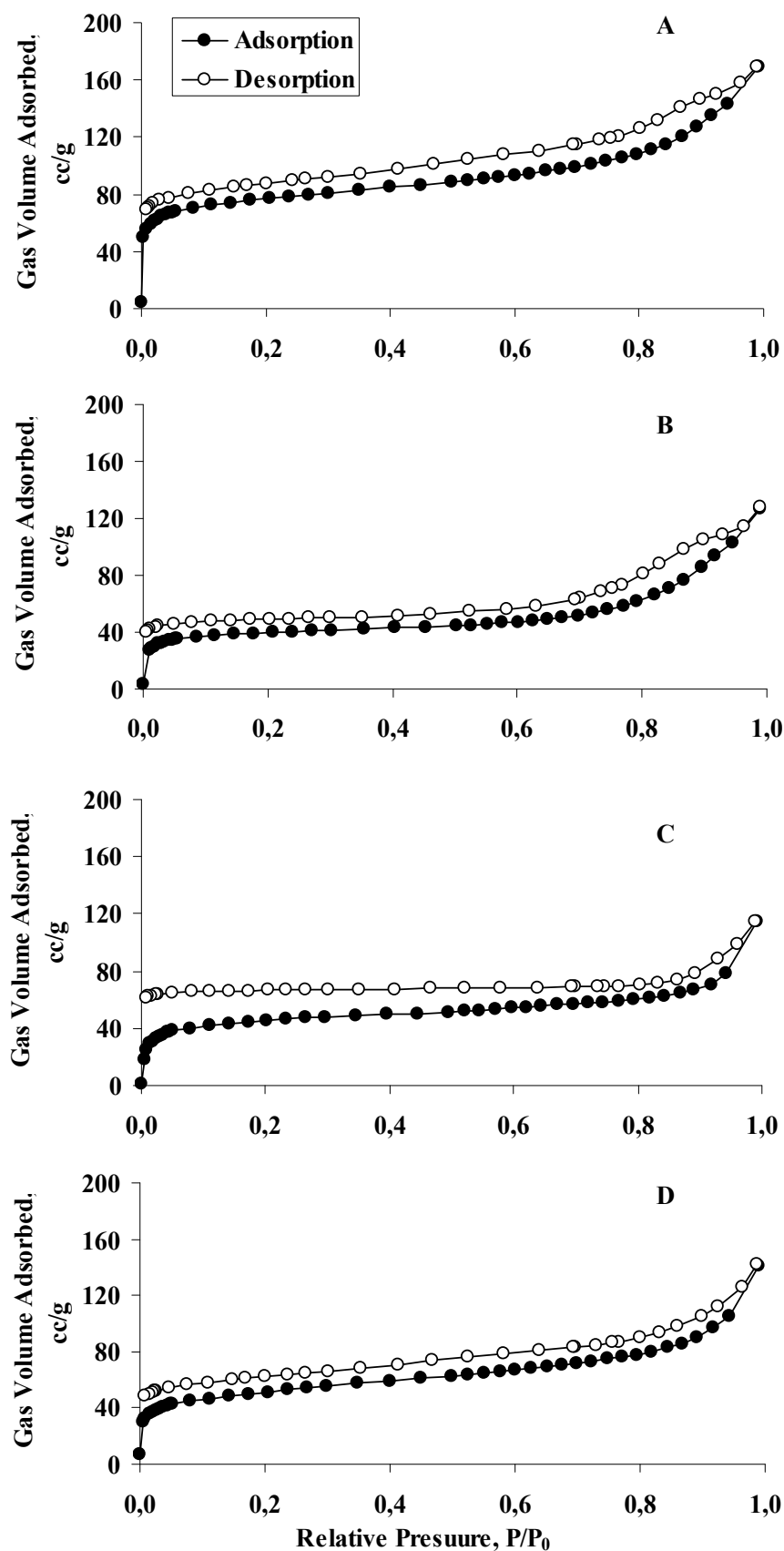
Figure 4.41. N$_2$ adsorption/desorption isotherms of AlPO$_4$-5 templated carbons, carbonized at **A.** 700°C, **B.** 800°C, **C.** 900°C and **D.**1000°C.
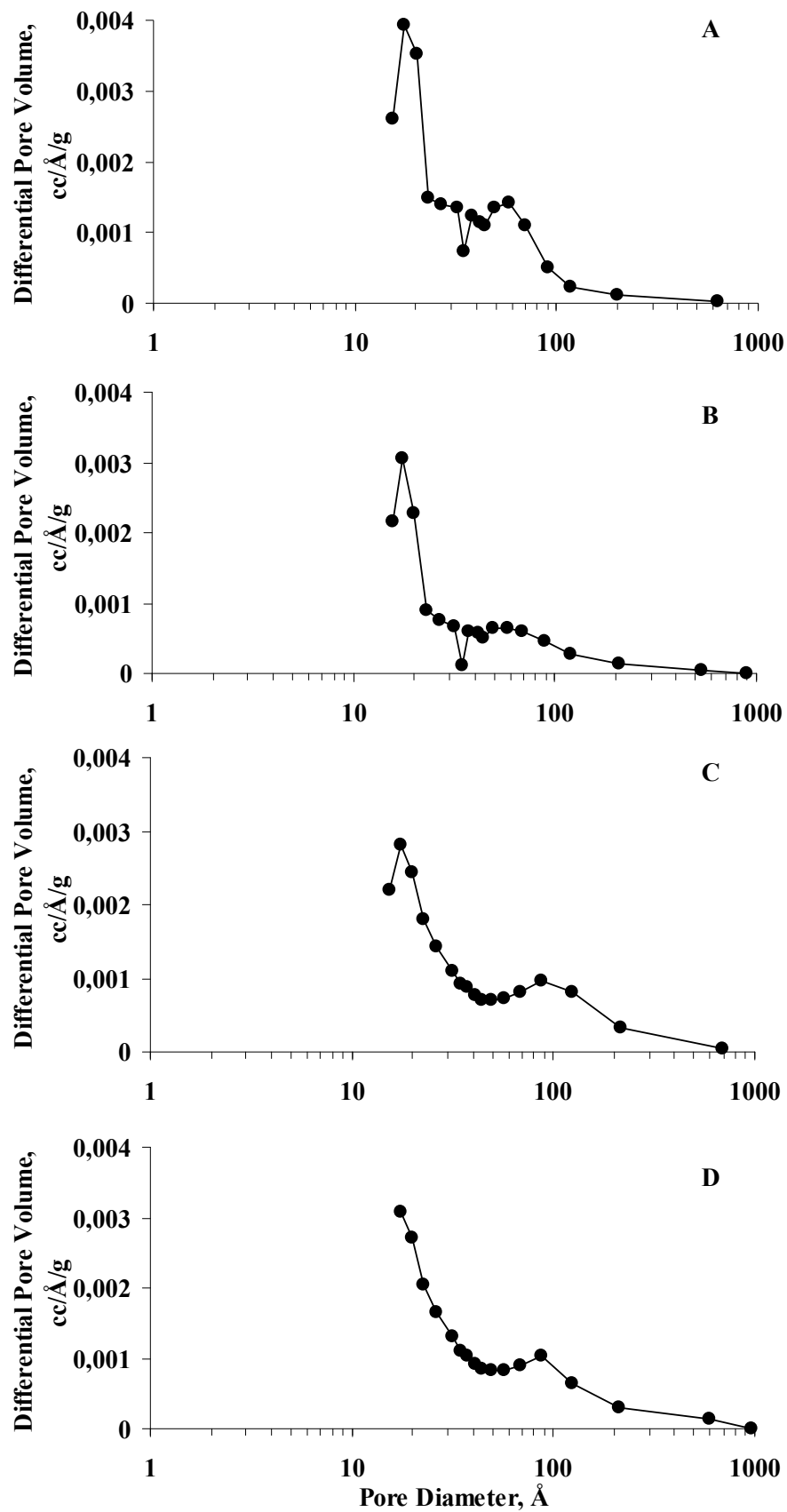
Figure 4.42. Pore size distribution of AlPO$_4$-5 templated carbons, carbonized at **A.** 700°C, **B.** 800°C, **C.** 900°C and **D.** 1000°C.

SEM images of $AlPO_4$-5 templated carbons are shown in Figure 4.43. Porous carbons reflected a honeycomb structure in all of the carbonization temperatures. The SEM images illustrated that some of the carbon materials formed on the outside of the walls of $AlPO_4$-5 crystals. The synthesis route of these pores formed was shown in Figure 4.44. After washing with HF, the $AlPO_4$-5 crystals disappeared, leaving hexagonal shaped holes.

Kyotani et al. [135] synthesized templated porous carbons using various kinds of zeolites as templates and poly(furfuryl alcohol) and propylene as carbon sources. They found that some particles observed in SEM are hollow inside. They concluded that the presence of such hollow particles specified that carbon deposition took place mostly on the external surface of zeolite particles [135]. Previously, Han et al [120,122,123] used the same procedure to produce porous carbons. They polymerized and carbonized sucrose and resorcinol-formaldehyde, RF, in the presence of inorganic silica sol particles. The BET surface area measured was 400-800 m^2/g [122]. Also Ma et al. [136] synthesized porous carbon using zeolites. They also concluded that there is carbon deposition on the external surface of the particles regardless of the type of the synthesis methods.

Electron dispersive spectroscopy (EDS) results of natural zeolite templated carbons at different temperatures are presented in Table 4.6. Carbon contents of the porous carbons detected in EDS were 92%, 90%, 96% and 82% C at 700, 800, 900 and 1000°C, respectively. Carbon contents seemed to decrease with the carbonization temperature. As it was in natural zeolite templated carbons, some fluorine residues still remained in the structure due to the washing solution. Acid washing mostly eliminated the aluminium and phosphorus structures.

Table 4.6. EDS analyses of $AlPO_4$-5 templated porous carbons.

Element	Atom. C, At. %			
	700°C	800°C	900°C	1000°C
Carbon	92.39	90.21	96.00	81.77
Aluminium	0.96	1.34	0.30	3.42
Phosphorus	1.04	1.29	0.55	1.35
Fluorine	4.41	1.45	0.07	5.73
Oxygen	1.20	5.71	3.08	7.73
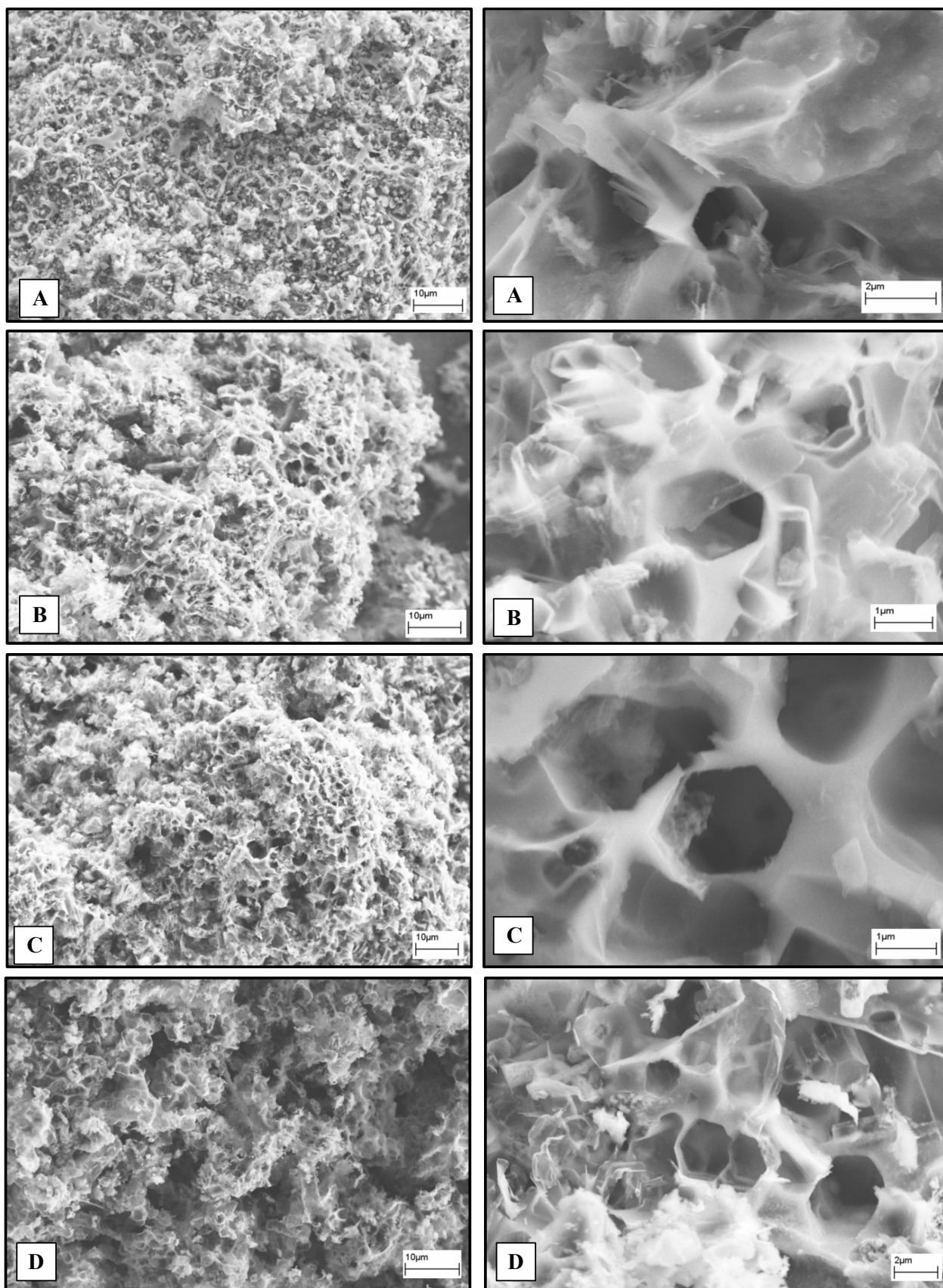
Figure 4.43. SEM images of AlPO$_4$-5 templated carbons, carbonized at **A.** 700°C, **B.** 800°C, **C.** 900°C and **D.** 1000°C.
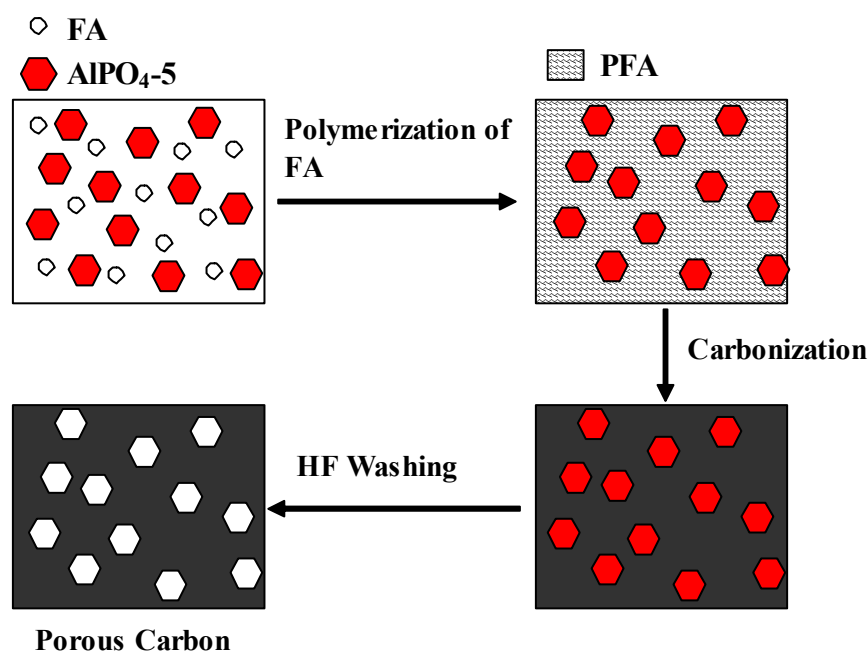
Figure 4.44. Schematic diagram for the synthesis of porous carbon formed on the outside of the walls of $AlPO_4$-5 through polymerization and carbonization of FA and $AlPO_4$-5.

The FT-IR spectra of $AlPO_4$-5 templated porous carbons that were obtained at different temperatures are presented in Figure 4.45. Broad peaks in the 3500-3400 cm^{-1} range due to O-H stretchings are observed in all of the spectra. The bands at the ranges of 2913-2924 cm^{-1} and 2847-2857 cm^{-1} were due to the presence of -CH$_3$ or -CH$_2$- structures. Olefinic C=C stretching bands observed in the range of 1400-1600 cm^{-1}. Broad bands at 1300–1000 cm^{-1} have been assigned to C–O stretching [335]. Peaks observed between 1450-1200 cm^{-1} are due to =C-H stretching band, -C=C-H in-plane C-H bend and -C≡C-H bend overtone respectively [332,333]. The band observed at 1734 cm^{-1} and 868 cm^{-1} was due to keto C=O and aryl C-H groups.
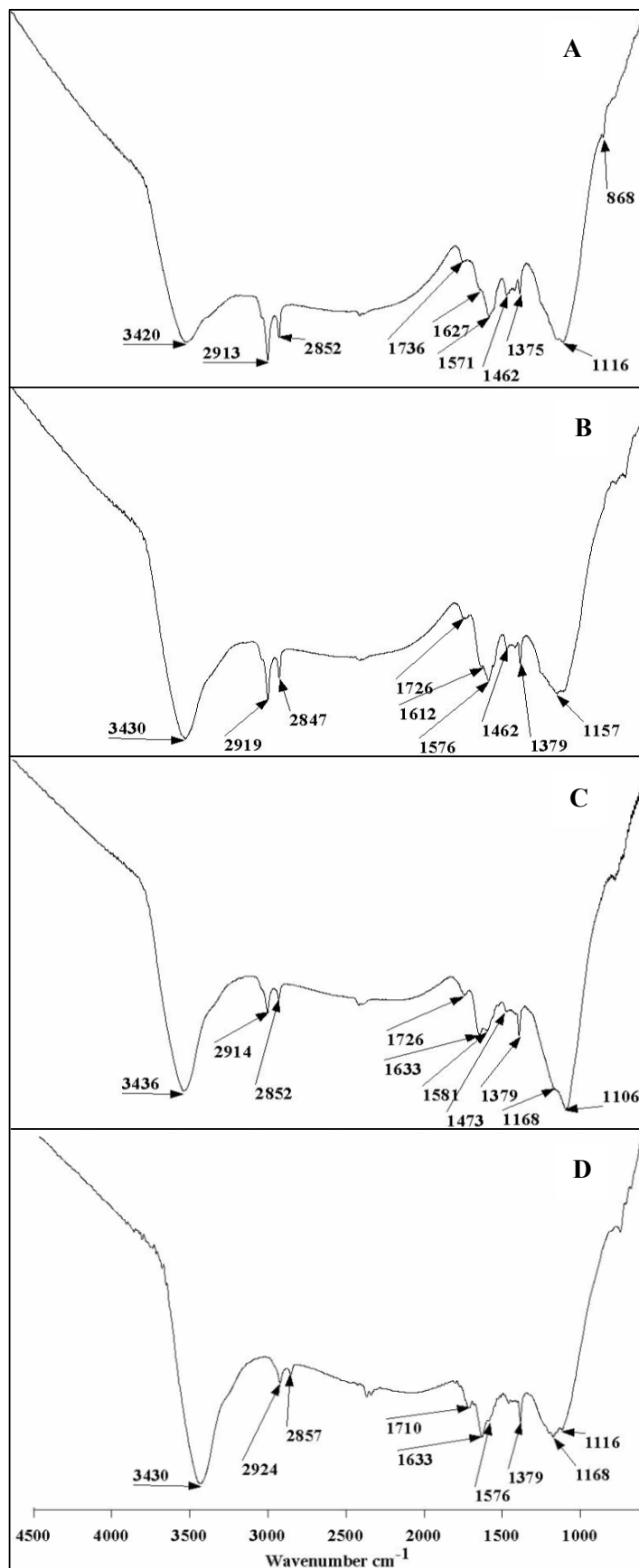
Figure 4.45. FT-IR spectra of AlPO$_4$-5 templated carbons, carbonized at **A**. 700°C, **B.** 800°C, **C.** 900°C and **D.**1000°C.

126

The d_{002} values were calculated from XRD patterns of porous carbons obtained at different temperatures, are shown in Figure 4.46. The resultant porous carbons display two large diffraction peaks near $2\theta = 26°$ and $44°$, which are characteristic of a disordered carbonaceous structure as discussed in the previous sections. A broad peak at $2\theta = 26°$ represents *(002)* reflection of carbon due to the stacking structure of aromatic layers [2].
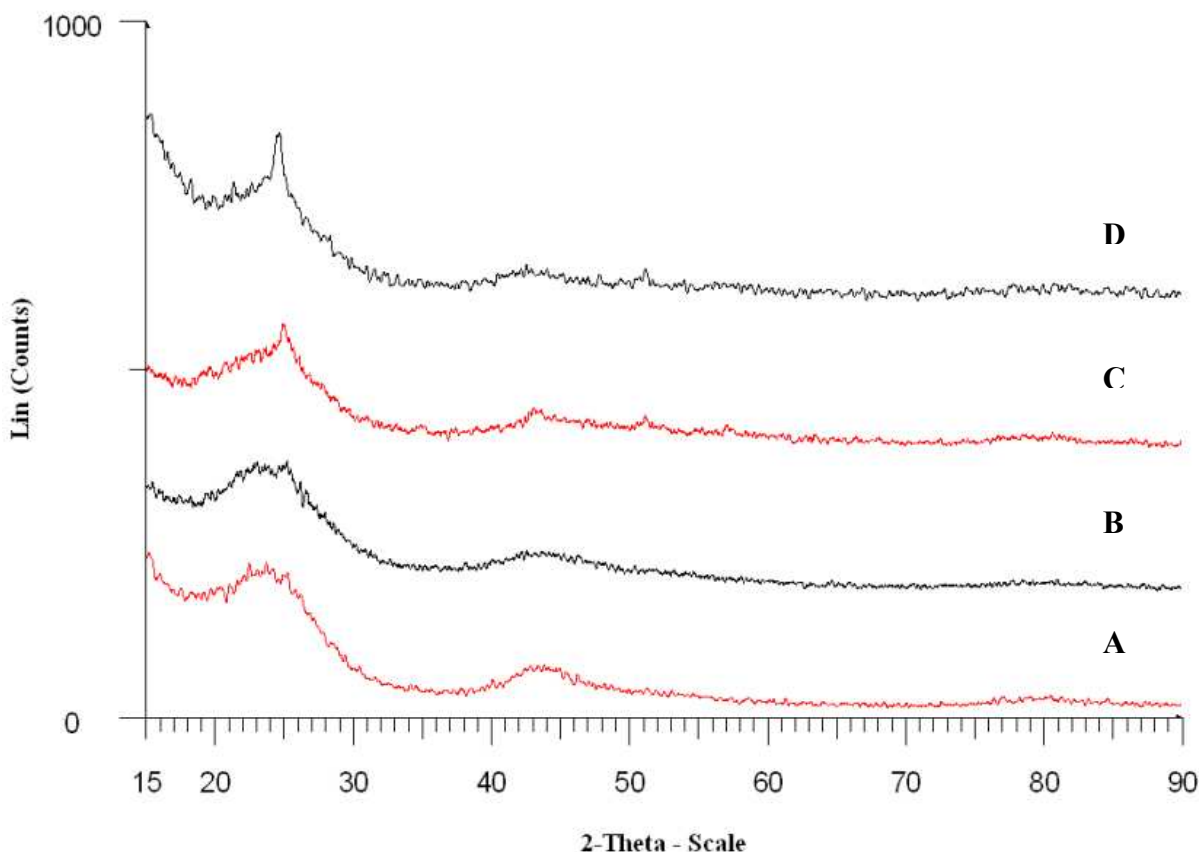
Figure 4.46. XRD of AlPO$_4$-5 templated carbons, carbonized at **A.** 700°C, **B.** 800°C, **C.** 900°C and **D.**1000°C.

The d_{002} values of the AlPO$_4$-5 templated porous carbons are presented in Table 4.7, at different temperatures. The relative intensities of the (*002*) peaks were 1.00, 1.00, 0.81 and 0.79 for carbons obtained at 700, 800, 900 and 1000°C, respectively. These can be considered as indications for the presence of turbostratic (fully disordered) structures in the temperature range of 700-1000°C. The intensity of d_{002} values decreased with increasing temperature. Same results were obtained also in the natural zeolite templated porous carbons. The decrease could be explained by the loss of amounts of carbon as discussed before.

Table 4.7. Change of interlayer spacing of carbons AlPO$_4$-5 templated carbons carbonized at different temperatures.

Carbonization Temperature, °C	d_{002}, nm	Relative intensity of (*002*) peak
700°C	0.358	1.00
800°C	0.358	1.00
900°C	0.362	0.81
1000°C	0.363	0.79

The L_c values, L_a values and the average number of graphene sheets per stack increased with increasing temperature which was calculated from XRD patterns are presented in Figure 4.47, Figure 4.48 and Figure 4.49 respectively. L_c values increased from 1.48 nm to 2.06 nm, L_a values increased from 5.71 nm to 9.46 nm and average number of graphene sheets increased from 4 to 6 when temperature was increased from 700 to 1000°C. Kercher and Nagle [15] found that L_c values of carbons increased from 1.7 to 2.4 nm, L_a values increased from 4.4 to 8.4 nm and average number of graphene sheets increased from 5 to 7 with increasing the carbonization temperature. The disordered carbon is low-density carbonaceous material, which decomposes and gets incorporated into the large graphene sheets of the turbostratic carbon with increasing carbonization temperature [15]. Some graphene sheets grow extensively, and other sheets become terminated and pinned by structural defects. The conversion of low-density disordered carbon into high density graphene sheets causes the volumetric contraction observed during carbonization [15]. BET surface areas of AlPO$_4$-5 templated porous carbons slightly decreased with temperature due to volumetric contraction. Darmstadt et al. [329] pointed out that L_c and L_a values increased with decreasing surface area. Yoshizawa et al. [368] indicated that the number of layers decreased continuously with the increase in surface area.

Emmerich [369] studied the variation of the dimensions L_c and L_a of the graphite-like crystallites of graphitizable carbons with heat treatment using XRD techniques. It was observed that the temperature separating the vegetative increase and the coalescent increase of L_c and L_a depends largely on carbon used.

L_c values obtained from AlPO$_4$-5 were lower than that of natural zeolite. The increasing trend of the values in AlPO$_4$-5 templated porous carbons was also different from natural zeolite templated porous carbons. Slope of the curves seemed to increase steadily, this showed that the growing of the crystallites did not reach the equilibrium state as in

natural zeolite templated carbons Figure 4.12. Grumer et al. [370] found that above a certain temperature L_c and L_a increased sharply with increase of heat treatment
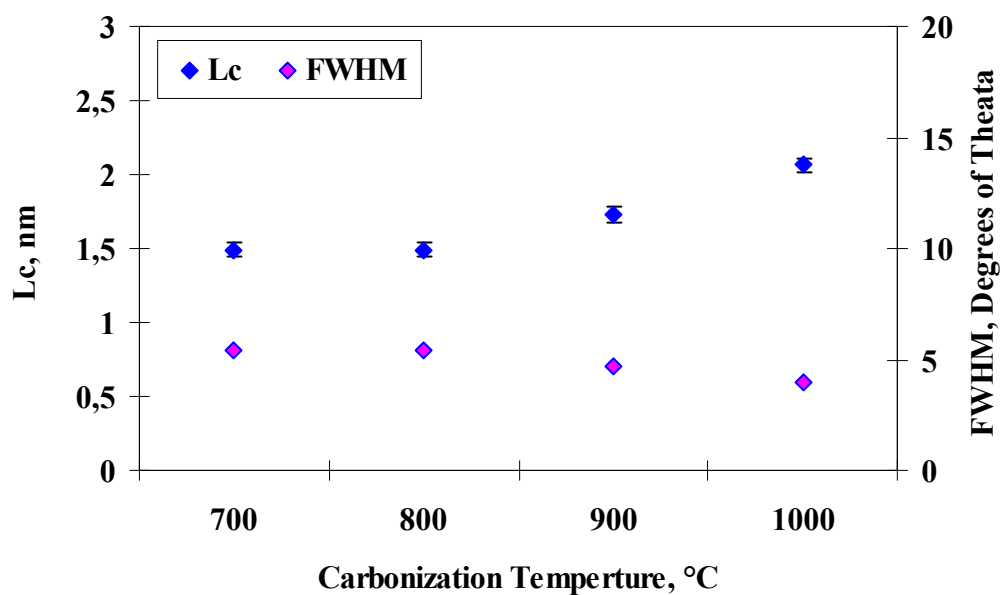
Figure 4.47. Change of FWHM and L_c values of AlPO$_4$-5 templated carbons carbonized at different temperatures.
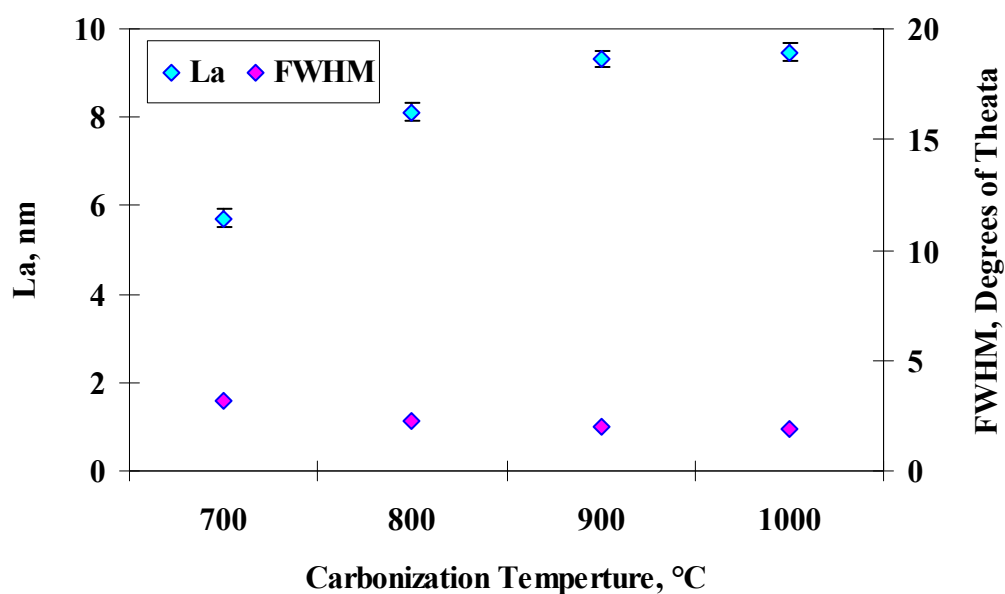
Figure 4.48. Change of FWHM and L_a values of AlPO$_4$-5 templated carbons carbonized at different temperatures.
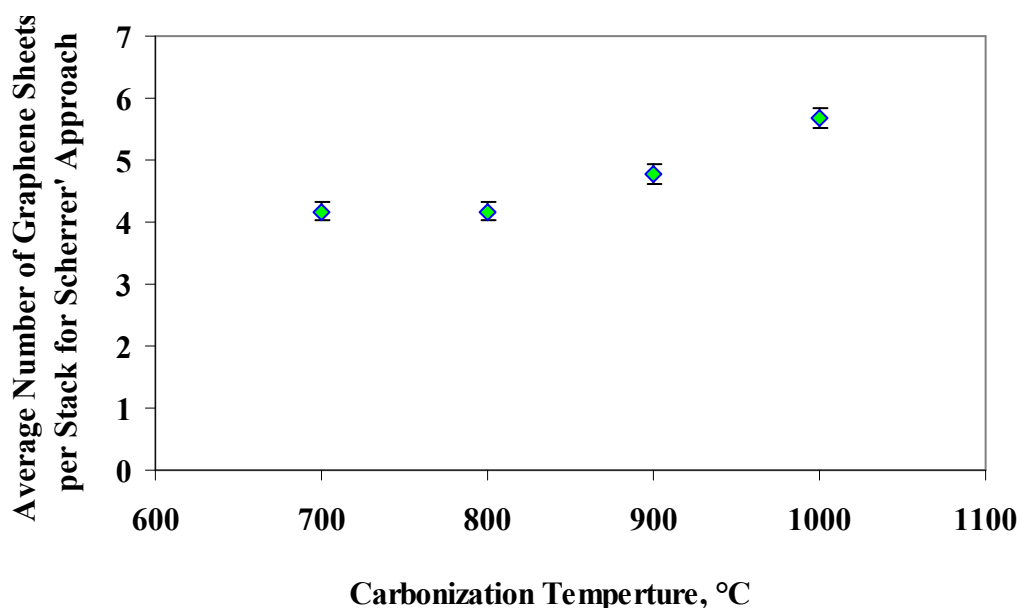
Figure 4.49. Change of the average number of graphene sheets of carbons $AlPO_4$-5 templated carbons carbonized at different temperatures.

4.4 Diffusion of Volatile Organic Chemicals in Porous Media

4.4.1 Natural Zeolite as a Porous Media

The zeolite used in the present study contains 40.2% micro, 57.9% mesopores and 1.9% macropores, Table 3.1. It seemed that the zeolite enclosed the material diffused in it, mainly inside the meso and micropores. Alcohol molecules might have been sorbed on the pore walls, which was in equilibrium with the intra-zeolitic free gas phase. The sorbed molecules probably could not escape the force field of the surrounding pore wall atoms which might be considered as the Brønsted acid sites that methanol was initially adsorbed [371]. Therefore the maximum value attained could be attributed to the adsorption of alcohols mainly to the surface sites of the zeolite.

The coefficients of diffusion of methanol, ethanol, n-propanol, i-propanol and n-butanol at 24.0, 26.0 and 28.0°C are presented in Table 4.8. It is seen that the higher the molecular weight of alcohols, the lower the coefficients of diffusion they had, thus lower amounts of higher alcohols were transported relative to the lower alcohols at the same temperatures due to steric hindrances. The entry of the diffusing molecules into the zeolite channels is strongly influenced by the critical size of the molecules [372]. At sufficiently low temperature or at short time scales *Case a* detailed in the Introduction section, must

prevail, but at increasingly higher temperature and time scales all the other cases will eventually occur [274]. Therefore, the effective relatively longer time ($\approx$10 minutes) scale coefficients of diffusion calculated in the present work might be the result of a complex mechanism and will depend on the different coefficients of diffusion characteristic each of the considered cases stated above.

Increasing the temperature increased the kinetic energy of the molecules and therefore, caused increases also in the coefficients of diffusion; for example coefficients of diffusion of methanol at 24.0, 26.0 and 28.0°C were measured as 4.53×10^{-14}, 4.76×10^{-14} and 5.00×10^{-14} m^2/s, respectively. Dyer and Amin [373] studied the liquid phase self diffusion of ethanol and n-butanol in heteroionic zeolites, coefficients of diffusion measured by these workers are much lower ($\approx 1.15 \times 10^{-18}$m^2/s and $\approx 1.94 \times 10^{-18}$m^2/s) than those measured in the present work. This is definitely due to the difference of liquid phase uptake of ethanol and n-butanol in the work of Dyer and Amin [373] and gas phase diffusion of the same alcohols measured in the present report. Sorption/diffusion in the zeolite from the liquid phase and gas (or vapor) phase differs from each other in the intra-crystalline mass transfer for the entry of sorbate molecules to the zeolite channels [372].

Table 4.8. Coefficients of diffusion of volatile alcohols in natural zeolite.

Alcohol Type	$T, \ ^\circ C$	$D, m^2/s$
Methanol	24.0	4.53×10^{-14}
	26.0	4.76×10^{-14}
	28.0	5.00×10^{-14}
Ethanol	24.0	3.48×10^{-14}
	26.0	4.29×10^{-14}
	28.0	4.46×10^{-14}
n-Propanol	24.0	2.20×10^{-14}
	26.0	3.00×10^{-14}
	28.0	3.40×10^{-14}
i-Propanol	24.0	3.08×10^{-14}
	26.0	3.31×10^{-14}
	28.0	3.88×10^{-14}
n-Butanol	24.0	2.04×10^{-14}
	26.0	2.31×10^{-14}
	28.0	3.32×10^{-14}

The coefficients of diffusion measured in the present work were lower than those reported by Bludau et al. [309] for pyridine diffusion into mordenite and H-ZSM-5, ($D = 1\text{x}10^{-12}$ m^2/s and $D = 6\text{x}10^{-11}$ m^2/s, respectively), who claimed the transport of pyridine into the micropores was the rate-determining step. The reason for the lower values of coefficients of diffusion in the case of alcohols might be due to stronger polar interactions of alcohols with the zeolitic intracrystalline surfaces. It has been found that occurrence of various factors such as intra- and inter-particle transport, might affect the overall rate of the sorption process [311]. Keipert and Baerns [318] also mention that zeolite crystal radius and length of the zeolite layer strongly affect the estimated values of the intracrystalline coefficient of diffusion.

The diffusion rate constants, diffusion exponents and transport mechanisms of different alcohols in the natural zeolite presented in Table 4.9. Analysis of the linearity of these plots gave acceptable regressional coefficients (R^2) in all cases; R^2 values in all of the experiments were equal to or greater than 0.98 indicating a linear relationship between ln (M_t/M_∞) and ln t. It seemed that diffusion of alcohols in zeolite could be approximated with a first-order rate law for all of the alcohols studied. Diffusion rate constants slightly increased as the temperature was increased and decreased as the molecular weight increased, for all of the samples in the range of 24.0 – 28.0^{o}C. Diffusion rate constant of i-propanol was lower than those of n-propanol. Timescale of the intracrystalline diffusion is influenced by smaller crystals leading to shorter diffusion times [318]. Crystal size distribution and deviations from the spherical shape are assumed further to influence accuracy. The reason of different rate constants in this paper was the zeolite type that is used and the crystalline structures varieties found in this natural zeolite clinoptilolite.

The diffusion exponents, n, were calculated to be between 0.96–1.00 in all experiments done at all temperatures indicating an anomalous diffusion mechanism. The calculations were done assuming the diffusion mechanism is Fickian. Although the literature results closer to our results, it is clear those different techniques, models and assumptions (crystal shape, size) may strongly affect the results. Further progress in zeolite diffusion may be achieved by simultaneous fitting of experiments for different zeolite types.

Table 4.9. Diffusion rate constants, diffusion exponents, and transport mechanisms of volatile alcohols in natural zeolite.

Alcohol Type	T, °C	k ,s^{-1}	n	R^2	Activation Energy of Diffusion, kJ/mol
Methanol	24.0	1.36×10^{-3}	1.00	0.988	
	26.0	1.65×10^{-3}	0.99	0.994	18.3
	28.0	1.76×10^{-3}	0.97	0.997	
Ethanol	24.0	1.27×10^{-3}	0.97	0.997	
	26.0	1.51×10^{-3}	0.96	0.991	46.4
	28.0	1.57×10^{-3}	0.98	0.989	
n-Propanol	24.0	1.24×10^{-3}	1.00	0.999	
	26.0	1.50×10^{-3}	1.00	0.997	79.7
	28.0	2.17×10^{-3}	1.00	0.999	
i-Propanol	24.0	6.77×10^{-4}	1.00	0.998	
	26.0	1.07×10^{-3}	1.00	0.982	57.3
	28.0	1.27×10^{-3}	0.99	0.994	
n-Butanol	24.0	7.35×10^{-4}	0.98	0.998	
	26.0	9.26×10^{-4}	0.99	0.996	90.1
	28.0	9.99×10^{-4}	0.99	0.998	

Calculated activation energies were 18.3, 46.4, 79.7, 57.3 and 90.1 kJ/mol for methanol, ethanol, n-propanol, i- propanol and n-butanol, respectively. There should be a strong influence of chain length, polarity, critical molecular size and configuration of diffusing molecules on the diffusion coefficients and activation energies. With increasing molecular weight of the volatile alcohols the activation energies also increased. Activation energy of i-propanol was lower than n-propanol. Branching of the molecule resulted in higher coefficients of diffusion. Activation energies measured were also in accord with the values of diffusion coefficients of alcohols for different temperatures. The activation energies might be thought of as the energy required producing the diffusive motion of one mole of penetrant molecules [298]. Large activation energy results in a relatively small diffusion coefficient. The activation energy of methanol in the zeolite was measured to be the smallest among those of alcohols and of diffusion coefficients methanol at all temperatures was the greatest.

4.4.2   Natural Zeolite Templated Porous Carbons as a Porous Media

The coefficients of diffusion of methanol, ethanol, n-propanol, and n-butanol at 24.0, 26.0 and 28.0°C into porous carbons which carbonized at 700, 800, 900 and 1000°C were presented in Table 4.10, Table 4.11, Table 4.12 and Table 4.13, respectively.

In all of the samples the coefficients of diffusion increased with an increase in the diffusion temperature due to higher mobility of volatile molecules. The coefficient of diffusion of methanol in the porous carbon, carbonized at 700°C, increased from 2.05×10^{-14} m^2/g to 3.37×10^{-14} m^2/g when the diffusion temperature was elevated from 24.0 to 28.0°C, respectively. Seferinoglu and Yürüm [298] also observed that the diffusion of pyridine in the coal is increased with increasing temperature. Prasetyo et al. [374] studied the surface diffusion of hydrocarbon vapors on activated carbon by using a constant molar flow method. They concluded that the surface diffusivity increases with temperature according to the Arrhenius law, and decreases with the molecular weight of the adsorbate.

Higher the molecular weight of the alcohol, the lower coefficient of diffusion was observed in all porous carbons, carbonized at different temperatures, owing to steric hindrances. The diffusion of methanol in the porous carbons seemed to be less, compared to those of the other alcohols. The coefficients of diffusion of methanol, ethanol, n-propanol and n-butanol in the porous carbon, carbonized at 700°C, were 2.05×10^{-14}, 9.98×10^{-15}, 8.57×10^{-15} and 1.59×10^{-15} m^2/g at 24.0°C, respectively. Prasetyo et al. [374] studied the surface diffusion ethanol under constant flow over the porous carbons. Coefficients of diffusion measured by these workers are much higher (7.09×10^{-11} m^2/s) than those measured in the present work.

Do and coworkers [375-377] proposed a model for diffusion of adsorbed species in activated carbon. In that model, it was assumed that the carbon is composed of units of graphitic layers. Molecules enter one end of the unit, diffuse within the graphitic units and then evaporate from the other end of the unit. The process of entering the pore and leaving the pore would have energy equivalent to that of adsorption. Therefore the "observed" activation energy for surface diffusion will fall between the activation energy for diffusion within the graphitic unit and the heat of adsorption. This seems reasonable as for larger molecules, one would expect that the penetration into the graphitic network is more

difficult than that of smaller molecules. This is the case that one would observe for carbon molecular sieve.

The calculated coefficients of diffusion of volatile molecules in the porous carbons were lower than that of observed in the natural zeolite. The large number and array of different functional groups on carbon surface (e.g., carboxylic, carbonyl, hydroxyl, ether, quinone, lactone, anhydride, etc.) imply that there are many types of solute–adsorbent interaction [378]. The electrostatic interaction between the hydroxyl group of alcohols and the functional groups such as carboxylic acid on carbon surface can explain such results.

The experiments were carried out under same operating conditions for screening the various porous carbons, carbonized at different temperatures. As observed in the Table 4.10 to Table 4.13, the coefficients of diffusion for the volatile molecules over porous carbons followed the same trend.

The diffusion rate constants, diffusion exponents and transport mechanisms of different alcohols in the porous carbons, carbonized at 700°C, 800°C, 900°C and 1000°C presented in Table 4.14, Table 4.15, Table 4.16 and Table 4.17, respectively. In all samples acceptable regression coefficients (R^2) were observed. It seemed that diffusion of alcohols in porous carbons could be also approximated with a first-order rate law for all of the alcohols studied.

As the temperature of diffusion was increased, diffusion rate constants increased for all the samples. Diffusion rate constant of methanol over porous carbon, carbonized at 700°C, was increased from 3.13 x 10^{-4} s^{-1} to 5.15 x 10^{-3} s^{-1} when diffusion temperature increased from 24.0 to 28.0°C.

The diffusion exponents, n, were calculated to be between 0.58–1.00 in all experiments done at all temperatures indicating an anomalous diffusion mechanism. The anomalous coefficients of diffusion in the literature usually are in the range of 0.6-1.0 [285,294,379]. Although the literature is similar to our results, it is clear those different techniques, models and assumptions (crystal shape, size) may strongly affect the results.

Table 4.10. Coefficients of diffusion of volatile alcohols in natural zeolite templated porous carbon, carbonized at 700°C.

Alcohol Type	$T, °C$	$D, m^2/s$
Methanol	24.0	2.05×10^{-14}
	26.0	2.95×10^{-14}
	28.0	3.37×10^{-14}
Ethanol	24.0	9.98×10^{-15}
	26.0	1.54×10^{-14}
	28.0	2.49×10^{-14}
n-Propanol	24.0	8.57×10^{-15}
	26.0	1.96×10^{-14}
	28.0	2.11×10^{-14}
n-Butanol	24.0	1.59×10^{-15}
	26.0	2.97×10^{-15}
	28.0	5.21×10^{-15}

Table 4.11. Coefficients of diffusion of volatile alcohols in natural zeolite templated porous carbon, carbonized at 800°C.

Alcohol Type	$T, °C$	$D, m^2/s$
Methanol	24.0	1.31×10^{-14}
	26.0	1.87×10^{-14}
	28.0	2.37×10^{-14}
Ethanol	24.0	1.18×10^{-14}
	26.0	1.25×10^{-14}
	28.0	2.52×10^{-14}
n-Propanol	24.0	3.85×10^{-15}
	26.0	1.12×10^{-14}
	28.0	1.81×10^{-14}
n-Butanol	24.0	1.45×10^{-15}
	26.0	3.00×10^{-15}
	28.0	4.10×10^{-15}

Table 4.12. Coefficients of diffusion of volatile alcohols in natural zeolite templated porous carbon, carbonized at 900°C.

Alcohol Type	$T,$ °C	$D, m^2/s$
Methanol	24.0	1.92×10^{-14}
	26.0	2.41×10^{-14}
	28.0	2.86×10^{-14}
Ethanol	24.0	1.21×10^{-14}
	26.0	1.41×10^{-14}
	28.0	2.13×10^{-14}
n-Propanol	24.0	7.85×10^{-15}
	26.0	1.57×10^{-14}
	28.0	1.66×10^{-14}
n-Butanol	24.0	3.21×10^{-15}
	26.0	5.00×10^{-15}
	28.0	7.99×10^{-15}

Table 4.13. Coefficients of diffusion of volatile alcohols in natural zeolite templated porous carbon, carbonized at 1000°C.

Alcohol Type	$T,$ °C	$D, m^2/s$
Methanol	24.0	1.49×10^{-14}
	26.0	1.86×10^{-14}
	28.0	2.18×10^{-14}
Ethanol	24.0	1.57×10^{-14}
	26.0	2.08×10^{-14}
	28.0	2.35×10^{-14}
n-Propanol	24.0	7.23×10^{-15}
	26.0	1.33×10^{-14}
	28.0	1.42×10^{-14}
n-Butanol	24.0	2.41×10^{-15}
	26.0	2.51×10^{-15}
	28.0	7.46×10^{-15}

Table 4.14. Diffusion rate constants, diffusion exponents, and transport mechanisms of volatile alcohols in natural zeolite templated porous carbon, carbonized at 700°C.

Alcohol Type	T, °C	k, s^{-1}	n	R^2	Activation Energy of Diffusion, kJ/mol
Methanol	24.0	3.13×10^{-4}	0.96	0.984	
	26.0	1.33×10^{-3}	0.73	0.983	92.3
	28.0	5.15×10^{-3}	0.62	0.966	
Ethanol	24.0	3.94×10^{-4}	1.00	0.963	
	26.0	7.38×10^{-4}	0.99	0.969	169.7
	28.0	4.30×10^{-3}	0.71	0.953	
n-Propanol	24.0	2.55×10^{-4}	1.00	0.995	
	26.0	2.90×10^{-4}	1.00	0.991	167.8
	28.0	2.00×10^{-3}	0.69	0.988	
n-Butanol	24.0	1.15×10^{-4}	1.00	0.994	
	26.0	3.31×10^{-4}	1.00	0.985	220.7
	28.0	1.18×10^{-3}	0.95	0.970	

Table 4.15. Diffusion rate constants, diffusion exponents, and transport mechanisms of volatile alcohols in natural zeolite templated porous carbon, carbonized at 800°C.

Alcohol Type	T, °C	k, s^{-1}	n	R^2	Activation Energy of Diffusion, kJ/mol
	24.0	5.33×10^{-4}	0.98	0.935	
Methanol	26.0	3.82×10^{-3}	0.67	0.945	111.1
	28.0	4.14×10^{-3}	0.67	0.948	
	24.0	4.19×10^{-4}	0.98	0.998	
Ethanol	26.0	3.19×10^{-3}	0.62	0.996	140.7
	28.0	4.28×10^{-3}	0.54	0.998	
	24.0	3.61×10^{-5}	1.00	0.990	
n-Propanol	26.0	5.87×10^{-4}	0.99	0.977	191.2
	28.0	2.82×10^{-3}	0.74	0.976	
	24.0	3.11×10^{-4}	1.00	0.958	
n-Butanol	26.0	4.59×10^{-4}	1.00	0.990	193.0
	28.0	8.61×10^{-4}	0.96	0.967	

Table 4.16. Diffusion rate constants, diffusion exponents, and transport mechanisms of volatile alcohols in natural zeolite templated porous carbon, carbonized at 900°C.

Alcohol Type	T, °C	k, s^{-1}	n	R^2	*Activation Energy of Diffusion, kJ/mol*
Methanol	24.0	1.90×10^{-3}	0.85	0.992	
	26.0	3.45×10^{-3}	0.81	0.981	74.2
	28.0	4.66×10^{-3}	0.75	0.978	
Ethanol	24.0	4.83×10^{-4}	1.00	0.983	
	26.0	9.03×10^{-4}	0.49	0.987	104.4
	28.0	4.00×10^{-3}	1.00	0.989	
n-Propanol	24.0	2.29×10^{-4}	1.00	0.992	
	26.0	3.20×10^{-4}	1.00	0.993	139.6
	28.0	8.89×10^{-4}	1.00	0.978	
n-Butanol	24.0	3.00×10^{-4}	0.98	0.998	
	26.0	3.40×10^{-4}	0.99	0.996	169.3
	28.0	1.00×10^{-3}	0.99	0.998	

Table 4.17. Diffusion rate constants, diffusion exponents, and transport mechanisms of volatile alcohols in natural zeolite templated porous carbon, carbonized at 1000°C.

Alcohol Type	T, °C	k, s^{-1}	n	R^2	*Activation Energy of Diffusion, kJ/mol*
Methanol	24.0	5.65×10^{-4}	1.00	0.972	
	26.0	4.39×10^{-3}	0.95	0.960	70.6
	28.0	5.35×10^{-3}	0.87	0.962	
Ethanol	24.0	2.31×10^{-4}	0.97	0.997	
	26.0	9.60×10^{-4}	0.96	0.991	76.2
	28.0	5.00×10^{-3}	0.98	0.989	
n-Propanol	24.0	3.22×10^{-4}	1.00	0.979	
	26.0	1.07×10^{-3}	0.89	0.963	125.5
	28.0	1.36×10^{-3}	0.84	0.981	
n-Butanol	24.0	4.00×10^{-4}	1.00	0.979	
	26.0	5.00×10^{-4}	0.59	0.956	208.9
	28.0	4.00×10^{-4}	0.58	0.971	
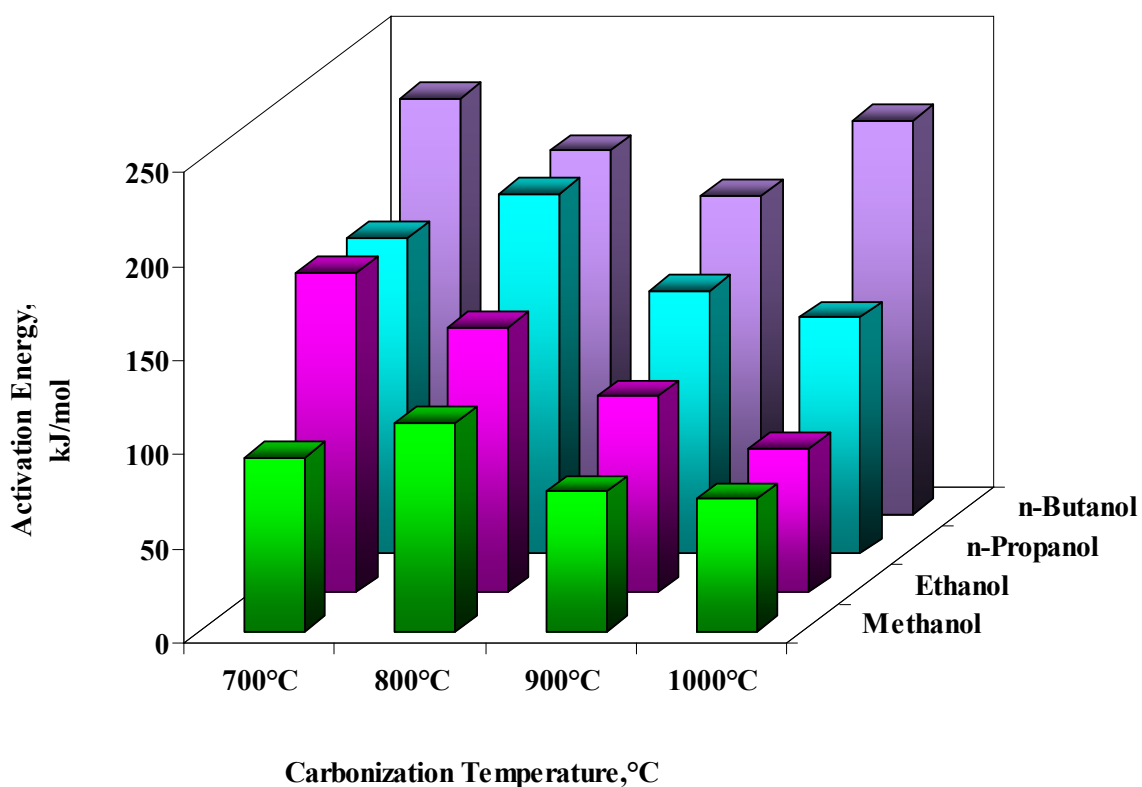
Figure 4.50. Activation energies of diffusion for the alcohols

The activation energies of diffusion measured for methanol, ethanol, n-propanol, and n-butanol over porous carbons were presented in Figure 4.50. With increasing molecular weight of the volatile alcohols the activation energies also increased. The activation energy of methanol in the porous carbons was measured to be the smallest among those of alcohols and of diffusion coefficients methanol at all temperatures was the greatest. The similar results were observed in the diffusion of alcohols in natural zeolites.

It is interesting to compare the activation energies measured in natural zeolite and natural zeolite templated porous carbons. The activation energies for diffusion of methanol were 90.1 kJ/mol and 220.7 kJ/mol over natural zeolite and porous carbon, carbonized at 700°C, respectively. Although the operating conditions are the same, the diffused methanol molecule over porous carbon has to overcome an energy barrier twice as much as that of natural zeolite. This is most likely due to the polarity of alcohols. Compounds containing the –OH group are generally highly polar and have an appreciable electrostatic field due to

the resultant dipoles [380]. Being a polar molecule, alcohols have stronger interaction with carbon surface which is dispersed with functional groups.

Since the morphology of porous carbon is very complex, obtaining reliable data is one of the major problems in our quest for determining coefficient of diffusions of volatile molecules in this material. The irregularity of the pore structure, resulting in energetic heterogeneity of the solid surface, makes the nature of the diffusion on porous carbon materials very complicated. A detailed pore structure for this material cannot be fully determined due to the complexity of the morphology of templated porous carbons. Nevertheless, informative description can be obtained by measuring the physical properties (e.g. porosity, pore size distribution, BET surface area) and the diffusion characteristics of organic volatile molecules on this material.

CONCLUSIONS

1. Porous carbons were synthesized by using natural zeolites and microwave assisted AlPO$_4$-5 as a template. Furfuryl alcohol, FA, was used as carbon precursor in both cases. Diffusion of volatile organic chemicals in natural zeolites and natural zeolite templated porous carbons were investigated. Coefficients of diffusion, mode of transport and activation energies of simple alcohols into the porous structure of a Turkish natural zeolite and natural zeolite templated porous carbons were studied.

2. The template carbonization method has been utilized successfully for the production of mesoporous carbons templated from Turkish natural zeolite. Hydrofluoric acid, HF was used to dissolve the templates.

3. BET surface areas of natural zeolite templated carbons were 397, 350, 405 and 367 m^2/g at 700, 800, 900 and 1000°C, respectively. Templated porous carbons were mesoporous with 11 nm average pore diameter. BET area of TEOS-FA carbon was 804 m^2/g.

4. The d_{002} values of the porous carbons synthesized by carbonization of FA in the channels of zeolite were 0.358, 0.347, 0.349 and 0.346 nm at 700, 800, 900 and 1000°C, respectively. L_c values and average number of graphene sheets per stack were increasing with carbonization temperature. The size of the microcrystallites increases quickly with increasing pyrolytic temperature L_c values were increased from 2.79 nm to 6.64 nm, and average number of graphene sheets increased from 8 to 19 when temperature was increased from 700°C to 1000°C.

5. EDS analyses showed that 91-99% carbon was obtained with the carbonization of PFA in the zeolite at 700-1000°C. The success of the demineralization step was indicated by both the high carbon content and the small quantities of silicon and aluminum.

6. The presence of sp^3 C, sp^2 C and sp hybridized carbons was detected by solid state ^{13}C MAS NMR spectroscopy.

7. During removal of the zeolite template by washing with HF, organoaluminum fluoride structures were formed. In the SEM image of natural zeolite templated carbons, some flower-like structures were observed, which consisted of mainly fluorine, carbons and aluminum. According to ^{19}F MAS NMR spectra of carbons, Al_2F_2, $AlFC_3$, AlF_2C_2, and AlF_3C groups were observed. In the XRD pattern, peaks belonged to aluminum hydroxide fluoride. The d_{002} value of the carbon was 0.358 nm.

8. The structural differences in the natural zeolite templated carbons obtained after HCl, NaOH, HCl-NaOH, and HF-NaOH washings solutions besides HF were investigated. BET surface area of porous carbons were 58, 163, 140 and 98 m^2/g in obtained with HCl, NaOH, HCl-NaOH, and HF-NaOH washings solutions, respectively. HF washed carbon had the highest surface area with 397 m^2/g. The d_{002} values of the carbons were calculated as 0.341, 0.329, 0.330, 0.358 and 0.313 nm for those washed with HCl, NaOH, HCl-NaOH, HF and HF-NaOH solutions, respectively. The resultant carbons indicated the presence of turbostratic structures.

9. The systematic study of the parameters of $AlPO_4$-5 microwave synthesis was examined to use for the further templating purposes. Powdered $AlPO_4$-5 crystals of high quality can be synthesized using a microwave heating technique. Utilizing microwave heating leads to improved control of the synthesis of molecular sieve crystals and for the synthesis of AFI type structures it drastically reduced the crystallization times. It is concluded that the crystal growth depended on the initial gel composition. The results showed that the morphology, orientation, and the size of the $AlPO_4$-5 crystals can be controlled by varying the gel composition, water content, amount of organic template, heating power and crystallization time.

10. Perfect hexagonal $AlPO_4$-5 products with rod-like shape, well-defined edges and faces formed with ca. 5 μm length. This shape is one of the characteristic morphologies of $AlPO_4$-5 crystals. It is confirmed that the $AlPO_4$-5 powder of the H4 sample, produced by the method described in the present study is of sufficient quality to be used as the container for guest material and for studying its properties in detail. BET surface area of selected $AlPO_4$-5 for the further steps was 107 m^2/g and average pore diameter was 1.7 nm.

11. In addition to natural zeolites, porous carbons were produced by using microwave-assisted $AlPO_4$-5 as a template. BET surface areas of $AlPO_4$-5 templated carbons were measured as 149, 125, 122 and 108 m^2/g at 700, 800, 900 and 1000°C, respectively BET surface areas seemed to decrease slightly with increasing temperature. The surface areas of natural zeolite templated porous carbons, were higher than those of $AlPO_4$-5 templated porous carbons, due to higher accessibility to the pores in natural zeolite.

12. Average pore diameter of all the porous carbons were 1.7 nm, carbonized at 700, 800, 900 and 1000°C, respectively, besides some larger pores with 6 nm and 9 nm pore diameters.

13. Highly microporous carbons were synthesized. These results indicated that, carbons were mostly formed inside the pores of the $AlPO_4$-5 as well as some formed on the outside walls of the $AlPO_4$-5 crystals. Carbon contents of the porous carbons detected in EDS were 92%, 90%, 96% and 82% carbon at 700, 800, 900 and 1000°C, respectively.

14. The d_{002} values of the $AlPO_4$-5 templated porous carbons synthesized were 0.358, 0.358, 0.362 and 0.363 nm at 700, 800, 900 and 1000°C, respectively. L_c values and average number of graphene sheets per stack increased with carbonization temperature. The size of the microcrystallites increased with increasing pyrolytic temperature, L_c values increased from 1.48 nm to 2.06 nm, L_a values increased from 5.71 nm to 9.46 nm and average number of graphene sheets increased from 4 to 6 when temperature was increased from 700 to 1000°C.

15. As the molecular weight of the solvent increases; coefficients of diffusion decrease, activation energy for diffusion increases, and time necessary to come to equilibrium increases. The diffusion of n-butanol both in the natural zeolite and natural zeolite templated carbons seemed to be less, compared to those of the smaller alcohols. In all of the samples the coefficients of diffusion increased linearly with an increase in the temperature. The diffusion of alcohols in the zeolite and porous carbons obeyed anomalous transport mechanism. Diffusion rate constants slightly increased as the temperature was increased.

16. The calculated coefficients of diffusion of volatile molecules in the porous carbons were lower than that of observed in the natural zeolite. The large number and array of

different functional groups on carbon surface imply that there are many types of solute–adsorbent interactions. The electrostatic interaction between the hydroxyl group of alcohols and the functional groups such as carboxylic acid on carbon surface can explain such results.

17. It is interesting to compare the activation energies measured in natural zeolite and natural zeolite templated porous carbons. The activation energies for diffusion of methanol were 90.1 kJ/mol and 220.7 kJ/mol for natural zeolite and porous carbon, carbonized at 700°C, respectively. This is most likely due to the polarity of alcohols. Compounds containing the –OH group are generally highly polar and have an appreciable electrostatic field due to the resultant dipoles. Being a polar molecule, alcohols have stronger interaction with carbon surface which is dispersed with functional groups.

REFERENCES

[1]   Weeks. M.E. *J Chem Educ. Public.* (1956), 1 (2), 58-89.

[2]   Sakintuna B., Yürüm Y. *Energy Fuels* (2004), 18, 883-888.

[3]   Fitzer E., Köchling K.H., Boehm H.P., Marsh H. Recommended Terminology for the Description of Carbon as a Solid. Pure and Applied Chemistry: IUPAC Subcommittee on Terminology and Characterization of Carbon, ICCTC, 1995. 473-506.

[4]   Warren B.E. *Phys. Rev.* (1934), 2, 551.

[5]   Warren B.E. *Phys. Rev.* (1941), 59, 693-699.

[6]   Brindley G.W., Mering J. *Acta Cryst.* (1951), 4, 441.

[7]   Hirsch P.B. *Proc Roy Soc Ser A* (1954), 226, 143.

[8]   Diamond R. *Acta Cryst.* (1957), 10, 359.

[9]   Diamond R. *Acta Cryst.* (1958), 11, 129.

[10]   Short M.A., Walker J.P.L. *Carbon* (1963), 1, 3.

[11]   Bacon R., Walker J.P.L. Chemistry and Physics of Carbon, Marcel Dekker, In: Thrawer P, Eds, editor. New York, 1973. pp. 1-95.

[12]   Franklin R.E. *Proc Roy Soc* (1951), 209, 196-218.

[13]   Franklin R.E. *Acta Cryst.* (1951), 4, 253-261.

[14]   Oberlin A. *Carbon* (1984), 22, 521.

[15]   Kercher A.K., Nagle D.C. *Carbon* (2003), 41, 15-27.

[16]   Fujimoto H., Shiraishi M. *Carbon* (2001), 39, 1753.

[17]   Feng B., Bhatia S.K., Barry J.C. *Carbon* (2002), 40, 481.

[18]   Sharma A., Kyotani T., Tomita A. *Carbon* (2000), 38, 1977.

[19]   Babu V.S., Seehra M.S. *Carbon* (1996), 34, 1259.

[20]   Oberlin A., Bonnamy S., Lafdi K., Donnet J-B, Wang T.K., Reboyuillat S, Peng J.C.M. Structure and Texture of Carbon Fibers. In: Carbon Fibers. New York: Dekker M., 1998.

[21]   Sakintuna B., Aktas Z., Yürüm Y. Abstracts of Papers of the American Chemical Society 228: Fuel Chemistry Division, 2004.

[22]   Armbruster T. Clinoptilolite-Heulandite: Applications and Basic Research. editor: J. Vedrine, In: Studies in Surface Science and Catalysis, Zeolites and Mesoporous Materielas at the Dawn of the 21st Century, 2001.

[23]   Coombs D.S., Alberti A., Armbruster T.H., Artioli G., Colella C., Galli E., Grice J.D., Liebau F., Mandarino J.A., Minato H., Nickel E.H., Passaglia E., Peacor D.R., Quartieri S., Rinaldi R., Ross M., Sheppard R.A., Tillmanns E., Vezzalini G. *Min. Mag.* (1998), 62, 533.

[24]   Gottardi G., Galli E. Natural Zeolites. Berlin: Springer-Verlag, 1985.

[25]   Sakintuna B., Yürüm Y. *Ind. Eng. Chem. Res.* (2005), 44, 2893-2902.

[26]   IUPAC Compendium of Chemical Terminology 2nd Edition (1997), 1972.

[27]   IUPAC Compendium of Chemical Terminology 2nd Edition (1997), 1976.

[28]   Ryoo R., Joo S.H., Kruk M., Jaroniec M. *Adv. Mater.,* (2001), 13 (9), 677-681.

[29]   Fan S., Chapline M.G., Franklin N.R., Tombler T.W., Cassell A.M., Dai H. *Science* (1999), 283, 512-514.

[30]   Subramoney S. *Adv. Mater.* (1998), 10 (15), 1157-1171.

[31]   Davis M.E. *Nature* (2002), 417, 813-821.

[32]   Kyotani T. *Carbon* (2000), 38, 269-286.

[33]   Tamai H., Kakii T., Hirota Y., Kumamoto T., Yasuda H. *Chem. Mater* (1996), 8, 454-462.

[34]   Zhonghua H., Madapusi P.S., Ni Y. *Adv. Mater.* (2000), 12 (1), 62-65.

[35]   Lu W., Chung D.D.L. *Carbon* (1997), 35 (3), 427-436.

[36]   Planeix J.M., Coustel N., Coq J.B., Brotons J.V., Kumbhar P.S., Dutartre R., Geneste P., Bernier P., Ajayan P.M. *J Am. Chem. Soc.* (1994), 116, 7935-7936.

[37]   Rodriguez N.M., Chambers A., Baker R.T.K. *Langmuir* (1995), 11, 3862-3866.

[38]   Lee J., Han S., Kim H., Koh J.H., Hyeon T., Moon S.H. *Catal. Today* (2003), 86, 141.

[39]   Rueckes T., Kim K., Joselevich E., Tseng G.Y., Cheung C.L., Lieber C.M. *Science* (2000), 289, 94-97.

[40]   Hyeon T., Han S., Sung Y.E., Park K.W., Kim Y.W. *Angew. Chem.* (2003), 2003 (Int. Ed.), 4352.

[41]   Dillon A.C. *Nature* (1997), 386, 377-379.

[42]   Lee J., Han S., Hyeon T. *J Mater. Chem.* (2004), 14, 478-486.

[43]   Lee J., Yoon S., Oh S.M., Shin C.H., Hyeon T. *Adv. Mater.* (2000), 12 (5), 359-362.

[44]   Lee J., Yoon S., Hyeon T., Oh S.M., Kim K.B. *Chem. Commun.* (1999), 2177-2178.

[45]   Parthasarathy R.V., Martin C. *Nature* (1994), 369 (6478), 298-301.

[46]   Johnson S.A., Ollivier P.J., Mallouk T.E. *Science* (1999), 282, 963-965.

[47]   Martin C.R. *Adv. Mater.* (1991), 3 (9), 457-459.

[48]   Klein J.D., Herrick R.D.I., Palmer D., Sailor M.J., Brumlik C.J., Martin C.R. *Chem. Mater.* (1993), 5 (7), 902-904.

[49]   Martin C.R. *Chem. Mater.* (1996), 8, 1739-1746.

[50]   Cao G., Rabenberg L.K., Nunn C.M., Mallouk T.E. *Chem. Mater.* (1991), 3, 149-156.

[51]   Ozin G.A., Steele M.R., Holmes A.J. *Chem. Mater.* (1994), 6, 999-1010.

[52]   Brigham E.S., Weisbecker C.S., Rudzinski W.E., Mallouk T.E. *Chem. Mater.* (1996), 8 (2121-2127).

[53]   Zarbin A.J.G., De Paoli M.A., Alves O.L. *Synth. Met.* (1999), 99, 227-235.

[54]   Asefa T., MacLachlan M.J., Coombs N., Ozin G.A. *Nature* (1999), 402, 867.

[55]   Heywood B.R., Mann S. *J Am. Chem. Soc.* (1992), 114, 4681-4686.

[56] Ukrainczyk L., Bellman R.A., Anderson A.B. *J Phys. Chem. B* (1997), 101, 531-539.

[57] Nguyen C.V., Carter K.R., Hawker C.J., Hedrick J.L., Jaffe R.L., Miller R.D., Remenar J.F., Rhee H.W., Rice P.M., Toney M.F., Trollsas M., Yoon D.Y. *Chem. Mater.* (1999), 11, 3080-3085.

[58] Feng P., Bu X., Pine D.J. *Langmuir* (2000), 16, 5304-5310.

[59] Beck J.S., Vartuli J.C., Roth W.J., Leonowisc M.E., Kresge C.T., Schmitt K.D., Chu C.T-W., Olson D.H., Sheppard E.W, McCullen S.B., Higgens J.B., Schlenker J.L. *J Am. Chem. Soc.* (1992), 114, 10834-10843.

[60] Braun P.V., Osenar P., Tohver V., Kennedy S.B., Stupp S.I. *J Am. Chem. Soc.* (1999), 121, 7302-7309.

[61] Putyeraa K., Bandosz T.J., Jagieob J., Schwarz J.A. *Carbon* (1996), 34 (12), 1559-1567.

[62] Bandosz T.J., Jagie J., Putyera K., Schwarz J.A. *Chem. Mater.* (1996), 8, 2023-2029.

[63] Li J., Moskovits M., Haslett T.L. *Chem. Mater.* (1998), 10, 1963-1967.

[64] Knox J.H., Kaur B., Millward G.R. *J Chromatogr.* (1986), 352, 3.

[65] Gilbert M.T., Knox J.H., Kaur B. *Chromatographia* (1982), 16, 138.

[66] Brunauer S., Emmett P.H., Teller E. *J Am. Chem. Soc.* (1938), 60, 309.

[67] Che G., Lakshmi B.B., Martin C.R., Fisher E.R. *Langmuir* (1999), 15, 750-758.

[68] Che G., Lakshmi B.B., Martin C.R., Fisher E.R., Ruoff R.S. *Chem. Mater.* (1998), 10, 260-267.

[69] Pradhan B.K., Toba T., Kyotani T., Tomita A. *Chem. Mater.* (1998), 10, 2510-2515.

[70] Liu S., Yue J., Cai T., Andersony K.L. *J Colloid Interface Sci* (2000), 225, 254-256.

[71] Kyotani T., Tsai L., Tomita A. *Chem. Mater.* (1996), 8, 2109-2113.

[72] Kyotani T., Tsai L., Tomita A. *Chem. Mater.* (1995), 7 (8), 1427-1428.

[73] Shindo A., Izumino K. *Carbon* (1994), 32 (7), 1233-1243.

[74] Zhang X., Solomon D.H. *Chem. Mater.* (1999), 11, 384-391.

[75] Domingo-Garcia M., Lopez-Garzon F.J., Perez-Mendoza M. *Carbon* (2000), 38, 555-563.

[76] Müller H., Rehak P., Jager C., Hartmann J., Meyer N., Spange S. *Adv. Mater.* (2000), 12 (22), 1671-1675.

[77] Wang Z., Lu Z., Huang X., Xue R., Chen L. *Carbon* (1998), 36 (1-2), 51-59.

[78] Schüth F., Schmdt W. *Adv. Mater.* (2002), 14 (9), 629-638.

[79] Schüth F. *Angew. Chem.* (2003), 42 (31), 3604-3622.

[80] Che G., Lakshmi B.B., Fisher E.R., Martin C.R. *Nature* (1998), 393 (6683), 346-349.

[81] Ryoo R., Joo S.H., Jun S. *J Phys. Chem. B.* (1999), 103 (37), 7743-7746.

[82] Kresge C.T., Leonowisc M.E., Roth W.J., Vartuli J.C., Beck J. S. *Nature* (1992), 359, 710-712.

[83] Kruk M., Jaroniec M., Ryoo R., Kim J. M. *Chem. Mater* (1999), 11, 2568-2572.

[84] Kruk M., Jaroniec M., Ryoo R., Joo S.H. *J Phys. Chem. B.* (2000), 104, 7960-7968.

[85] Kaneda M., Tsubakiyama T., Carlsson A., Sakamoto Y., Ohsuna T., Terasaki O., Joo S.H., Ryoo R. *J Phys. Chem. B.* (2002), 106, 1256-1266.

[86] Ryoo R., Joo S.H., Kim J.M. *J Phys. Chem. B.* (1999), 103, 7435-7440.

[87] Kruk M., Jaroniec M. *Chem. Mater.* (2000), 12, 1414-1421.

[88] Ryoo R., Jun S., Kim J.M., Kim M. J. *Chem. Commun.* (1997), 2225-2226.

[89] Solovyov L.A., Zaikovskii V.I., Shmakov A.N., Belousov O.V., Ryoo R. *J Phys. Chem. B.* (2002), 106, 12198-12202.

[90] Joo S.H., Jun S., Ryoo R. *Microporous Mesoporous Mater.* (2001), 44-45, 153-158.

[91] Jun S., Joo S.H., Ryoo R., Kruk M., Jaroniec M., Liu Z., Ohsuna T., Terasaki O. *J Am. Chem. Soc.* (2000), 122, 10712-10713.

[92] Joo S.H., Choi S.J., Oh I., Kwak J., Liu Z., Terasaki O., Ryoo R. *Nature* (2001), 412, 169-172.

[93] Kruk M., Jaroniec M., Sakamoto Y., Terasaki O., Ryoo R., Ko C.H. *J Phys. Chem. B.* (2000), 104, 292-301.

[94] Kruk M., Jaroniec M., Ryoo R., Kim J. M. *Microporous Mater.* (1997), 12, 93-106.

[95] Kruk M., Jaroniec M., Sayari A. *J Phys. Chem. B.* (1997), 101, 583-589.

[96] Ryoo R., Ko C.H., Park I.-S. *Chem. Commun.* (1999), 1413-1414.

[97] Ryoo R., Kim J.M., Ko C.H., Shin C.H. *J Phys. Chem.* (1996), 100 (45), 17718-17721.

[98] Kim J.M., Stucky G.D. *Chem. Commun.* (2000), 1159-1160.

[99] Lee J.-S., Joo S.H., Ryoo R. *J Am. Chem. Soc.* (2002), 124 (7), 1156-1157.

[100] Zhao D., Feng J., Huo Q., Melosh N., Fredirckson G.H., Chemlka B.F., Stucky G.D. *Science* (1998), 279, 548.

[101] Galindo C., Ming D.W., Morgan A., Pickering K. Program and Abstracts. Zeolite. Ischia, Naples, 1997. 154.

[102] Shin H.J., Ryoo R., Kruk M., Jaroniec M. *Chem. Commun.* (2001), 349-350.

[103] Darmstadt H., Roy C., Kaliaguine S. , Choi S.J., Ryoo R. *Carbon* (2002), 40, 2673-2683.

[104] Darmstadt H., Roy C., Kaliaguine S., Kim T.W., Ryoo R. *Chem. Mater.* (2003), 15, 3300-3307.

[105] Joo S.H., Ryoo R., Kruk M., Jaroniec M. *J Phys. Chem. B.* (2002), 106, 4640-4646.

[106] Solovyov L.A., Shmakov A.N., Zaikovskii V.I., Joo S.H., Ryoo R. *Carbon* (2002), 40, 2277-2481.

[107] Ryoo R., Ko C.H., Kruk M., Antochshuk V., Jaroniec M. *J Phys. Chem. B.* (2000), 104, 11465-11471.

[108] Kim S.S., Pauly T.R., Pinnavaia T.J. *Chem. Commun.* (2000), 17, 1661-1662.

[109]   Lee J., Sohn K., Hyeon T. *Chem. Commun.* (2002), 2674-2675.

[110]   Li Z., Jaroniec M.. *J Am. Chem. Soc.* (2001), 123 (37), 9208-9209.

[111]   Li Z., Jaroniec M. *Carbon* (2001), 39 (13), 2080-2082.

[112]   Taguchi A., Smatt J.H., Linden M. *Adv. Mater.* (2003), 15 (14), 1209.

[113]   Li W.Z., Xie S.S., Qian L.X., Chang B.H., Zou B.S., Zhou W.Y., Zhao R.A., Wang G. *Science* (1996), 274 (5293), 1701-1703.

[114]   Zakhidov A.A., Baughman R.H., Iqbal Z., Changxing Cui, Ilyas Khayrullin, Dantas S.O., Marti J., Ralchenko G.V. *Science* (1998), 282 (5390), 897-901.

[115]   Zarbin A.J.G., Bertholdo R., Oliveira M.A.F.C. *Carbon* (2002), 40, 2413-2422.

[116]   Kamegawa K., Yoshida H. *Carbon* (1997), 35 (5), 631-639.

[117]   Strano M.S., Agarwal H., Pedrick J., Redman D., Foley H.C. *Carbon* (2003), 41, 2501-2508.

[118]   Tamon H., Ishizaka H., Mikami M., Olazaki M. *Carbon* (1997), 35 (6), 791-796.

[119]   Ozaki J., Endo N., Ohizumi W., Igarashi K., Nakahara M., Oya A. *Carbon* (1997), 35 (7), 1031-1033.

[120]   Han S., Kim M., Hyeon T. *Carbon* (2003), 41, 1525-1532.

[121]   Han S, Hyeon T. *Carbon* (1999), 37, 1645-1647.

[122]   Han S, Sohn K., Hyeon T. *Chem. Mater.* (2000), 12, 3337-3341.

[123]   Han S, Hyeon T. *Chem. Commun.* (1999), 1955-1956.

[124]   Fuertes A.B., Nevskaia D.M. *Microporous Mesoporous Mater.* (2003), 62, 177-190.

[125]   Alvarez S., Fuertes A.B. *Carbon* (2004), 42, 423-460.

[126]   Ferey G., Cheetham A.K. *Science* (1999), 283 (5405), 1125-1126.

[127]   Mirasol J.R., Cordero T., Radovic L.R., Rodriquez J.J. *Chem. Mater.* (1998), 10, 550-558.

[128]   Davis M.E., Lobo R.F. *Chem. Mater.* (1992), 4, 756-768.

[129]   Kyotani T., Nagai T., Inoue S., Tomita A. *Chem. Mater.* (1997), 9, 609-615.

[130]   Johnson S.A., Brigham E.S., Ollivier P.J., Mallouk T.E. *Chem. Mater.* (1997), 9, 2448-2458.

[131]   Sakintuna B., Aktas Z., Yürüm Y. Abstracts of Papers of the American Chemical Society 226 (2003), U538-U538 056-Fuel Part 1 (September).

[132]   Ma Z., Kyotani T., Tomita A. *Chem. Commun.* (2000), 2365-2366.

[133]   Ma Z., Kyotani T., Liu Z., Terasaki O., Tomita A. *Chem. Mater.* (2001), 13, 4413-4415.

[134]   Cordero T., Thrower P.A., Radovic L. R. *Carbon* (1992), 30 (3), 365-374.

[135]   Kyotani T., Ma Z., Tomita A. *Carbon* (2003), 41, 1451-1459.

[136]   Ma Z., Kyotani T., Tomita A. *Carbon* (2002), 40, 2367-2374.

[137]   Enzel P., Bein T. *Chem. Mater.* (1992), 4, 819-824.

[138]   Cox S., Stucky G.D. *J Phys. Chem.* (1991), 95, 710-720.

[139]   Sonobe N., Kyotani T., Tomita A. *Carbon* (1988), 26 (4), 573-578.

[140]   Sonobe N., Kyotani T., Tomita A. *Carbon* (1990), 28 (4), 483-488.

[141] Kyotani T., Yamada H., Sonobe N., Tomita A. *Carbon* (1994), 32 (4), 627-635.

[142] Bandosz T.J., Putyeraa K., Jagieoa J., Schwarza J.A. *Carbon* (1994), 32 (4), 659-664.

[143] Bandosz T.J., Putyeraa K., Jagieoa J., Schwarza J.A. *Langmuir* (1995), 11, 3964-3969.

[144] Sonobe N., Kyotani T., Tomita A. *Carbon* (1991), 29 (1), 61-67.

[145] Sandi G., Thiyagarajan P., Carrado K.A., Winans R.E. *Chem. Mater.* (1999), 11, 235-240.

[146] Kyotani T., Mori T., Tomita A. *Chem. Mater.* (1994), 6, 2138-2142.

[147] Rodrigues P.M.B., Mays T.J., Moggridge G.D. *Carbon* (2003), 41, 2231-2246.

[148] Meyers C.J., Shah S.D., Patel S.C., Sneeringer R.M., Bessel C.A., Dollahon N.R., Leising R.A., Takeuchi E.S. *J Phys. Chem. B.* (2001), 105, 2143-2152.

[149] Wen J., Wilkes G.L. *Chem. Mater.* (1996), 8, 1667-1681.

[150] Mann S., Burkett S.L., Davis S.A., Fowler C.E., Mendelson N.H., Sims S.D., Walsh D., Whilton N.T. *Chem. Mater.* (1997), 9, 2300-2310.

[151] Kawashima D., Aihara T., Kobayashi Y., Kyotani T., Tomita A. *Chem. Mater.* (2000), 12, 3397-3401.

[152] Breck D.W. Zeolite Molecular Sieves. New York, 1974.

[153] Flanigen, E.M., Bennett J.M., Grose R.W., Cohen J.P., Patton R.L., Kirchner R.M., Smith J.V. *Nature* (1978), 271, 512.

[154] Wilson S.T., Lok B.M., Messina C.A., Cannan T.R., Flanigen E.M. *J Am. Chem. Soc.* (1982), 104 (4), 1146-1147.

[155] Tapp N.J., Cardile C.M. *Zeolites* (1990), 10, 680.

[156] Finger G., Richter-Mendav J., Bulow M., Kornatowski J. *Zeolites* (1991), 11, 443-448.

[157] Choi K.J., Jhon M.S., No K.T. *Bull. Korean Chem. Soc.* (1987), 8 (3), 155-157.

[158] Meier W.M., Olson D.H. Atlas of Zeolite Structure Types. London, 1992.

[159] Miyake M., Uehara H., Suzuki H., Yao Z., Matsuda M., Sato M. *Microporous Mesoporous Mater.* (1999), 32, 45-52.

[160] Ehrl M., Deeg F.W., Brauchle C., Franke O., Sobbi A., Schulz-Ekloff G., Wöhrle D. *J Phys. Chem.* (1994), 98, 47.

[161] Deeg F.W., Ehrl M., Brauchle C., Hoppe R., Schulz-Ekloff G., Wöhrle D. *Luminescence* (1992), 53, 219.

[162] Cox S.D., Gier T.E., Stucky G.D., Bierlein J. *J Am. Chem. Soc.* (1990), 110, 609.

[163] Werner L., Caro J., Finger G., Kornatowski J. *Zeolites* (1992), 12, 658.

[164] Caro J., Finger G., Kornatowski J., Richter-Mendau J., Werner B., Zibrowius L. *Adv. Mater.* (1992), 4, 273.

[165] Marlow F., Caro J., Werner L., Kornatowski J., Dahne S. *J Phys. Chem.* (1993), 97, 11286.

[166] Caro J., Marlow F., Wübbenhorst M. *Adv. Mater.* (1994), 6, 413.

[167] Martin C., Tosi-Pellenq N., Patarin J., Coulomb J.P. *Langmuir* (1998), 14, 1774-1778.

[168] Qiu S., Piang Q., Kessler H., Guth J.L. *Zeolites* (1989), 9, 440-444.

[169] Demuth D., Stucky G.D., Unger K., Schüth F. *Microporous Mater.* (1995), 3, 473.

[170] Schuth F., Demuth D., Zibrowius B., Kornatowski J., Finger G. *J Am. Chem. Soc.* (1994), 116, 1090.

[171] Schnabel K., Finger G., Kornatowski J., Loffler E., Peuker C., Pilz W. *Microporous Mater.* (1997), 11, 293.

[172] Newalkar B., Kamath B., Jasra R., Bhat S. *Zeolites* (1997), 18, 286.

[173] Prasad S., Liu S. *Microporous Mater.* (1995), 4, 391

[174] Chen C.-M., Jehng J.-M. *Catal. Letters* (2003), 85 (1-2), 73-80.

[175] Demontis P., Gonzalez J.G., Suffritti G.B., Tilocca A., Pozas C.D.L. *Microporous Mesoporous Mater.* (2001), 42, 103-111.

[176] Bennett J.M., Cohen J.P., Flanigen E.M., Pluth J.J., Smith J.V. ACS Symp. Ser (1983), 218, 109.

[177] Wilson S.T., Lok B.M., Messina C.A., Cannan T.R., Flanigen E.M. ACS Symp. Ser (1983), 218, 79.

[178] Robson H., Lillerud K.P. Verified Synthesis of Zeolitic Materials. Amsterdam: Elsevier Science, 2001.

[179] Eldik R.V., Hubbard C.D. Chemistry under Extreme of Non-Classical Conditions. New York: Wiley, 1996.

[180] Scott A.W. Understanding Microwaves. New York: John Wiley & Sons, Inc., 1993.

[181] Gabriel C., Gabriel S., Grant E.H., Halsteed B.S.J., Mingos D.P. *Chem. Soc. Rev.* (1998), 27, 213.

[182] Rao K.J., Vaidhyanathan B., Ganguli M., Ramakrishnan P.A. *Chem. Mater.* (1999), 11, 882.

[183] Park S.-E., Chang J.-S., Hwang Y.K., Kim D.S., Jhung S.H., Hwang J.S. *Catal. Surveys Asia* (2004), 8 (2), 91-110.

[184] Mingos D.M.P., Whittaker A.G. *J. Chem. Soc. Dalton Trans* (1992), 2751.

[185] Smith F., Cousins B., Bozic J., Flora W. *Anal. Chim. Acta.* (1985), 177, 243.

[186] Sutton W.H.. *Am. Ceram. Soc. Bull.* (1989), 68 (2), 376–386.

[187] Lidström P., Tierney J., Wathey B., Westman J. *Tetrahedron* (2001), 57, 9225.

[188] Kingston H.M., Haswell S.J. Microwave-Enhanced Chemistry, Fundamentals, Sample Preparation, and Application. Washington DC, 1997.

[189] Roussy G., Chenot P. *J Phys. Chem.* (1981), 85, 2199.

[190] Tatsuo O., Akiko W. *Phys. Chem. Commun.* (2001), 3, 1.

[191] Roussy G., Hilaire S., Thiebaut J.M., Maire G., Garin F., Ringler S. *Appl. Catal. A: Gen.* (1997), 156, 167.

[192] Bond G., Moyes R.B., Whan D.A. *Catal. Today* (1993), 17, 427.

[193] Berry F.J., Smart L.E., Sai Prasad P.S., Lingaiah N., Kanta P. *Rao Appl. Catal. A: Gen.* (2000), 204, 191.

[194] Wang Y., Zhu J.H., Cao J.M., Chun Y., Xu Q.H. *Microporous Mesoporous Mater.* (1998), 26, 175.

[195] Zhang X., Hayward D.O., Mingos D.M.P. *Ind. Eng. Chem.Res.* (2001), 40, 2810.

[196] Margolis S.M., Jasse L., Kingston H. M. *J Aut. Chem.* (1991), 13, 93.

[197] Sanders A., Wetzel H., Kunst M., Snyder Jr. W., Sutton W.H., Iskander M., Johnson D. L. MRS. Pittsburgh, PA, 1990. pp. 403.

[198] Elsamak G.G., Altuntaş Ö.N., Yürüm Y. *Fuel* (2003), 82, 531-537.

[199] Cundy C.S., Plaisted R.J., Zhao J. P. *Chem. Commun.* (1998), 1465.

[200] Lidstrom P., Tierney J., Wathey B., Westman J. *Tetrahedron* (2001), 57, 9225.

[201] Cundy C.S. *Collect. Czech, Chem. Commun.* (1998), 63, 1699.

[202] Zhu J., Polchik O., Chen S., Gedanken A. *J Phys. Chem. B* (2000), 104, 7344.

[203] Chu P., Dwyer F.G., Vartuli J. C. US Patent 4778 666, 1988.

[204] Arafat A., Jansen J.C., Ebaid A.R., Bekkum H.V., Occelli M.L., Robson H.E. In Synthesis of Microporous Mater., Reinhold VN, editor. New York, 1992. pp. 507.

[205] Arafat A., Jansen J.C., Ebaid A.R., Bekkum H.V. *Zeolites* (1993), 13, 162.

[206] Girnus I., Jancke K., Vetter R., Richter-Mendau J., Caro J. *Zeolites* (1995), 15, 33-39.

[207] Carmona J.C., Clemente R.R., Morales J.G. *Zeolites* (1997), 18, 340-346.

[208] Wu C.G., Bein T. *Chem. Commun.* (1996), 925.

[209] Park S.-E., Kim D.S., Chang J.-S., Kim W.Y. *Catal. Today* (1998), 44, 301.

[210] Sung-Suh H.M., Kim D.S., Park S.-E. *J. Ind. Eng. Chem.* (1999), 5, 191.

[211] Sun Y., Lin W., Chen J., Yue Y., Pang W. *Stud. Surf. Sci.Catal. Today* (1997), 105A, 77.

[212] Wu C.-G., Bein T. *Chem. Commun.* (1996), 925.

[213] Zhang Y., Zhao S., Sun G., Wang Z., Xuebao C. (2000), 21, 345.

[214] Newalkar B.L., Komarneni S., Katsuki H. *Chem.Commun.* (2000), 2389.

[215] Newalkar B.L., Komarneni S. *Chem. Mater.* (2001), 13, 4573.

[216] Newalkar B.L., Olanrewaju J., Komarneni S. *Chem. Mater.* (2001), 13, 552.

[217] Hwang Y.K., Chang J.-S., Kwon Y.-U., Park S.-E. *Stud.Surf. Sci. Catal.* (2003), 146, 101.

[218] Park M., Komarneni S. *Microporous and Mesoporous Materials* (1998), 20, 39-44.

[219] Brückner A., Lohse U., Mehner H.. *Microporous Mesoporous Mater.* (1998), 20, 207-215.

[220] Xu X., Yang W., Liu J., Lin L. *Separation Purification Tech.* (2001), 25, 241-249.

[221] Braun I., Schulz-Ekloff G., Bockstette M., Wöhrle D. *Zeolites* (1997), 19, 128-132.

[222] Min F., Hongbin D., Wenguo X., Xianping M., Wenqin P. *Microporous Mater.* (1997), 9 (1-2), 59-61.

[223] Mintova S., Mo S., Bein T. *Chem. Mater.* (1998), 10, 4030-4036.

[224] Kodaira T., Miyazawa K., Ikeda T., Kiyozumi Y. *Microporous Mesoporous Mater.* (1999), 29, 329-337.

[225] Girnus I., Jancke K., Vetter R., Richter-Mendau J., Caro J. *Zeolites* (1995), 15, 33-39.

[226] Fang M., Du H., Xu W., Meng X., Pang W. *Microporous Mater.* (1997), 9, 59-61.

[227] Slangen P.M., Jansen J.C., Bekkum H.V. *Microporous Mater.* (1997), 9, 259.

[228] I. Braun, Ekloff G.S., M. Bocktette, D.Wöhrle. *Zeolites* (1997), 19, 128.

[229] Tsai T.-G., Chao K.-J., Guo X.-J., Sung S.-L., Wu C.-N., Wang Y.-L., H.-C. S. *Adv. Mater.* (1997), 9, 1154.

[230] Mintova S., Schoeman B.J., Valtchev V., Sterte J., Mo S., Bein T. *Adv. Mater.* (1997), 9, 585.

[231] Ikeda T., Miyazawab K., Izumic F., Huangd Q., Santorod A. *J Phys. Chem. Solids* (1999), 60, 1531-1535.

[232] Klap G.J., Koningsveld H.V., Grafasma H., Schreurs A.M.M. *Microporous Mesoporous Mater.* (2000), 38, 403-412.

[233] Wilson S.T., Lok B.M., Flanigen E.M.. US Patent (1982), 4, 310, 440.

[234] Müller U., Unger K.K. *Zeits. Kristallogr.* (1988), 182, 190.

[235] Girnus I., Pohl M.-M., Richter-Mendau J., Schneider M., Noack M., Venzke D., Caro J. *Adv. Mater.* (1995), 8, 711.

[236] Park M., Komarneni S. *Microporous Mesoporous Mater.* (1998), 20, 39.

[237] Braun I., Schulz-Ekloff G., Wohrle D., Lautenschlager W. *Microporous Mesoporous Mater.* (1998), 23, 79-81.

[238] Du H., Fang M., Xu W., Meng X., Pang W. *J Mater. Chem.* (1997), 7 (3), 551-555.

[239] Jhung S.H., Chang J.-S., Kim D.S. Park S.-E. *Microporous Mesoporous Mater.* (2004), 71, 135-142.

[240] Ganschow M., Schulz-Ekloff G., Wark M., Wendschuh-Josties M., Wohrle D. *J. Mater. Chem.* (2001), 11, 1823-1827.

[241] Lin J-C., Dipre J.T., Yates M.Z. *Langmuir* (2004), 20, 1039-1042.

[242] Weyda H., Lechert H. *Zeolites* (1990), 10, 251.

[243] Iwasaki A., Sano T., Kiyozumi Y. *Microporous Mesoporous Mater.* (1998), 25, 119.

[244] Iwasaki A., Sano T., Kodaira T., Kiyozumi Y. *Microporous Mesoporous Mater.* (2003), 64, 145-153.

[245] Ahn S., Chon H. *Microporous Mater.* (1997), 8, 113.

[246] Kornatowski J., Zadrozna G., Rozwadowski M., Zibrowius B., Marlow F., Lercher J. A. *Chem. Mater.* (2001), 13, 4447.

[247] Kessler H., Patarin J., Schott-Darie C. *Stud. Surf. Sci. Catal.* (1994), 85, 75.

[248] Jhung S.H., Hwang Y.K., Chang J.-S., Park S.-E. *Microporous Mesoporous Mater.* (2004), 67, 151-157.

[249] Iijima S. *Nature* (1991), 345, 56.

[250] Guo T., Nikolaev P., Thess A., Colbert D.T., Smalley R. E. *Chem. Phys. Lett.* (1995), 243, 49.

[251] Journet C., Maser W.K., Bernier P., Loiseau A., Lamy de la Chapelle M., Lefrant S., Deniard P., Lee R., Fischer J. E. *Nature* (1997), 388, 756.

[252] Dubay O., Kresse G. *Carbon* (2004), 42, 979-982.

[253] Tang Z.K., Sun H.D., Wang J., Chen J., Li G. *App. Phys. Lett.* (1998), 73 (16), 2287-2289.

[254] Wang N., Tang Z.K., Li G.D., Chen J.S. *Nature* (2000), 408, 50.

[255] Launois P., Moret R., Le Bolloc'h D., Albouy P.A., Tang Z.K., Li G., Chen J. *Solid State Commun.* (2000), 116, 99-103.

[256] Sun H.D., Tang Z.K., Chen J., Li G.D. *App. Phys. A* (1999), 69, 381.

[257] Tang Z.K., Zhang L.Y., Wang N., Zhang X.X., Wang J.N., Li G.D., Li Z.M., Wen G.H., Chan C.T., Sheng P. *Synth. Met.* (2003), 133-134, 689-693.

[258] Caro J., Marlow F. *Zeolites* (1992), 12, 433.

[259] Miyake M., Yoshida M., Matsuda M., Kiguchi M., Taniguchi Y., Uehara H., Sato M. *J Mat. Sci.* (1999), 34, 5509-5512.

[260] Ihlein G., Junges B., Junges U., Laeri F., Schüth F., Vietze U. *App. Organomet. Chem.* (1998), 12, 305-314.

[261] Reck G., Marlow F., Kornatowski J., Hill W., Caro J. *J Phys. Chem.* (1996), 100, 1698.

[262] Finger G., Kornatowski J. *Zeolites* (1990), 10, 615.

[263] Wöhrle D., Sobbi A.K., Franke O., Schulz-Ekloff G. *Zeolites* (1995), 15 (540).

[264] Kowalak S., Balkus Jr. K.J. *Collect. Czech. Chem.Commun.* (1992), 57, 774.

[265] Wohlrab S., Hoppe R., Schulz-Ekloff G., Wöhrle D. *Zeolites* (1992), 12, 862.

[266] Hoppe R., Schulz-Ekloff G., Wöhrle D., Shpiro E.S., Tkachenko O.P. *Zeolites* (1993), 13, 222.

[267] Hoppe R., Schulz-Ekloff G., Rathousky J., Starek J., Zukal A. *Zeolites* (1994), 14, 126.

[268] Bockstette M., Wöhrle D., Braun I., Schulz-Ekloff G. *Microporous Mesoporous Mater.* (1998), 23, 83-96.

[269] Wang N., Li G.D., Tang Z.K. *Chem. Phys. Lett.* (2001), 339, 47-52.

[270] Seiler M., Schenk U., Hunger M. *Catal. Lett.* (1999), 62, 139–145.

[271] Bjørgen M., Kolboe S. *App. Catal. A* (2002), 225, 285–290.

[272] Stich I., Gale J.D., Terkura K., Payn e. M. C. *Chem. Phys. Lett.* (1998), 283, 402-408.

[273] Hutchings G.J., Watson G.W., Willock D.J. *Microporous Mesoporous Mater.* (1999), 29, 67–77.

[274] Domontis P., Suffritti G.B. *Chem. Rev.* (1997), 97, 2845-2878.

[275] Haberlandt R. *Thin Solid Films* (1998), 330, 34-45.

[276] Lood W.P., Verheijen P.J.T., Moulijn J.A. *Chem. Eng. Sci.* (2000), 55, 51-65.

[277] Benes N., Verweij H. *Langmuir* (1999), 15 (23), 8292–8299.

[278] Weisz. P.B. *Chem. Tech.* (1973), 3, 498–505.

[279] Chen N.Y., Degnan Jr T.F., Smith C.M. Molecular Transport and Reaction in Zeolites-Design and Application of Shape Selective Catalysis. New York: VCH Publishers, (1994).

[280] Fick A. *Ann. Phys.* (1855), 94, 59–86.

[281] Barrer R.M., Jost W. *Trans. Faraday Soc.* (1949), 45, 928–930.

[282] Ruthven D.M. *Chem. Eng. Science* (2004), 59, 4531-4545.

[283] Hall P.J., Thomas K.M., Marsh H. *Fuel* (1992), 71, 1271-1275.

[284] Inglezakis V.J., Grigoropoulou H.P. *J Colloid Interface Sci* (2001), 234, 434-441.

[285] Peppas N.A., Lucht L.M. *Chem. Eng. Commun* (1985), 37, 333.

[286] Crank J. The Mathematics of Diffusion. London.: Clarendon Press, Oxford, 1976.

[287] Ndaji F.E., Thomas K.M. *Fuel* (1993), 72, 1525-1530.

[288] Xiao J., Wei J. *Chem. Eng. Sci.* (1992), 47 (5), 1123–1141.

[289] Callister W.D. Material Science and Engineering. New York, 1991.

[290] Riekert L. *Adv. Catal.* (1970), 21, 281.

[291] Otake Y., Suuberg E. M. *Energy Fuels* (1997), 11, 1155-1164.

[292] Gao H., Nolura M., Murata S., Artok L. *Energy Fuels* (1999), 13, 518-528.

[293] Peppas N.A., Franson N.M. *Polymer Phys. Ed.* (1983), 21, 983-997.

[294] Seferinoglu M., Yürüm Y. *Energy Fuels* (2001), 15, 135.

[295] Ruthven D.M. Principles of Adsorption and Adsorption Processes. New York: Wiley, 1984.

[296] Karger J., Ruthven D.M. Diffusion in Zeolites and Other Microporous Solids. New York: Wiley & Sons, (1992).

[297] Karger J., Ruthven D.M. "Diffusion and Adsorption in Porous Solids" in Handbook of Porous Solids. Weinheim: Wiley-VHC, (2002).

[298] Seferinoglu M., Yürüm Y. *Energy Fuels* (2001), 15, 135-140.

[299] Karger J., Heitjans P., Haberlandt R. Diffusion in Condensed Matter. Braunschweig/Wiesbaden: Vieweg, 1998.

[300] Karger J., Pfeifer H. *Zeolites* (1987), 7, 90–107.

[301] Karger J., Caro J. *J Chem. Soc. Faraday I* (1977), 73, 1363–1376.

[302] Jobic H. Diffusion Studies Using Quasi-Elastic Neutron Scattering. In: Recent Advances in Gas Separation by Microporous Ceramic Membranes., editor: Kanellopoulos N.K. Amsterdam: Elsevier, 2000. pp. 109–138.

[303] Karger J. *Adsorption* (2003), 9, 29-35.

[304] Boersma-Klein W., Moulijn J.A. *Chem. Eng. Sci.* (1979), 34 (7), 959–969.

[305] Sakintuna B., Fakıoğlu E., Yürüm Y. *Energy Fuels* (2005), Submitted.

[306] Sakintuna B., Fakıoğlu E., Yürüm Y. Abstracts of Papers of the American Chemical Society 228th National Meeting, Colloid and Surface Chemistry Division. Philadelphia, 2004.

[307] Ritger P.L., Peppas N.A. *Fuel* (1987), 66, 1379-1388.

[308] Howell B.D., Peppas N.A. *Chem. Eng. Commun.* (1985), 43, 301-315.

[309] Bludau H., Karge H.G., Niessen. *Microporous Mesoporous Mater.* (1998), 22, 297-308.

[310] Dyer A., White K.J. *Thermochim. Acta* (1999), 340-341, 341-348.

[311] Aleksandra M., Mianowski. *Fuel* (1998), 77 (14), 1691-1696.

[312] Zhu W., Graaf J.M., Broeke L.J.P., Kapteijn F., Moulijn J.A. *Ind. Eng. Chem. Res.* (1998), 37 (5), 1934–1942.

[313] Caro J., Hocevar S., Kaerger J., Riekert L. *Zeolites* (1986), 6, 213.

[314] Haynes H.W., Sarma P.N. *AIChE J.* (1973), 19 (5), 1043–1046.

[315] Anderson B.G., Noordhoek N.J., Gauw F.J.M.M., IJzendoorn L.J., Voigt M.J.A., Santen R.A. *Ind. Eng. Chem. Res.* (1998), 37 (3), 815–824.

[316] Eic M., Ruthven D. *Zeolites* (1988), 8, 40–45.

[317] Nijhuis T.A., Broeke L.J.P., Linders M.J.G., Graaf J.M., F. Kapteijn, Makkee M., Moulijn J.A. *Chem. Eng. Sci.* (1999), 54, 4423–4436.

[318] Keipert O.P., Baerns M. *Chem. Eng. Sci.* (1998), 53 (20), 3623-3634.

[319] Anderson B.G., Jong A.M., Santen R.A. In situ Measurement of Heterogeneous Catalytic Reactor Phenomena using Positron Emission, in: In-situ Spectroscopy in Heterogeneous Catalysis. In: Haw JA, editor. Weinheim: Wiley-VCH, 2002. pp. 195–237.

[320] Karger J., Pfeifer H., Heink W. *Adv. Magn. Res.* (1988), 12, 1.

[321] Gladden L.F., Sousa-Goncalves J.A., Alexander P. *J Phys. Chem. B.* (1997), 101 (48), 10121–10127.

[322] Schaefer D.J., Favre D.E., Wilhelm M., Weigel S.J., Chmelka B.F. *J Am. Chem. Soc.* (1997), 119 (39), 9252–9267.

[323] Favre D.E., Schaefer D.J., Auerbach S.M., Chmelka B.F. *Phys. Rev. Lett.* (1998), 81 (26), 5852–5855.

[324] Jobic H., Bee M., Kearley G.J. *J Phys. Chem.* (1994), 98, 4660–4665.

[325] Schemmert U., Karger J., Weitkamp J. *Microporous Mesoporous Mater.* (1999), 32, 101–110.

[326] Levitt H.M. Spin Dynamics: Basics of Nuclear Magnetic Resonance. England: Wiley and Sons, 2001.

[327] Barrett E.P., Joyner L.G., Halenda P.H. *J Am. Chem. Soc.* (1951), 73, 373-380.

[328] Bac C.G., Bernier P., Latil S., Jourdain V., Rubio A., Jhnag S.H., Lee S.W., Park Y.W., Hozinger M., Hirsch A.. *Current App. Phys.* (2001), 1, 149-155.

[329] Darmstadt H., Roy C., Kaliaguine S., Xu G., Auger M., A T. *Carbon* (2000), 38 (9), 1279-1287.

[330] Golzan M.M., Lukins P.B., Mackenzie D.R., Vassalo A.M., JV. H. *Chem. Phys.* (1995), 193 (1-2), 167-172.

[331] Biniak S., Szymanski G., Siedlewski J., Swietkowski A. *Carbon* (1997), 35 (12), 1799-1810.

[332] Svehla G. Comprehensive Analytical Chemistry. New York, (1976).

[333] Pavia D.L., Lampman G.M., George S. Kriz J. Introduction to Spectroscopy: A Guide for Students of Organic Chemistry. Philadelphia, (1983).

[334] Jung M.-W., Ahn K.-H., Lee Y., Kim K.-P., Rhee J.-S., Park J.T., Paeng K.-J. *Microchem. J* (2001), 70, 123-131.

[335] Guo J., Lua A.C. *Separation Purification Tech.* (2000), 18, 47-55.

[336] Pinkasa J., Roeskyb H.W. *J Fluorine Chem.* (2003), 122, 125-150.

[337] Ziegler K., Holzkamp E., Koster R., Lehmkuhl H. *Angew. Chem.* (1955), 67, 213–214.

[338] Müller M., Harvey G., Prins R. *Microporous Mesoporous Mater.* (2000), 34, 281-290.

[339] Steel K.M., Patrick J.W. *Fuel Process. Tech.* (2004), 86, 179-190.

[340] Ganapathy S., Kumar R., Montouillout V., Fernandez C., Amoureux J.P. *Chem. Phys. Lett.* (2004), 390, 79-83.

[341] Bruker FTIR Handbook, 3,4488A, 4481, 4880B, 4481, 4851C (2005).

[342] Giraudet J., Dubois M., Inacio J., Hamwi A. *Carbon* (2003), 41, 453-463.

[343] Gupta V., Nakajima T., Ohzawa Y., Zemva B. *J Fluorine Chem.* (2003), 120, 143-150.

[344] Nanse G., Papirer E., Fioux P., Moguet F., Tressaud A. *Carbon* (1997), 35, 175-194.

[345] Yamamoto S., Sugiyama S., Matsuoka O., Kohmura K., Honda T., Banno Y., Nozoye H. *J Phys. Chem.* (1996), 100, 18474-18482.

[346] Scott C. *J Am. Chem. Soc.* (1948), 70, 105.

[347] Ando S., Harris R.K., Hirschinger J., Reinsberg S.A., Scheler U. *Macromolecules* (2001), 34, 66-75.

[348] Chen J., Chen T., Guan N., Wang J. *Catal.Today* (2004), 93–95, 627–630.

[349] Fyfe C.A., Bretherton J.L., Lan. L.Y. *J Am. Chem. Soc.* (2001), 123, 5285.

[350] Man P.P., Klinowski J. *J. Chem. Soc.- Chem. Commun.* (1988), 19, 1291-1294.

[351] Poborchii V.V., Kolobov A.V., Caro J., Zhuravlev V.V., Tanaka K. *Chem. Phys. Lett.* (1997), 280, 17-23.

[352] Richardson Jr., J.W., Pluth J.J., Smith J.V. *Acta Crystallogr.* (1987), C43, 1469.

[353] Vietze U., Krauss O., Laeri F., Ihlein G., Schuth F., Limburg B., Abraham M. *Phys. Rev. Lett.* (1998), 81, 4628-4631.

[354] Thong N., Schwarzenbach D. *Acta Crystallogr.* (1979), 53, 35.

[355] Jahn E., Müller D., Wieker W., Richter-Mendau J. *Zeolites* (1989), 9 (177).

[356] Christensen A.N., Jensen T.R., Norby P., Hanson J.C. *Chem. Mater.* (1998), 10, 1688.

[357] Zhu G.S., Xia F.S., Qui S.L., Hun P.C., Xu R.R., Ma S.J., Terasaki O. *Microporous Mater.* (1997), 11, 269.

[358] Gougeon R.D., Brouwer E.B., Bodart P.R., Delmotte L., Marichal C., Chezeau J.-M., Harris R.K. *J Phys. Chem. B.* (2001), 105, 12249-12256.

[359] Araki T., Finney J.J., Zoltai T. *Am. Mineral.* (1968), 53, 1096.

[360] Mooney R.C.L. *Acta Crystallogr.* (1956), 9, 728.

[361] Walker J. *Sci Am.* (1987), 256, 98.

[362] Symons M.C.R. *Acc. Chem. Res.* (1981), 14, 179.

[363] Brunner G.O. *Zeolites* (1992), 12, 428.

[364] Handerson S.J., White J.W. *J Appl. Cryst.* (1988), 21 (744).

[365] Dutta P.K., Bronic J. *Zeolites* (1994), 14, 251.

[366] Zhdanov S.P. *Adv. Chem. Ser.* (1971), 101, 21.

[367] Flanigen E.M. *Adv. Chem. Ser.* (1973), 121, 119.

[368] Yoshizawa N., Maruyama K., Yamada Y., Zielinska-Blajet M. *Fuel* (2000), 79, 1461-1466.

[369] Emmerich F.G. *Carbon* (1995), 33 (12), 1709.

[370] Grumer T., Zerda T.W., Gerspacher M. *Carbon* (1994), 32 (7), 1377.

[371] Mirth G., Lercher J.A., Anderson M.W., Klinowski J. *J Chem. Soc., Faraday Trans.* (1990), 86, 3039.

[372] Choudhary V.R. *Chem. Eng. Sci.* (1997), 52 (20), 3543-3552.

[373] Dyer A., Amin S. *Microporous Mesoporous Mater.* (2001), 46, 163-176.

[374] Prasetyo I., Do H. D., Do D.D. *Chem. Eng. Sci.* (2002), 57, 133-141.

[375] Do D.D. *Chem. Eng. Sci.* (1996), 51, 4145–4158.

[376] Do D.D., Wang K. *A.I.Ch.E. J* (1998), 44, 68.

[377] Do D.D., Wang K. *Carbon* (1998), 36, 1539.

[378] Figueiredo J.L., Pereira M.F.R., Freitas M.M.A., Orfao J.J.M. *Carbon* (1999), 37, 1379.

[379] Peppas N. A. *Polymer* (1997), 38, 3425.

[380] Glasstone S., Lewis D. Element of Physical Chemistry. London: Macmillan, (1946).

APPENDIX I. Polymerization of Furfuryl Alcohol

PFA can be synthesized by a polycondensation reaction of FA with various cationically active initiators, e.g., CF$_3$COOH, silica, HCl, or Lewis acids, Figure A.1. The resulting polymeric PFA materials are either soluble fractions or insoluble dark brown solids that contain conjugated sequences and crosslinked structures [76].
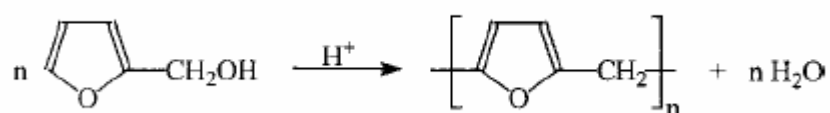
Figure A.1. Cationically induced polycondensation of FA (ideal structure formation).

APPENDIX II. Synthesis of Microwave-Assisted AlPO$_4$-5

AII.1. Synthesis of AlPO$_4$-5's Labeled A to D

Heating rates and heating times were changed in A1, A2, A3, A4 and A5. SEM micrographs of the samples A1 to A5 were shown in Figure A.2. Platelet crystals were formed in A1 and A3. Although in A1, plates arranged in superposing, crystals exhibits in A3 was more scattered. By increasing the heating time small rhombohedral crystals were produced in A2. However, miscellaneous, stuck together crystals were formed in A4 and A5.
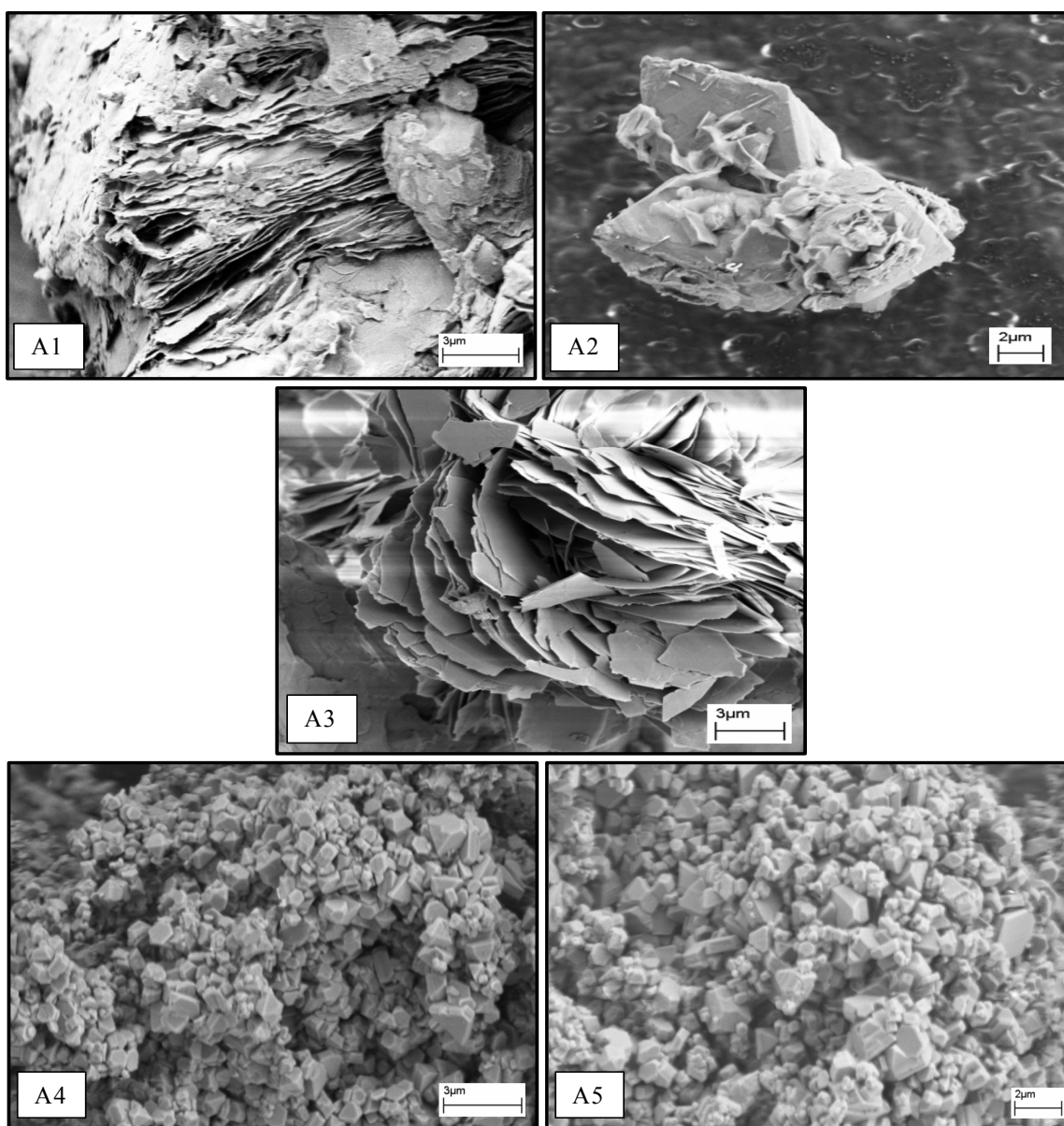
Figure A.2. SEM micrographs of A1, A2, A3, A4 and A5.

AFI type crystals could not obtained without HF. Spherical crystals were obtained in the samples labeled B, C and D, underlying the role of HF in shortening the crystallization time [168,206]. Therefore, HF was always present in the following synthesis. The concomitant use of amines or quaternary ammonium cations as templates and of a fluoride medium appears to be a prerequisite for the formation of both large and well-crystallized single crystals of $AlPO_4$-5 [206].
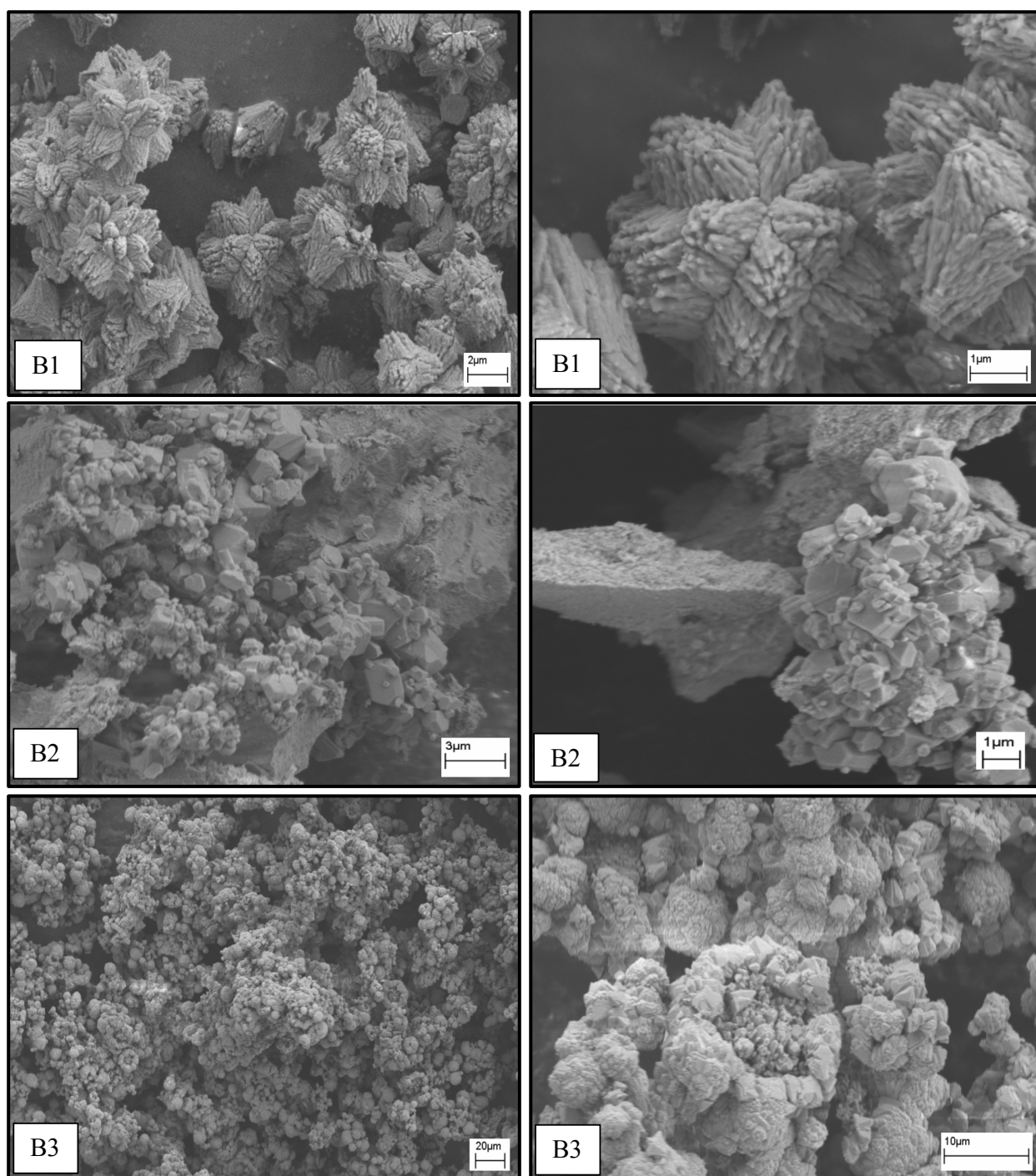
Figure A.3. SEM micrographs of B1, B2, and B3.

SEM micrographs of B1, B2 and B3 were shown in Figure A.3. B1 contains radial shape crystals, developing uniformly around a central axis with ca. 4 μm diameter that has needle-like projections, getting narrower outwards. Increasing heating time to 600 s, these crystals replaced with different geometrical shaped ones in B2. At 1200 s, all assorted crystals, in a mixed fashion, have been arranged in an order in a ring-shaped orientation. They have bigger clusters than that of crystallized at shorter time periods. In B4 and B5, ring shaped crystals have also been formed, shown in Figure A.4; however they have smaller sizes compared to B3.
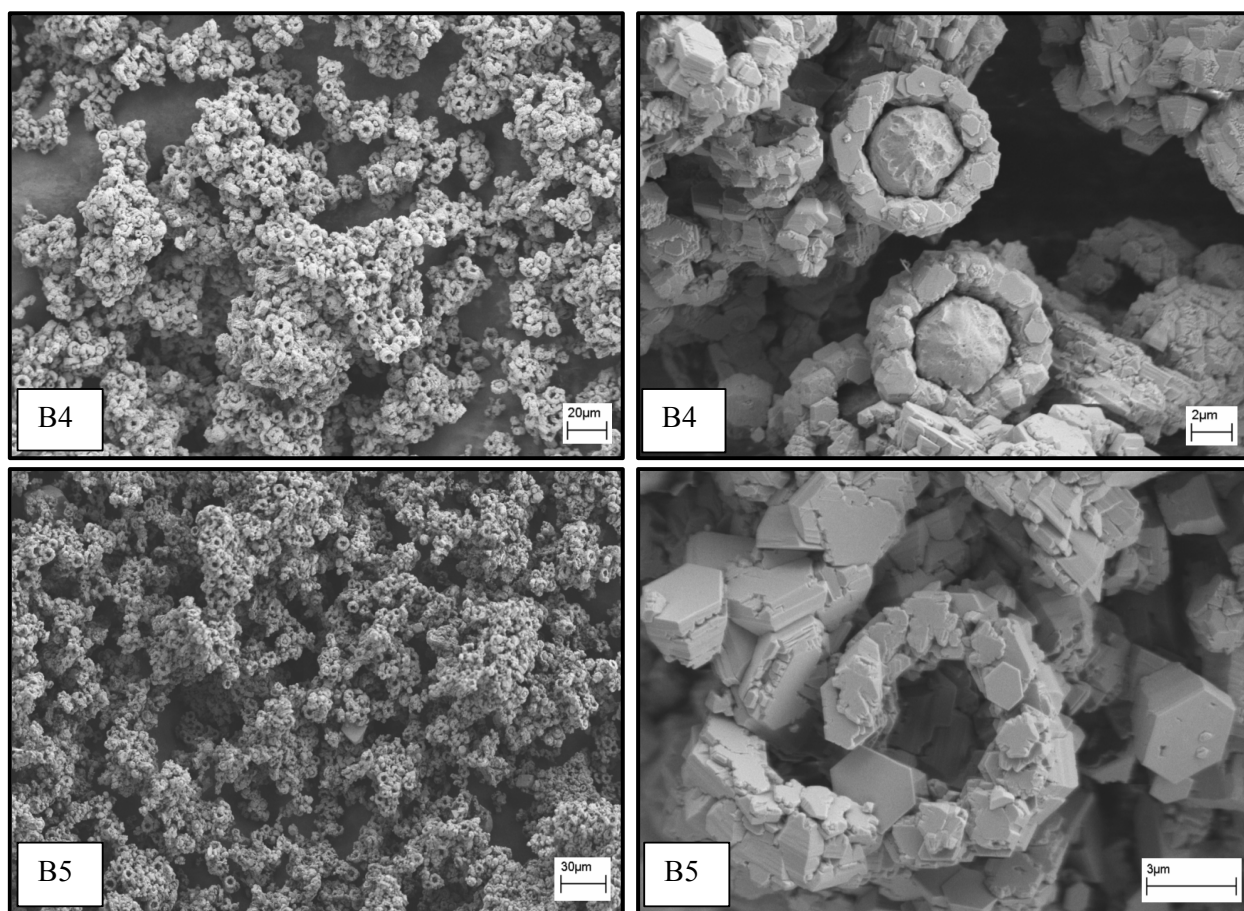
Figure A.4. SEM micrographs of B4 and B5.

The same molar composition resulted in different crystallites at higher power of crystallization, 200W. SEM micrographs of B6, B7 and B8 were represented in Figure A.5. Although B6 has no distinctive crystal shape, confirmed in XRD pattern (Figure A.6), B7 exhibits cambered globoids inside the ring shaped crystals, in ca. 6 μm diameter. Whereas B8 displays globules in ca. 4 μm width made up of little needles. XRD patterns of B4, B5, B6 and B7 were given in Figure A.6. Aluminum phosphate hydrate was observed matched with the patterns found in XRD software.

The synthesis products observed in C1 represent flatted faced spheres ca. 6 μm width, found in aggregates (Figure A.7). In C2, tightly arranged needles formed a group, to form pimpled spheres. Clusters found in B1 made sporadically assembled bigger agglomerates with holes in prickles in C3. XRD patterns of C5 and C6 were shown in Figure A.8, similar to Figure A.6. Analyzing D1, one can notice that no distinctive feature was observed, shown in Figure A.9. Whereas, in D2 small balls grabbing hold of AlPO$_4$ islands was observed.
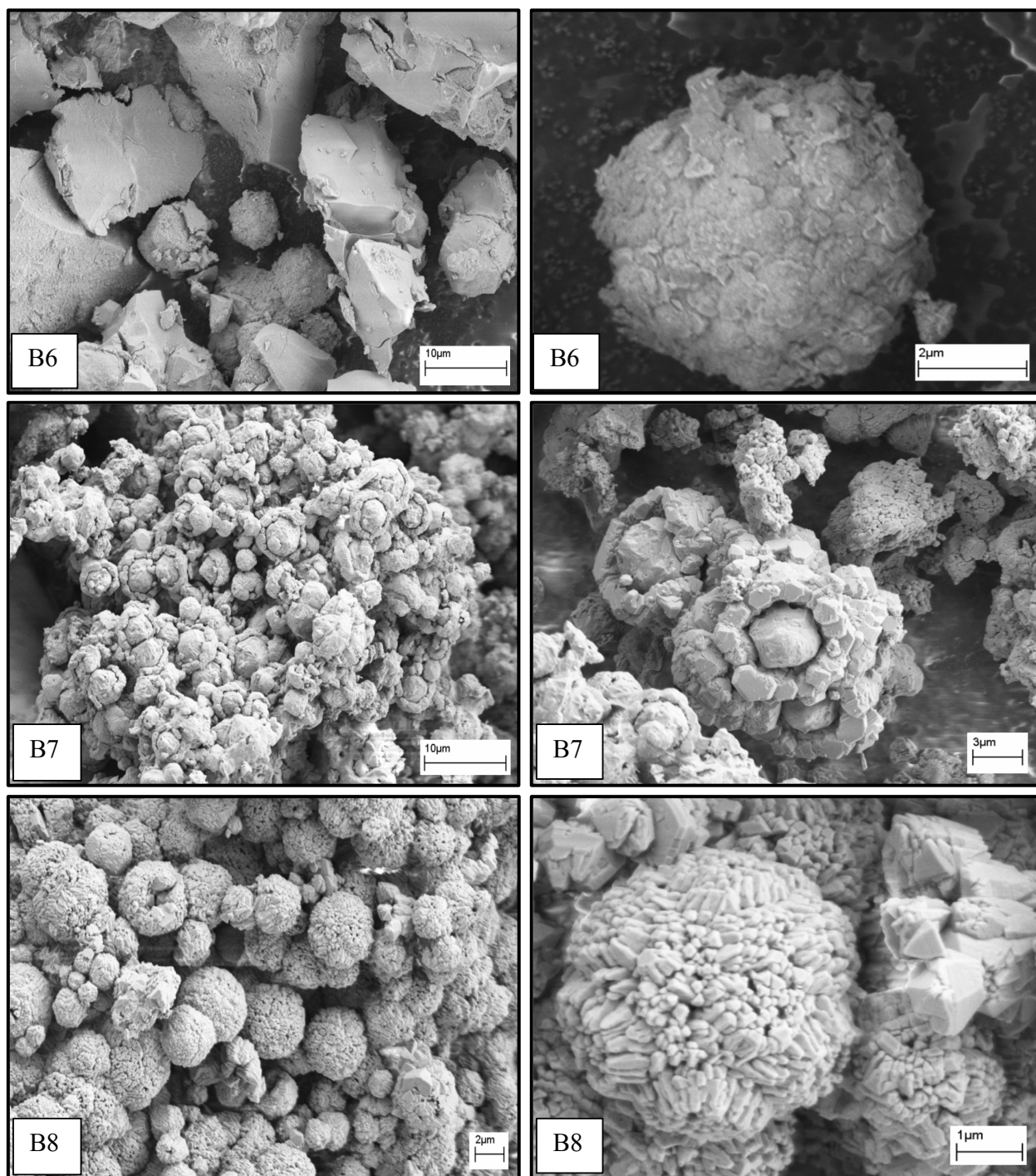
Figure A.5. SEM micrographs of B6, B7 and B8.
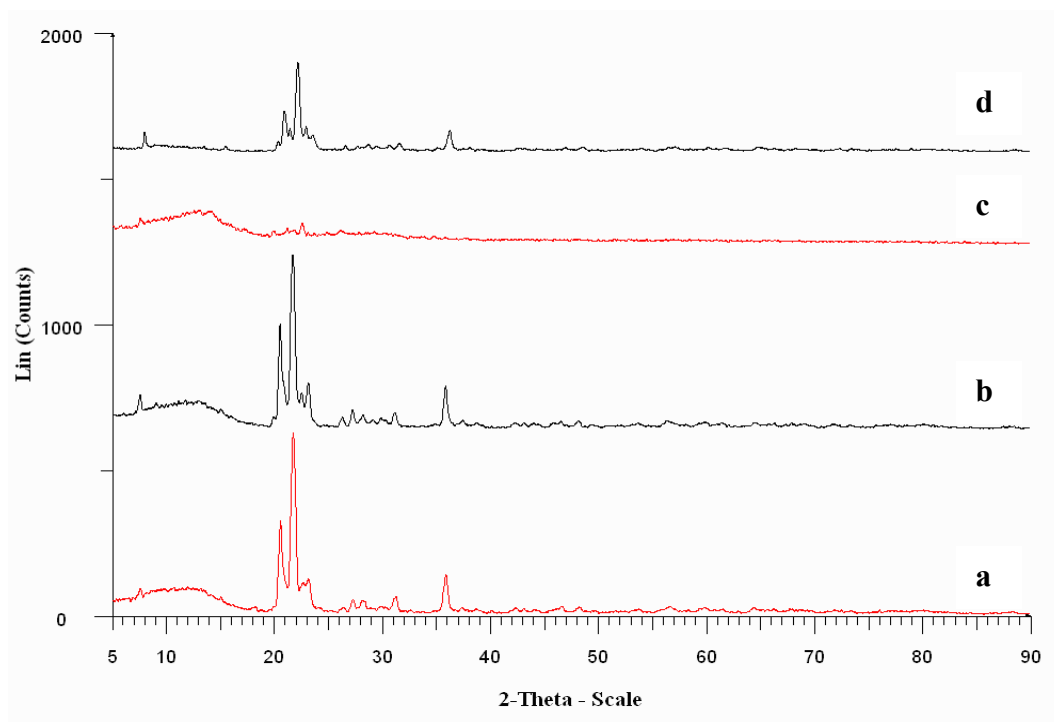
Figure A.6. XRD patterns of **a.** B4, **b.** B5, **c.** B6 and **d**. B7.
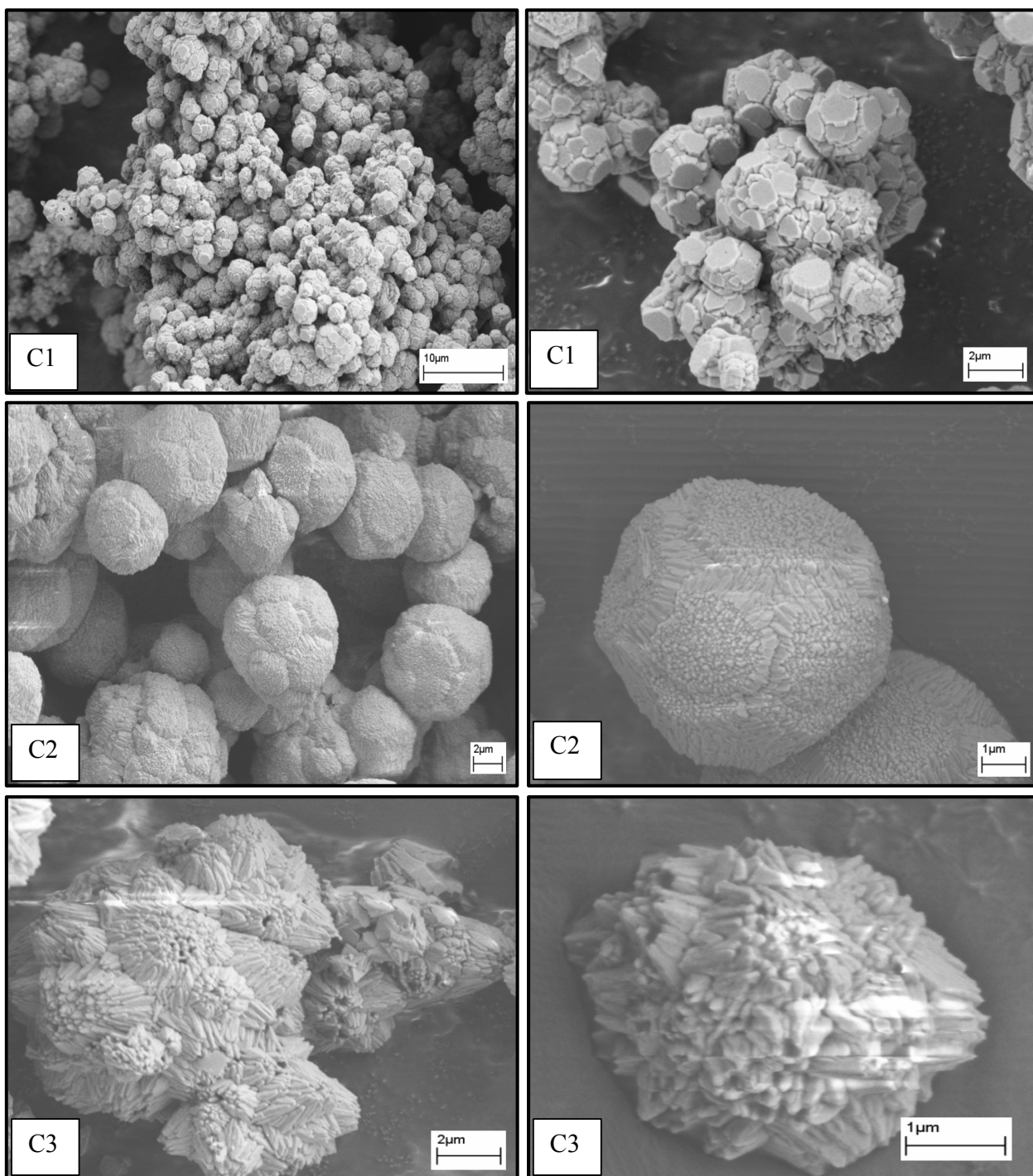
Figure A.7. SEM micrographs of C1, C2 and C3.
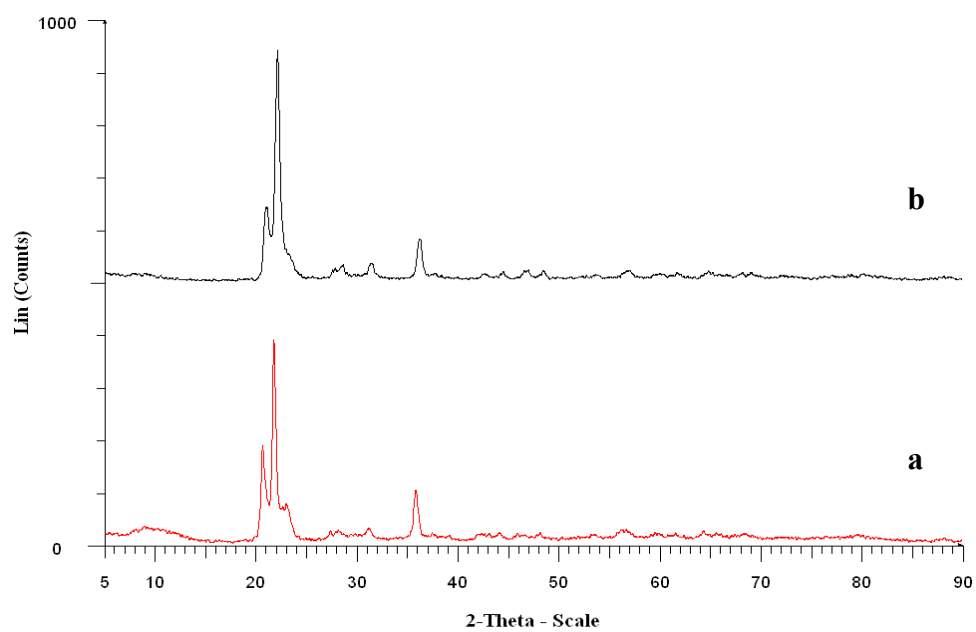
Figure A.8. XRD patterns of **a.** C5 and **b.** C6.
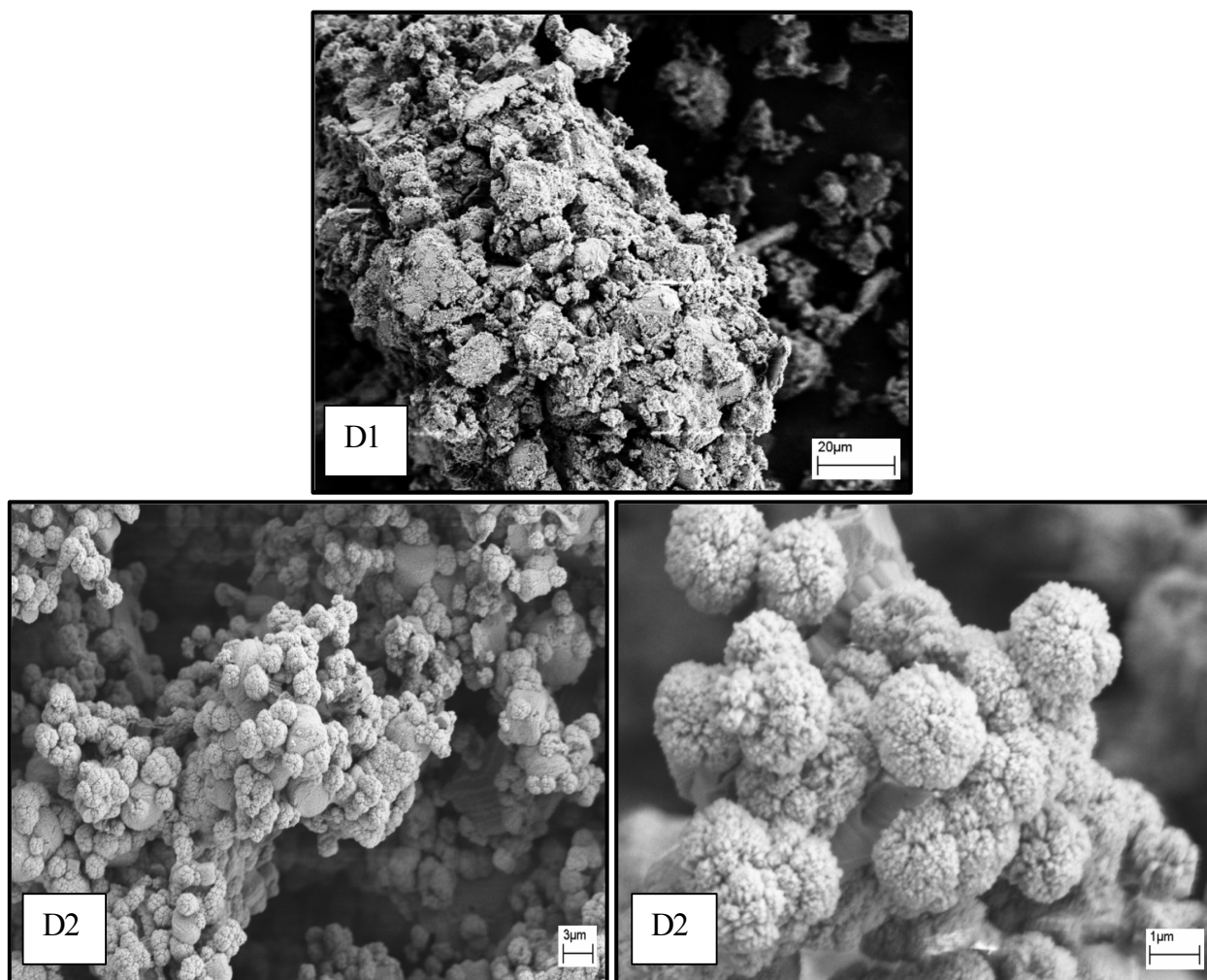
Figure A.9. SEM micrographs of D1 and D2.

AII.2. Synthesis of AlPO$_4$-5's Labeled E

No distinguishing crystals were detected in E1, E2 and E3 (Figure A.10). Rising the heating time to 8 minute in the second step, pudgy hexagonal AlPO$_4$-5's dispersed in the scanned area was formed in E4 (Figure A.11). Some unreacted fragments were also observed.
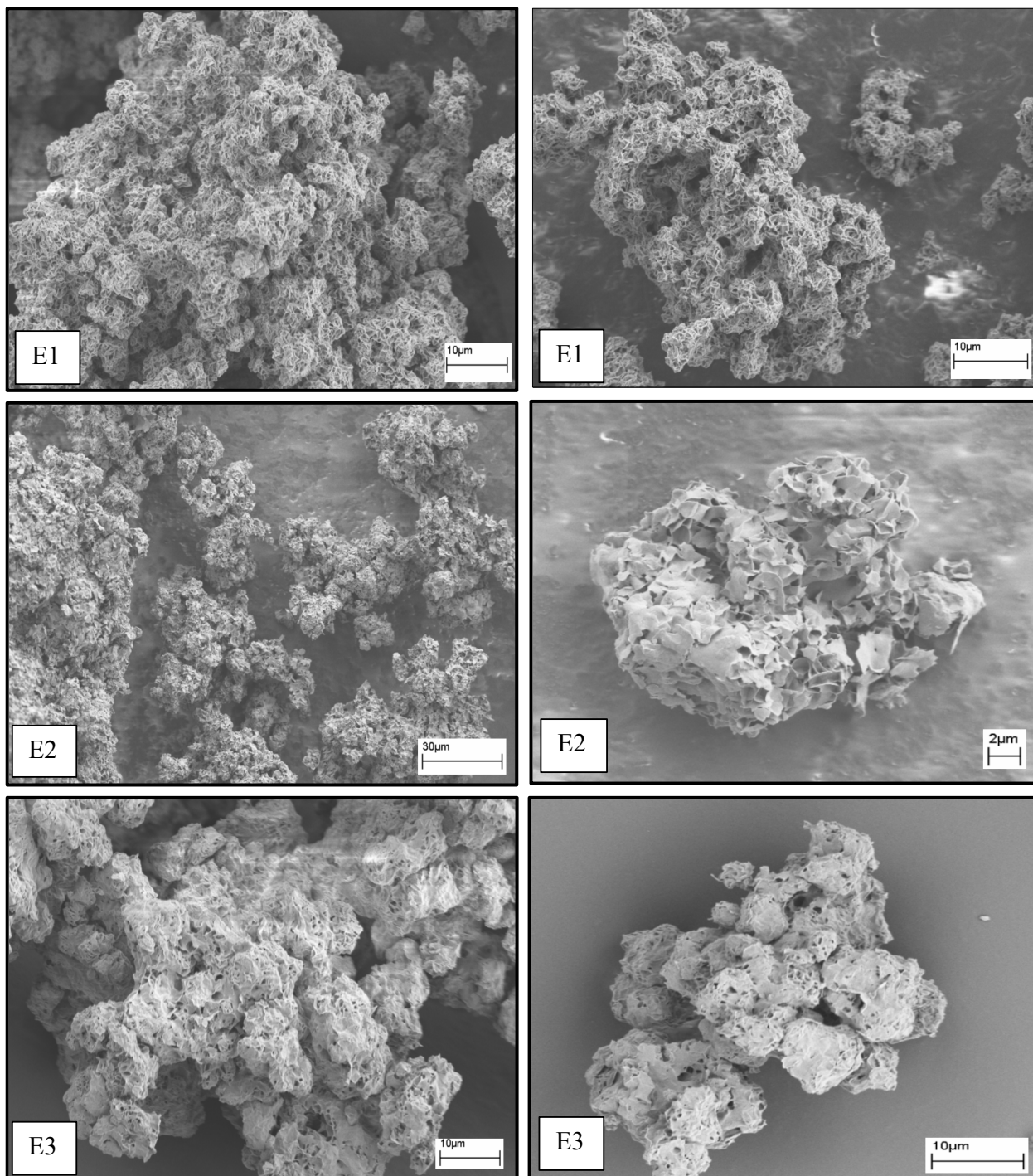
Figure A.10. SEM micrographs of E1, E2 and E3.
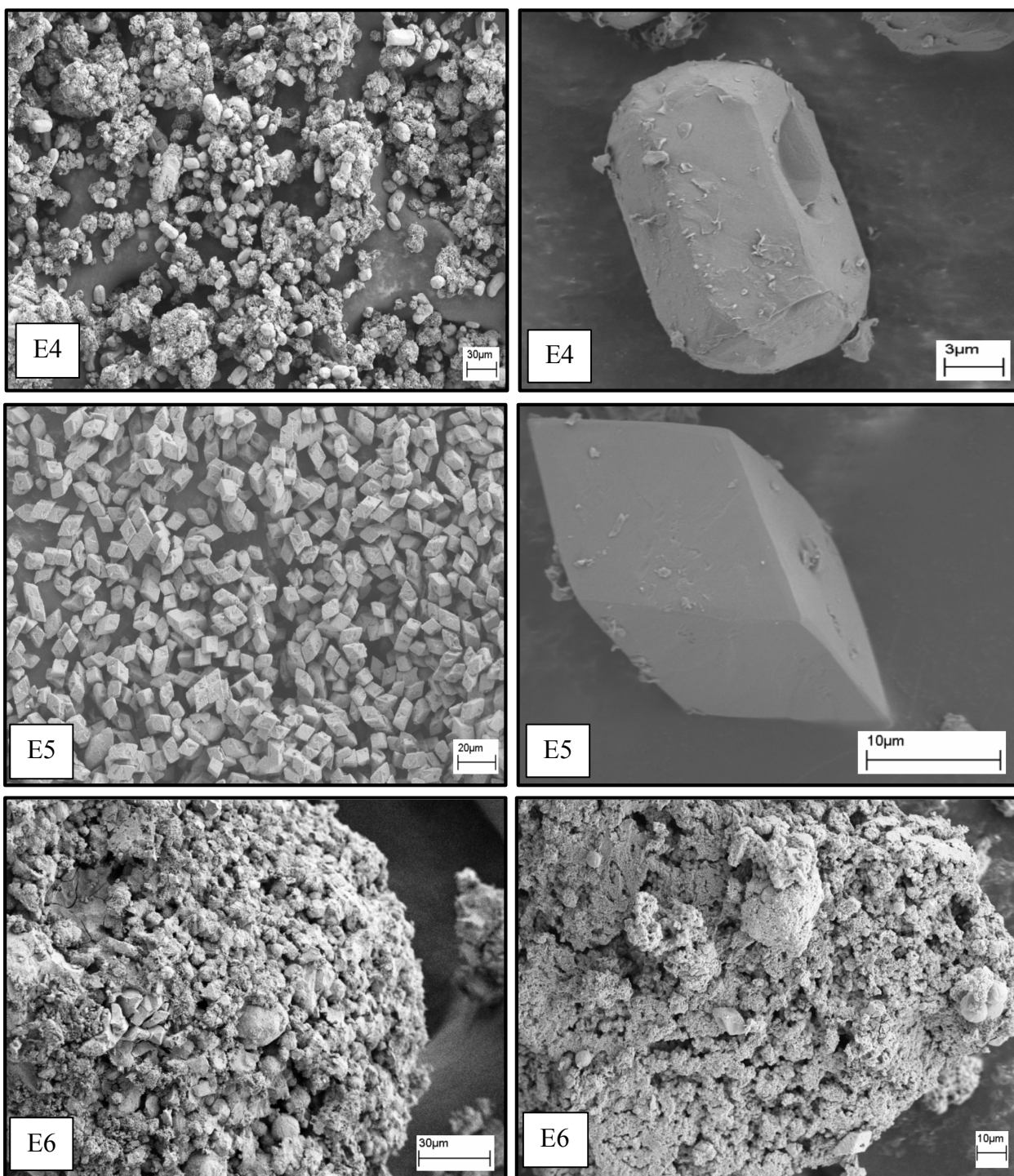
Figure A.11. SEM micrographs of E4, E5, E6 and E7.

Increasing the heating time to 600 s in the second step, perfect rhombohedral crystals were formed without unreacted gels (Figure A.11). These diamonds have ca. 10 μm in length of one side. Finger et al. [156] also observed such rhomohedral crystals. XRD patterns of E1, E2, E3 and E5 were shown in Figure A.12. Peaks observed in E5 matched with both berlinite [354] and aluminum phosphate hydrate [172] structures. When heating time was increased to 900 s and 1200 s, in E6 and E7, no significant crystal shapes were

formed (Figure A.11) Increasing heating time in the second step resulted in losing the crystal shapes.
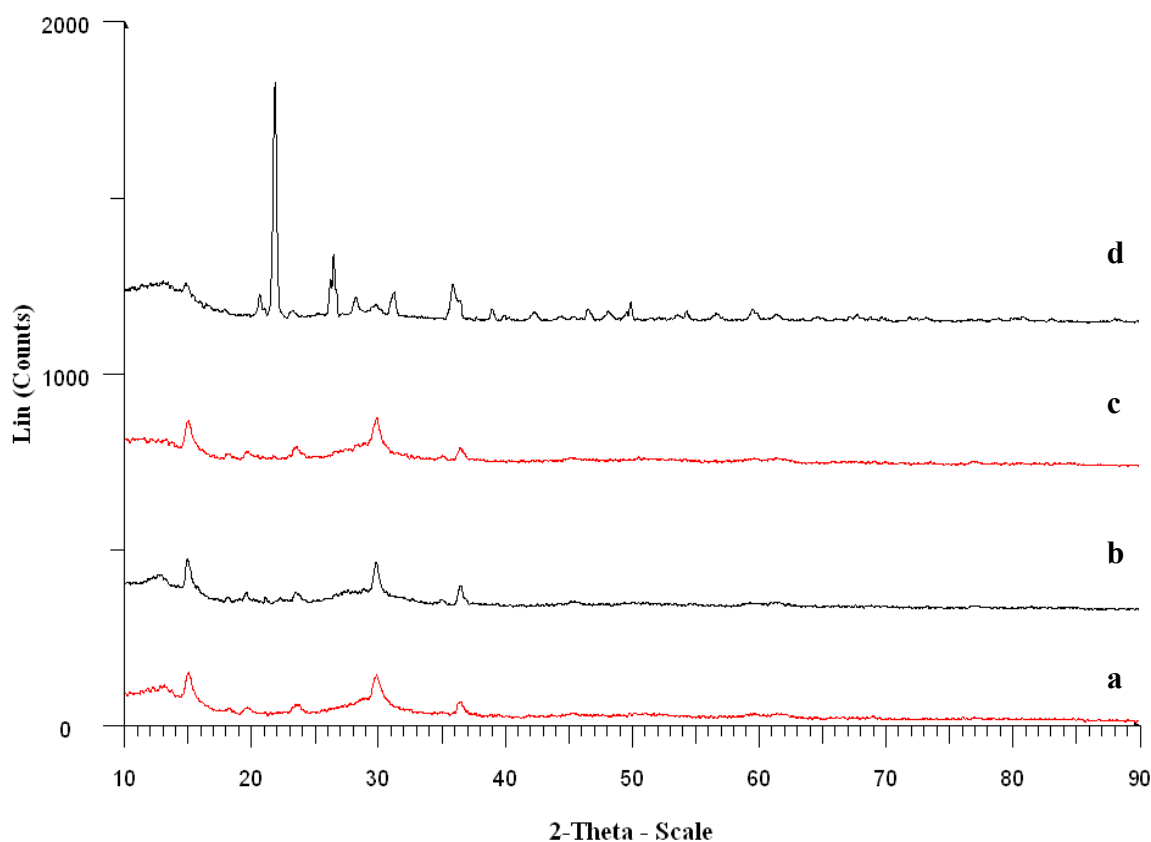
Figure A.12. XRD patterns of **a.** E1, **b.** E2, **c.** E3 and **d.** E5.

SEM micrographs of E8, E9, E10, E11 and E12 were given in Figure A.13. No preheating was applied for these samples. While some cubic structures were formed in E8, there are no distinctive forms in E9. In E10, scanned area was consisted of rectangular prisms in different dimensions. SEM micrographs of E13, E14 and E15 were shown in Figure A.14. Scattered layers of $AlPO_4$-5's constitute E11 and E15. Cubic structures were observed in E13 and E14.

The samples F1, F2 and F3 produced by using half amount of water were presented in E3, E5 and E6 respectively. F1 has no distinctive crystal shapes like E3, shown in Figure A.15. Decreasing water content in E5 resulted in changing the crystal shapes from cubic to hexagonal, long ones, which have ca.10 μm width and ca.40 μm length.

The HF concentration was decreased in G1, G2 and G3, compared to E1, E2 and E3 respectively, represented in Figure A.16. While E1, E2 and E3 have no observed crystalline shapes; decreasing HF amount affected the crystal formation. Although some

unreacted phase was present, hexagonal AlPO$_4$-5's were observed in G1. The ends of the crystals become convex with increasing the heating time. Increasing heating rate to 200W changed the crystal shapes to amorphous types in G4, G5 and G6, shown in Figure A.17. XRD patterns of G1, G3, G4 and G5 were shown in Figure A.18. XRD patterns observed in G1 belongs to base-centered orthorhombic aluminum phosphate [360], matched with pattern found in XRD software. XRD pattern of G3 was more likely synthetic berlinite [354] matched with patterns found XRD software.
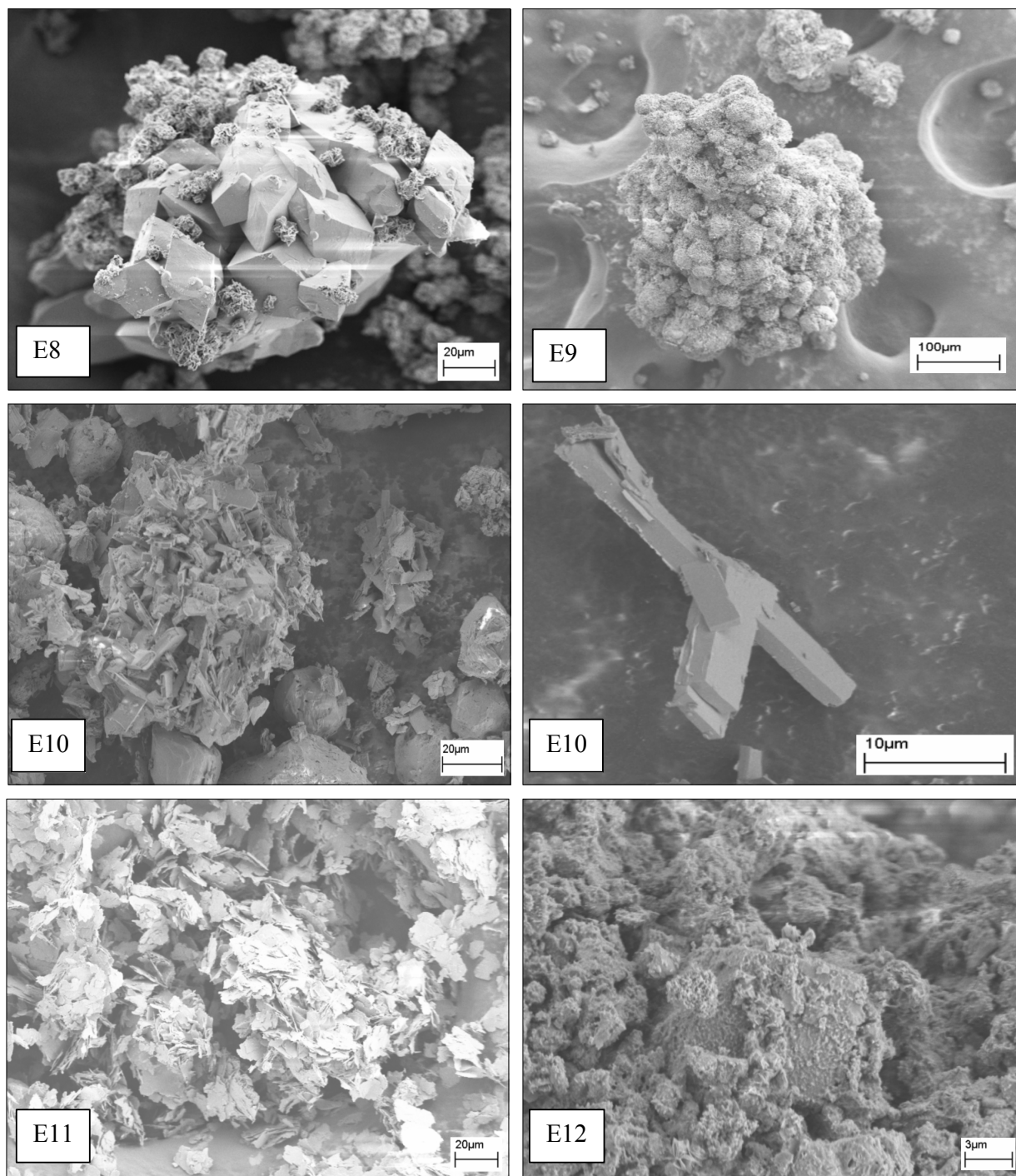
Figure A.13. SEM micrographs E8, E9, E10, E11 and E12.
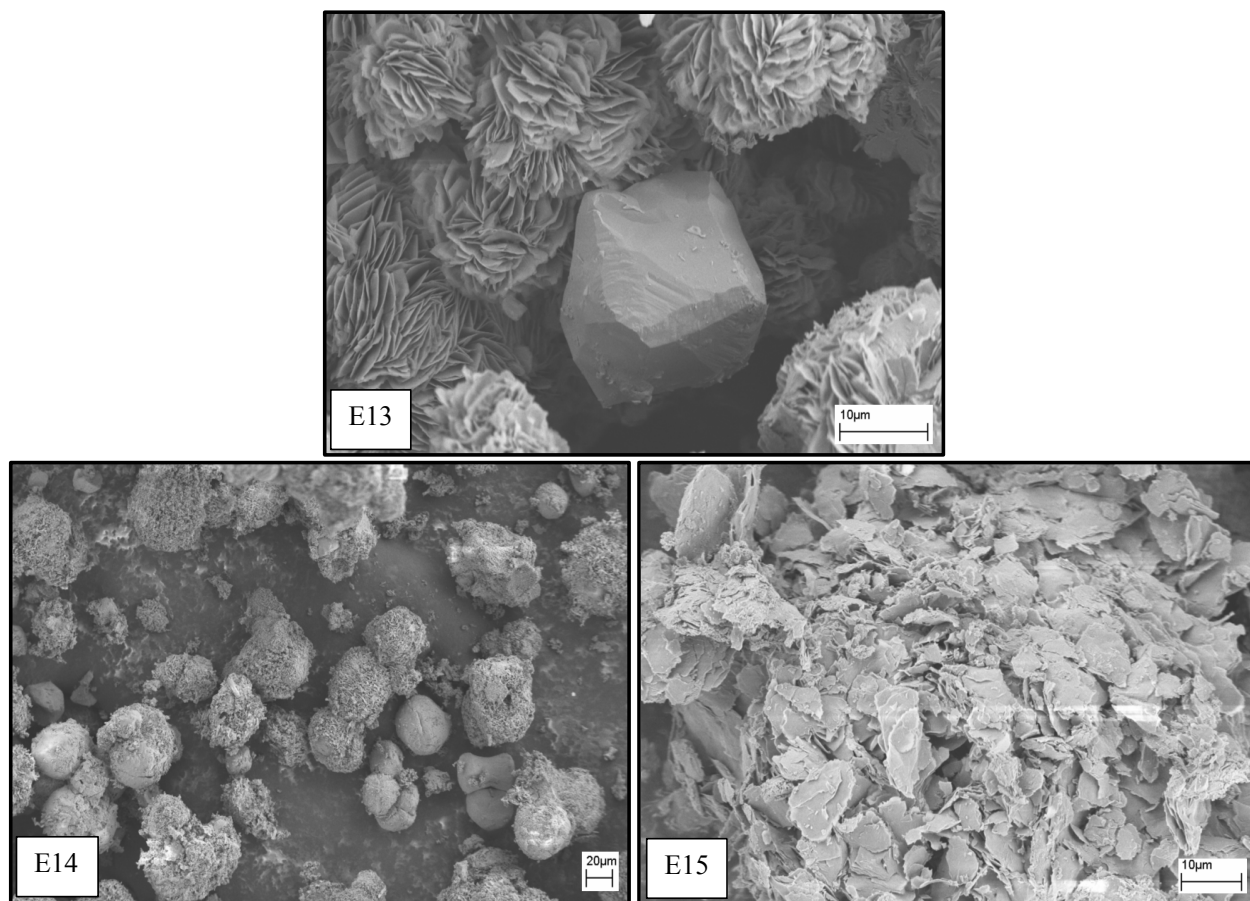
Figure A.14. SEM micrographs of E13, E14 and E15.
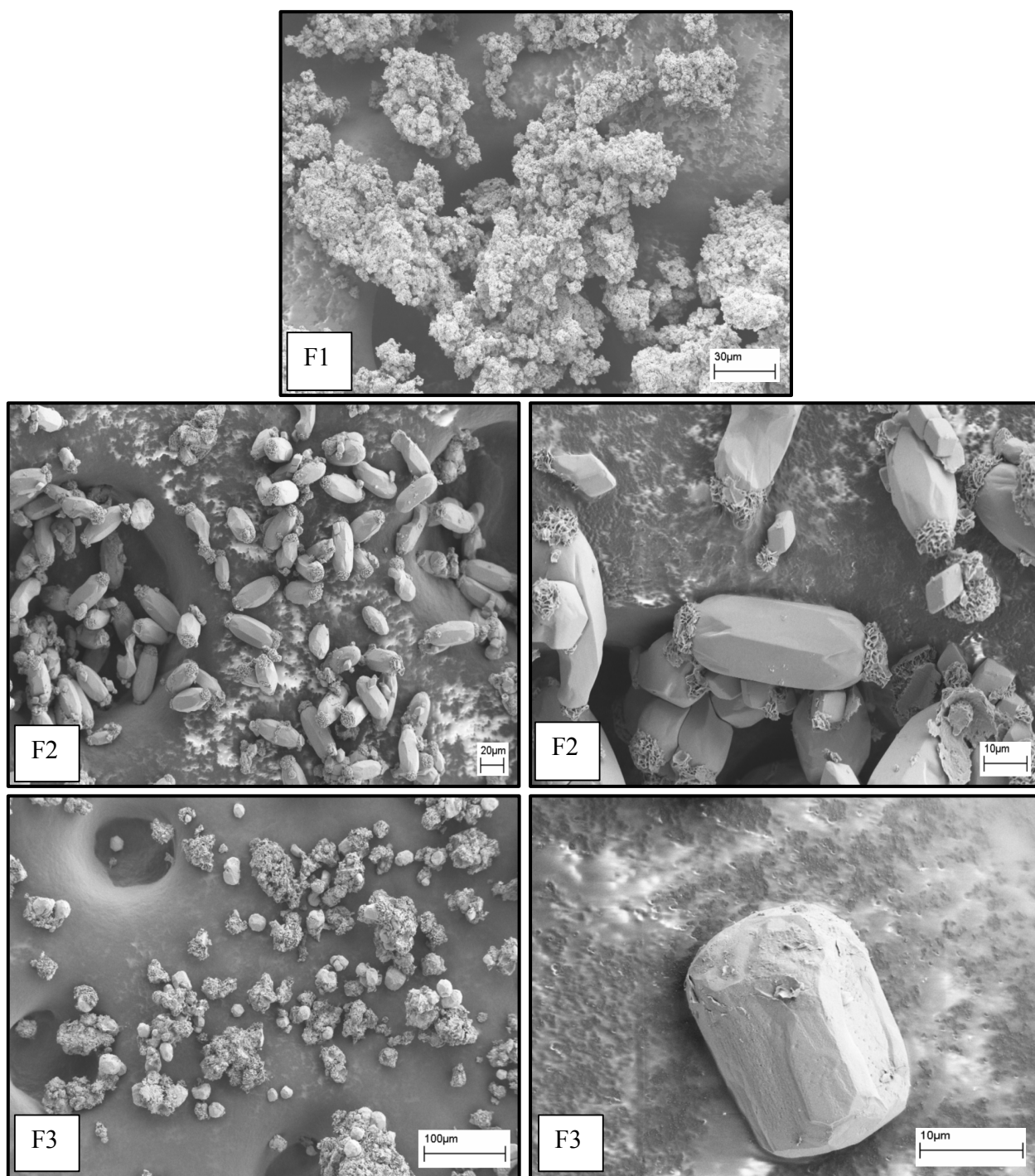
Figure A.15. SEM micrographs of F1, F2 and F3.
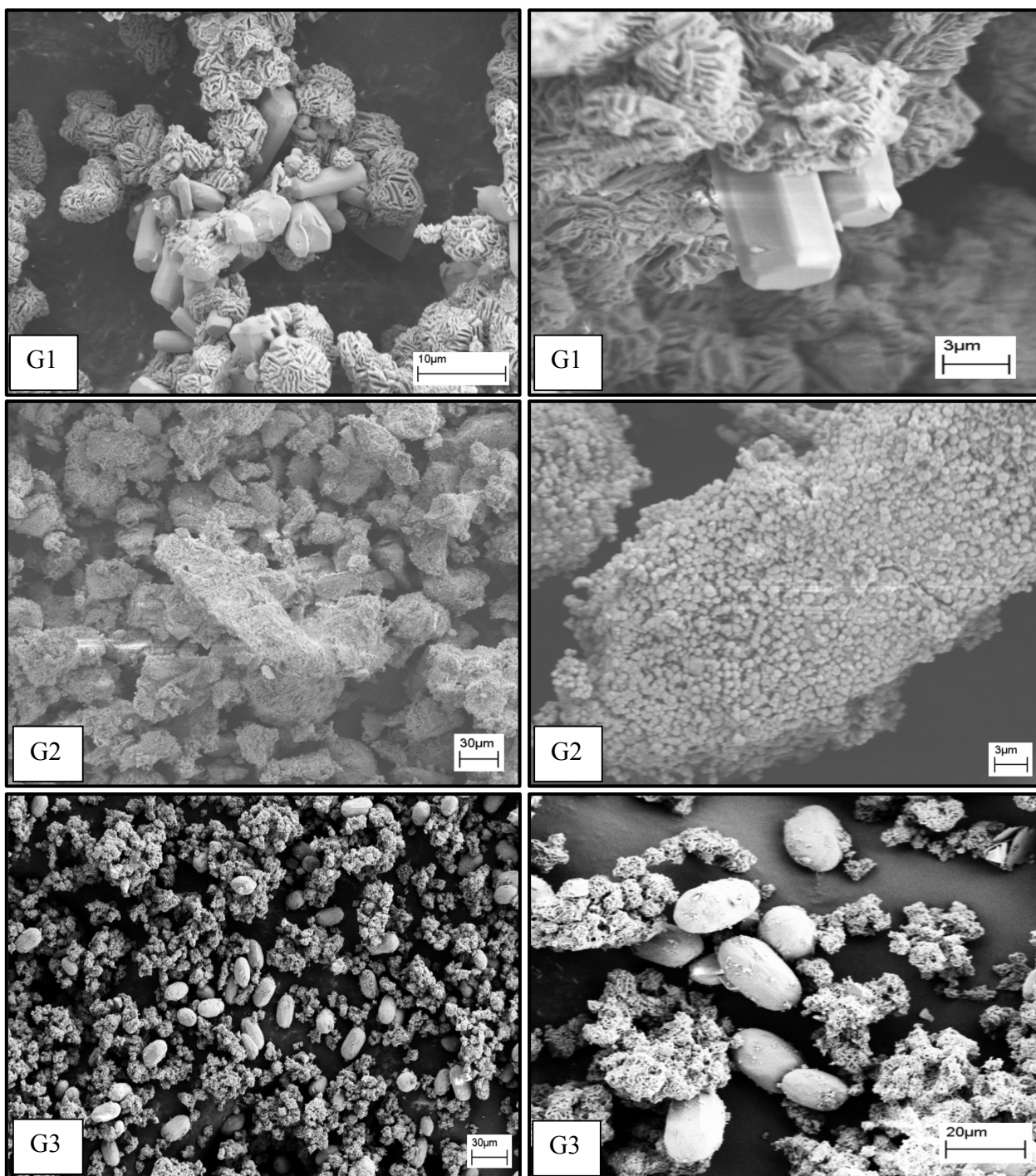
Figure A.16. SEM micrographs of G1, G2 and G3.
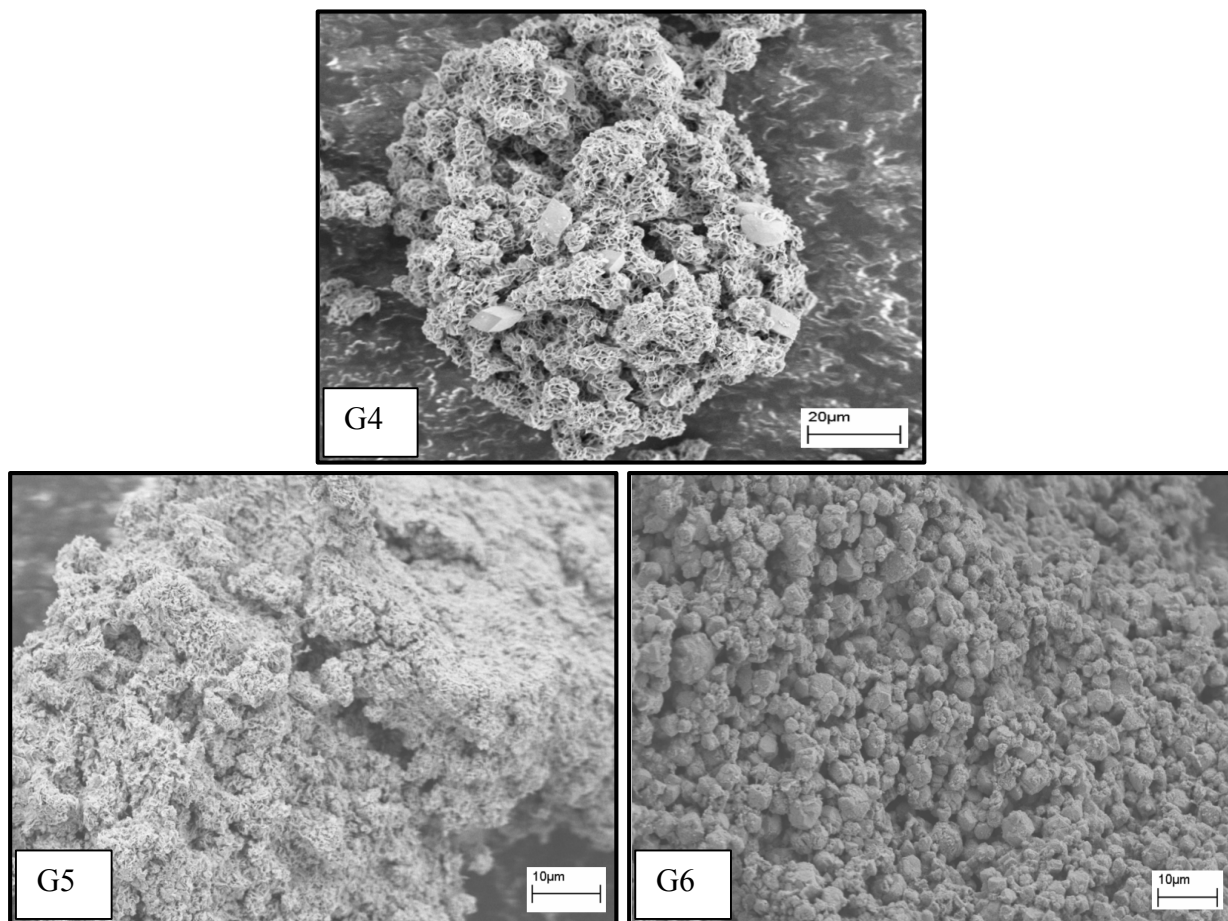
Figure A.17. SEM micrographs of G4, G5 and G6.
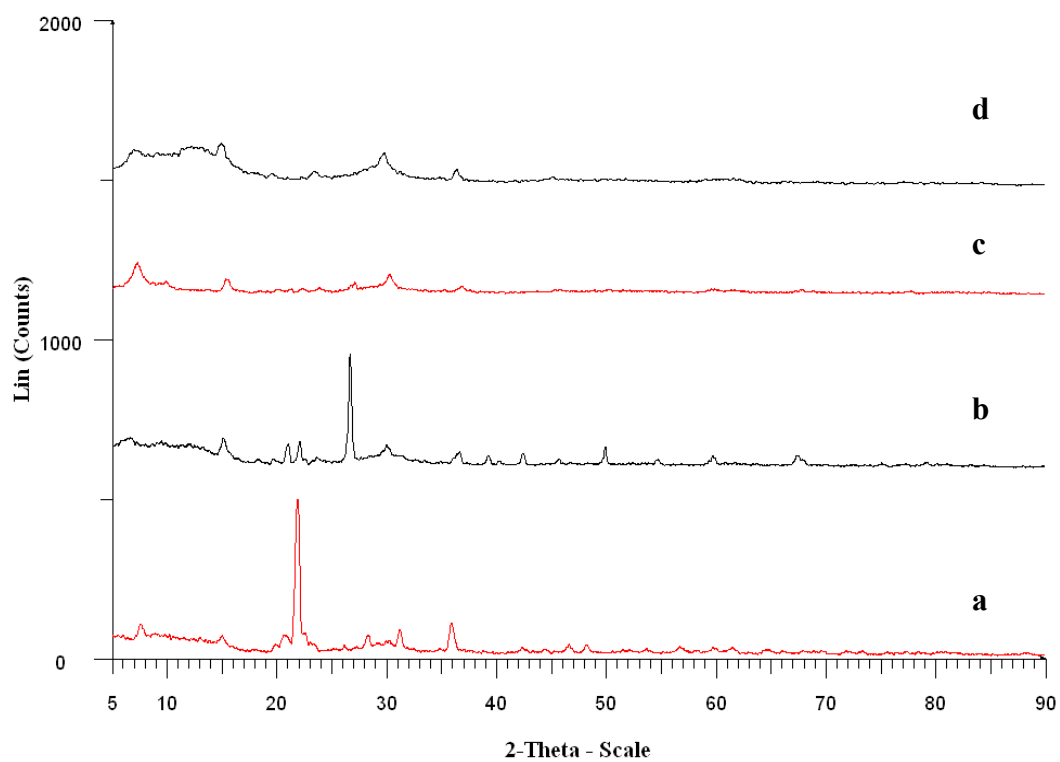
Figure A.18. XRD patterns of **a.** G1, **b.** G3, **c.** G4 and **d.** G5.

AII.3. Synthesis of AlPO$_4$-5's Labeled J to M

AII.3.1. Effect of Template Concentration on the Synthesis of AlPO$_4$-5 Labeled J

The effect of templating agent concentration in the initial solution of AlPO$_4$-5 formation was investigated by comparing the results H5 and H8 with J1 and J2. When the concentration of TEA was doubled, AlPO$_4$-5 crystals were thinner and agglomerated and stucked each other. Even though well-arranged hexagonal crystals were formed in H5, that contains 1.3 molar composition of TEA, after the composition was increased to 2.6, in J1, adherent and thinner crystals were formed (Figure A.19). Increasing heating time to 300 s, in J2, crystals were deteriorated. The comparison of XRD patterns of H5, J1, H8 and J2, were presented in Figure A.20. XRD patterns observed in H5 and H8 showed AFI structure, however J1 and J2 exhibit berlinite structure [360]. Finger et al. [156] observed rose-like crystals or vicinal crystals at high concentration of TEA in the synthesis mixture.
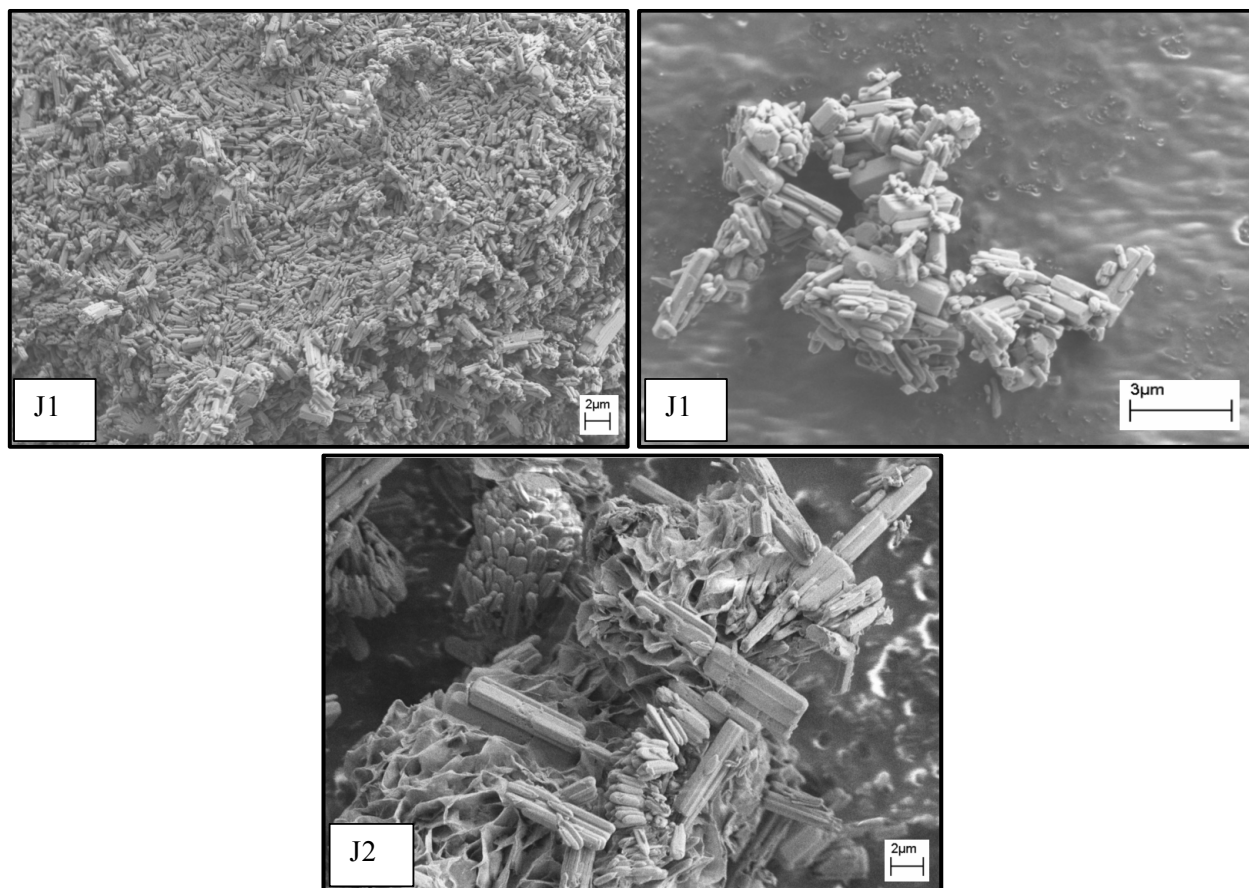
Figure A.19. SEM micrographs, J1 and J2.

The solubility of gels for the synthesis of the $AlPO_4$ molecular sieve can be increased with a high concentration of template [245] instead of increased water concentration or incorporation of fluoride. It has also been known that the nucleation rate increases and, therefore, the crystal size decreases with an increase in the concentration of the template [372,172,238].
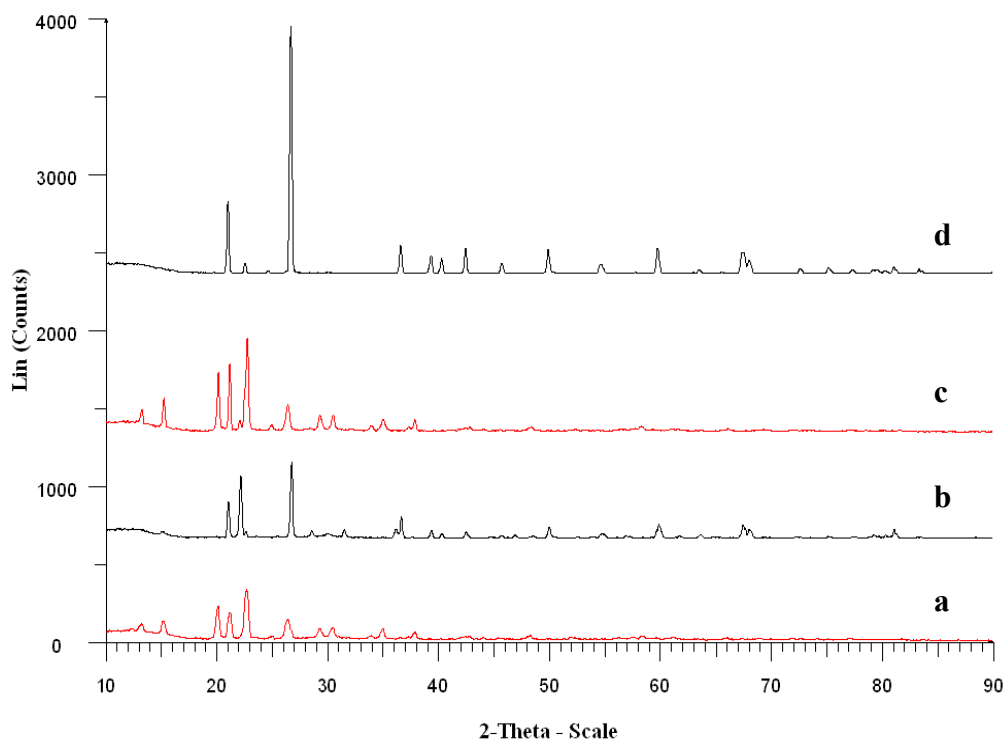
Figure A.20. XRD patterns of **a.** H5, **b.** J1, **c**. H8 and **d.** J2.

AII.3.2. Effect of H_2O Concentration on the Synthesis of $AlPO_4$-5 Labeled K

Variation of the water content results in changes to both the nucleation rate and the crystal growth rate, as indicated by Du et al. [238]. Dilution of the sample has a dramatic effect on the $AlPO_4$-5 structure [206,156,174]. When the initial reaction mixture is dilute, not many nucleation sites were present. Crystals grown in the diluted solution has a considerably more elongated form [244]. In the twice-diluted solution, the growth in the c-axis direction continued whereas that in the a-axis direction was almost completed. This coincides with the fact that the secondary crystals nucleated in the exhausted gel at the late stage were very thin [244].

177

It should be mentioned that for those samples, the molar composition of H_2O was half of that of the samples labeled H. Dilution of the initial solution resulted in the growth of thinner crystals and, as well; the samples are more contaminated by undesired byproducts. SEM micrographs of K1, K2 and K3 were shown in Figure A.21. The ball type crystals were formed in K1, while perfect hexagonal crystals were formed in H1, which has double amounts of water. Narrow and bush like crystals were formed in K2 and K3.
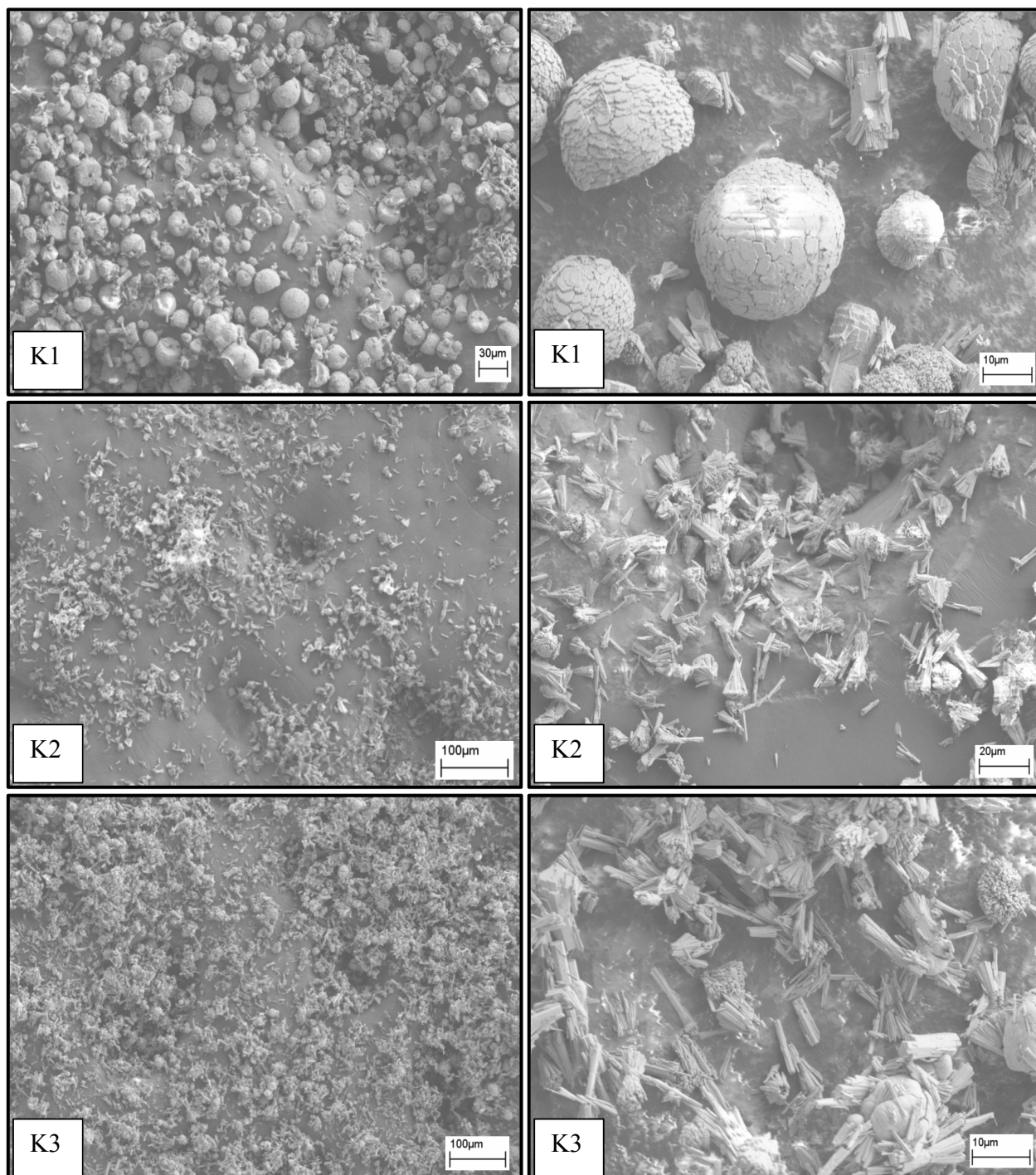
Figure A.21. SEM micrographs of K1, K2 and K3.

AII.3.3. Effect of TPA Used as a Templete on the Synthesis of AlPO$_4$-5 Labeled L

In the samples labeled L, TPA was used instead of TEA as an organic template. Several studies [156,355,242] have been devoted to the synthesis of the AlPO$_4$-5 phase, which can be prepared with different templates. SEM micrographs of L1, L2 and L3 were shown in Figure A.22. L1 and L2 have no significant crystal shapes. L3 consists of bars knitted with leafs. These crystalline morphologies were also confirmed with XRD patterns.
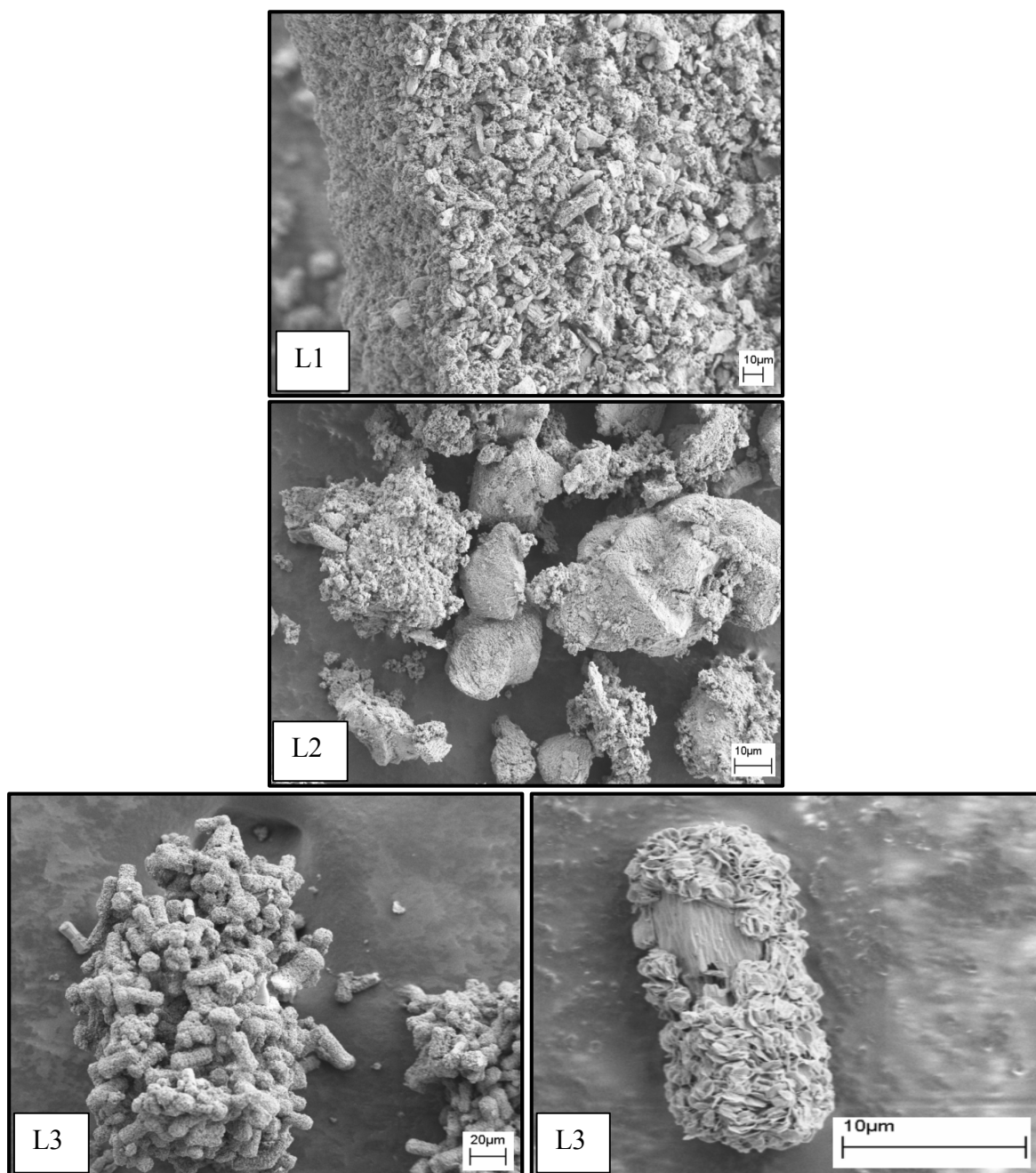
Figure A.22. SEM micrographs of L1, L2 and L3.
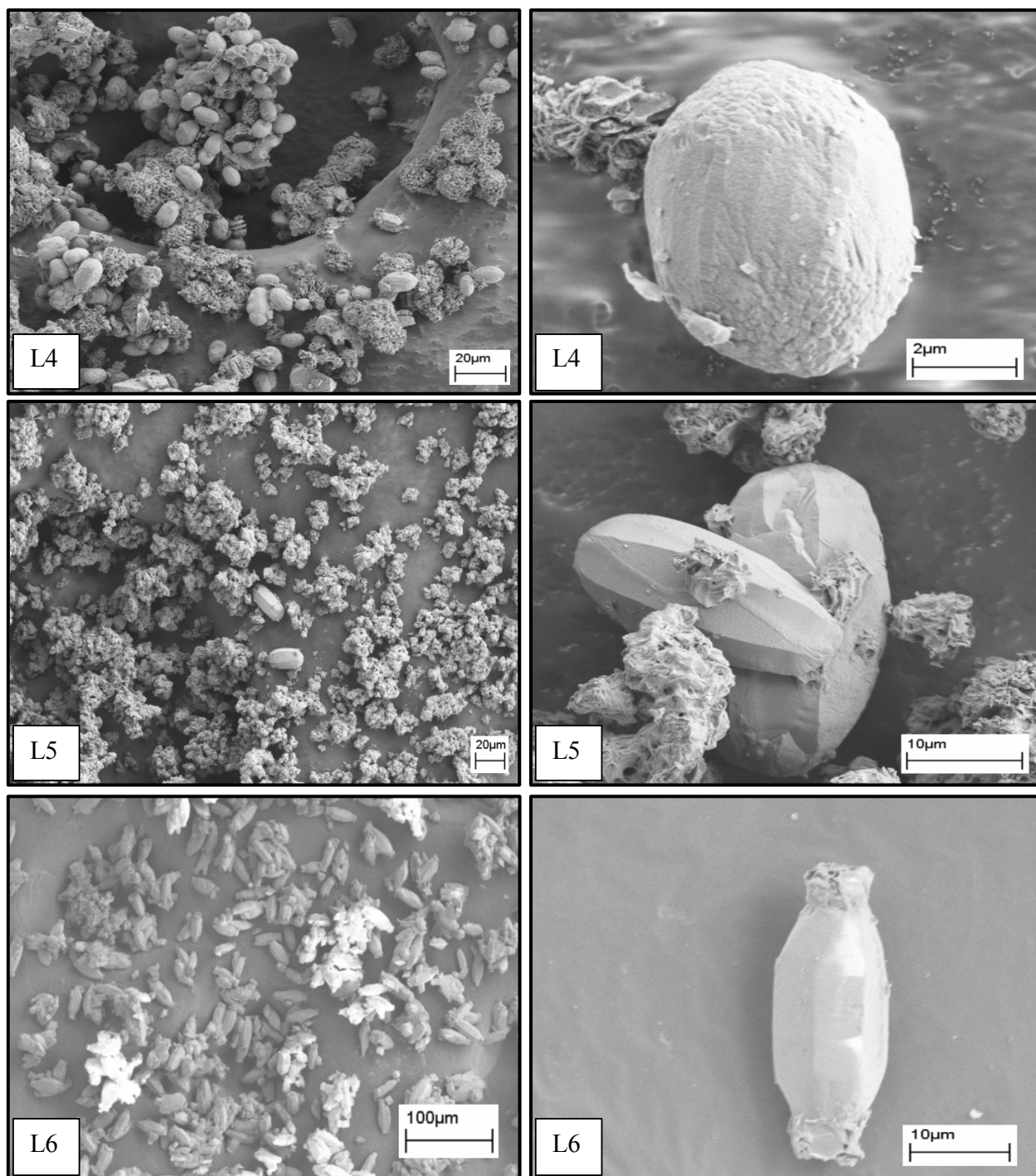
Figure A.23. SEM micrographs of L4, L5 and L6.

The crystal size was increased when TPA using as a template at 200W. SEM micrographs of L4, L5 and L6 were shown in Figure A.23. Different morphologies were observed at these samples. Spherical crystals were grown in L4 whereas in L5 angled bars were formed. Increasing heating time resulted in hexagonal crystals with unreacted and still growing ends in c-axis in L6. Wider hexagonals were formed when heating time was

360 s and 420 s, in L7 and L8 (Figure A.24). XRD patterns of L5, L6, L7 and L8 were shown in Figure A.26. Peaks observed in L5, L6, L7 and L8 matched with synthetic berlinite [354].
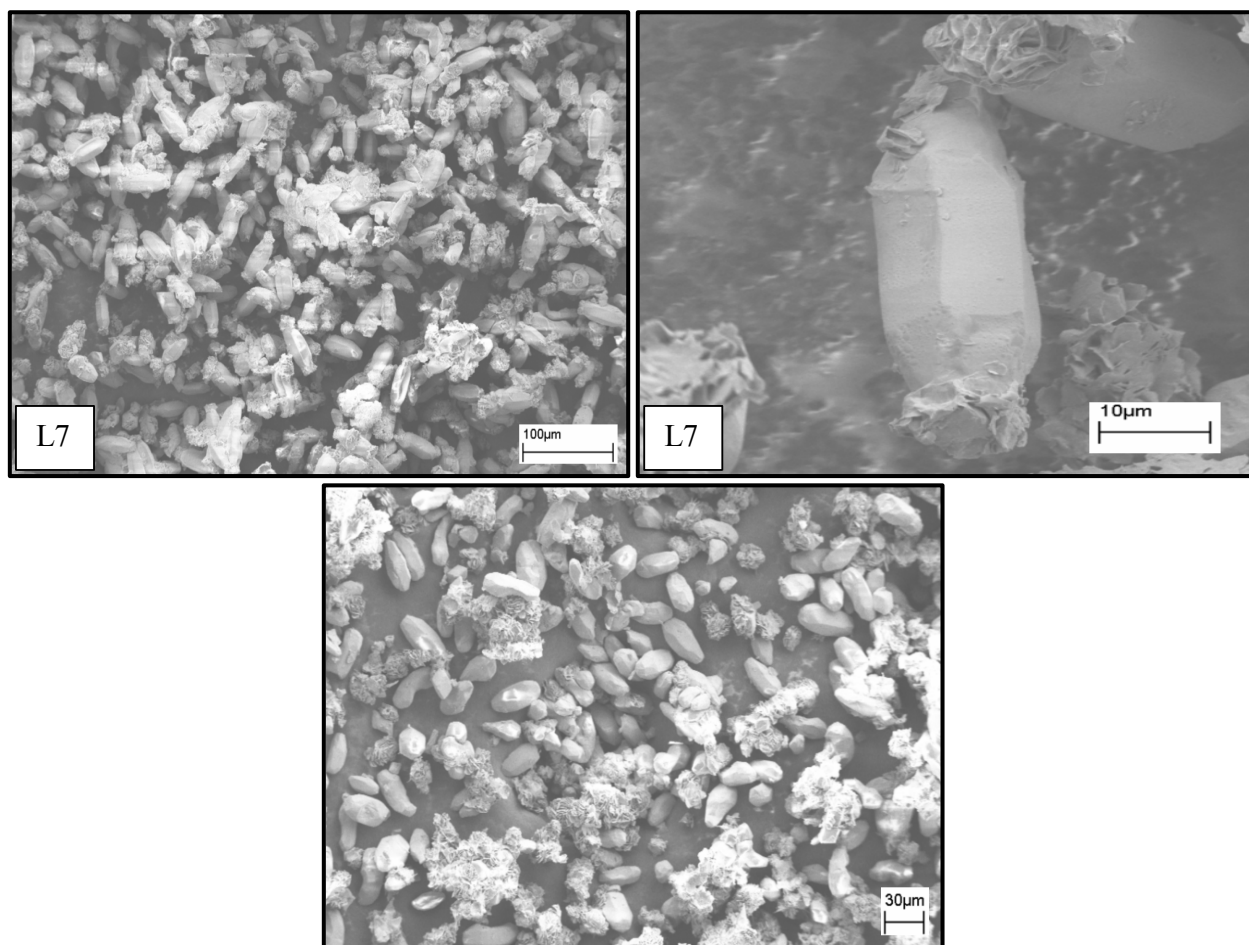
Figure A.24. SEM micrographs of L7 and L8.

SEM micrographs of L9, L10 and L11 were shown in Figure A.25. L9 and L10 have no significant shape, In L11, crystals grew in triangular fashion. In L12 (Figure A.25) wider and longer crystals were formed with perfect hexagonal and narrower ended. Finger et al. [156] proved that rising amine content forces the system to form the AFI phase by acceleration of the nucleation rate. XRD patterns of L9, L11, L12 and L13 were shown in Figure A.27. XRD pattern of L9 and L13 was corresponding to berlinite [354] and L11 and L12 was aluminum phosphate structure [360].

Du et al. [238] investigated the influence of the template content on the synthesis of $AlPO_4$-5. The tetraethyl ammonium hydroxide as a template favors the formation of small crystallites of $AlPO_4$-5, in contrast to triethylamine as the template, which usually favors the formation of large $AlPO_4$-5 crystals [156].
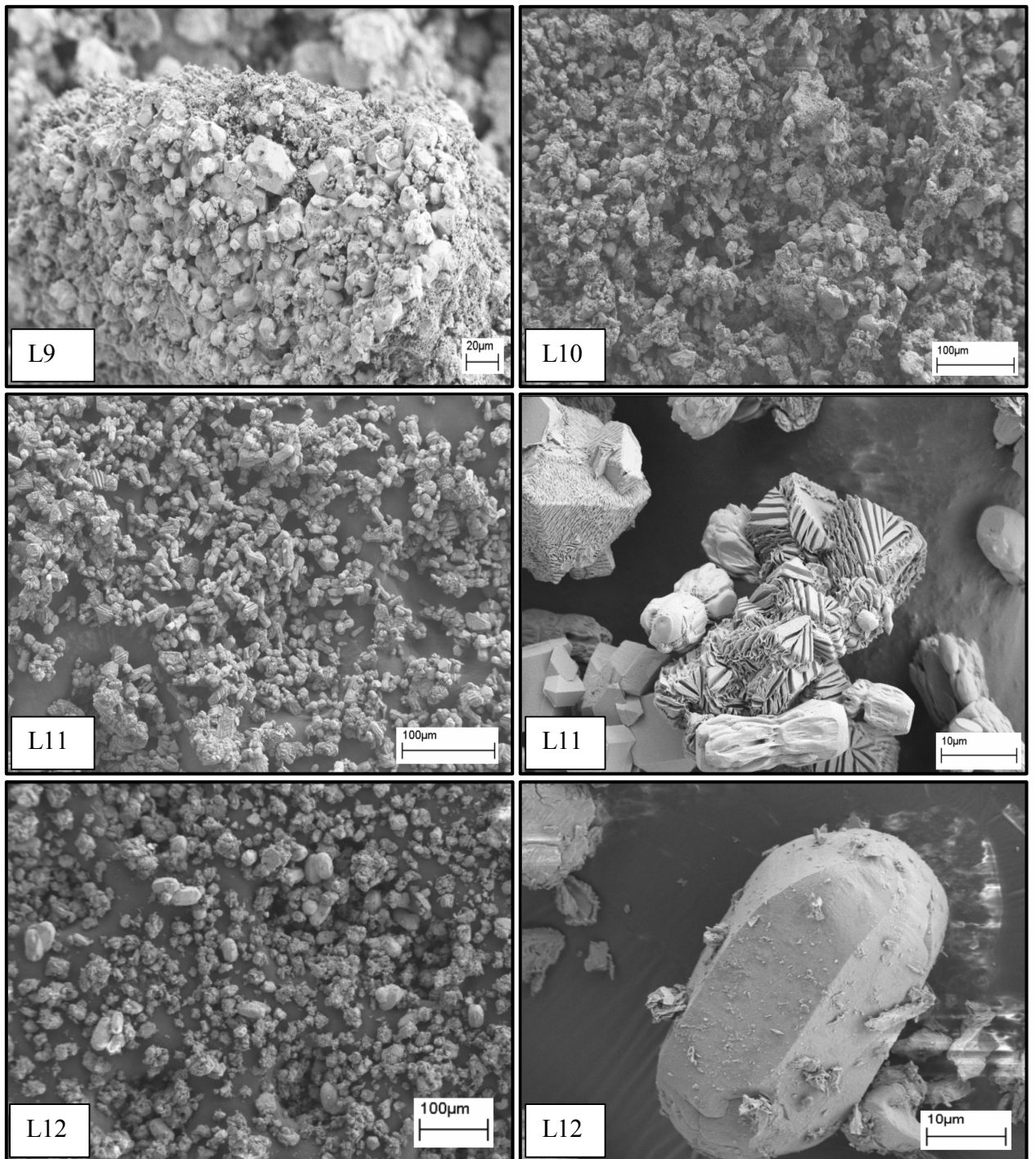
Figure A.25. SEM micrographs L9, L10, L11 and L12.
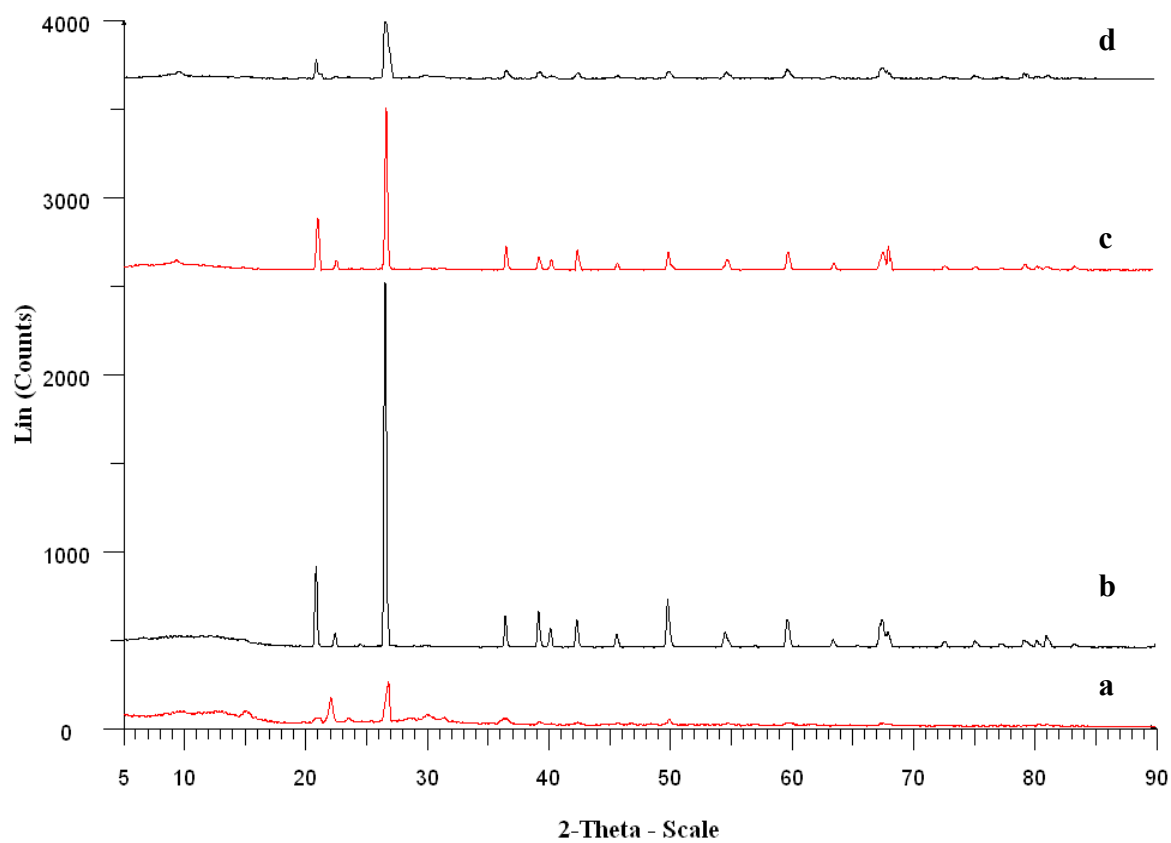
Figure A.26. XRD patterns of **a.** L5, **b.** L6, **c.** L7and **d**. L8.
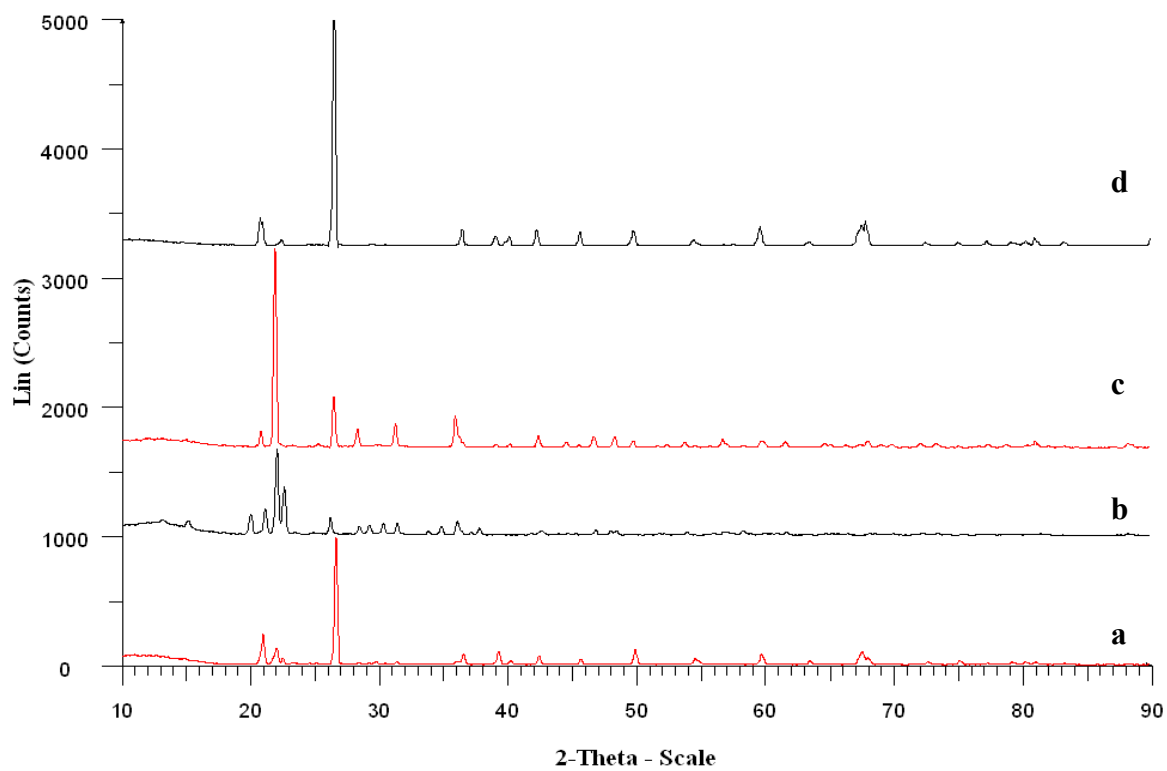
Figure A.27. XRD patterns of **a.** L9, **b.** L11, **c.** L12 and **d**. L13.

AII.3.4. Effect of TPA Concentration on the Synthesis of AlPO$_4$-5 Labeled M

Increasing TPA concentration resulted in formation of triangular-faced crystals in M1. In M2, rounded ended hexagons were formed, shown in Figure A.28. In M3, shown in Figure A.28, all scanned area was full of perfect, ca. 30 μm long hexagonals. XRD patterns of M1, M2 and M3 were shown in Figure A.29. M1 was corresponding to aluminum phosphate structure [360] whereas peaks observed in M2 and M3 belongs to berlinite [354].
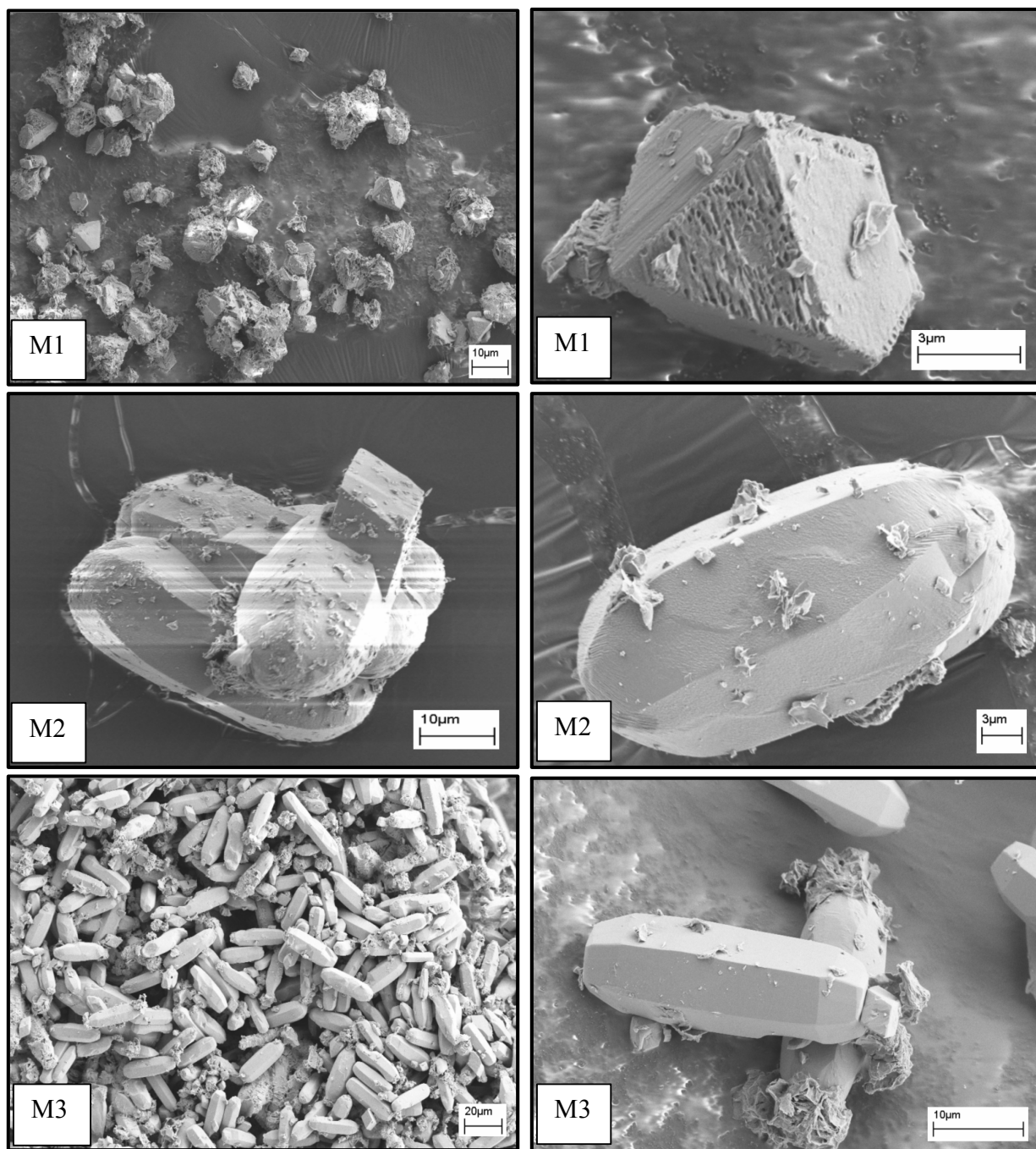
Figure A.28. SEM micrographs of M1, M2 and M3.
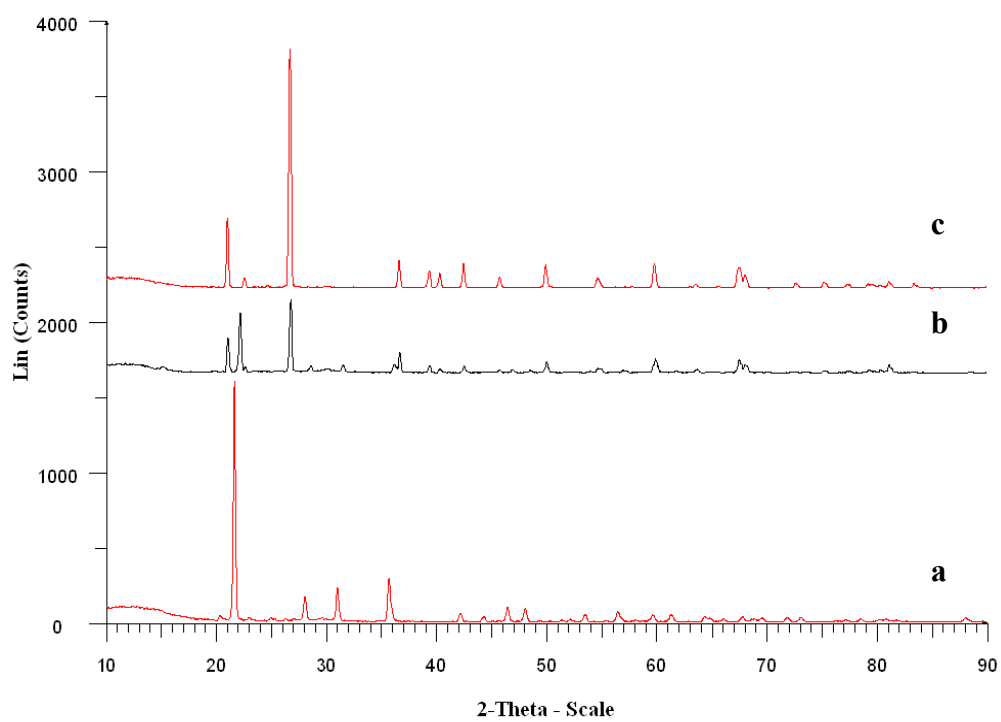
Figure A.29. XRD patterns of **a.** M1, **b.** M2 and **c.** M3.

APPENDIX III. Calculating Coefficients of Diffusion

The alcohol uptake of the samples was recorded until equilibrium was attained. As the molecular weight of alcohols was increased, time needed to reach equilibrium also increased. The change of the propanol uptake to the natural zeolite with time at 24.0°C is presented as an example, in the Figure A.30. The steady state value of 0.0612 g was reached at about 3,000th s. The experiment was continued until the 10,000th s at which the uptake was recorded as 0.0631 g of propanol.
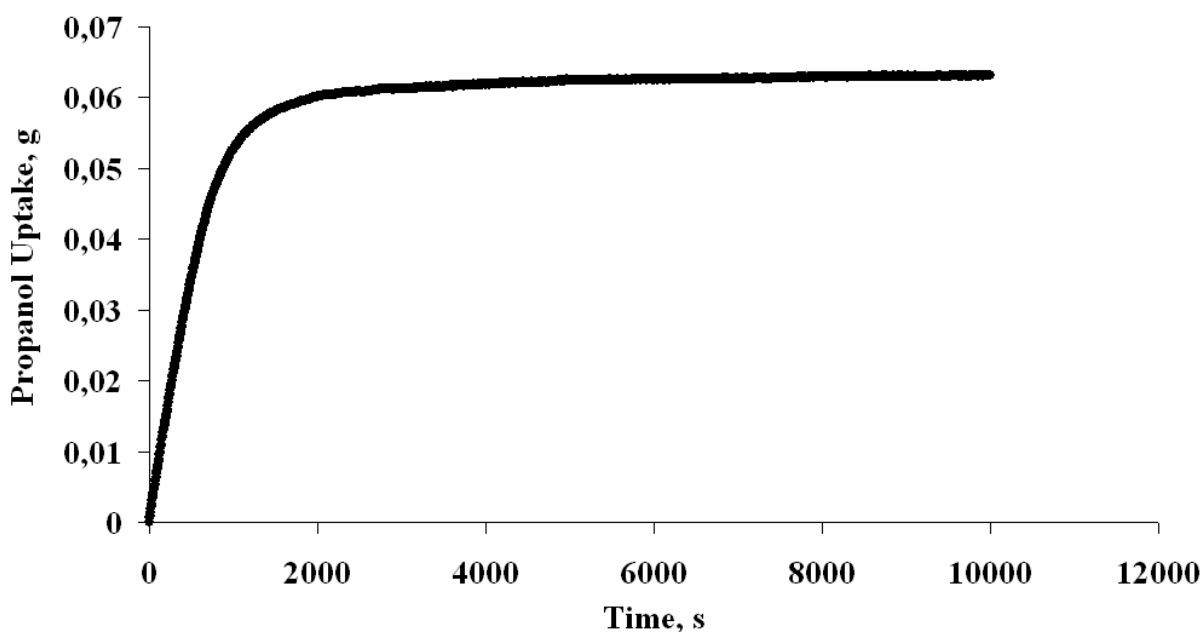
Figure A.30. n-Propanol uptake of the zeolite at 24.0°C.

Since it was assumed [283,293,294] that diffusion occurred linearly during the first 60 percent of the ramp (≈10 minutes), all the calculations for coefficients of diffusion and the activation energy were based on the data in this region. Graphs of M_t/M_∞ versus $t^{1/2}$ for the alcohol diffusion in the zeolite were plotted in order to calculate the coefficients of diffusion, Figure A.31 is presented as an example for the calculation of coefficient of diffusion of propanol at 24.0°C. The coefficients of diffusion were measured from the slope of such graphs.
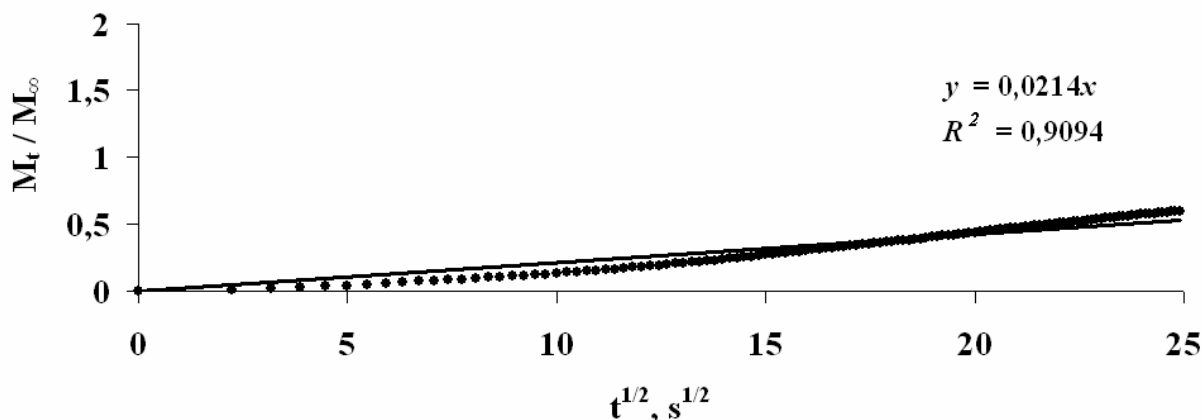
Figure A.31. M_t/M_∞ versus $t^{1/2}$ graph of the n-propanol diffusion in the zeolite at 24.0 °C.

The type of transport mechanisms of alcohols in the zeolitic porous structure can be speculated by the values of the diffusion rate constants, k, and diffusion exponents, n, which were calculated using $\ln (M_t/M_\infty)$ vs $\ln t$ graphs, an example for such graphs is presented in Figure A.32 for the diffusion of n-propanol at 24.0°C. The value of R^2, for the graph was 0.9997 indicating a linear relationship between $\ln (M_t/M_\infty)$ and $\ln t$. Diffusion rate constant, k, was calculated as 1.24×10^{-3} s^{-1}. The activation energy was calculated from the slope of the straight line of the graph $\ln D$ versus $1/T$.
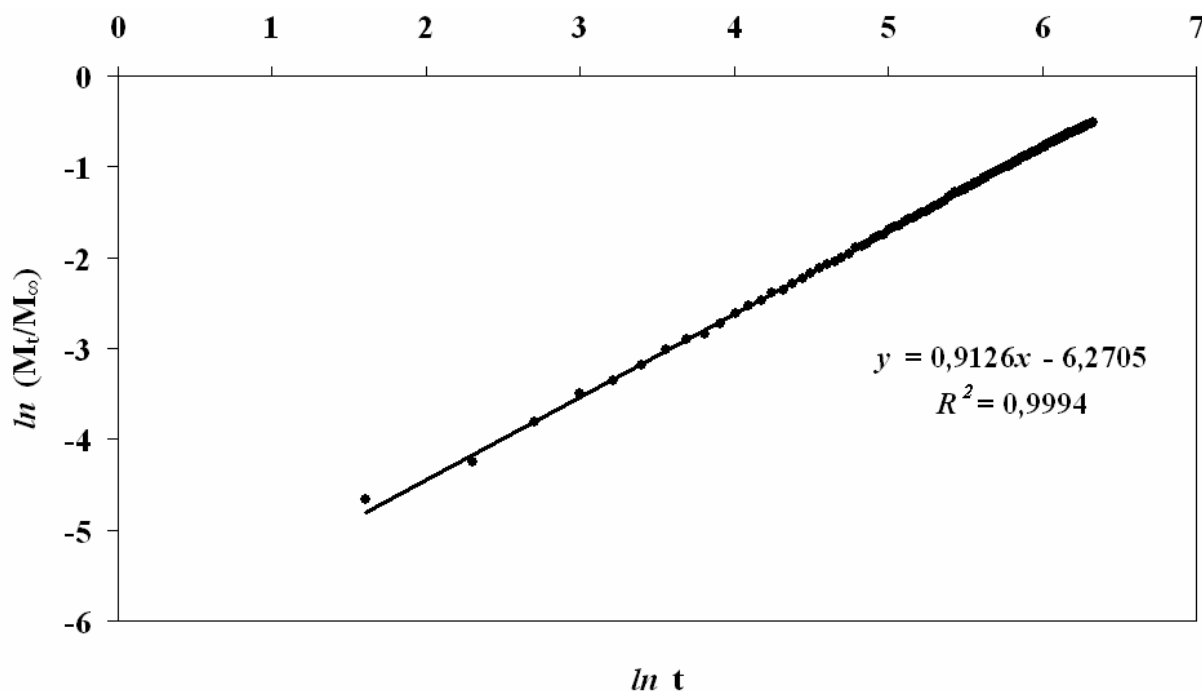
Figure A.32. $\ln (M_t/M_\infty)$ versus $\ln t$ graph of the n-propanol diffusion in the zeolite at 24.0 °C.

BİLLUR SAKİNTUNA

Sabanci University,
Materials Science & Engineering Dept.,
MDBF 34956, Tuzla / Istanbul
billur@su.sabanciuniv.edu

Education:

Ph.D. Sabanci University, Material Science and Engineering Department, Istanbul, Turkey, 2001 – Recent,
Thesis Title: Synthesis and Characterization of Porous Carbons using Natural Zeolites and $AlPO_4$-5 as Templates and Diffusion of Volatile Organic Chemicals in These Porous Media
Project: Synergy Effects of Co-Processing of Biomass with Coal and Non-Toxic Wastes for Heat and Power Generation, supported by EU FP6 Co power Project

M.S. Middle East Technical University, Chemical Engineering Department, Ankara 1998-2001,
Thesis Title: Enzymatic Hydrolysis of Wheat Starch.
Projects: Separation of Turkish Wheat Flour into Starch and Gluten, Hydrolysis of Freshly Prepared Wheat Starch Fractions and Commercial Wheat Starch Using Alpha-Amylase

B.S. Hacettepe University, Chemical Engineering Department, Ankara 1994-1998

Work Experience:

- Teaching Assistant, Department of Materials Science & Engineering, Sabanci University, Istanbul, September 2001- Recent.
  Teaching Experience: MAT 202-Kinetics and Kinetics Lab., MAT 312-Material Characterization Lab., MAT 401-Surface Chemistry, NS 101-Science of Nature I, CHEM 301-Inorganic Chemistry.
  Hands-on experience: XRD, SEM, FTIR, NMR, Confocal Microscopy, TGA/DSC, GC/MS and LC/MS.
- Scientific researcher, Hacettepe University Doping Control Centre, Ankara, Analysis of Doping Materials, 7 / 1999 - 9 / 1999
- Internship, TAI, Turkish Aerospace Industries, Akinci, Ankara, Composite Materials Department, 8 / 1998 - 9 / 1998
- Internship, DUSA Industrial Yarn Manufacturing and Trading Inc., Alikahya, Izmit, Quality Control Laboratory, 8 / 1999 - 9 / 1999

Journal Articles:

1. <u>Billur Sakintuna</u> and Yuda Yürüm, "Preparation and Characterization of Porous Carbons Using Zeolitic Templates: 2. Organoaluminum Fluoride Structures", <u>Industrial & Engineering Chemistry Research</u>, *Submitted,* 2004

2. <u>Billur Sakintuna</u>, Enis Fakıoğlu and Yuda Yürüm, "Diffusion of Volatile Organic Chemicals in Porous Media, 1. Alcohol/Natural Zeolite Systems", Energy and Fuels, *Submitted,* 2005

3. Serkan Bas, <u>Billur Sakintuna</u>, Burak Birkan, Yusuf Menceloğlu, Alpay Taralp and Yuda Yürüm, "Lyophilization-Induced Structural Changes in Solvent Swollen and Supercritical Carbon Dioxide Treated Low Rank Turkish Coals and Characterization of their Extracts", Energy and Fuels 19: 1056-1064, 2005

4. <u>Billur Sakintuna</u> and Yuda Yürüm, "Preparation and Characterization of Porous Carbons Using Zeolitic Templates: 1. Natural Clinoptilolite as Template", Industrial & Engineering Chemistry Research, *Submitted,* 2004

5. <u>Billur Sakintuna</u>, N.Suzan Kıncal, Tunay Dik, Füsun Yöndem-Makascıoğlu, "Enzymatic Dextrinization of Freshly Prepared Wheat Starch", Food Research International, *Submitted,* 2004

6. <u>Billur Sakintuna</u> and Yuda Yürüm, **"**Templated Porous Carbons - A Review Article", Industrial & Engineering Chemistry Research 44: 2893-2902, 2005

7. Demet Erçin, Mahmut Eken Zeki Aktas Sevil Çetinkaya, <u>Billur Sakintuna</u> and Yuda Yürüm "Effect of γ-irradiation of activated carbons on the generation of new free radicals and porosity" Radiation Physics and Chemistry, 73 (5): 263-271 2005

8. Billur <u>Sakintuna</u>, Yuda Yürüm and Sevil Çetinkaya, "Evolution of microstructures during activated carbon production from Turkish Elbistan lignite in the temperature range 700 - 1000°C" Energy and Fuels 18 (3): 883-888 May-Jun 2004

9. Yeşim Başaran, Adil Denizli, <u>Billur Sakintuna</u>, Alpay Taralp and Yuda Yürüm, "Bio-liquefaction/solubilization of Two Low-Rank Turkish Lignites", Energy and Fuels 17 (4): 1068-1074 Jul-Aug 2003

10. <u>Billur Sakintuna</u>, Okan Budak, Tunay Dik, Füsun Yöndem-Makascıoğlu and N.Suzan Kıncal, "Hydrolysis of Freshly Prepared Wheat Starch Fractions and Commercial Wheat Starch Using Alpha-amylase", Chemical Engineering Communications 190 (5-8): 883-897 May-Aug 2003

Journal Articles in Progress:

1. <u>Billur Sakintuna</u>, Esra Altuntaş and Yuda Yürüm, "Preparation and characterization of microwave assisted $AlPO_4$-5"

Conference Proceedings:

1. <u>Billur Sakintuna</u> and Yuda Yürüm, "Preparation and characterization of Porous Carbons Using Zeolitic Templates: Natural Clinoptilolite as Template" *Gordon Research Conference*, Ventura, California, January 8-14, 2005, *Poster presentation was awarded*.

2. Billur Sakintuna, Zeki Aktaş and Yuda Yürüm, "Templated Synthesis of Porous Carbons and Flower-Like Carbon Fluorides Using Natural Zeolite" *American Chemical Society 228th National Meeting*, Philadelphia, Fuel Chemistry Division. August 21-27, 2004. Abstracts of Papers of The American Chemical Society 228: U669-U669 102-Fuel Part 1 Aug 22 2004

3. Serkan Bas, Billur Sakintuna, Burak Birkan, Yusuf Menceloğlu, Alpay Taralp, and Yuda Yürüm, "Investigation of the structural changes in freeze-dried low-rank Turkish coals and in their supercritical extracts" *American Chemical Society 228th National Meeting*, Philadelphia, Fuel Chemistry Division. August 21-27, 2004. Abstracts of Papers of The American Chemical Society 228: U669-U669 101-Fuel Part 1 Aug 22 2004

4. Demet Erçin, Mahmut Eken Zeki Aktas Sevil Çetinkaya, Billur Sakintuna and Yuda Yürüm "Effect of gamma-irradiation of activated carbons on the generation of new free radicals and porosity" *American Chemical Society 228th National Meeting*, Philadelphia, Fuel Chemistry Division. August 21-27, 2004. Abstracts of Papers of The American Chemical Society 228: U668-U668 100-Fuel Part 1 Aug 22 2004

5. Billur Sakintuna, Enis Fakıoğlu and Yuda Yürüm, "Diffusion of volatile organic materials in a natural zeolite" *American Chemical Society 228th National Meeting*, Philadelphia, Colloid and Surface Chemistry Division. August 21-27, 2004. Abstracts of Papers of The American Chemical Society 228: U452-U452 013-Coll Part 1 Aug 22 2004

6. Ahu Gümrah Dumanlı, Billur Sakintuna And Yuda Yürüm, "Determination of the oxidation Characteristics of Fir (*Abies Bornmulleriana*) Wood" *American Chemical Society 228th National Meeting*, Philadelphia, Colloid and Surface Chemistry Division. August 21-27, 2004. Abstracts of Papers of The American Chemical Society 228: U676-U676 153-Fuel Part 1 Aug 22 2004

7. Billur Sakintuna, Enis Fakıoğlu and Yuda Yürüm, "Organik Solventlerin Dogal Zeolitteki Difüzyon Sabitlerinin Ölçülmesi", *V. National Chromatography Congress*, Eskişehir, 30 June-2 July 2004

8. Billur Sakintuna, Zeki Aktas, and Yuda Yürüm, "Synthesis of Porous Carbon Materials by Carbonization of Carbonaceous Material in Natural Zeolite Nanochannels", *Nanocat Summer School,* Torino, Italy, 14-20 September 2003

9. Billur Sakintuna, Tunay Dik, Füsun Yöndem Makascioglu, and N. Suzan Kıncal, "Enzymatic Dextrinization Of Freshly Prepared Wheat Starch", *AIChE, American Institute of Chemical Engineers*, San Francisco, CA, CoFE - Conference on Food Engineering, November 16-21, 2003

10. Billur Sakintuna, Zeki Aktas, and Yuda Yürüm, "Synthesis of porous carbon materials by carbonization in natural zeolite nanochannels" *American Chemical Society 226th National Meeting*, New York City, N.Y., Abstracts of Papers of the American Chemical Society 226: U538-U538 056-Fuel Part 1, Fuel Chemistry Division. September 7-11, 2003

11. <u>Billur Sakintuna</u>, Sevil Çetinkaya Zeki Aktas, and Yuda Yürüm, "Effect of temperature on the surface area change and formation of crystal structures during activated carbon production from fir (*Abies Bornmulleriana*) wood" *3rd Chemical Engineering Conference for Collaborative Research in Eastern Mediterranean, EMCC-3*, Thessalonica, Greece, Synthesis of Nanoscale Materials (T-6), Third Paper, May13-15, 2003

12. Sevil Çetinkaya, <u>Billur Sakintuna</u> and Yuda Yürüm, "Formation of crystal structures during activated carbon production from Turkish Elbistan lignite" *American Chemical Society 225th National Meeting*, New Orleans, LA, Abstracts of Papers of the American Chemical Society 225: U848-U848 FUEL Part 1,-Fuel Chemistry Division Preprints, 48 (1), 67, March 23-27, 2003

13. <u>Billur Sakintuna</u>, Tunay Dik, Füsun Yöndem Makascioglu, and N. Suzan Kıncal, "Effect of wheat-water-solubles and starch granule size on the hydrolysis of wheat starch using a thermo-stable alpha-amylase" *AACC, Annual Meeting Charlotte*, North Carolina, Poster Presentation, Charlotte Convention Center, October 14-18, 2001

14. <u>Billur Sakintuna</u>, Tunay Dik, Füsun Yöndem Makascıoğlu, N. Suzan Kıncal, "Hydrolysis of Freshly Prepared Wheat Starch Fractions and Commercial Wheat Starch Using Alpha-amylase", *2nd Chemical Engineering Conference for Collaborative Research in Eastern Mediterranean, EMCC-2,* Middle East Technical University, Ankara, Turkey, Book of Abstracts, page 79 May 20-24, 2001

15. <u>Billur Sakintuna</u>, Tunay Dik, Füsun Yöndem Makascıoğlu, Suzan Kıncal, "Hydrolysis of Wheat Starch in a Flow System", *12. National Biotechnology Congress*, Ayvalık-Balikesir, Turkey, Book of Abstracts, page 30-34. 17-19 September 2001

16. <u>Billur Sakintuna</u>, Tunay Dik, Füsun Yöndem Makascıoğlu, N. Suzan Kıncal, "Enzymatic Hydrolysis of Wheat Starch", *IV. National Chemical Engineering Congress*, Istanbul University, Turkey, 1999

Membership in Societies:
    Member of *American Chemical Society*

Scholarship:
    Full scholarship from Sabanci University

REFERENCES

[1]   Weeks. M.E. *J Chem Educ. Public.* (1956), 1 (2), 58-89.

[2]   Sakintuna B., Yürüm Y. *Energy Fuels* (2004), 18, 883-888.

[3]   Fitzer E., Köchling K.H., Boehm H.P., Marsh H. Recommended Terminology for the Description of Carbon as a Solid. Pure and Applied Chemistry: IUPAC Subcommittee on Terminology and Characterization of Carbon, ICCTC, 1995. 473-506.

[4]   Warren B.E. *Phys. Rev.* (1934), 2, 551.

[5]   Warren B.E. *Phys. Rev.* (1941), 59, 693-699.

[6]   Brindley G.W., Mering J. *Acta Cryst.* (1951), 4, 441.

[7]   Hirsch P.B. *Proc Roy Soc Ser A* (1954), 226, 143.

[8]   Diamond R. *Acta Cryst.* (1957), 10, 359.

[9]   Diamond R. *Acta Cryst.* (1958), 11, 129.

[10]   Short M.A., Walker J.P.L. *Carbon* (1963), 1, 3.

[11]   Bacon R., Walker J.P.L. Chemistry and Physics of Carbon, Marcel Dekker, In: Thrawer P, Eds, editor. New York, 1973. pp. 1-95.

[12]   Franklin R.E. *Proc Roy Soc* (1951), 209, 196-218.

[13]   Franklin R.E. *Acta Cryst.* (1951), 4, 253-261.

[14]   Oberlin A. *Carbon* (1984), 22, 521.

[15]   Kercher A.K., Nagle D.C. *Carbon* (2003), 41, 15-27.

[16]   Fujimoto H., Shiraishi M. *Carbon* (2001), 39, 1753.

[17]   Feng B., Bhatia S.K., Barry J.C. *Carbon* (2002), 40, 481.

[18]   Sharma A., Kyotani T., Tomita A. *Carbon* (2000), 38, 1977.

[19]   Babu V.S., Seehra M.S. *Carbon* (1996), 34, 1259.

[20]   Oberlin A., Bonnamy S., Lafdi K., Donnet J-B, Wang T.K., Reboyuillat S, Peng J.C.M. Structure and Texture of Carbon Fibers. In: Carbon Fibers. New York: Dekker M., 1998.

[21]   Sakintuna B., Aktas Z., Yürüm Y. Abstracts of Papers of the American Chemical Society 228: Fuel Chemistry Division, 2004.

[22]   Armbruster T. Clinoptilolite-Heulandite: Applications and Basic Research. editor: J. Vedrine, In: Studies in Surface Science and Catalysis, Zeolites and Mesoporous Materielas at the Dawn of the 21st Century, 2001.

[23]   Coombs D.S., Alberti A., Armbruster T.H., Artioli G., Colella C., Galli E., Grice J.D., Liebau F., Mandarino J.A., Minato H., Nickel E.H., Passaglia E., Peacor D.R., Quartieri S., Rinaldi R., Ross M., Sheppard R.A., Tillmanns E., Vezzalini G. *Min. Mag.* (1998), 62, 533.

[24]   Gottardi G., Galli E. Natural Zeolites. Berlin: Springer-Verlag, 1985.

[25]   Sakintuna B., Yürüm Y. *Ind. Eng. Chem. Res.* (2005), 44, 2893-2902.

[26]   IUPAC Compendium of Chemical Terminology 2nd Edition (1997), 1972.

[27]   IUPAC Compendium of Chemical Terminology 2nd Edition (1997), 1976.

[28]   Ryoo R., Joo S.H., Kruk M., Jaroniec M. *Adv. Mater.,* (2001), 13 (9), 677-681.

[29]   Fan S., Chapline M.G., Franklin N.R., Tombler T.W., Cassell A.M., Dai H. *Science* (1999), 283, 512-514.

[30]   Subramoney S. *Adv. Mater.* (1998), 10 (15), 1157-1171.

[31]   Davis M.E. *Nature* (2002), 417, 813-821.

[32]   Kyotani T. *Carbon* (2000), 38, 269-286.

[33]   Tamai H., Kakii T., Hirota Y., Kumamoto T., Yasuda H. *Chem. Mater* (1996), 8, 454-462.

[34]   Zhonghua H., Madapusi P.S., Ni Y. *Adv. Mater.* (2000), 12 (1), 62-65.

[35]   Lu W., Chung D.D.L. *Carbon* (1997), 35 (3), 427-436.

[36]   Planeix J.M., Coustel N., Coq J.B., Brotons J.V., Kumbhar P.S., Dutartre R., Geneste P., Bernier P., Ajayan P.M. *J Am. Chem. Soc.* (1994), 116, 7935-7936.

[37]   Rodriguez N.M., Chambers A., Baker R.T.K. *Langmuir* (1995), 11, 3862-3866.

[38]   Lee J., Han S., Kim H., Koh J.H., Hyeon T., Moon S.H. *Catal. Today* (2003), 86, 141.

[39]   Rueckes T., Kim K., Joselevich E., Tseng G.Y., Cheung C.L., Lieber C.M. *Science* (2000), 289, 94-97.

[40]   Hyeon T., Han S., Sung Y.E., Park K.W., Kim Y.W. *Angew. Chem.* (2003), 2003 (Int. Ed.), 4352.

[41]   Dillon A.C. *Nature* (1997), 386, 377-379.

[42]   Lee J., Han S., Hyeon T. *J Mater. Chem.* (2004), 14, 478-486.

[43]   Lee J., Yoon S., Oh S.M., Shin C.H., Hyeon T. *Adv. Mater.* (2000), 12 (5), 359-362.

[44]   Lee J., Yoon S., Hyeon T., Oh S.M., Kim K.B. *Chem. Commun.* (1999), 2177-2178.

[45]   Parthasarathy R.V., Martin C. *Nature* (1994), 369 (6478), 298-301.

[46]   Johnson S.A., Ollivier P.J., Mallouk T.E. *Science* (1999), 282, 963-965.

[47]   Martin C.R. *Adv. Mater.* (1991), 3 (9), 457-459.

[48]   Klein J.D., Herrick R.D.I., Palmer D., Sailor M.J., Brumlik C.J., Martin C.R. *Chem. Mater.* (1993), 5 (7), 902-904.

[49]   Martin C.R. *Chem. Mater.* (1996), 8, 1739-1746.

[50]   Cao G., Rabenberg L.K., Nunn C.M., Mallouk T.E. *Chem. Mater.* (1991), 3, 149-156.

[51]   Ozin G.A., Steele M.R., Holmes A.J. *Chem. Mater.* (1994), 6, 999-1010.

[52]   Brigham E.S., Weisbecker C.S., Rudzinski W.E., Mallouk T.E. *Chem. Mater.* (1996), 8 (2121-2127).

[53]   Zarbin A.J.G., De Paoli M.A., Alves O.L. *Synth. Met.* (1999), 99, 227-235.

[54]   Asefa T., MacLachlan M.J., Coombs N., Ozin G.A. *Nature* (1999), 402, 867.

[55]   Heywood B.R., Mann S. *J Am. Chem. Soc.* (1992), 114, 4681-4686.

[56] Ukrainczyk L., Bellman R.A., Anderson A.B. *J Phys. Chem. B* (1997), 101, 531-539.

[57] Nguyen C.V., Carter K.R., Hawker C.J., Hedrick J.L., Jaffe R.L., Miller R.D., Remenar J.F., Rhee H.W., Rice P.M., Toney M.F., Trollsas M., Yoon D.Y. *Chem. Mater.* (1999), 11, 3080-3085.

[58] Feng P., Bu X., Pine D.J. *Langmuir* (2000), 16, 5304-5310.

[59] Beck J.S., Vartuli J.C., Roth W.J., Leonowisc M.E., Kresge C.T., Schmitt K.D., Chu C.T-W., Olson D.H., Sheppard E.W, McCullen S.B., Higgens J.B., Schlenker J.L. *J Am. Chem. Soc.* (1992), 114, 10834-10843.

[60] Braun P.V., Osenar P., Tohver V., Kennedy S.B., Stupp S.I. *J Am. Chem. Soc.* (1999), 121, 7302-7309.

[61] Putyeraa K., Bandosz T.J., Jagieob J., Schwarz J.A. *Carbon* (1996), 34 (12), 1559-1567.

[62] Bandosz T.J., Jagie J., Putyera K., Schwarz J.A. *Chem. Mater.* (1996), 8, 2023-2029.

[63] Li J., Moskovits M., Haslett T.L. *Chem. Mater.* (1998), 10, 1963-1967.

[64] Knox J.H., Kaur B., Millward G.R. *J Chromatogr.* (1986), 352, 3.

[65] Gilbert M.T., Knox J.H., Kaur B. *Chromatographia* (1982), 16, 138.

[66] Brunauer S., Emmett P.H., Teller E. *J Am. Chem. Soc.* (1938), 60, 309.

[67] Che G., Lakshmi B.B., Martin C.R., Fisher E.R. *Langmuir* (1999), 15, 750-758.

[68] Che G., Lakshmi B.B., Martin C.R., Fisher E.R., Ruoff R.S. *Chem. Mater.* (1998), 10, 260-267.

[69] Pradhan B.K., Toba T., Kyotani T., Tomita A. *Chem. Mater.* (1998), 10, 2510-2515.

[70] Liu S., Yue J., Cai T., Andersony K.L. *J Colloid Interface Sci* (2000), 225, 254-256.

[71] Kyotani T., Tsai L., Tomita A. *Chem. Mater.* (1996), 8, 2109-2113.

[72] Kyotani T., Tsai L., Tomita A. *Chem. Mater.* (1995), 7 (8), 1427-1428.

[73] Shindo A., Izumino K. *Carbon* (1994), 32 (7), 1233-1243.

[74] Zhang X., Solomon D.H. *Chem. Mater.* (1999), 11, 384-391.

[75] Domingo-Garcia M., Lopez-Garzon F.J., Perez-Mendoza M. *Carbon* (2000), 38, 555-563.

[76] Müller H., Rehak P., Jager C., Hartmann J., Meyer N., Spange S. *Adv. Mater.* (2000), 12 (22), 1671-1675.

[77] Wang Z., Lu Z., Huang X., Xue R., Chen L. *Carbon* (1998), 36 (1-2), 51-59.

[78] Schüth F., Schmdt W. *Adv. Mater.* (2002), 14 (9), 629-638.

[79] Schüth F. *Angew. Chem.* (2003), 42 (31), 3604-3622.

[80] Che G., Lakshmi B.B., Fisher E.R., Martin C.R. *Nature* (1998), 393 (6683), 346-349.

[81] Ryoo R., Joo S.H., Jun S. *J Phys. Chem. B.* (1999), 103 (37), 7743-7746.

[82]   Kresge C.T., Leonowisc M.E., Roth W.J., Vartuli J.C., Beck J. S. *Nature* (1992), 359, 710-712.

[83]   Kruk M., Jaroniec M., Ryoo R., Kim J. M. *Chem. Mater* (1999), 11, 2568-2572.

[84]   Kruk M., Jaroniec M., Ryoo R., Joo S.H. *J Phys. Chem. B.* (2000), 104, 7960-7968.

[85]   Kaneda M., Tsubakiyama T., Carlsson A., Sakamoto Y., Ohsuna T., Terasaki O., Joo S.H., Ryoo R. *J Phys. Chem. B.* (2002), 106, 1256-1266.

[86]   Ryoo R., Joo S.H., Kim J.M. *J Phys. Chem. B.* (1999), 103, 7435-7440.

[87]   Kruk M., Jaroniec M. *Chem. Mater.* (2000), 12, 1414-1421.

[88]   Ryoo R., Jun S., Kim J.M., Kim M. J. *Chem. Commun.* (1997), 2225-2226.

[89]   Solovyov L.A., Zaikovskii V.I., Shmakov A.N., Belousov O.V., Ryoo R. *J Phys. Chem. B.* (2002), 106, 12198-12202.

[90]   Joo S.H., Jun S., Ryoo R. *Microporous Mesoporous Mater.* (2001), 44-45, 153-158.

[91]   Jun S., Joo S.H., Ryoo R., Kruk M., Jaroniec M., Liu Z., Ohsuna T., Terasaki O. *J Am. Chem. Soc.* (2000), 122, 10712-10713.

[92]   Joo S.H., Choi S.J., Oh I., Kwak J., Liu Z., Terasaki O., Ryoo R. *Nature* (2001), 412, 169-172.

[93]   Kruk M., Jaroniec M., Sakamoto Y., Terasaki O., Ryoo R., Ko C.H. *J Phys. Chem. B.* (2000), 104, 292-301.

[94]   Kruk M., Jaroniec M., Ryoo R., Kim J. M. *Microporous Mater.* (1997), 12, 93-106.

[95]   Kruk M., Jaroniec M., Sayari A. *J Phys. Chem. B.* (1997), 101, 583-589.

[96]   Ryoo R., Ko C.H., Park I.-S. *Chem. Commun.* (1999), 1413-1414.

[97]   Ryoo R., Kim J.M., Ko C.H., Shin C.H. *J Phys. Chem.* (1996), 100 (45), 17718-17721.

[98]   Kim J.M., Stucky G.D. *Chem. Commun.* (2000), 1159-1160.

[99]   Lee J.-S., Joo S.H., Ryoo R. *J Am. Chem. Soc.* (2002), 124 (7), 1156-1157.

[100]   Zhao D., Feng J., Huo Q., Melosh N., Fredirckson G.H., Chemlka B.F., Stucky G.D. *Science* (1998), 279, 548.

[101]   Galindo C., Ming D.W., Morgan A., Pickering K. Program and Abstracts. Zeolite. Ischia, Naples, 1997. 154.

[102]   Shin H.J., Ryoo R., Kruk M., Jaroniec M. *Chem. Commun.* (2001), 349-350.

[103]   Darmstadt H., Roy C., Kaliaguine S. , Choi S.J., Ryoo R. *Carbon* (2002), 40, 2673-2683.

[104]   Darmstadt H., Roy C., Kaliaguine S., Kim T.W., Ryoo R. *Chem. Mater.* (2003), 15, 3300-3307.

[105]   Joo S.H., Ryoo R., Kruk M., Jaroniec M. *J Phys. Chem. B.* (2002), 106, 4640-4646.

[106]   Solovyov L.A., Shmakov A.N., Zaikovskii V.I., Joo S.H., Ryoo R. *Carbon* (2002), 40, 2277-2481.

[107]   Ryoo R., Ko C.H., Kruk M., Antochshuk V., Jaroniec M. *J Phys. Chem. B.* (2000), 104, 11465-11471.

[108]   Kim S.S., Pauly T.R., Pinnavaia T.J. *Chem. Commun.* (2000), 17, 1661-1662.

[109] Lee J., Sohn K., Hyeon T. *Chem. Commun.* (2002), 2674-2675.

[110] Li Z., Jaroniec M.. *J Am. Chem. Soc.* (2001), 123 (37), 9208-9209.

[111] Li Z., Jaroniec M. *Carbon* (2001), 39 (13), 2080-2082.

[112] Taguchi A., Smatt J.H., Linden M. *Adv. Mater.* (2003), 15 (14), 1209.

[113] Li W.Z., Xie S.S., Qian L.X., Chang B.H., Zou B.S., Zhou W.Y., Zhao R.A., Wang G. *Science* (1996), 274 (5293), 1701-1703.

[114] Zakhidov A.A., Baughman R.H., Iqbal Z., Changxing Cui, Ilyas Khayrullin, Dantas S.O., Marti J., Ralchenko G.V. *Science* (1998), 282 (5390), 897-901.

[115] Zarbin A.J.G., Bertholdo R., Oliveira M.A.F.C. *Carbon* (2002), 40, 2413-2422.

[116] Kamegawa K., Yoshida H. *Carbon* (1997), 35 (5), 631-639.

[117] Strano M.S., Agarwal H., Pedrick J., Redman D., Foley H.C. *Carbon* (2003), 41, 2501-2508.

[118] Tamon H., Ishizaka H., Mikami M., Olazaki M. *Carbon* (1997), 35 (6), 791-796.

[119] Ozaki J., Endo N., Ohizumi W., Igarashi K., Nakahara M., Oya A. *Carbon* (1997), 35 (7), 1031-1033.

[120] Han S., Kim M., Hyeon T. *Carbon* (2003), 41, 1525-1532.

[121] Han S, Hyeon T. *Carbon* (1999), 37, 1645-1647.

[122] Han S, Sohn K., Hyeon T. *Chem. Mater.* (2000), 12, 3337-3341.

[123] Han S, Hyeon T. *Chem. Commun.* (1999), 1955-1956.

[124] Fuertes A.B., Nevskaia D.M. *Microporous Mesoporous Mater.* (2003), 62, 177-190.

[125] Alvarez S., Fuertes A.B. *Carbon* (2004), 42, 423-460.

[126] Ferey G., Cheetham A.K. *Science* (1999), 283 (5405), 1125-1126.

[127] Mirasol J.R., Cordero T., Radovic L.R., Rodriquez J.J. *Chem. Mater.* (1998), 10, 550-558.

[128] Davis M.E., Lobo R.F. *Chem. Mater.* (1992), 4, 756-768.

[129] Kyotani T., Nagai T., Inoue S., Tomita A. *Chem. Mater.* (1997), 9, 609-615.

[130] Johnson S.A., Brigham E.S., Ollivier P.J., Mallouk T.E. *Chem. Mater.* (1997), 9, 2448-2458.

[131] Sakintuna B., Aktas Z., Yürüm Y. Abstracts of Papers of the American Chemical Society 226 (2003), U538-U538 056-Fuel Part 1 (September).

[132] Ma Z., Kyotani T., Tomita A. *Chem. Commun.* (2000), 2365-2366.

[133] Ma Z., Kyotani T., Liu Z., Terasaki O., Tomita A. *Chem. Mater.* (2001), 13, 4413-4415.

[134] Cordero T., Thrower P.A., Radovic L. R. *Carbon* (1992), 30 (3), 365-374.

[135] Kyotani T., Ma Z., Tomita A. *Carbon* (2003), 41, 1451-1459.

[136] Ma Z., Kyotani T., Tomita A. *Carbon* (2002), 40, 2367-2374.

[137] Enzel P., Bein T. *Chem. Mater.* (1992), 4, 819-824.

[138] Cox S., Stucky G.D. *J Phys. Chem.* (1991), 95, 710-720.

[139] Sonobe N., Kyotani T., Tomita A. *Carbon* (1988), 26 (4), 573-578.

[140] Sonobe N., Kyotani T., Tomita A. *Carbon* (1990), 28 (4), 483-488.

[141] Kyotani T., Yamada H., Sonobe N., Tomita A. *Carbon* (1994), 32 (4), 627-635.

[142] Bandosz T.J., Putyeraa K., Jagieoa J., Schwarza J.A. *Carbon* (1994), 32 (4), 659-664.

[143] Bandosz T.J., Putyeraa K., Jagieoa J., Schwarza J.A. *Langmuir* (1995), 11, 3964-3969.

[144] Sonobe N., Kyotani T., Tomita A. *Carbon* (1991), 29 (1), 61-67.

[145] Sandi G., Thiyagarajan P., Carrado K.A., Winans R.E. *Chem. Mater.* (1999), 11, 235-240.

[146] Kyotani T., Mori T., Tomita A. *Chem. Mater.* (1994), 6, 2138-2142.

[147] Rodrigues P.M.B., Mays T.J., Moggridge G.D. *Carbon* (2003), 41, 2231-2246.

[148] Meyers C.J., Shah S.D., Patel S.C., Sneeringer R.M., Bessel C.A., Dollahon N.R., Leising R.A., Takeuchi E.S. *J Phys. Chem. B.* (2001), 105, 2143-2152.

[149] Wen J., Wilkes G.L. *Chem. Mater.* (1996), 8, 1667-1681.

[150] Mann S., Burkett S.L., Davis S.A., Fowler C.E., Mendelson N.H., Sims S.D., Walsh D., Whilton N.T. *Chem. Mater.* (1997), 9, 2300-2310.

[151] Kawashima D., Aihara T., Kobayashi Y., Kyotani T., Tomita A. *Chem. Mater.* (2000), 12, 3397-3401.

[152] Breck D.W. Zeolite Molecular Sieves. New York, 1974.

[153] Flanigen, E.M., Bennett J.M., Grose R.W., Cohen J.P., Patton R.L., Kirchner R.M., Smith J.V. *Nature* (1978), 271, 512.

[154] Wilson S.T., Lok B.M., Messina C.A., Cannan T.R., Flanigen E.M. *J Am. Chem. Soc.* (1982), 104 (4), 1146-1147.

[155] Tapp N.J., Cardile C.M. *Zeolites* (1990), 10, 680.

[156] Finger G., Richter-Mendav J., Bulow M., Kornatowski J. *Zeolites* (1991), 11, 443-448.

[157] Choi K.J., Jhon M.S., No K.T. *Bull. Korean Chem. Soc.* (1987), 8 (3), 155-157.

[158] Meier W.M., Olson D.H. Atlas of Zeolite Structure Types. London, 1992.

[159] Miyake M., Uehara H., Suzuki H., Yao Z., Matsuda M., Sato M. *Microporous Mesoporous Mater.* (1999), 32, 45-52.

[160] Ehrl M., Deeg F.W., Brauchle C., Franke O., Sobbi A., Schulz-Ekloff G., Wöhrle D. *J Phys. Chem.* (1994), 98, 47.

[161] Deeg F.W., Ehrl M., Brauchle C., Hoppe R., Schulz-Ekloff G., Wöhrle D. *Luminescence* (1992), 53, 219.

[162] Cox S.D., Gier T.E., Stucky G.D., Bierlein J. *J Am. Chem. Soc.* (1990), 110, 609.

[163] Werner L., Caro J., Finger G., Kornatowski J. *Zeolites* (1992), 12, 658.

[164] Caro J., Finger G., Kornatowski J., Richter-Mendau J., Werner B., Zibrowius L. *Adv. Mater.* (1992), 4, 273.

[165] Marlow F., Caro J., Werner L., Kornatowski J., Dahne S. *J Phys. Chem.* (1993), 97, 11286.

[166] Caro J., Marlow F., Wübbenhorst M. *Adv. Mater.* (1994), 6, 413.

[167] Martin C., Tosi-Pellenq N., Patarin J., Coulomb J.P. *Langmuir* (1998), 14, 1774-1778.

[168] Qiu S., Piang Q., Kessler H., Guth J.L. *Zeolites* (1989), 9, 440-444.

[169] Demuth D., Stucky G.D., Unger K., Schüth F. *Microporous Mater.* (1995), 3, 473.

[170] Schuth F., Demuth D., Zibrowius B., Kornatowski J., Finger G. *J Am. Chem. Soc.* (1994), 116, 1090.

[171] Schnabel K., Finger G., Kornatowski J., Loffler E., Peuker C., Pilz W. *Microporous Mater.* (1997), 11, 293.

[172] Newalkar B., Kamath B., Jasra R., Bhat S. *Zeolites* (1997), 18, 286.

[173] Prasad S., Liu S. *Microporous Mater.* (1995), 4, 391

[174] Chen C.-M., Jehng J.-M. *Catal. Letters* (2003), 85 (1-2), 73-80.

[175] Demontis P., Gonzalez J.G., Suffritti G.B., Tilocca A., Pozas C.D.L. *Microporous Mesoporous Mater.* (2001), 42, 103-111.

[176] Bennett J.M., Cohen J.P., Flanigen E.M., Pluth J.J., Smith J.V. ACS Symp. Ser (1983), 218, 109.

[177] Wilson S.T., Lok B.M., Messina C.A., Cannan T.R., Flanigen E.M. ACS Symp. Ser (1983), 218, 79.

[178] Robson H., Lillerud K.P. Verified Synthesis of Zeolitic Materials. Amsterdam: Elsevier Science, 2001.

[179] Eldik R.V., Hubbard C.D. Chemistry under Extreme of Non-Classical Conditions. New York: Wiley, 1996.

[180] Scott A.W. Understanding Microwaves. New York: John Wiley & Sons, Inc., 1993.

[181] Gabriel C., Gabriel S., Grant E.H., Halsteed B.S.J., Mingos D.P. *Chem. Soc. Rev.* (1998), 27, 213.

[182] Rao K.J., Vaidhyanathan B., Ganguli M., Ramakrishnan P.A. *Chem. Mater.* (1999), 11, 882.

[183] Park S.-E., Chang J.-S., Hwang Y.K., Kim D.S., Jhung S.H., Hwang J.S. *Catal. Surveys Asia* (2004), 8 (2), 91-110.

[184] Mingos D.M.P., Whittaker A.G.*J. Chem. Soc. Dalton Trans* (1992), 2751.

[185] Smith F., Cousins B., Bozic J., Flora W. *Anal. Chim. Acta.* (1985), 177, 243.

[186] Sutton W.H.. *Am. Ceram. Soc. Bull.* (1989), 68 (2), 376–386.

[187] Lidström P., Tierney J., Wathey B., Westman J. *Tetrahedron* (2001), 57, 9225.

[188] Kingston H.M., Haswell S.J. Microwave-Enhanced Chemistry, Fundamentals, Sample Preparation, and Application. Washington DC, 1997.

[189] Roussy G., Chenot P. *J Phys. Chem.* (1981), 85, 2199.

[190] Tatsuo O., Akiko W. *Phys. Chem. Commun.* (2001), 3, 1.

[191] Roussy G., Hilaire S., Thiebaut J.M., Maire G., Garin F., Ringler S. *Appl. Catal. A: Gen.* (1997), 156, 167.

[192] Bond G., Moyes R.B., Whan D.A. *Catal. Today* (1993), 17, 427.

[193] Berry F.J., Smart L.E., Sai Prasad P.S., Lingaiah N., Kanta P. *Rao Appl. Catal. A: Gen.* (2000), 204, 191.

[194] Wang Y., Zhu J.H., Cao J.M., Chun Y., Xu Q.H. *Microporous Mesoporous Mater.* (1998), 26, 175.

[195] Zhang X., Hayward D.O., Mingos D.M.P. *Ind. Eng. Chem.Res.* (2001), 40, 2810.

[196] Margolis S.M., Jasse L., Kingston H. M. *J Aut. Chem.* (1991), 13, 93.

[197] Sanders A., Wetzel H., Kunst M., Snyder Jr. W., Sutton W.H., Iskander M., Johnson D. L. MRS. Pittsburgh, PA, 1990. pp. 403.

[198] Elsamak G.G., Altuntaş Ö.N., Yürüm Y. *Fuel* (2003), 82, 531-537.

[199] Cundy C.S., Plaisted R.J., Zhao J. P. *Chem. Commun.* (1998), 1465.

[200] Lidstrom P., Tierney J., Wathey B., Westman J. *Tetrahedron* (2001), 57, 9225.

[201] Cundy C.S. *Collect. Czech, Chem. Commun.* (1998), 63, 1699.

[202] Zhu J., Polchik O., Chen S., Gedanken A. *J Phys. Chem. B* (2000), 104, 7344.

[203] Chu P., Dwyer F.G., Vartuli J. C. US Patent 4778 666, 1988.

[204] Arafat A., Jansen J.C., Ebaid A.R., Bekkum H.V., Occelli M.L., Robson H.E. In Synthesis of Microporous Mater., Reinhold VN, editor. New York, 1992. pp. 507.

[205] Arafat A., Jansen J.C., Ebaid A.R., Bekkum H.V. *Zeolites* (1993), 13, 162.

[206] Girnus I., Jancke K., Vetter R., Richter-Mendau J., Caro J. *Zeolites* (1995), 15, 33-39.

[207] Carmona J.C., Clemente R.R., Morales J.G. *Zeolites* (1997), 18, 340-346.

[208] Wu C.G., Bein T. *Chem. Commun.* (1996), 925.

[209] Park S.-E., Kim D.S., Chang J.-S., Kim W.Y. *Catal. Today* (1998), 44, 301.

[210] Sung-Suh H.M., Kim D.S., Park S.-E. *J. Ind. Eng. Chem.* (1999), 5, 191.

[211] Sun Y., Lin W., Chen J., Yue Y., Pang W. *Stud. Surf. Sci.Catal. Today* (1997), 105A, 77.

[212] Wu C.-G., Bein T. *Chem. Commun.* (1996), 925.

[213] Zhang Y., Zhao S., Sun G., Wang Z., Xuebao C. (2000), 21, 345.

[214] Newalkar B.L., Komarneni S., Katsuki H. *Chem.Commun.* (2000), 2389.

[215] Newalkar B.L., Komarneni S. *Chem. Mater.* (2001), 13, 4573.

[216] Newalkar B.L., Olanrewaju J., Komarneni S. *Chem. Mater.* (2001), 13, 552.

[217] Hwang Y.K., Chang J.-S., Kwon Y.-U., Park S.-E. *Stud.Surf. Sci. Catal.* (2003), 146, 101.

[218] Park M., Komarneni S. *Microporous and Mesoporous Materials* (1998), 20, 39-44.

[219] Brückner A., Lohse U., Mehner H.. *Microporous Mesoporous Mater.* (1998), 20, 207-215.

[220] Xu X., Yang W., Liu J., Lin L. *Separation Purification Tech.* (2001), 25, 241-249.

[221] Braun I., Schulz-Ekloff G., Bockstette M., Wöhrle D. *Zeolites* (1997), 19, 128-132.

[222] Min F., Hongbin D., Wenguo X., Xianping M., Wenqin P. *Microporous Mater.* (1997), 9 (1-2), 59-61.

[223] Mintova S., Mo S., Bein T. *Chem. Mater.* (1998), 10, 4030-4036.

[224] Kodaira T., Miyazawa K., Ikeda T., Kiyozumi Y. *Microporous Mesoporous Mater.* (1999), 29, 329-337.

[225] Girnus I., Jancke K., Vetter R., Richter-Mendau J., Caro J. *Zeolites* (1995), 15, 33-39.

[226] Fang M., Du H., Xu W., Meng X., Pang W. *Microporous Mater.* (1997), 9, 59-61.

[227] Slangen P.M., Jansen J.C., Bekkum H.V. *Microporous Mater.* (1997), 9, 259.

[228] I. Braun, Ekloff G.S., M. Bocktette, D.Wöhrle. *Zeolites* (1997), 19, 128.

[229] Tsai T.-G., Chao K.-J., Guo X.-J., Sung S.-L., Wu C.-N., Wang Y.-L., H.-C. S. *Adv. Mater.* (1997), 9, 1154.

[230] Mintova S., Schoeman B.J., Valtchev V., Sterte J., Mo S., Bein T. *Adv. Mater.* (1997), 9, 585.

[231] Ikeda T., Miyazawab K., Izumic F., Huangd Q., Santorod A. *J Phys. Chem. Solids* (1999), 60, 1531-1535.

[232] Klap G.J., Koningsveld H.V., Grafasma H., Schreurs A.M.M. *Microporous Mesoporous Mater.* (2000), 38, 403-412.

[233] Wilson S.T., Lok B.M., Flanigen E.M.. US Patent (1982), 4, 310, 440.

[234] Müller U., Unger K.K. *Zeits. Kristallogr.* (1988), 182, 190.

[235] Girnus I., Pohl M.-M., Richter-Mendau J., Schneider M., Noack M., Venzke D., Caro J. *Adv. Mater.* (1995), 8, 711.

[236] Park M., Komarneni S. *Microporous Mesoporous Mater.* (1998), 20, 39.

[237] Braun I., Schulz-Ekloff G., Wohrle D., Lautenschlager W. *Microporous Mesoporous Mater.* (1998), 23, 79-81.

[238] Du H., Fang M., Xu W., Meng X., Pang W. *J Mater. Chem.* (1997), 7 (3), 551-555.

[239] Jhung S.H., Chang J.-S., Kim D.S. Park S.-E. *Microporous Mesoporous Mater.* (2004), 71, 135-142.

[240] Ganschow M., Schulz-Ekloff G., Wark M., Wendschuh-Josties M., Wohrle D. *J. Mater. Chem.* (2001), 11, 1823-1827.

[241] Lin J-C., Dipre J.T., Yates M.Z. *Langmuir* (2004), 20, 1039-1042.

[242] Weyda H., Lechert H.*Zeolites* (1990), 10, 251.

[243] Iwasaki A., Sano T., Kiyozumi Y. *Microporous Mesoporous Mater.* (1998), 25, 119.

[244] Iwasaki A., Sano T., Kodaira T., Kiyozumi Y. *Microporous Mesoporous Mater.* (2003), 64, 145-153.

[245] Ahn S., Chon H. *Microporous Mater.* (1997), 8, 113.

[246] Kornatowski J., Zadrozna G., Rozwadowski M., Zibrowius B., Marlow F., Lercher J. A. *Chem. Mater.* (2001), 13, 4447.

[247] Kessler H., Patarin J., Schott-Darie C. *Stud. Surf. Sci. Catal.* (1994), 85, 75.

[248] Jhung S.H., Hwang Y.K., Chang J.-S., Park S.-E. *Microporous Mesoporous Mater.* (2004), 67, 151-157.

[249] Iijima S. *Nature* (1991), 345, 56.

[250] Guo T., Nikolaev P., Thess A., Colbert D.T., Smalley R. E. *Chem. Phys. Lett.* (1995), 243, 49.

[251] Journet C., Maser W.K., Bernier P., Loiseau A., Lamy de la Chapelle M., Lefrant S., Deniard P., Lee R., Fischer J. E. *Nature* (1997), 388, 756.

[252] Dubay O., Kresse G. *Carbon* (2004), 42, 979-982.

[253] Tang Z.K., Sun H.D., Wang J., Chen J., Li G. *App. Phys. Lett.* (1998), 73 (16), 2287-2289.

[254] Wang N., Tang Z.K., Li G.D., Chen J.S. *Nature* (2000), 408, 50.

[255] Launois P., Moret R., Le Bolloc'h D., Albouy P.A., Tang Z.K., Li G., Chen J. *Solid State Commun.* (2000), 116, 99-103.

[256] Sun H.D., Tang Z.K., Chen J., Li G.D. *App. Phys. A* (1999), 69, 381.

[257] Tang Z.K., Zhang L.Y., Wang N., Zhang X.X., Wang J.N., Li G.D., Li Z.M., Wen G.H., Chan C.T., Sheng P. *Synth. Met.* (2003), 133-134, 689-693.

[258] Caro J., Marlow F. *Zeolites* (1992), 12, 433.

[259] Miyake M., Yoshida M., Matsuda M., Kiguchi M., Taniguchi Y., Uehara H., Sato M. *J Mat. Sci.* (1999), 34, 5509-5512.

[260] Ihlein G., Junges B., Junges U., Laeri F., Schüth F., Vietze U. *App. Organomet. Chem.* (1998), 12, 305-314.

[261] Reck G., Marlow F., Kornatowski J., Hill W., Caro J. *J Phys. Chem.* (1996), 100, 1698.

[262] Finger G., Kornatowski J. *Zeolites* (1990), 10, 615.

[263] Wöhrle D., Sobbi A.K., Franke O., Schulz-Ekloff G. *Zeolites* (1995), 15 (540).

[264] Kowalak S., Balkus Jr. K.J. *Collect. Czech. Chem.Commun.* (1992), 57, 774.

[265] Wohlrab S., Hoppe R., Schulz-Ekloff G., Wöhrle D. *Zeolites* (1992), 12, 862.

[266] Hoppe R., Schulz-Ekloff G., Wöhrle D., Shpiro E.S., Tkachenko O.P. *Zeolites* (1993), 13, 222.

[267] Hoppe R., Schulz-Ekloff G., Rathousky J., Starek J., Zukal A. *Zeolites* (1994), 14, 126.

[268] Bockstette M., Wöhrle D., Braun I., Schulz-Ekloff G. *Microporous Mesoporous Mater.* (1998), 23, 83-96.

[269] Wang N., Li G.D., Tang Z.K. *Chem. Phys. Lett.* (2001), 339, 47-52.

[270] Seiler M., Schenk U., Hunger M. *Catal. Lett.* (1999), 62, 139–145.

[271] Bjørgen M., Kolboe S. *App. Catal. A* (2002), 225, 285–290.

[272] Stich I., Gale J.D., Terkura K., Payn e. M. C. *Chem. Phys. Lett.* (1998), 283, 402-408.

[273] Hutchings G.J., Watson G.W., Willock D.J. *Microporous Mesoporous Mater.* (1999), 29, 67–77.

[274] Domontis P., Suffritti G.B. *Chem. Rev.* (1997), 97, 2845-2878.

[275] Haberlandt R. *Thin Solid Films* (1998), 330, 34-45.

[276] Lood W.P., Verheijen P.J.T., Moulijn J.A. *Chem. Eng. Sci.* (2000), 55, 51-65.

[277] Benes N., Verweij H. *Langmuir* (1999), 15 (23), 8292–8299.

[278] Weisz. P.B. *Chem. Tech.* (1973), 3, 498–505.

[279] Chen N.Y., Degnan Jr T.F., Smith C.M. Molecular Transport and Reaction in Zeolites-Design and Application of Shape Selective Catalysis. New York: VCH Publishers, (1994).

[280] Fick A. *Ann. Phys.* (1855), 94, 59–86.

[281] Barrer R.M., Jost W. *Trans. Faraday Soc.* (1949), 45, 928–930.

[282] Ruthven D.M. *Chem. Eng. Science* (2004), 59, 4531-4545.

[283] Hall P.J., Thomas K.M., Marsh H. *Fuel* (1992), 71, 1271-1275.

[284] Inglezakis V.J., Grigoropoulou H.P. *J Colloid Interface Sci* (2001), 234, 434-441.

[285] Peppas N.A., Lucht L.M. *Chem. Eng. Commun* (1985), 37, 333.

[286] Crank J. The Mathematics of Diffusion. London.: Clarendon Press, Oxford, 1976.

[287] Ndaji F.E., Thomas K.M. *Fuel* (1993), 72, 1525-1530.

[288] Xiao J., Wei J. *Chem. Eng. Sci.* (1992), 47 (5), 1123–1141.

[289] Callister W.D. Material Science and Engineering. New York, 1991.

[290] Riekert L. *Adv. Catal.* (1970), 21, 281.

[291] Otake Y., Suuberg E. M. *Energy Fuels* (1997), 11, 1155-1164.

[292] Gao H., Nolura M., Murata S., Artok L. *Energy Fuels* (1999), 13, 518-528.

[293] Peppas N.A., Franson N.M. *Polymer Phys. Ed.* (1983), 21, 983-997.

[294] Seferinoglu M., Yürüm Y. *Energy Fuels* (2001), 15, 135.

[295] Ruthven D.M. Principles of Adsorption and Adsorption Processes. New York: Wiley, 1984.

[296] Karger J., Ruthven D.M. Diffusion in Zeolites and Other Microporous Solids. New York: Wiley & Sons, (1992).

[297] Karger J., Ruthven D.M. "Diffusion and Adsorption in Porous Solids" in Handbook of Porous Solids. Weinheim: Wiley-VHC, (2002).

[298] Seferinoglu M., Yürüm Y. *Energy Fuels* (2001), 15, 135-140.

[299] Karger J., Heitjans P., Haberlandt R. Diffusion in Condensed Matter. Braunschweig/Wiesbaden: Vieweg, 1998.

[300] Karger J., Pfeifer H. *Zeolites* (1987), 7, 90–107.

[301] Karger J., Caro J. *J Chem. Soc. Faraday I* (1977), 73, 1363–1376.

[302] Jobic H. Diffusion Studies Using Quasi-Elastic Neutron Scattering. In: Recent Advances in Gas Separation by Microporous Ceramic Membranes., editor: Kanellopoulos N.K. Amsterdam: Elsevier, 2000. pp. 109–138.

[303] Karger J. *Adsorption* (2003), 9, 29-35.

[304] Boersma-Klein W., Moulijn J.A. *Chem. Eng. Sci.* (1979), 34 (7), 959–969.

[305] Sakintuna B., Fakıoğlu E., Yürüm Y. *Energy Fuels* (2005), Submitted.

[306] Sakintuna B., Fakıoğlu E., Yürüm Y. Abstracts of Papers of the American Chemical Society 228th National Meeting, Colloid and Surface Chemistry Division. Philadelphia, 2004.

[307] Ritger P.L., Peppas N.A. *Fuel* (1987), 66, 1379-1388.

[308] Howell B.D., Peppas N.A. *Chem. Eng. Commun.* (1985), 43, 301-315.

[309] Bludau H., Karge H.G., Niessen. *Microporous Mesoporous Mater.* (1998), 22, 297-308.

[310] Dyer A., White K.J. *Thermochim. Acta* (1999), 340-341, 341-348.

[311] Aleksandra M., Mianowski. *Fuel* (1998), 77 (14), 1691-1696.

[312] Zhu W., Graaf J.M., Broeke L.J.P., Kapteijn F., Moulijn J.A. *Ind. Eng. Chem. Res.* (1998), 37 (5), 1934–1942.

[313] Caro J., Hocevar S., Kaerger J., Riekert L. *Zeolites* (1986), 6, 213.

[314] Haynes H.W., Sarma P.N. *AIChE J.* (1973), 19 (5), 1043–1046.

[315] Anderson B.G., Noordhoek N.J., Gauw F.J.M.M., IJzendoorn L.J., Voigt M.J.A., Santen R.A. *Ind. Eng. Chem. Res.* (1998), 37 (3), 815–824.

[316] Eic M., Ruthven D. *Zeolites* (1988), 8, 40–45.

[317] Nijhuis T.A., Broeke L.J.P., Linders M.J.G., Graaf J.M., F. Kapteijn, Makkee M., Moulijn J.A. *Chem. Eng. Sci.* (1999), 54, 4423–4436.

[318] Keipert O.P., Baerns M. *Chem. Eng. Sci.* (1998), 53 (20), 3623-3634.

[319] Anderson B.G., Jong A.M., Santen R.A. In situ Measurement of Heterogeneous Catalytic Reactor Phenomena using Positron Emission, in: In-situ Spectroscopy in Heterogeneous Catalysis. In: Haw JA, editor. Weinheim: Wiley-VCH, 2002. pp. 195–237.

[320] Karger J., Pfeifer H., Heink W. *Adv. Magn. Res.* (1988), 12, 1.

[321] Gladden L.F., Sousa-Goncalves J.A., Alexander P. *J Phys. Chem. B.* (1997), 101 (48), 10121–10127.

[322] Schaefer D.J., Favre D.E., Wilhelm M., Weigel S.J., Chmelka B.F. *J Am. Chem. Soc.* (1997), 119 (39), 9252–9267.

[323] Favre D.E., Schaefer D.J., Auerbach S.M., Chmelka B.F. *Phys. Rev. Lett.* (1998), 81 (26), 5852–5855.

[324] Jobic H., Bee M., Kearley G.J. *J Phys. Chem.* (1994), 98, 4660–4665.

[325] Schemmert U., Karger J., Weitkamp J. *Microporous Mesoporous Mater.* (1999), 32, 101–110.

[326] Levitt H.M. Spin Dynamics: Basics of Nuclear Magnetic Resonance. England: Wiley and Sons, 2001.

[327] Barrett E.P., Joyner L.G., Halenda P.H. *J Am. Chem. Soc.* (1951), 73, 373-380.

[328] Bac C.G., Bernier P., Latil S., Jourdain V., Rubio A., Jhnag S.H., Lee S.W., Park Y.W., Hozinger M., Hirsch A.. *Current App. Phys.* (2001), 1, 149-155.

[329] Darmstadt H., Roy C., Kaliaguine S., Xu G., Auger M., A T. *Carbon* (2000), 38 (9), 1279-1287.

[330] Golzan M.M., Lukins P.B., Mackenzie D.R., Vassalo A.M., JV. H. *Chem. Phys.* (1995), 193 (1-2), 167-172.

[331] Biniak S., Szymanski G., Siedlewski J., Swietkowski A. *Carbon* (1997), 35 (12), 1799-1810.

[332] Svehla G. Comprehensive Analytical Chemistry. New York, (1976).

[333] Pavia D.L., Lampman G.M., George S. Kriz J. Introduction to Spectroscopy: A Guide for Students of Organic Chemistry. Philadelphia, (1983).

[334] Jung M.-W., Ahn K.-H., Lee Y., Kim K.-P., Rhee J.-S., Park J.T., Paeng K.-J. *Microchem. J* (2001), 70, 123-131.

[335] Guo J., Lua A.C. *Separation Purification Tech.* (2000), 18, 47-55.

[336] Pinkasa J., Roeskyb H.W. *J Fluorine Chem.* (2003), 122, 125-150.

[337] Ziegler K., Holzkamp E., Koster R., Lehmkuhl H. *Angew. Chem.* (1955), 67, 213–214.

[338] Müller M., Harvey G., Prins R. *Microporous Mesoporous Mater.* (2000), 34, 281-290.

[339] Steel K.M., Patrick J.W. *Fuel Process. Tech.* (2004), 86, 179-190.

[340] Ganapathy S., Kumar R., Montouillout V., Fernandez C., Amoureux J.P. *Chem. Phys. Lett.* (2004), 390, 79-83.

[341] Bruker FTIR Handbook, 3,4488A, 4481, 4880B, 4481, 4851C (2005).

[342] Giraudet J., Dubois M., Inacio J., Hamwi A. *Carbon* (2003), 41, 453-463.

[343] Gupta V., Nakajima T., Ohzawa Y., Zemva B. *J Fluorine Chem.* (2003), 120, 143-150.

[344] Nanse G., Papirer E., Fioux P., Moguet F., Tressaud A. *Carbon* (1997), 35, 175-194.

[345] Yamamoto S., Sugiyama S., Matsuoka O., Kohmura K., Honda T., Banno Y., Nozoye H. *J Phys. Chem.* (1996), 100, 18474-18482.

[346] Scott C. *J Am. Chem. Soc.* (1948), 70, 105.

[347] Ando S., Harris R.K., Hirschinger J., Reinsberg S.A., Scheler U. *Macromolecules* (2001), 34, 66-75.

[348] Chen J., Chen T., Guan N., Wang J. *Catal.Today* (2004), 93–95, 627–630.

[349] Fyfe C.A., Bretherton J.L., Lan. L.Y. *J Am. Chem. Soc.* (2001), 123, 5285.

[350] Man P.P., Klinowski J. *J. Chem. Soc.- Chem. Commun.* (1988), 19, 1291-1294.

[351] Poborchii V.V., Kolobov A.V., Caro J., Zhuravlev V.V., Tanaka K. *Chem. Phys. Lett.* (1997), 280, 17-23.

[352] Richardson Jr., J.W., Pluth J.J., Smith J.V. *Acta Crystallogr.* (1987), C43, 1469.

[353] Vietze U., Krauss O., Laeri F., Ihlein G., Schuth F., Limburg B., Abraham M. *Phys. Rev. Lett.* (1998), 81, 4628-4631.

[354] Thong N., Schwarzenbach D. *Acta Crystallogr.* (1979), 53, 35.

[355] Jahn E., Müller D., Wieker W., Richter-Mendau J. *Zeolites* (1989), 9 (177).

[356] Christensen A.N., Jensen T.R., Norby P., Hanson J.C. *Chem. Mater.* (1998), 10, 1688.

[357] Zhu G.S., Xia F.S., Qui S.L., Hun P.C., Xu R.R., Ma S.J., Terasaki O. *Microporous Mater.* (1997), 11, 269.

[358] Gougeon R.D., Brouwer E.B., Bodart P.R., Delmotte L., Marichal C., Chezeau J.-M., Harris R.K. *J Phys. Chem. B.* (2001), 105, 12249-12256.

[359] Araki T., Finney J.J., Zoltai T. *Am. Mineral.* (1968), 53, 1096.

[360] Mooney R.C.L. *Acta Crystallogr.* (1956), 9, 728.

[361] Walker J. *Sci Am.* (1987), 256, 98.

[362] Symons M.C.R. *Acc. Chem. Res.* (1981), 14, 179.

[363] Brunner G.O. *Zeolites* (1992), 12, 428.

[364] Handerson S.J., White J.W. *J Appl. Cryst.* (1988), 21 (744).

[365] Dutta P.K., Bronic J. *Zeolites* (1994), 14, 251.

[366] Zhdanov S.P. *Adv. Chem. Ser.* (1971), 101, 21.

[367] Flanigen E.M. *Adv. Chem. Ser.* (1973), 121, 119.

[368] Yoshizawa N., Maruyama K., Yamada Y., Zielinska-Blajet M. *Fuel* (2000), 79, 1461-1466.

[369] Emmerich F.G. *Carbon* (1995), 33 (12), 1709.

[370] Grumer T., Zerda T.W., Gerspacher M. *Carbon* (1994), 32 (7), 1377.

[371] Mirth G., Lercher J.A., Anderson M.W., Klinowski J. *J Chem. Soc., Faraday Trans.* (1990), 86, 3039.

[372] Choudhary V.R. *Chem. Eng. Sci.* (1997), 52 (20), 3543-3552.

[373] Dyer A., Amin S. *Microporous Mesoporous Mater.* (2001), 46, 163-176.

[374] Prasetyo I., Do H. D., Do D.D. *Chem. Eng. Sci.* (2002), 57, 133-141.

[375] Do D.D. *Chem. Eng. Sci.* (1996), 51, 4145–4158.

[376] Do D.D., Wang K. *A.I.Ch.E. J* (1998), 44, 68.

[377] Do D.D., Wang K. *Carbon* (1998), 36, 1539.

[378] Figueiredo J.L., Pereira M.F.R., Freitas M.M.A., Orfao J.J.M. *Carbon* (1999), 37, 1379.

[379] Peppas N. A. *Polymer* (1997), 38, 3425.

[380] Glasstone S., Lewis D. Element of Physical Chemistry. London: Macmillan, (1946).